The University Of Sheffield.

TRPC channels in human mast cells

Claire Tree-Booker

A thesis submitted for the degree of PhD

Department of Biomedical Science
University of Sheffield

October 2011

Author's declaration

I hereby certify that all writing and scientific figures presented in this thesis are original works by the author, unless otherwise stated in figure legends. All research displayed was carried out and processed by the author unless directly specified. All research findings, concepts and diagrams obtained from other sources have been clearly referenced with no known infringement of copyright. Permission to re-use figures from published work was sought where appropriate; figure legends indicate when permission was granted. This statement is true at the date of submission.

Claire Tree-Booker

Acknowledgements

I would firstly like to thank my supervisor Dr Liz Seward for her constant support, endless enthusiasm for my project, positivity and brilliant ideas. I have really enjoyed being part of such a friendly and dynamic lab. Thank you to my advisors Professor David Grundy and Dr Pete Monk for your guidance during my project. Pete, thank you for your continued support over the past few years and for all your helpful suggestions. Thank you also to the many people in BMS who have helped me during my PhD: Ivana Barbaric, Mark Jones, Bob and John, Gaynor Miller, Jamie Weiss and everyone in the Grundy lab.

I'd like to thank Rob for all your help when I was a newbie and for introducing me to the wonderful world of calcium imaging. Thank you to Reuben for your enthusiasm about PCR and for your help in reaching high places. Kathryn you're wonderful; I'm very lucky that I got to work with you for all my time in the lab. Thank you for everything you helped me with, for your appreciation of being organised, and for always knowing what to do. Jasmine, we've been in this together since day one and I couldn't have done it without you. Thank you for being my "counterpart", for your never-ending enthusiasm about patching and everything you've done for me. I'll miss your lengthy solution-making missions and your make-shift washing lines. Thank you both for making it fun to come into work every day.

Thank you to my family for all your love and support. Sarah, "The Bible" is now finished! Finally, a huge thank you to my husband-to-be John for always looking after me and for your unwavering confidence in me. I'll stop stressing about being unemployed now and you can have your desk back!

Abstract

Mast cells have an important role in the immune system, but they are centrally involved in the pathophysiology of asthma, along with a number of other allergic diseases including rhinitis, eczema and irritable bowel disease (Metcalfe *et al.*, 1997; Beaven, 2009). In the allergic response they are activated by IgE binding to high affinity receptors and subsequent cross-linking by antigen. A rise in intracellular Ca^{2+} is required for mast cells to become activated and release mediators into the surrounding areas, which give rise to the symptoms of allergic disease (Gilfillan & Tkaczyk, 2006). Elucidating the ion channels responsible for mast cell Ca^{2+} entry may unveil new therapeutic targets for the treatment of asthma and other allergic diseases.

Store-operated Ca^{2+} entry (SOCE) is a major mechanism for mast cell Ca^{2+} influx and is known to involve highly Ca^{2+}-selective Orai1 channels. TRPC channels are non-selective Ca^{2+} channels; TRPC1, 4 and 5 are thought to be involved in SOCE, whereas TRPC3, 6 and 7 are activated by diacylglycerol (DAG). Whilst a limited number of studies carried out in rodent mast cells suggest that TRPC channels could be important for Ca^{2+} entry and mediator release, their functional expression and roles in human mast cells have not been characterised.

This study showed that the LAD 2 human mast cell line and primary human lung mast cells (HLMCs) express mRNA for TRPC6. TRPC6-like currents were demonstrated for the first time in HLMCs, in response to direct activation by the DAG analogue OAG, and downstream of Gq protein-coupled $P2Y_1$ receptor stimulation by ADP. This study also revealed for the first time that TRPC1 channels are expressed in both LAD 2 cells and HLMCs, and that both TRPC1 and Orai1 channels are likely to be involved in SOCE. Importantly, this study also indicated that TRPC1 channels could be involved in Ca^{2+} entry and mediator release downstream of IgE receptor activation. TRPC channels could thus contribute to Ca^{2+} entry required for mast cell activation in allergic disease, and could represent a therapeutic target for the modulation of diseases such as asthma.

Contents

Index of figures

Index of tables

Abbreviations

2-APB	2-aminoethoxydiphenylborate
5HT	5-hydroxytryptamine
A/A	antibiotic/antimycotic solution
AA	arachidonic acid
ADP	adenosine diphosphate
AM ester	acetoxymethyl ester
ATP	adenosine triphosphate
AVP	arginine-vasopresin
BALF	broncoalveolar lavage fluid
BMMC	bone marrow-derived mast cell
BSA	bovine serum albumin
BTK	Bruton's tyrosine kinase
C3a	complement fragment 3a
CaM	calmodulin
CCD	charge-coupled device
CD	cluster of differentiation cell surface marker
CDS	cell dissociation solution
CHO	Chinese hamster ovary
COPD	chronic obstructive pulmonary disease
CTMC	connective tissue mast cell
DAG	diacylglycerol
DMEM	Dulbecco's modified Eagle's medium
DMSO	dimethyl sulphoxide
DN	dominant negative
DNA	deoxyribonucleic acid
EF-SAM	EF-hand domain and the sterile α-motif domain
EGTA	ethyleneglycoltetraacetic acid
ER	endoplasmic reticulum
FcεRI	high affinity IgE receptor
FCS	foetal calf serum
FSGS	focal segmental glomerulosclerosis
GPCR	G protein-coupled receptor
h	human
HBSS	Hank's buffered saline solution
HEK-293	human embryonic kidney cell line
HEK-TRPC5	HEK cell line expressing TRPC5 channels

HEK-TRPC6	HEK cell line expressing TRPC6 channels
HEPES	4-(2-hydroxyethyl)-1-piperazineethanesulphonic acid
HLMC	human lung mast cell
HMC-1	human mast cell-1 line
HR	hydrophobic residue
HSG	human salivary gland
I_{CRAC}	Ca^{2+} release-activated Ca^{2+} current
IgE	immunoglobulin E
IL	interleukin
$InsP_3$	inositol-1,4,5-triphosphate
I_{SOC}	store-operated current
ITAM	immunoreceptor tyrosine-based activation motif
I/V	current/voltage
K_v	voltage-gated K^+ channels
LAD	laboratory of allergic diseases
LAT	linker for activation of T cells
LPC	lysophosphatidylcholine
LT	leukotriene
MC_{TC}	tryptase and chymase-positive mast cells
MMC	mucosal mast cell
mMCP	mouse mast cell protease
NEAA	non-essential amino acids
NGF	nerve growth factor
NP-BSA	4-hydroxy-3-nitrophenylacetyl hapten conjugated to BSA
NTAL	non-T cell activation linker
OAG	1-Oleoyl-2-acetyl-*sn*-glycerol
OPT	*o*-phthaldialdehyde
PBS	phosphate buffered saline
PCR	polymerase chain reaction
PG	prostaglandin
PI3K	phosphatidylinositol 3-kinase
PKC	protein kinase C
PLC	phospholipase C
PMA	phorbol 12-myristate 13-acetate
PPADS	pyridoxalphosphate-6-azophenyl-2',4'-disulphonic acid
$PtdIns(4,5)P_2$	phosphatidylinositol-4,5-biphosphate
RBL-2H3	rat basophilic leukaemia cell line
RGS	regulator of G protein signalling
rhSCF	recombinant human SCF

ROI	region of interest
RPMI	Roswell Park memorial institute medium
Rs	series/access resistance
SD	standard deviation
SEM	standard error of the mean
S1P	sphingosine-1-phosphate
SCF	stem cell factor
SCID	severe combined immunodeficiency
SERCA	sarcoplasmic/endoplasmic reticulum Ca^{2+} ATPase
siRNA	small interfering RNA
SMC	smooth muscle cell
SNARE	soluble N-ethyl-maleimide-sensitive factor attachment protein receptor
SOAR	STIM1 Orai-activating region
SOC	store-operated Ca^{2+}
SOCE	store-operated Ca^{2+} entry
STIM1	stromal interaction molecule 1
Syk	spleen tyrosine kinase
TEA	tetraethylammonium
TGF	transforming growth factor
TLR	toll-like receptor
TM	transmembrane region
TNF	tumour necrosis factor
TRP	transient receptor potential channel
TRPA	ankyrin TRP channel
TRPC	canonical TRP channel
TRPM	melastatin TRP channel
TRPML	mucolipin TRP channel
TRPP	polycystin TRP channel
TRPV	vanilloid TRP channel
UTP	uridine triphosphate

Chapter 1: Introduction

1.1 Mast cells

1.1.1 Introduction to mast cells

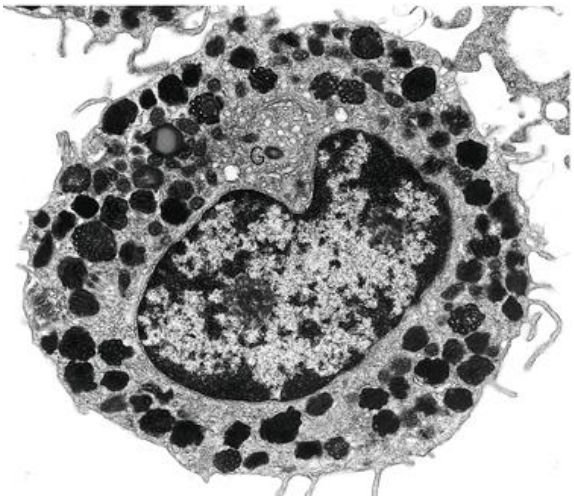

Figure 1.1. Electron micrograph of a human mast cell
Note the many cytoplasmic granules, which give rise to unique staining patterns.
Image (courtesy of Ann Dvorak) reproduced from cover of *Laboratory Investigation* **87** (10).

Mast cells are of haematopoietic origin and have long been recognised for their central role in anaphylaxis and allergic disease (Metcalfe *et al.*, 1997). They were first recognised by Paul Ehrlich in the 1800s, by the unique staining characteristics of their cytoplasmic granules (Metcalfe et al., 1997). Illustrated in figure 1.1 is an electron micrograph of a mast cell, showing the many cytoplasmic granules recognised by Ehrlich. He originally named mast cells "mastzellen" (from the Greek word *masto,* meaning *to feed*), after mistakenly believing that they consume their surrounding tissue. They are now considered immune cells, with a wide range of functions in the innate and adaptive immune responses (Metz & Maurer, 2007). Mast cells exert their functions by the secretion of a wide range of mediators, many of which are pre-formed and stored in the cytoplasmic granules (Metcalfe *et al.*, 1997). Whilst it is accepted that mast cells arise from $CD34^+/CD117^+$ pluripotent haematopoietic bone marrow stem cells (Kitamura *et al.*, 1978), controversy remains regarding their origins; a committed mast cell progenitor has been identified in adult mouse bone marrow that only gave rise to mast cells (Chen et al., 2005). However, bipotent progenitors have also been described in mouse spleen, which were found to be capable of differentiating into mast cells and basophils (Arinobu et al., 2005). Results so far obtained in human mast cells favour a multipotent progenitor; $CD34^+$ progenitors gave rise to mast cells, basophils, eosinophils and neutrophils when cultured in the presence of SCF (Kirshenbaum *et al.*, 1999).

Immature mast cells circulate in the blood, but require a tissue environment for full maturation (Metz & Maurer, 2007). They are preferentially located at sites where the host meets the external environment and infection is most likely to occur, for example the mucosa of the respiratory and gastrointestinal tract, and the skin (Sellge & Bischoff, 2006). The differentiation of progenitor cells into fully mature mast cells is dependent on the activation of c-kit receptors by stem cell factor (SCF) and subsequent dimerisation and auto-phosphorylation; KIT-deficient mice have considerably reduced mast cell numbers (Grimbaldeston *et al.*, 2005). Inhibition of c-kit activity by tyrosine kinase inhibitors in human mast cells induced apoptosis, indicating that the continued presence of SCF is also required for long-term mast cell survival (Metcalfe *et al.*, 1997). In mice, it has been shown that the $\alpha 4\beta 7$ integrin expressed on mast cell precursors and the mucosal address in cell adhesion molecule (MAdCAM)-1 expressed in the intestine are important for mast cell precursors homing to the gut (Gurish et al., 2001). In humans, however, it remains unidentified at which stage of maturation mast cell progenitors migrate from the blood into the tissues, and how this process is regulated (Sellge & Bischoff, 2006).

Tissue maturation of mast cells is dependent on other cells including T-cells and fibroblasts, and growth factors such as SCF and nerve growth factor (NGF). The complement of cytokines, chemokines and SCF at a particular site also determines the distribution and phenotype of mast cells (Metz & Maurer, 2007). This "mast cell heterogeneity" allows them to respond to diverse stimuli at different locations.

1.1.2 Classification

A great deal of evidence for mast cell heterogeneity has come from rodent studies. Traditionally they have been classified into two main types based on phenotypical differences observed between connective tissue mast cells (CTMC), for example in the peritoneal cavity and skin, and mucosal mast cells (MMC) in the intestine (Metcalfe et al., 1997). Phenotypical differences exist between the two types of rat mast cell include size, histamine content, and T-cell dependency; these differences are summarised in Table 1.1.

Human mast cells also display variations in properties such as size and granule ultrastructure (Dvorak, 1989). However, the two main subpopulations of human mast cells are distinguished based on their cytoplasmic granule protease content. TC mast cells are thus called because they contain tryptase and chymase, whereas T mast cells cells contain tryptase only (Irani et al., 1989). Human MC_T predominate in the gastrointestinal (GI) tract, where they comprise 2-3% of the lamina propria, and in the lungs. MC_T correspond more closely to rodent MMC, whereas MC_{TC} are found in the skin and small intestinal submucosa, and correspond to rodent CTMC (Metcalfe et al., 1997). Table 1.2 summarises the properties of human MC_T and MC_{TC}. The heterogeneity of both rodent and human mast cells at different sites indicates that the tissue microenvironment is an essential factor in determining mast cell phenotype.

Characteristics	Peritoneal Cavity Mast Cell	Intestinal Mucosa Mast Cell
Alternative names	Connective tissue mast cell Typical mast cell	Mucosal mast cell Atypical mast cell
Size	10–20 μm	5–10 μm
Formaldehyde fixation	Resistant	Sensitive
Staining	Safranin	Alcian blue
T-cell dependence in development	No	Yes
Protease content	Chymase (RMCP I)	Chymase (RMCP II)
Proteoglycans molecular mass	Heparin 750-1,000 kDa	Chondroitin sulfate di B 100–150 kDa
Histamine	10–20 pg/cell	1 pg/cell
5-Hydroxytryptamine	1–2 pg/cell	<0.5 pg/cell
Prostaglandin D_2	+	+
Leukotriene C_4	–	++
Activated by		
FcεRI aggregation	Yes	Yes
Compound 48/80	Yes	No
Substance P	Yes	No
Inhibited by sodium cromoglycate	Yes	No

RMCP, rat mast cell protease.

Table 1.1. Phenotypic characteristics of rodent peritoneal cavity mast cells (CTMCs) and intestinal mucosa mast cells (MMCs)

Reproduced from (Metcalfe *et al.*, 1997); permission not required for reproduction of figures from this article.

Characteristic	MC_T	MC_{TC}
Neutral protease	Tryptase (10)*	Tryptase Chymase Carboxypeptidase Cathepsin G
Granule ultrastructure	Scrolls	Lattice/grating
T-cell dependence	Yes	No
Inhibited by sodium cromoglycate	Yes	No
Distribution, %		
Skin	<1	>99
Alveolar tissue	93	7
Nasal mucosa	66	34
Tonsils	40	60
Small intestine		
Mucosa	81	19
Submucosa	23	77

MC_T, mast cells with tryptase only; MC_{TC}, mast cells with tryptase and chymase. * Cellular content (pg/cell).

Table 1.2. Characteristics of T and TC type human mast cells

Reproduced from (Metcalfe et al., 1997); permission not required for reproduction of figures from this article.

1.1.3 Model mast cells

Given the heterogeneity of mast cells between species, and between sites within the same organism, it would be ideal to use primary human mast cells for *in vitro* experiments. Cultured primary human lung mast cells have been used in a number of studies to investigate their activation mechanisms; such studies provide important insight into how mast cells may contribute to the asthmatic phenotype. However, difficulty in obtaining human tissue for mast cell isolation and limitations in cell numbers for functional assays mean that it is not always possible to use primary human mast cells. Model mast cell lines are thus frequently used.

The rat basophilic leukaemia (RBL)-1 cell line was originally derived from basophils (Eccleston *et al.*, 1973). Whilst this cell line was not able to respond to IgE-mediated stimulation (Siraganian *et al.*, 1975), it was used to develop the RBL-2H3 line, which degranulates in response to IgE receptor crosslinking (Barsumian *et al.*, 1981), reflecting the behaviour of mast cells and basophils. RBL-2H3 cells have a KIT mutation that gives rise to constitutive activation of the

receptor, allowing them to grow independently of SCF (Tsujimura *et al.*, 1995). This feature makes the cell line an economical alternative to primary mast cells, as cytokine-dependent culture is expensive. RBL-2H3 cells and primary rodent mast cells such as peritoneal mast cells have been used extensively to study mast cell function. Studying primary rodent mast cells from mice where a gene of interest has been knocked out can provide valuable information on the function of certain mast cell proteins. However, there are clear differences between rodent and human mast cells including tissue distribution, protease content, cytokine production and pharmacological activation (Bischoff, 2007). These species differences highlight the need to verify findings obtained in rodents using human mast cells.

LAD 1 and 2, two SCF-dependent human mast cell lines, were generated in the Laboratory of Allergic Diseases (LAD), from bone marrow aspirates taken from a patient with mast cell sarcoma/leukaemia. Mononuclear cells from five separate bone marrow aspirates were cultured in the presence of recombinant human SCF (rhSCF); mast cells persisted in culture and were established as cell lines 24 months later (Kirshenbaum *et al.*, 2003). LAD 1 and 2 cells were found to double in number approximately every 14 days when cultured with SCF. FACS analysis revealed that 98% of cells were positive for tryptase expression and 37% expressed both chymase and tryptase, therefore 37% of cells were of the TC type and 63% were of the T type. This expression profile most closely resembles that seen in mast cells found in the mucosal layers of organs such as the lung (Irani *et al.*, 1986). Antibody analysis of surface markers on LAD cells revealed the expression of CD117, the receptor for SCF, and the high affinity IgE receptor FcεRI, among others. The cells released β-hexosaminidase and histamine in response to FcεRI crosslinking (Kirshenbaum *et al.*, 2003), showing that the high affinity IgE receptor is functionally expressed in LAD 1 and 2 cells. Electron microscopy showed that LAD cells measure 8–15μM in diameter and have uneven surfaces; staining with toluidine blue showed round or oval-shaped cells with distinct metachromatic staining of the granules (Kirshenbaum *et al.*, 2003). Illustrated in figure 1.2 are the staining and surface features of LAD 2 cells.

To verify that the LAD 1 and 2 cell lines were derived from the original patient, DNA isolated from the patient's bone marrow and that from LAD cells was analysed using six primer pairs, and the band patterns were identical. LAD 3–5 cells remain in development (Kirshenbaum *et al.*, 2003). As LAD 2 cells closely resemble primary human mast cells, require SCF for growth and have functional high affinity IgE receptors, they are an extremely useful model for the study of human mast cell biology *in vitro*.

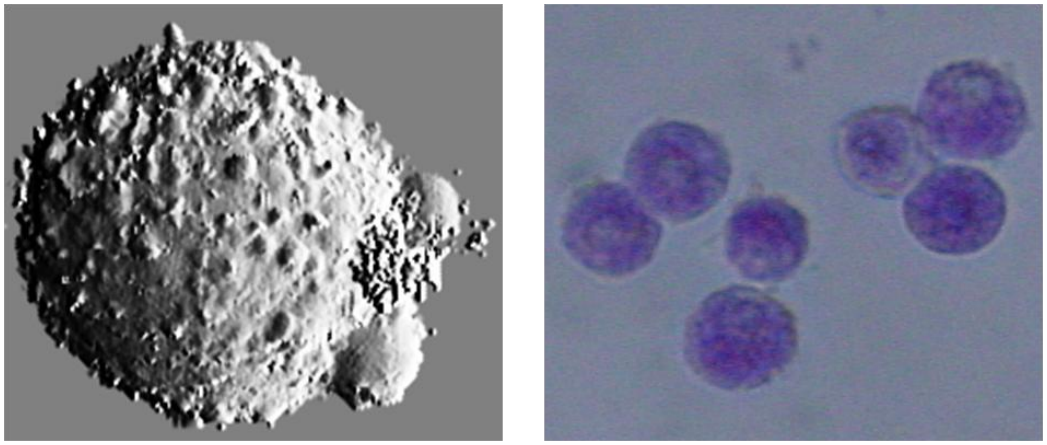

Figure 1.2. Images of LAD 2 mast cells

a: Scanning ion conductance microscopy image of a LAD 2 cell, courtesy of Robert Field, Ionscope Ltd.

b: Kimura stain of LAD 2 mast cells, showing characteristic metachromatic granule staining

An alternative human mast cell line, HMC-1 (Butterfield *et al.*, 1988) , is available, but it has some limitations. Firstly, like RBL-2H3 cells, HMC-1 cells have a KIT activating mutation (Asp816Val) (Nilsson *et al.*, 1994), which causes CD117 phosphorylation to occur independently of SCF, rendering the cells growth factor-independent. This activating mutation is not present in LAD 2 cells; they require SCF for proliferation, therefore more closely resemble mature primary human mast cells. Additionally, HMC-1 cells do not consistently degranulate in response to IgE receptor crosslinking (Butterfield *et al.*, 1988), as surface expression of the high affinity IgE receptor is variable (Nilsson *et al.*, 1994). These limitations restrict the usefulness of HMC-1 for the study of human mast cells. Very recently a new human mast cell line, LUVA, was developed from haematopoietic progenitor cells (Laidlaw *et al.*, 2011). LUVA cells express c-kit and FcεRI, and degranulate in response to FcεRI cross-linking. They can be grown in the absence of SCF but do not have an activating KIT mutation, suggesting that growth occurs by a c-kit-independent mechanism (Laidlaw *et al.*, 2011). The reasons for lack of dependence on SCF are at present being investigated in the authors' laboratory.

To summarise, a number of models exist for the study of mast cells. Due to the species- and site-dependent mast cell heterogeneity that exists, primary human mast cells should ideally be used for investigations. In the absence of their availability, LAD 2 cells represent a useful model for the *in vitro* study of human mast cell biology.

1.1.4 The role of mast cells in the immune system

Whilst mast cells are most well-known for their role in allergic reactions, a number of studies have indicated that they are involved in innate and adaptive immune responses. Mast cell-deficient mice have been used to show that they are crucial for the development of host immunity and survival in bacterial infections including septic peritonitis (Echtenacher *et al.*, 1996). It is now known that mast cells provide protection only after being activated by signals from both host and pathogen, such as mannose-binding lectin (bacterial surface protein) and host-derived products of the complement cascade (Henz *et al.*, 2001; Metz & Maurer, 2007). Following mast cell activation in response to infection, they secrete mediators that recruit other inflammatory cells such as neutrophils and macrophages (Metz & Maurer, 2007). Mast cells have also been suggested as effector cells in the innate immune response, causing phagocytosis of bacteria (Malaviya *et al.*, 1996). They have long been thought to contribute to innate defence against parasitic infections; mouse models of nematode infection have been used to show that mast cell numbers in the intestinal mucosa are increased during infection, and activation stimulates the release of mouse mast cell protease (mMCP)-1m, which contributes to nematode expulsion (McDermott *et al.*, 2003).

There is also increasing evidence to suggest that mast cells are important in acquired (adaptive) immunity. Studies in mice showed that the recruitment of T cells to draining lymph nodes following *Escherichia coli* infection was enhanced following mast cell activation (McLachlan *et al.*, 2003). The effect was mimicked by injection of tumour necrosis factor (TNF), suggesting that mast cell-derived TNF has a role in T cell recruitment (McLachlan *et al.*, 2003; Metz & Maurer, 2007).

Mast cells thus have important roles in the initiation and maintenance of host responses to pathogens, which are summarised in figure 1.3. However, it must be considered that studies addressing the role of mast cells in immunity have mostly been carried out in rodents. Caution must be applied when extrapolating results obtained in mice to humans. Human mast cells can release a range of immunomodulatory mediators but species differences exist in the production of some cytokines and expression of receptors (Bischoff, 2007); these differences could affect the role of mast cells in human immunity.

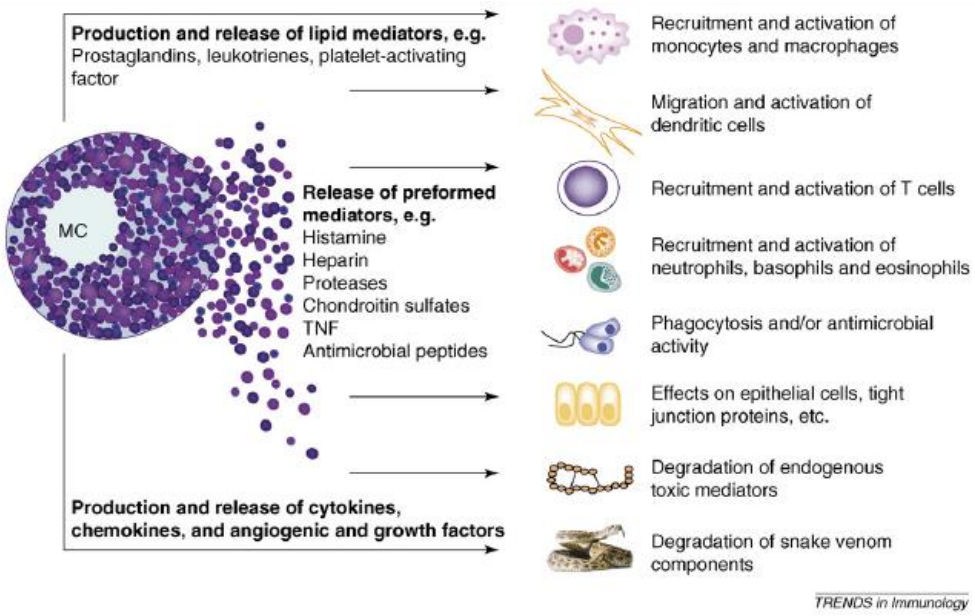

Figure 1.3. The effects of mast cells on pathogens and other cells of the immune system
Reproduced with permission from (Metz & Maurer, 2007)

1.1.5 The role of mast cells in allergic disease

Scientific investigations into allergic disease began in 1869, when Charles Blakely performed a skin test on himself to show that his hayfever was caused by pollen, which gave rise to an urticarial reaction (Beaven, 2009). The term anaphylaxis was introduced in 1902 when *Physalia* tentacle extracts caused anaphylactic shock in dogs that had previously been given an injection of the extracts (Beaven, 2009). Subsequent studies showed that histamine could cause the symptoms of anaphylactic shock (Riley, 1953), and a correlation was observed between mast cell count and histamine levels in urticaria lesions (Riley & West, 1952). Further evidence for the involvement of mast cells in anaphylactic reactions was provided by the enhanced presence of histamine in dog mastocytomas (Cass *et al.*, 1954). IgE antibodies were identified as the factor responsible for sensitivity to allergens in 1967 (Ishizaka & Ishizaka, 1967). The role of mast cells in allergic disease is now more fully characterised, and the allergic response is described as a type 1 hypersensitivity reaction (Beaven, 2009). Hypersensitivity is an abnormally high immune response to a normally harmless molecule such as dust, leading to cell and tissue damage.

Chronic mast cell activation is now known to contribute to the pathophysiology of many allergic diseases, including allergic asthma. Asthma is a chronic lung disease that is characterised by reversible airway obstruction caused by bronchial hyper-responsiveness, excess mucus production and narrowing of the airways (Owen, 2007). Following allergen exposure, an asthmatic reaction is initiated by a type 1 hypersensitivity reaction; mast cell mediators are present at higher levels from bronchoalveolar lavage fluid (BALF) from patients with asthma compared with non-asthmatic controls at this stage (Broide *et al.*, 1991). Mast cell mediators are capable of causing mucus secretion, bronchoconstriction and mucosal oedema, all of which

contribute to the symptoms of asthma (Bradding *et al.*, 2006). Mast cells are present in increased numbers within the airway smooth muscle in asthmatic patients compared with non-asthmatics (Brightling *et al.*, 2002), a factor that is thought to contribute to airway hyper-responsiveness (Bradding *et al.*, 2006). Localisation of mast cells to the bronchial epithelium and airway mucous glands also occurs in asthmatics; in the epithelium they are in close proximity to aeroallergens that cause mast cell activation, and they are thought to contribute to mucous gland hyperplasia (Bradding *et al.*, 2006). Mast cells are also thought to be involved in the symptoms of chronic asthma; mast cell mediators are present at higher levels in BALF from patients with chronic asthma compared with non-asthmatics (Broide *et al.*, 1991), and human lung mast cells (HLMCs) can release the mediators histamine, leukotriene C_4 (LTC_4) and interleukin (IL)-8 a week after initial exposure to IgE (Cruse *et al.*, 2005).

Current statistics from *Asthma UK* indicate that asthma currently affects 5.4 million people in the UK; it is the most common long-term medical condition, and 1.1 million working days were lost due to breathing difficulties in 2008–2009. Several mast cell-stabilising drugs are used in the treatment of asthma including disodium cromoglycate, which causes weak (10–20%) inhibition of HLMC histamine release *in vitro* (Church & Hiroi, 1987), and β2-adrenoceptor agonists such as salbutamol, which has a more potent effect on mast cell function *in vitro* but has limited efficacy with chronic administration (Church & Hiroi, 1987; Swystun *et al.*, 2000). Omalizumab, a recently-licensed treatment for asthma, is a humanised monoclonal antibody that binds circulating IgE and prevents it from binding to FcεRI on mast cells in the airway (Thomson *et al.*, 2011). It has been shown to improve symptoms in patients with allergic asthma and reduce airway inflammation (Walker *et al.*, 2006; Rodrigo *et al.*, 2011), highlighting the importance of the mast cell as a therapeutic target. The impact of asthma on quality of life, along with the economic toll and inadequacy of current therapies in some patients, highlights the need for improved asthma treatments. Given the central role of the mast cell in the disease process, further research into human lung mast cell activation and inhibition is necessary to reveal potential new therapeutic targets for asthma.

In addition to asthma, mast cells play a major part in the manifestation of other allergic disorders including allergic rhinitis, peanut allergy and eczema (Owen, 2007), along with gastrointestinal disorders such as inflammatory bowel disease and coeliac disease (Barbara *et al.*, 2006; Sellge & Bischoff, 2006). Their detrimental effects also extend to autoimmune diseases (Beaven, 2009); mast cells have been found to accumulate in the synovial fluid of patients with rheumatoid arthritis (Nigrovic & Lee, 2007), and correlations have been found between disease progression and mast cell localisation in multiple sclerosis (Beaven, 2009). Further research into mast cell activation mechanisms will thus be of great benefit for the understanding of a wide range of conditions in which they are involved, and could lead to the development of new treatments.

1.1.6 Mast cell mediators

The many biological and pathophysioloical roles of mast cells are made possible by the heterogeneous group of mediators that they synthesise and release. Mast cell mediators can be divided into three categories; preformed granule-associated mediators, lipid-derived mediators and cytokines (Metcalfe *et al.*, 1997).

1.1.6.1 Granule-associated mediators

Mast cells store a plethora of pro- and anti-inflammatory mediators in their cytoplasmic granules that are released upon degranulation. Degranulation is an immediate reaction that occurs following mast cell activation, taking place within minutes (Metcalfe *et al.*, 1997). The biogenic amine histamine is released upon degranulation; histamine possesses a range of biological activities, including vasodilation, bronchoconstriction, increased capillary permeability and airway smooth muscle contraction (Lundequist & Pejler, 2011). Mice deficient in histidine decarboxylase (HDC), the enzyme catalysing histamine production, have provided further insight, suggesting that histamine has a role in allergic airway inflammation (Koarai *et al.*, 2003) and autoimmune encephalitis (Musio *et al.*, 2006). It has been known since the 1950s that serotonin is present in mast cell granules; it was previously thought to be restricted to rodent mast cells (Lundequist & Pejler, 2011) but has recently been shown to be present in human peripheral blood-derived mast cells (Kushnir-Sukhov *et al.*, 2007). The major pathophysiological effects of serotonin are vasoconstriction and pain (Theoharides *et al.*, 2007). Mast cell granules also contain a number of enzymes that are present in lysosomes. β-hexosaminidase is the most well-known, and is ubiquitously present in mast cells from all species (Lundequist & Pejler, 2011). It is thought to have a role in carbohydrate processing (Theoharides *et al.*, 2007). β-hexosaminidase release is frequently used experimentally to quantify the extent of mast cell degranulation.

Proteoglycans are a major constituent of mast cell granules (Lundequist & Pejler, 2011); heparin and chondroitin sulphate E are both found in human mast cells (Metcalfe *et al.*, 1979; Metcalfe *et al.*, 1997) and stabilise mast cell proteases. Mast cell granule proteoglycans are thought to give rise to their staining by Toluidine Blue (Lundequist & Pejler, 2011), as metachromatic staining is not visible in mast cells from mice lacking the proteolgycan serglycin (Abrink *et al.*, 2004). Mast cell granules are a major site of stored proteases, which account for 25% of total mast cell protein (Schwartz *et al.*, 1987). As discussed above, human mast cells are classified based on their tryptase and chymase protease content. Chymase gives rise to tissue damage and pain when released from the mast cell, whereas tryptase has a role in protease-activated receptor (PAR) activation, inflammation and pain (Theoharides *et al.*, 2007). Granule-associated mediators thus contribute to the symptoms of asthma and other allergic diseases through their multifaceted effects when they are released following mast cell activation.

1.1.6.2 Lipid-derived mediators

In addition to the range of granule-associated mediators released by the mast cell, newly-synthesised mediators are produced upon mast cell activation. It is known that mast cells are

capable of differential mediator release without degranulation as they are involved in the pathogenesis of inflammatory diseases without causing anaphylactic shock (Theoharides *et al.*, 2007). The *de novo* synthesis of lipid-derived mediators derived from arachidonic acid is an important event following activation, as they possess potent pro-inflammatory activity (Metcalfe *et al.*, 1997). Cyclo-oxygenase metabolites of arachidonic acid include prostaglandins and thromboxanes; lipoxygenase products include leukotrienes. LTC_4, LTD_4 and LTE_4 are all produced by the lipoxygenase pathway; they induce skin reactions, promote bronchial mucus secretion and bronchial constriction, enhance vascular permeability and induce smooth muscle cell constriction (Drazen & Austen, 1987; Metcalfe *et al.*, 1997). Prostaglandin (PG) D_2 is also generated following mast cell activation; it is an inhibitor of platelet aggregation, causes bronchoconstriction and pain, and is a neutrophil chemoattractant (Metcalfe *et al.*, 1997; Theoharides *et al.*, 2007). Lipid-derived mediators thus have a number of pro-inflammatory effects in the lung, which contribute to the pathogenesis of asthma.

1.1.6.3 Cytokines

Cytokines are protein or glycoprotein molecules with a broad spectrum of biological activities that are synthesised and secreted by cells (Metcalfe *et al.*, 1997). Following initial events that occur upon mast cell activation, an enhancement of gene expression occurs, followed by the production of cytokines (Gilfillan & Tkaczyk, 2006). Since the first demonstration of mast cell cytokine production in 1986, when they were shown to produce granulocyte-macrophage colony-stimulating factor (Chung *et al.*, 1986), mast cells have been shown to generate a vast array of cytokines (Metcalfe *et al.*, 1997). The expression of mRNAs for IL-1, IL-3, IL-5, IL-6, interferon (IFN)-γ and monocyte chemotactic protein (MCP)-1 were detected in an early study of mouse mast cells (Burd *et al.*, 1989); human mast cells are known to express tumour necrosis factor (TNF)-α, IL-4, IL-5, IL-6 and IL-8 (Bradding *et al.*, 1992; Ohkawara *et al.*, 1992; Moller *et al.*, 1993; Metcalfe *et al.*, 1997). These cytokines can have a profound effect on surrounding tissues, inducing inflammation, leukocyte migration, cellular hyperplasia and angiogenesis, for example (Theoharides *et al.*, 2007). The pro-inflammatory cytokine TNF-α is important in the development of the asthmatic phenotype; it induces bronchial hyper-responsiveness and neutrophil accumulation in the sputum when inhaled (Bradding *et al.*, 2006). TNF-α protein expression is enhanced in BALF in patients with severe asthma compared with non-asthmatics, and mRNA expression is elevated in the bronchial mucosa (Howarth *et al.*, 2005; Berry *et al.*, 2006). In addition to *de novo* synthesis, it has also been shown that mast cells can store pre-formed TNF-α in their granules, along with IL-4 and IL-15 (Gordon & Galli, 1990; Lundequist & Pejler, 2011).

To summarise, numerous mediators released by mast cell degranulation and synthesised upon activation give rise to the various pro- and anti-inflammatory actions of mast cells in various tissue types. The types and effects of the various mast cell mediators are summarised in table 1.3.

	Mediators	Biological effects
Granule-associated	Histamine	vasodilation SMC contraction airway inflammation autoimmune encephalitis
	Serotonin	vasoconstriction pain
	B-hexosaminidase	carbohydrate processing
	Proteoglycans	stablilise mast cell proteases
	Tryptase	PAR activation inflammation pain
	Chymase	tissue damage pain
Lipid-derived	Leukotrienes LTC_4, LTD_4, LTE_4	skin reactions bronchial mucus secretion bronchial constriction increased vascular permeability SMC constriction
	Prostaglandin D_2	inhibits platelet aggregation bronchoconstriction pain neutrophil chemoattraction
Cytokines	IL-1, IL-3, IL-5, IL-6, IL-8 IFNγ, MCP-1, TNF-α	inflammation leukocyte migration cellular hyperplasia leukocyte activation pain angiogenesis

Table 1.3. Summary of mast cell mediators and their biological effects

LTC, leukotriene; SMC, smooth muscle cell; IL, interleukin; IFN, interferon; MCP, monocyte chemotactic protein; TNF, tumour necrosis factor.

Composed from (Metcalfe *et al.*, 1979; Schwartz *et al.*, 1987; Metcalfe *et al.*, 1997; Koarai *et al.*, 2003; Abrink *et al.*, 2004; Musio *et al.*, 2006; Theoharides *et al.*, 2007; Lundequist & Pejler, 2011)

1.2 Mast cell activation

IgE-mediated mast cell activation is considered a critical event in the allergic response (Gilfillan & Tkaczyk, 2006). This section will describe the series of events leading from mast cell IgE binding through to the synthesis and release of the variety of mediators discussed above. The activation of mast cells by other stimuli will also be considered.

1.2.1 Activation via the high affinity IgE receptor

In the allergic response, IgE antibodies to a normally harmless molecule (an allergen, such as dust or pollen) are produced by B cells. These antibodies bind to high affinity IgE receptors (FcεRI) on the surface of mast cells (Kinet, 1999). Following re-exposure, the allergen cross-links IgE bound to FcεRI. This tetrameric receptor consists of the α chain, which binds IgE, along with one β and two disulphide-linked γ chains, which together initiate signalling (Gilfillan & Tkaczyk, 2006). IgE cross-linking by allergen leads to the juxtaposition of two or more FcεRI receptors, commencing signalling cascades that ultimately lead to the release of the mediators discussed above that are involved in allergic inflammation. It has been shown that early signalling events involve interactions of the aggregated receptors with lipid rafts in the membrane (Field et al., 1999), followed by activation of SRC family kinases and phosphorylation of FcεRI on tyrosine residues in immunoreceptor tyrosine-based activation motifs (ITAMs) (Paolini et al., 1991). The SRC family kinases Lyn and Syk phosphorylate the adaptor molecule LAT (linker for activation of T cells), resulting in its recruitment of cytosolic adaptor molecules such as GRB2 and GADS (Gilfillan & Tkaczyk, 2006). The resulting signalling complex allows downstream signalling, leading to the release of various mediators. Figure 1.4 details the pathway of FcεRI- mediated mast cell activation.

As shown in figure 1.4, activation of the mitogen-activated protein kinase (MAPK) pathway generates eicosanoids, including leukotriene C_4 and prostaglandin D_2. Degranulation occurs following increased cytosolic Ca^{2+} as a result of phospholipase C γ (PLCγ) and protein kinase C (PKC) activation. Activated PLCγ catalyses the cleavage of phosphatidylinositol-4,5-biphosphate (PtdIns(4,5)P_2) to produce inositol-1,4,5-triphosphate ($InsP_3$) and diacylglycerol (DAG), which cause calcium release from stores and PKC activation, respectively. It has been shown that the PLCγ inhibitor U73122 inhibits both cytosolic calcium rises and degranulation in human mast cells (Gilfillan & Tkaczyk, 2006), demonstrating the importance of PLCγ in the process. Mast cells express two isoforms of PLCγ: $PLC\gamma_1$ and $PLC\gamma_2$ (Wilde & Watson, 2001). Whilst it is known that in cells of the rat mast cell line RBL-2H3 both isoforms are activated following FcεRI-mediated stimulation, it has been difficult to detect $PLC\gamma_2$ activation in human mast cells (Tkaczyk et al., 2003), suggesting that $PLC\gamma_1$ may be the predominant form in humans.

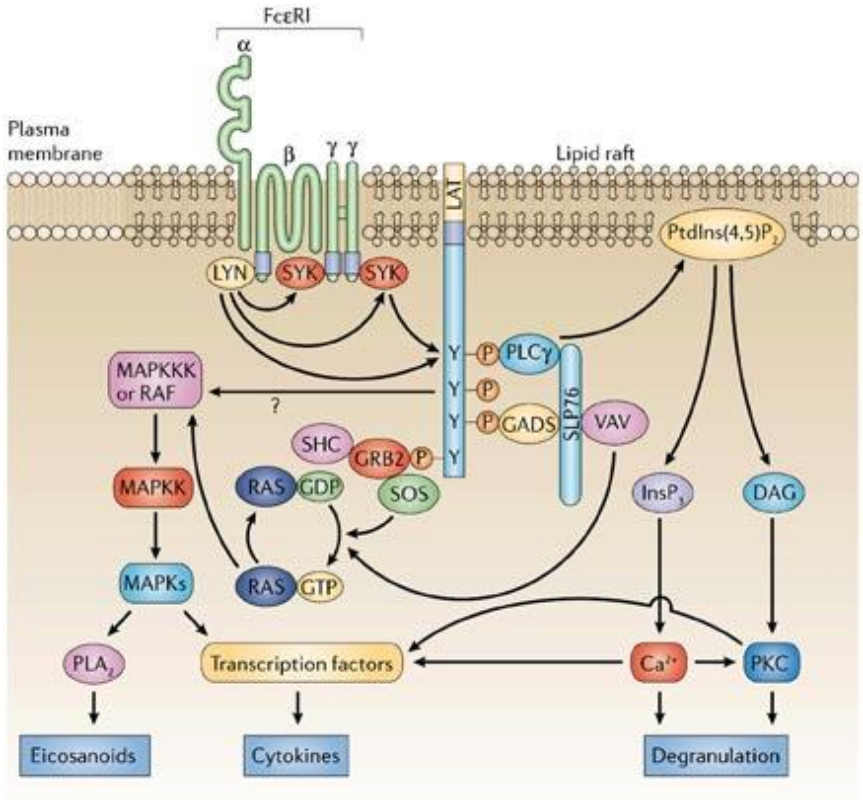

Figure 1.4. The FcεRI-mediated pathway for mast cell activation

Following FcεRI cross-linking, LAT becomes phosphorylated by Src family kinases LYN and SYK. This results in interactions between LAT and cytosolic adaptor molecules such as GRB2 (growth-factor-receptor-bound protein 2) and GADS (GRB2-related activator protein). The production of eicosanoids occurs following activation of the mitogen-activated protein kinase (MAPK) pathway, whereas degranulation takes place when PLCγ is activated, leading to Ca^{2+} mobilisation and protein kinase C (PKC) generation.

Reproduced with permission from (Gilfillan & Tkaczyk, 2006)

In addition to the primary signalling pathway described above, it is believed that a "complementary activation pathway" exists for FcεRI- mediated mast cell activation (Gilfillan & Tkaczyk, 2006). It has been shown that another SRC family kinase, Fyn, is required for degranulation (Parravicini *et al.*, 2002; Sanchez-Miranda *et al.*, 2010); this forms part of a pathway that does not involve LAT-dependent PLCγ activation, but leads to the activation of phosphatidylinositol 3-kinase (PI3K). Described in figure 1.5 is the complementary signalling pathway.

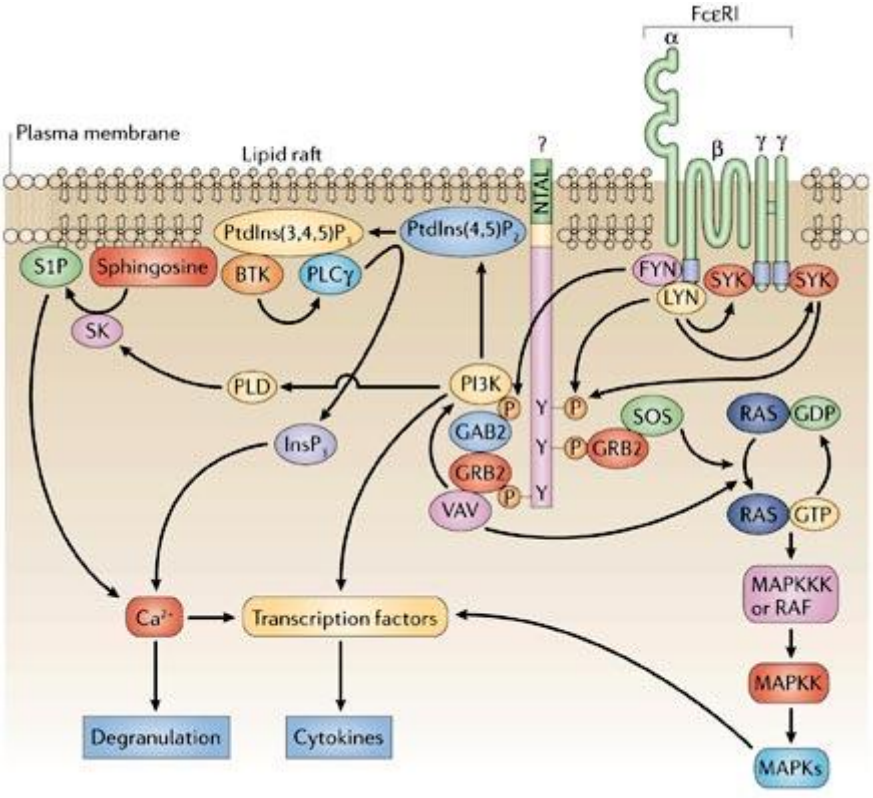

Figure 1.5. The complementary pathway for mast cell activation (only one receptor shown for clarity)

Following receptor cross-linking, the tyrosine kinase Fyn becomes activated, leading to phosphorylation of GAB2 (growth-factor-receptor-bound protein 2), a cytosolic adaptor molecule. Consequently, phosphatidylinositol 3-kinase (PI3K) binds to GAB2, which causes PLCγ phosphorylation by Bruton's tyrosine kinase (BTK). This produces $InsP_3$ via PLCγ-dependent cleavage of $PtdIns(4,5)P_2$, which causes increased calcium mobilisation and degranulation.

Reproduced with permission from (Gilfillan & Tkaczyk, 2006)

PI3K can phosphorylate plasma membrane-associated phosphoinositides via pleckstrin-homology domains (Vanhaesebroeck *et al.*, 2001; Gilfillan & Tkaczyk, 2006), thereby providing a docking site for the recruitment of signalling molecules to the plasma membrane. Signalling molecules involved in mast cell activation that contain pleckstrin homology domains include PLCγ and Bruton's tyrosine kinase (BTK) (Vanhaesebroeck *et al.*, 2001); these molecules can be recruited to the membrane by PI3K. It is thought that this parallel signalling pathway is in place to maintain or amplify the calcium signal generated by the PLCγ- mediated signalling pathway, in order to optimise mast cell activation (Gilfillan & Tkaczyk, 2006). There are a number of possible reasons why multiple signalling cascades exist to mediate FcεRI-dependent mediator release; it could ensure that if a mutation occurs in an essential gene encoding a signalling molecule then activation still occurs, or may allow flexibility in signalling (Gilfillan & Tkaczyk, 2006). Another possibility is that the complementary pathways could allow the integration of other signalling pathways that affect FcεRI -mediated activation.

1.2.2 IgE-independent mast cell activation

Whilst IgE-mediated mast cell activation is regarded as a key event in the allergic response, mast cells express receptors for other physiological ligands, which may induce degranulation, promote survival, growth or chemotaxis of mast cells, prime cells for activation by FcεRI cross-linking, or provide co-stimulatory signals.

1.2.2.1 c-kit

One of the best studied examples is of IgE-independent mast cell activation is via c-kit, the receptor for SCF. It has been shown, using studies with knockout mice and cultured human mast cells, that SCF-dependent activation of c-kit is necessary for mast cell growth, differentiation and survival (Galli et al., 1993; Galli et al., 2005). It has also been found that the presence of SCF is necessary for the long term culture of mast cells isolated and purified from the human lung and intestine; it is a survival factor, and induces proliferation if present in the growth medium at a concentration greater than 10ng/ml (Bischoff *et al.*, 1999; Sanmugalingam *et al.*, 2000; Bischoff, 2007).

SCF, whilst not inducing degranulation alone, enhances FcεRI-mediated responses (Tkaczyk et al., 2004). It has been demonstrated, using human intestinal mast cells, that the release of histamine and LTC_4 in response to FcεRI cross-linking is enhanced after 6 days of culture with SCF compared to controls (Bischoff et al., 1999). For SCF to enhance antigen-mediated degranulation, the two signalling pathways must interact; figure 1.6 details the c-kit signalling pathway.

As shown in Figure 1.6, SCF signalling via c-kit shares many common responses with the FcεRI pathway; PLCγ activation, calcium mobilisation and PI3K activation, for example. SCF, however, cannot by itself activate PKC (Hundley et al., 2004); this could explain its inability to induce degranulation in the absence of antigen. SCF itself does not induce LAT phosphorylation but does phosphorylate NTAL, which is part of the complementary pathway of mast cell activation (see figure 1.5). Therefore SCF can enhance the main antigen-mediated activation pathway by activating the complementary pathway.

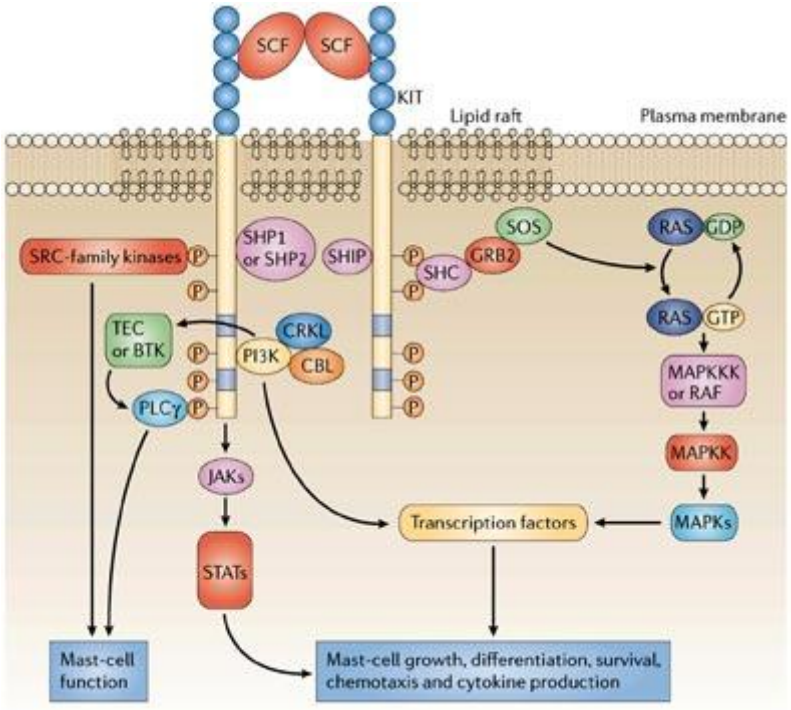

Figure 1.6. The mast cell signalling pathway mediated by stem cell factor (SCF) binding to KIT

Upon SCF binding to KIT and subsequent receptor aggregation, tyrosine residues in the cytoplasmic tail of KIT autophosphorylate. Cytosolic adaptor molecules such as SHC (SRC homology 2-domain-containing transforming protein C) and signalling enzymes such as PLCγ and PI3K are then recruited. Activation of these signalling enzymes, along with the mitogen-activated protein kinase (MAPK) and JAK-STAT (Janus kinase-signal transducer and activator of transcription) pathways, leads to mast cell growth, differentiation, survival, chemotaxis and cytokine production.
Reproduced with permission from (Gilfillan & Tkaczyk, 2006)

1.2.2.2 G protein-coupled receptors

In addition to c-kit, there is increasing evidence demonstrating the influence of members of the G-protein coupled receptor (GPCR) superfamily on mast cells. They have been shown to have a wide range of effects, including both enhancement and inhibition of FcεRI-mediated responses, and increased chemotaxis (Kuehn & Gilfillan, 2007). C3a, an anaphylotoxin that forms part of the complement cascade, can act as a mast cell chemoattractant when bound to its G protein-coupled C3a receptor (C3aR) (Hartmann et al., 1997). Its effects on antigen-mediated degranulation vary depending on the type of mast cell; in RBL-2H3 cells C3a has been shown to inhibit mediator release by a C3a receptor-independent mechanism (Erdei et al., 1995), whereas in the HMC-1 and LAD 2 human mast cell lines it induces degranulation through the C3a receptor (Venkatesha et al., 2005). Sphingosine-1-phosphate (S1P) is a lysophospholipid that binds to a family of five GPCRs, two of which ($S1P_1$ and $S1P_2$) have been shown to be expressed by RBL-2H3 cells (Jolly et al., 2004). They are thought to be important in regulating chemotaxis and degranulation; $S1P_1$ induces chemotaxis, whereas $S1P_2$ induces degranulation but inhibits

chemotaxis (Jolly et al., 2004). A higher concentration of S1P is required to bind to $S1P_2$ than $S1P_1$. It has therefore been proposed that in allergic reactions, lower concentrations of S1P cause mast cells to migrate to their target tissues through binding to S1P, whereas higher S1P concentrations activate the $S1P_2$ receptor to cause degranulation and inhibit chemotaxis once at the target tissue (Olivera & Rivera, 2005). $S1P_2$-mediated enhancement of FcεRI –mediated degranulation has been demonstrated in $S1P_2$-deficient bone marrow mast cells (BMMCs), where there was a reduction in antigen-dependent mediator release compared to wild-type cells (Jolly et al., 2004).

1.2.2.3 Purinergic signalling

Adenosine has been reported to produce contrasting responses in mast cell activation; when bound to the A_3 adenosine GPCR, it enhances FcεRI-dependent mediator release in RBL-2H3 cells (Gilfillan et al., 1990) and HLMCs when added after challenge with anti-human IgE (Hughes et al., 1984) . However, it has also been shown to inhibit FcεRI- dependent degranulation in HLMCs when added before immunological challenge (Hughes et al., 1984). These diverse responses are thought to be due to the multiple P1 purinoceptors for adenosine expressed on mast cells (A_{2A}, $A2_B$ and A_3) producing distinct responses when bound to adenosine (Forsythe & Ennis, 1999).

The nucleotides ATP, ADP and UTP influence cellular behaviour by binding to P2 purinoceptors on the cell surface (Abbracchio & Burnstock, 1994). The P2 purinoceptors are divided into two subgroups; P2X receptors, which are ligand-gated ion channels, and G-protein coupled P2Y receptors (Dubyak & el-Moatassim, 1993). These nucleotides, like adenosine, have been shown to produce distinct responses; in rat mast cells ATP has been reported to induce degranulation via P2X and P2Y receptors (Jaffar & Pearce, 1990), and enhance FcεRI- mediated histamine release (Osipchuk & Cahalan, 1992). Similarly, in HLMCs ATP and UTP have been shown to enhance FcεRI- dependent degranulation, probably mediated through P2Y receptors (Schulman et al., 1999). The functional expression of ATP-activated $P2X_1$, $P2X_4$ and $P2X_7$ has been demonstrated in both LAD 2 cells and HLMCs in our laboratory (Wareham *et al.*, 2009), indicating that these receptors could be important in human mast cell signalling.

In contrast to their augmentation of FcεRI-mediated responses, ADP and ATP have been shown to block cytokine production in response to a toll-like receptor (TLR)2 agonist in human cord blood-derived mast cells (Feng et al., 2004). These findings suggest that, as with adenosine receptors, the expression of multiple purinoceptors in mast cells allows ATP, ADP and UTP to instigate distinct responses. The observation that cord blood-derived human mast cells express $P2Y_1$, $P2Y_2$, $P2Y_{11}$, $P2Y_{12}$ and $P2Y_{13}$ (Feng et al., 2004) supports this idea.

In summary, GPCRs can either provoke mast cell activation, or modify FcεRI-dependent degranulation. However, it must be noted that many of the previously described studies have been carried out in mouse or rat, as opposed to human, mast cells. From the studies carried out

in human mast cells it is apparent that they may behave significantly differently to mouse mast cells (Kuehn & Gilfillan, 2007). It is therefore necessary to investigate further the expression of GPCRs modulating responses in human mast cells, and to examine to what extent they contribute to diseases associated with human mast cells. How GPCR signalling itself is regulated in mast cells also remains incompletely understood. The role of regulator of G protein signalling (RGS) proteins in human MCs has recently been investigated using the HMC-1 and LAD 2 cell lines; it has been shown that the RGS13 protein restricts particular GPCR responses (Bansal et al., 2008), thus representing a therapeutic target for allergic inflammatory diseases.

1.2.3 The importance of Ca^{2+} in mast cell activation

It is well established that a sustained increase in cytosolic Ca^{2+} levels is an essential signal for degranulation in mast cells (Cochrane & Douglas, 1974; Ozawa *et al.*, 1993; Gilfillan & Tkaczyk, 2006). Regulated exocytosis, the process by which degranulation occurs, is controlled by soluble N-ethyl-maleimide-sensitive factor attachment protein receptor (SNARE) proteins (Puri & Roche, 2008). Typically vesicular (v) SNAREs interact with SNAREs on the target membrane (t-SNAREs); this process is Ca^{2+}-dependent and regulated by Ca^{2+} sensors (Melicoff *et al.*, 2009). Ca^{2+} is also required for the *de novo* synthesis of eicosanoids, whose production is dependent on the Ca^{2+} sensitive enzyme PLA_2, and in the transcriptional regulation of cytokine production (Melicoff *et al.*, 2009).

1.3 Ca^{2+} entry mechanisms

There are a number of different routes for Ca^{2+} entry in MCs; one of the most well-studied is via store-operated calcium (SOC) channels. Non-store-operated mechanisms include Ca^{2+} entry via the nucleotide-activated P2X and P2Y receptors discussed above, and through store-independent TRP channels, which are discussed below in section 1.3.2. Figure 1.7 illustrates the mechanisms responsible for Ca^{2+} fluxes in stimulated mast cells, and the importance of Ca^{2+} for mast cell mediator release.

1.3.1 Store-operated Ca^{2+} entry

Store-operated Ca^{2+} entry (SOCE), or capacitative Ca^{2+} entry, is the process by which the depletion of Ca^{2+} stores in the endoplasmic reticulum (ER) by $InsP_3$ binding to its receptor activates Ca^{2+} entry from outside the cell (Parekh & Putney, 2005). The concept of SOCE was first proposed in 1986, when it was suggested that Ca^{2+} influx in non-excitable cells is controlled by the amount of Ca^{2+} in intracellular stores (Putney, 1986). Direct evidence for SOCE was provided by a combination of electrophysiological studies and fura-2 Ca^{2+} measurements in rat mast cells (Hoth & Penner, 1992, 1993); the authors showed that depletion of intracellular Ca^{2+} stores gave rise to a current called Ca^{2+} release-activated Ca^{2+} current (I_{CRAC}). I_{CRAC} is a highly Ca^{2+}-selective, inwardly-rectifying, non-voltage activated current. In the absence of Ca^{2+}, I_{CRAC} currents readily permeate Na^+ ions, giving rise to current amplification (Parekh & Putney, 2005). The biophysical properties of I_{CRAC} currents are illustrated in figure 1.8 Although I_{CRAC} was the first store-operated current to be identified and is the best characterised, it is not believed to be the only SOCE current (Parekh & Putney, 2005; Cheng *et al.*, 2011; Ma & Beaven, 2011). Early studies showed that Ba^{2+} and Sr^{2+} ions, which pass through TRPC channels but not I_{CRAC} channels (Lis *et al.*, 2007; Ma & Beaven, 2011), can support degranulation in rat peritoneal mast cells in the absence of extracellular Ca^{2+} (Foreman & Mongar, 1972); later studies in RBL cells revealed that TRPC5 channels permit Sr^{2+} entry following store depletion (Ma *et al.*, 2008). Various currents with distinct biophysical properties are now thought to be involved in SOCE (Parekh & Putney, 2005).

1.3.1.1 STIM1, Orai1 and I_{CRAC}

The molecular components of I_{CRAC} remained elusive until recently; a key question was how the ER Ca^{2+} store content is linked to plasma membrane channels. This was resolved with the discovery of stromal interaction molecule 1 (STIM1), an ER-resident Ca^{2+} sensor that regulates SOCE, in two independent studies (Liou *et al.*, 2005; Roos *et al.*, 2005). In a siRNA screen to identify genes involved in SOCE in *Drosophila* S2 cells, Roos *et al.* (2005) showed that knock-down of *Stim* inhibited thapsigargin-evoked Ca^{2+} entry and I_{CRAC} currents activated by passive store depletion. The authors showed that knock-down of the human homologue STIM1 similarly inhibited I_{CRAC} in Jurkat T cells, and over-expression of STIM1 in HEK-293 cells enhanced SOCE, concluding that STIM1 has an essential role in SOCE (Roos *et al.*, 2005).

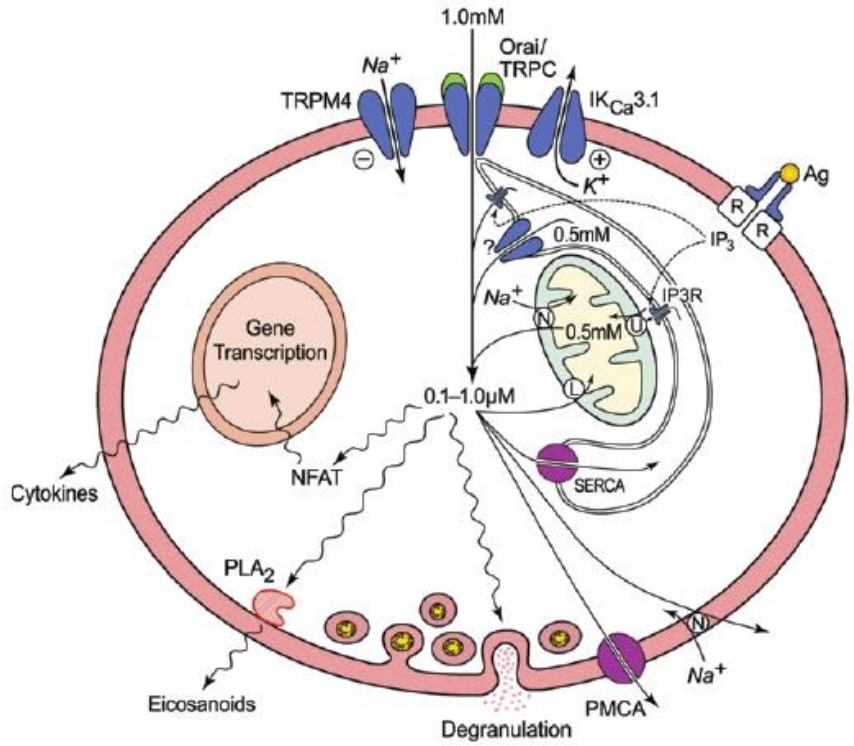

Figure 1.7. Ca^{2+} fluxes in stimulated mast cells

Following FcεRI-evoked signalling, $InsP_3$ binding leads to Ca^{2+} release from the ER through the $InsP_3$ receptors. Ca^{2+} released close to mitochondria is taken up by the mitochondrial uniporter (U). Ca^{2+} store depletion causes the formation of punctae (not shown) that bring together the Ca^{2+} sensor STIM1 into close contact with Orai and TRPC plasma membrane channels. Ca^{2+} influx leads to store replenishment through uptake by the SERCA pump; equilibrium is maintained by Ca^{2+} extrusion via Na+/Ca^{2+} exchangers and the ATP-dependent PMCA pump.

Reproduced with permission from (Ma & Beaven, 2011)

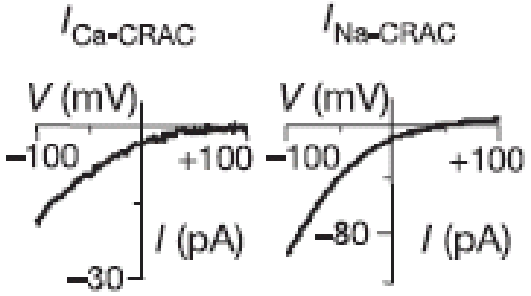

Figure 1.8. Biophysical properties of I_{CRAC} currents

Current-voltage relationships of I_{CRAC} currents activated by BAPTA-mediated passive store depletion in the presence of extracellular Ca^{2+} (left) or Na^+ (right). I_{CRAC} currents are Ca^{2+}-selective and inwardly-rectifying, with a positive reversal potential. In the absence of Ca^{2+}, I_{CRAC} channels are permeable for Na^+, causing amplification of the current.

Reproduced with permission from (Feske *et al.*, 2006)

In a separate siRNA screen, Liou *et al*. (2005) identified STIM1 and STIM2 as important proteins for SOCE in HeLa cells. Using fluorescently tagged STIM1, the authors showed that following store depletion, STIM1 redistributes into punctae at the plasma membrane (Liou *et al.*, 2005). Recombinant expression studies revealed that the Ca^{2+}-sensing EF-hand domain and the sterile α-motif (SAM) domain (EF-SAM domain) are responsible for initiating STIM1 puncta formation upon store depletion (Stathopulos *et al.*, 2006).

The molecular identity of the CRAC channel was revealed in 2006; genome screening and mutagenesis studies showed that Orai1, also called CRACM1, is the channel mediating I_{CRAC} (Feske *et al.*, 2006; Prakriya *et al.*, 2006; Vig *et al.*, 2006b). Feske *et al.* (2006) reported that a missense mutation in Orai1 is linked to severe combined immunodeficiency (SCID), where it is responsible for defective SOCE in T cells. Orai1 channels have four transmembrane regions with intracellular N- and C-termini; conserved glutamate residues form the pore and confer Ca^{2+} selectivity (Prakriya *et al.*, 2006). STIM1 and Orai1 were shown to functionally interact by co-over-expression studies in HEK-293 and Jurkat T cells (Peinelt *et al.*, 2006); whilst over-expression of either protein alone did not significantly amplify I_{CRAC}, over-expression of STIM1 and Orai1 greatly potentiated the current. It is now known that a highly conserved SOAR (STIM1 Orai-activating region) domain in STIM1 activates Orai1 channels (Yuan *et al.*, 2009), and no other interactions are required for channel opening (Lee *et al.*, 2010). The importance of STIM1 and Orai1 in mast cell function was highlighted using mice lacking the proteins; foetal liver-derived mast cells from STIM1-deficient mice were shown to have reduced IgE-activated Ca^{2+} entry, degranulation and activation of the transcription factors NFκB and NFAT, leading to impaired cytokine production (Baba *et al.*, 2008). Mast cells from Orai1-deficient mice were shown to exhibit reduced degranulation and cytokine production (Vig *et al.*, 2008). Investigating the contribution of STIM1 and Orai1 to SOCE in human mast cells remains to be investigated, but it can be hypothesised from studies using rodents that they are essential for human mast cell function.

Orai1 channels are highly selective for Ca^{2+} over other ions, giving rise to the Ca^{2+} selectivity of I_{CRAC}. Previous studies recording I_{CRAC} currents in RBL cells and Jurkat T cells showed that that equimolar replacement of Ca^{2+} ions with Ba^{2+} in the extracellular recording solution leads to a reduction, but not complete inhibition, of the I_{CRAC} current (Hoth, 1995; Zweifach & Lewis, 1995). However, these results were obtained in solutions where both Na^+ and Ba^{2+} were present; a recent study showed that replacement of Ca^{2+} with Ba^{2+} ions when Na^+ ions were replaced with tetraethyl ammonium (TEA) caused abolition of I_{CRAC} currents mediated by Orai1, 2 and 3 in HEK-293 cells (Lis *et al.*, 2007). The authors re-examined Ba^{2+} permeation of I_{CRAC} in Jurkat T cells in the presence and absence of Na^+, reporting that currents are inhibited in the absence of Na^+. It was concluded that I_{CRAC} currents are abolished when Ba^{2+} is the sole charge carrier, and that Na^+ ions carry the current observed in the absence of Ca^{2+} previously thought to be

mediated by Ba^{2+}(Lis *et al.*, 2007). Orai1-mediated I_{CRAC} currents are therefore highly Ca^{2+} selective, a property that can be used to distinguish them from other store-operated currents.

1.3.1.2 Methods to study I_{CRAC}

Physiologically, Ca^{2+} store release is evoked by $InsP_3$ binding to its receptor in the ER. Experimental methods for store depletion include dialysis of the cytosol with $InsP_3$ or a high concentration of Ca^{2+} chelators such as EGTA or BAPTA to prevent store refilling. Sarcoplasmic/endoplasmic reticulum Ca^{2+} ATPase (SERCA) inhibitors such as thapsigargin or cyclopiazonic acid (CPA) can also be used to prevent Ca^{2+} store refilling, causing passive store depletion (Parekh & Putney, 2005). Ca^{2+} imaging is commonly used to monitor SOCE following thapsigargin-evoked store depletion; currents are directly monitored using the patch-clamp technique, which allows direct application of Ca^{2+} chelators and $InsP_3$ into the cytosol (Parekh & Putney, 2005).

As Orai1 channels have very low conductance (Hogan *et al.*, 2010), they are very difficult to detect under standard recording conditions. Ca^{2+} ions are frequently replaced with Na^+ ions when recording I_{CRAC} currents to increase the conductance and facilitate identification (Lepple-Wienhues & Cahalan, 1996; Mercer *et al.*, 2006; Prakriya *et al.*, 2006; Scrimgeour *et al.*, 2009).

Commonly-used non-selective inhibitors of I_{CRAC} include the lanthanides La^{3+} and Gd^{3+} at low (~1) μM concentrations (Broad *et al.*, 1999; DeHaven *et al.*, 2009) and 2-aminoethoxydiphenylborate (2-APB) (Prakriya & Lewis, 2001). A selective small-molecule inhibitor of Orai1 channels, synta 66 (GSK1349571A, 3-fluoropyridine-4-carboxylic acid (2',5'-dimethoxybiphenyl-4-yl)amide), has recently been characterised. Synta compounds were developed by Synta pharmaceuticals from Astellas compounds (based on 5-pyrazol-5yl-2-thiophene-carboxamide), which are moderately potent SOCE inhibitors; the pyrazole ring of Astellas compounds was replaced with a phenyl ring in synta compounds (Sweeney *et al.*, 2009). Synta 66 was developed through small modifications of synta compounds ; it blocks I_{CRAC} currents in RBL cells with reported IC_{50} values of 3μM (Ng *et al.*, 2008) and 1.4μM (Di Sabatino *et al.*, 2009). The selectivity of synta 66 for I_{CRAC} inhibition was confirmed using a panel of radioligand binding assays, where its effects on other ion channels, receptors and enzymes were compared with known inhibitors of the targets. Little or no significant activity was observed against the targets tested, including GABA, muscarinic receptors, P2X receptors, K^+ channels, Cl^- channels and Na^+ channels, when synta 66 was used at a concentration causing maximal inhibition of I_{CRAC} (10μM) (Di Sabatino *et al.*, 2009). In vascular smooth muscle cells synta 66 has been shown to inhibit thapsigargin-evoked I_{CRAC}, whilst TRPC-mediated currents stimulated by thapsigargin were unaffected (Li *et al.*, 2011). The resistance of TRPC1-TRPC5 heteromeric channels to synta 66 was confirmed in HEK-293 cells; Ca^{2+} entry evoked by 100μM Gd^{3+} in HEK-TRPC1-TRPC5 cells was unaffected by the compound (Li *et al.*, 2011). Synta 66 can therefore be used as a selective I_{CRAC} inhibitor to determine the contribution of Orai1 channels to SOCE.

1.3.2 TRP channels

1.3.2.1 Overview, background and discovery

Transient receptor potential (TRP) channels are a superfamily of structurally-related channels, the majority of which are nonselective cation channels that are permeable to Ca^{2+}. The founding member of the superfamily was discovered in *Drosophila* photoreceptors, where a transient rather than a sustained current in response to light (transient receptor potential) was observed in flies carrying a *trp* mutation (Montell *et al.*, 1985; Hardie & Minke, 1992). The mutation gave rise to impaired Ca^{2+} entry, indicating that the TRP protein forms a Ca^{2+} influx channel in *Drosophila* photoreceptors (Hardie & Minke, 1992). Based on similarity to *Drosophila* TRP protein sequences, 28 mammalian TRP channels have since been cloned, which can be divided into six subfamilies on the basis of amino acid homology; see figure 1.9. These are TRPC (canonical), TRPV (vanilloid), TRPM (melastatin), TRPP (polycystin), TRPA (ankyrin) and TRPML (mucolipin) (Nilius *et al.*, 2007). The crystal structures of the TRP channels are not yet available (Flockerzi, 2007), but based on their amino acid analogy to other channels and the location of glycosylation sites, they are predicted to have six transmembrane domains (S1–S6). The N and C termini are thought to be located intracellularly, with the pore-forming loop located between S5 and S6; figure 1.10 illustrates the predicted topology of TRP channels. Cytosolic N-termini of TRP channels contain a variable number of protein-protein interaction motifs called ankyrin motifs; protein-protein interactions is the C termini differ between the various channels and include Ca^{2+}-calmodulin binding sites, $InsP_3$ interaction sites and PKC interaction sites (Birnbaumer, 2009). All TRP channels are permeable to Ca^{2+} except TRPM4 and TRPM5; these channels are only permeable to monovalent cations. Most Ca^{2+}-permeable TRP channels are poorly selective for Ca^{2+}, permeating other monovalent and divalent cations; TRPV5 and TRPV6, however, are highly selective for Ca^{2+}, with a permeability ratio relative to Na^+ of >100 (Nilius *et al.*, 2007). The following sections will discuss the different subfamilies of TRP channels, and will consider the role of TRPC channels in SOCE.

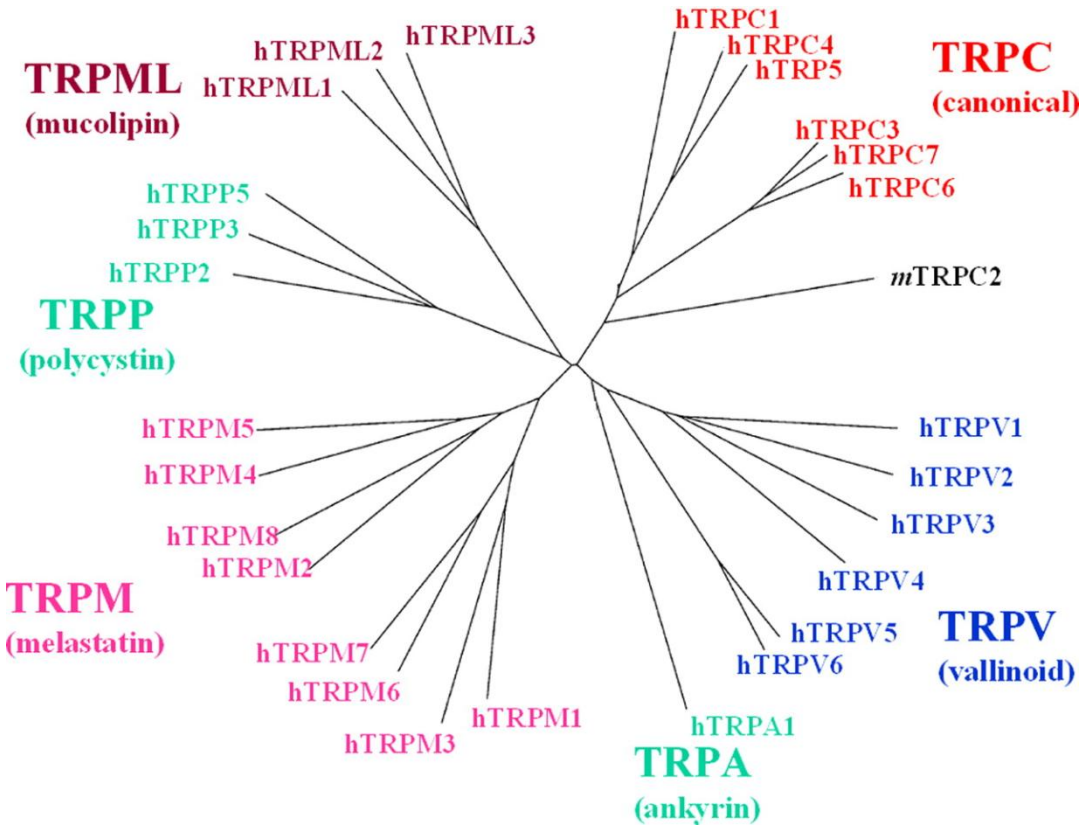

Figure 1.9. Phylogenetic tree of the TRP channels

The TRP superfamily is comprised of canonical (TRPC), vanilloid (TRPV), melastatin (TRPM), polycystin (TRPP), ankyrin (TRPA) and mucolipin (TRPML) channels.

Reproduced with permission from (Nilius *et al.*, 2007)

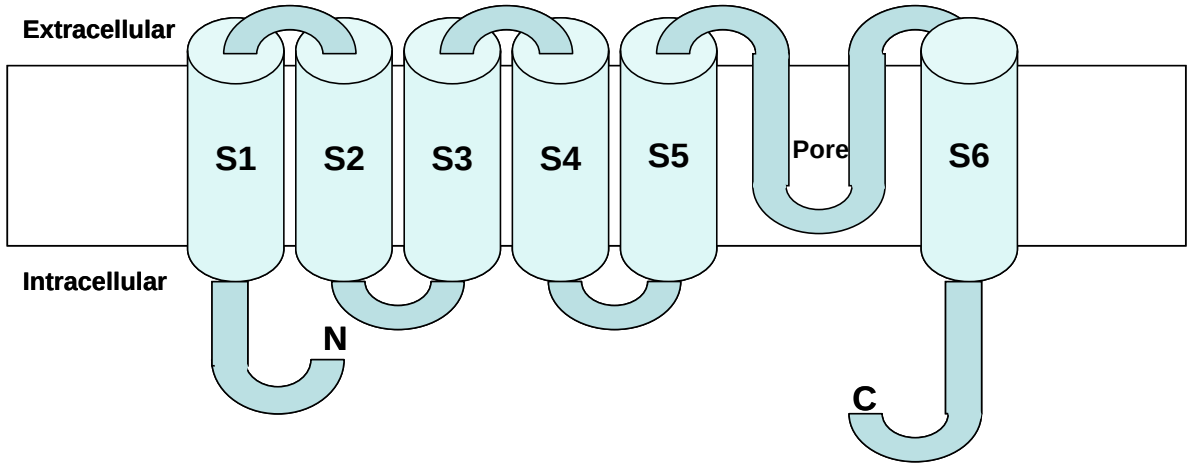

Figure 1.10. Predicted structure and membrane topology of TRP channels.

Based on sequence homology and glycosylation sites, TRP channels are predicted to have six transmembrane segments (S1–S6), with the pore located between S5 and S6.

Adapted from (Clapham *et al.*, 2001)

1.3.2.2 TRPV channels

TRPV1 was the first of the TRP-related channels to be discovered; it was identified in a cDNA screening assay to isolate the protein responsible for capsaicin sensitivity in neuronal cells (Caterina *et al.*, 1997). TRPV1 is a non-selective Ca^{2+} channel activated by vanilloids (such as capsaicin), heat and pH (Birnbaumer, 2009). There are six TRPV subfamily members; TRPV2, 3 and 4 were identified by their structural relationship to TRPV1 and are all activated by heat. TRPV1–3 can be activated by 2-APB, the commonly-used TRP channel and I_{CRAC} inhibitor (Colton & Zhu, 2007), and TRPV4 is sensitive to changes in osmolarity (Plant & Strotmann, 2007). TRPV5 and TRPV6, the only Ca^{2+}-selective channels in the TRP superfamily, are regulated by Ca^{2+} and hormones such as vitamin D_3 (Mensenkamp *et al.*, 2007; Wissenbach & Niemeyer, 2007).

TRPV channels are involved in the pathophysiology of some diseases; TRPV1 has been implicated in pain associated with conditions including inflammatory bowel disease, ulcerative colitis, osteoarthritis and pancreatitis (Yiangou *et al.*, 2001; Fernihough *et al.*, 2005; Nilius *et al.*, 2007). TRPV2 expression is up-regulated in muscle tissue from patients with Duchenne muscular dystrophy (Iwata *et al.*, 2003), and is thought to be involved in increased Ca^{2+} influx associated with the condition (Nilius *et al.*, 2007). The expression of TRPV6 is increased in prostate cancer tissue and is a putative target of oestrogen-based therapies for the disease (Zhuang *et al.*, 2002). Due to their Ca^{2+} selectivity, TRPV5 and TRPV6 are thought to play a role in Ca^{2+} homeostasis; Ca^{2+}-related disorders such as vitamin D-deficiency rickets type 1 and postmenopausal osteoporosis are also hypothesised to involve these channels (van Abel *et al.*, 2005).

TRPV2 mRNA has been detected in HLMCs by microarray analysis; more recent Western blot analyses of bone marrow-derived mast cells, RBL-2H3 cells and LAD 2 cells revealed protein expression for TRPV1, TRPV2 and TRPV6 (Turner *et al.*, 2007). Their role in mast cell function has not yet been determined, but TRPV channels are hypothesised to mediate Ca^{2+} entry in response to diverse stimuli including changes in the physical environment (Turner *et al.*, 2007).

1.3.2.3 TRPM channels

The first TRPM channel to be identified was melastatin (now called TRPM1), a protein that is down-regulated in melanoma cells (Duncan *et al.*, 1998). There are 8 TRPM channels; a feature of this subfamily is that three members have enzyme domains in the C terminus, conferring special properties. TRPM2 has an ADP-ribose phosphatase-related NUDIX domain that confers responsiveness to ADP-ribose (Eisfeld & Luckhoff, 2007); TRPM6 and TRPM7 contain a C-terminal atypical α-kinase domain, which permits protein-protein interactions in the assembly of signalling complexes (Birnbaumer, 2009). TRPM channels have variable permeability to divalent ions, ranging from Ca^{2+} impermeable (TRPM4 and TRPM5) (Vennekens & Nilius, 2007) to highly Ca^{2+} and Mg^{2+} permeable (TRPM6 and TRPM7) (Penner & Fleig, 2007). TRPM2 is activated by ADP ribose, H_2O_2 and heat (Eisfeld & Luckhoff, 2007); TRPM4 and TRPM5 are also heat-sensitive

channels (Birnbaumer, 2009). In contrast, TRPM8 is a cold-activated channel that is sensitive to cooling agents such as menthol (Voets *et al.*, 2007). TRPM6 and TRPM7 are regulated by intracellular Mg^{2+}; a study carried out in our laboratory showed that TRPM7 channels are expressed in human mast cells and are essential for their survival (Wykes *et al.*, 2007). TRPM channels have been implicated in a range of disorders, including malignant melanoma (TRPM1), taste dysfunction (TRPM5) and immune hyper-responsiveness (TRPM4).

1.3.2.4 TRPA channels

There is currently one mammalian TRPA family member, TRPA1, which is expressed in dorsal root ganglion (DRG) and trigeminal ganglion (TG) neurons (Garcia-Anoveros & Nagata, 2007). TRPA1 has a distinctive long N-terminal region, with 18 predicted ankyrin repeats. It is activated by pungent compounds, including isothiocyanates, which are found in mustard, wasabi and horseradish. Other activators include cinnamaldehyde, found in cinnamon, and allicin, produced from freshly crushed garlic (Garcia-Anoveros & Nagata, 2007). TRPA1 is thus considered a sensor of environmental irritants.

1.3.2.5 TRPP channels

Mutations in *PKD1* and *PKD2*, the genes encoding TRPP1 and TRPP2, are associated with autosomal-dominant polycystic kidney disease (Witzgall, 2007). TRPP1 and TRPP2 are thought to interact, with TRPP1 recruiting TRPP2 to the plasma membrane (Nilius *et al.*, 2007). There is limited knowledge about the activation mechanisms of TRPP channels; TRPP2 is activated by mechanical stress and Ca^{2+}, and TRPP3 is thought to form a complex with PKD2L3 to form a sour taste receptor (Nilius *et al.*, 2007).

1.3.2.6 TRPML channels

The TRPML subfamily consists of three mammalian members, TRPML1–3. TRPML1 is thought to be involved in the nuclear localisation of endosomes as it contains a nuclear localisation sequence. Mutations in the gene encoding TRPML1 (*MCONL1*) cause mucolipidosis type IV, a neurodegenerative lysosomal storage disorder (Nilius *et al.*, 2007). Relatively little is known about TRPML2 and TRPML3.

The TRP superfamily therefore represents a heterogeneous group of cation-permeable ion channels that are sensitive to a range of environmental stimuli and involved in the pathophysiology of various diseases. Channels from the TRPC subfamily, the focus of this thesis, are the most closely related to *Drosophila* TRP channels, and have a variety of physiological roles. The rest of this chapter will focus on TRPC channels, discussing their properties, functions and involvement in SOCE.

1.3.2.7 TRPC channels

The seven TRPC channels share a TRP box structure near the C-terminus, containing the conserved amino acid sequence EWKFAR (Nilius *et al.*, 2007). Like other TRP channels, the putative pore region of TRPC channels is located between S5 and S6; evidence for the importance of this conserved pore region was obtained from site-directed mutagenesis studies (Hofmann *et al.*, 2002). The exact location of the pore helix and selectivity filter, however, has not yet been elucidated for TRPC channels (Dietrich *et al.*, 2005b). TRPC channels are believed to function as tetrameric channel assemblies (Nilius *et al.*, 2007).

The TRPC channels are all non-selective, Ca^{2+}-permeable cation channels that are activated downstream of PLC. On the basis of structural homology and functional similarities they can be divided into two subgroups: TRPC1/4/5 and TRPC3/6/7. TRPC2 is a pseudogene in humans so will not be discussed further (Yildirim & Birnbaumer, 2007). TRPC3/6/7 channels are activated by DAG, whereas TRPC1/4/5 channels are insensitive to DAG and thought to be sensitive to store depletion (Clapham *et al.*, 2001). The following sections will discuss the properties of homomeric TRPC channels, along with their potential roles, activation mechanisms and heteromultimerisation potential.

1.3.2.8 The DAG-regulated TRPC channels: TRPC3, 6 and 7

TRPC3, 6 and 7 channels are a structurally- and functionally-related subfamily, sharing 70–80% amino acid homology and sensitivity to DAG (Hofmann *et al.*, 1999; Okada *et al.*, 1999).

1.3.2.8.1 TRPC3

Human (h) TRPC3 was the second member of the TRPC subfamily to be cloned using HEK-293 cell cDNA and a TRP channel-specific probe, R34716 (Zhu *et al.*, 1996). Human and mouse TRPC3 cDNA share 96.41% sequence homology, and both contain an additional exon to give rise to an alternative splice variant with an extended N-terminus (Yildirim *et al.*, 2005). As with other TRPC channels, there is limited information available on the pore region and selectivity filter of TRPC3; based on analogy to voltage-gated K^+ channels (K_v) and site-directed mutagenesis experiments with the related TRPC1 channel (Liu *et al.*, 2003), the pore is believed to be between S5 and S6 (Eder *et al.*, 2007). In support of this theory, expression of dominant-negative TRPC6 (with mutations in the putative pore region) in HEK-293 cells expressing TRPC3 suppressed TRPC3 channel activity (Hofmann *et al.*, 2002). The current-voltage (I/V) relationship of TRPC channel currents can be used to identify the channels present; when expressed in HEK-293 cells, TRPC3 forms a non-selective cation channel, showing both inward (negative voltages) and outward (positive voltages) current. The current is described as outwardly-rectifying, as the current at positive voltages is greater than that at negative voltages. A reversal potential (the voltage at which there is no net current flow) of 0mV is indicative of a non-selective ion channel. Shown in figure 1.11 is the current-voltage relationship of homomeric TRPC3 channels, along with the closely-related TRPC6 and 7 channels.

TRPC3 channels show considerable basal activity, which is thought to be linked to the glycosylation status of the channel (Dietrich *et al.*, 2003). Activity is enhanced in response to stimulation of PLC-linked receptors with ligands including carbachol, histamine and ADP (Eder *et al.*, 2007). In addition to direct activation by DAG produced by PLC, illustrated by application of the membrane-permeable analogue 1-Oleoyl-2-acetyl-*sn*-glycerol (OAG) to Chinese hamster ovary (CHO)-K1 cells expressing hTRPC3 (Hofmann *et al.*, 1999), regulation by store depletion downstream of PLC activation has also been suggested (Zhu *et al.*, 1996). Evidence for activation by store depletion remains limited, however, and will be discussed in section 1.3.2.11.

TRPC3 has been proposed to form a macromolecular signalling complex through interactions with other components of the Gq-coupled PLC signalling pathway including Gq proteins, PLCβ, $InsP_3$ receptors and caveolin-1, a marker of lipid raft domains in the plasma membrane (Lockwich *et al.*, 2001). Disruption of the actin cytoskeleton has been shown to reduce TRPC3 surface expression and attenuate TRPC3-mediated Sr^{2+} entry, suggesting that the cytoskeleton is responsible for TRPC3 surface expression (Lockwich *et al.*, 2001). Putative structural motifs in TRPC3 that mediate interactions with other signalling molecules and structural proteins include ankyrin repeats that interact with PLC and caveolin, a combined interaction domain in the C-terminus called CaM-$InsP_3$ receptor binding site (CIRB) and a PKC interaction domain (Eder *et al.*, 2007). It remains to be determined whether the targeting of TRPC3 to precise membrane microdomains is essential for gating by DAG, or whether interactions of the channel with caveolin are only involved in membrane trafficking (Eder *et al.*, 2007).

PKC has been implicated in the down-regulation of TRPC3 channels; it has been shown that DAG activation of TRPC3 channels expressed in the DT40 chicken B-cell line is prevented when cells were pre-treated with phorbol 12-myristate 13-acetate (PMA) to activate PKC (Venkatachalam *et al.*, 2003). Channel de-activation was retarded in the presence of a PKC inhibitor, suggesting that DAG induces biomodal regulation of TRPC3 channels, causing rapid activation followed by a slower, PKC-mediated deactivation phase (Venkatachalam *et al.*, 2003; Eder *et al.*, 2007).

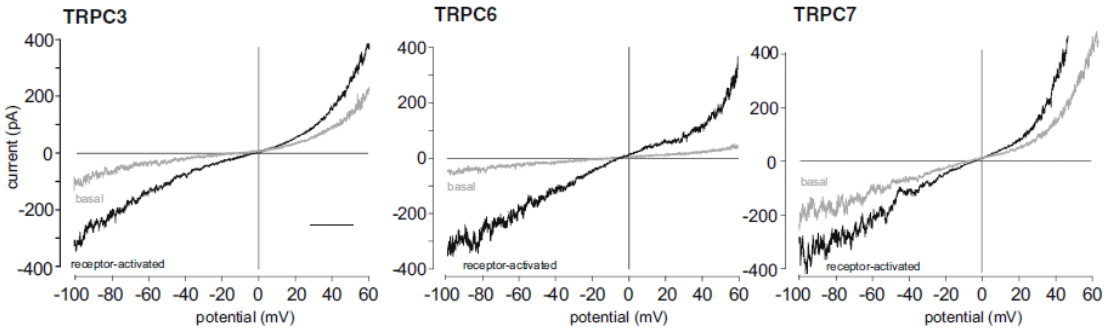

Figure 1.11. Current-voltage (I/V) relationships of TRPC3, 6 and 7 channels

Channels were expressed in HEK293 cells and activated downstream of receptor stimulation. TRPC3 and TRPC7 have high basal activity compared with TRPC6 (see grey traces). Note that voltage is displayed to -100mV in the negative direction and only +60mV in the positive direction; all channels are outwardly-rectifying with a reversal potential close to 0mV.

Reproduced with permission from (Dietrich *et al.*, 2005b)

TRPC3 is predominantly expressed in the specific regions of the brain (cerebellum, cortex and hippocampus), in the heart, and is present at high levels in embryonic tissues. It is therefore thought to have a role in development of neuronal and cardiac tissue (Eder *et al.*, 2007). TRPC3 knock-out mice showed defects in walking behaviour, indicating a critical role of TRPC3 in motor co-ordination (Hartmann *et al.*, 2008). Transgenic mice where TRPC3 is over-expressed specifically in the heart showed cardiomyopathy, which was inhibited by disruption of the calcineurin gene, and cardiac myocytes isolated from these mice displayed enhanced angiotensin II-evoked Ca^{2+} entry (Nakayama *et al.*, 2006). The role of TRPC3 channels in immune cells has not been extensively investigated, but has been suggested to be involved in T cell Ca^{2+} entry downstream of T cell receptor stimulation and PLCγ activation (Philipp *et al.*, 2003).The authors showed that the TRPC3 gene was defective in human T cell mutants with impaired Ca^{2+} entry; expression of wild-type TRPC3 in these mutants rescued Ca^{2+} currents. The role of TRPC3 channels in mast cell Ca^{2+} entry has not been investigated.

1.3.2.8.2 TRPC6

TRPC6 cDNA was first cloned from mouse brain in 1997, where it was shown to mediate La^{3+}- and SKF-96365- sensitive calcium entry in response to GPCR stimulation when expressed in COS cells (Boulay *et al.*, 1997). Human TRPC6 (hTRPC6) was isolated in 1999; expression in CHO-K1 cells resulted in calcium entry and outwardly-rectifying currents downstream of H1 histamine receptor activation, as well as direct activation by OAG and SAG, another DAG analogue (Hofmann *et al.*, 1999). hTRPC6 protein consists of 931 amino acids and is 93% homologous to mouse TRPC6 (mTRPC6) (Hofmann *et al.*, 1999). Three splice variants of hTRPC6 have been reported in airway smooth muscle cells; in addition to the full length hTRPC6 cloned by Hofmann

et al, Δ316-431 has a deletion in transmembrane region S1 and Δ377-431 has a shorter deletion in the same region (Corteling *et al.*, 2004).

Like TRPC3, TRPC6 is a Ca^{2+}-permeable non-selective cation channel; the I/V relationship of TRPC6 expressed in HEK-293 cells displays inward and outward current with outward rectification and a reversal potential close to 0mV (see figure 1.11). In HEK cells over-expressing TRPC6 channels (HEK-TRPC6 cells) it has been suggested that Ca^{2+} only forms a small percentage of whole-cell currents in the presence of Na^{+}; this was shown to be dependent on the membrane potential, with large increases in intracellular Ca^{2+} occurring at negative membrane potentials (between -50 and -80mV), and a greater contribution from Na^{+} ions when the potential was uncontrolled (Estacion *et al.*, 2006). These results suggest that the contribution of TRPC6 channels to Ca^{2+} entry is cell-type specific and dependent upon the membrane potential, which is determined by the complement of ion channels present (Estacion *et al.*, 2006; Dietrich & Gudermann, 2007).

Unlike TRPC3 and the closely related TRPC7, TRPC6 channels are not constitutively active. It is thought that post-translational protein modifications are responsible for the lack of basal activity; TRPC6 is glycosylated at two extracellular sites (loops 1 and 2), whereas TRPC3 is glycosylated on the first extracellular loop only (Dietrich *et al.*, 2003). When TRPC6 glycosylation mutants were expressed in HEK-293 cells, greater basal activity was observed, providing further evidence for the involvement of glycosylation status in basal activity (Dietrich *et al.*, 2003). The direct activation of hTRPC6 channels by DAG has been demonstrated by the application of OAG, SAG, DOG and the DAG lipase inhibitor RHC80267 to CHO-K1 cells expressing TRPC6 (Hofmann *et al.*, 1999). Activation is known to be independent of PKC, as current onset was shown to be unaffected by a PKC inhibitory peptide in HEK-TRPC6 cells (Shi *et al.*, 2004). Physiologically, TRPC6 currents are activated by DAG produced downstream of PLC-linked receptors; carbachol and histamine have been used to activate the channels in heterologous expression systems (Boulay *et al.*, 1997; Hofmann *et al.*, 1999; Inoue *et al.*, 2001; Venkatachalam *et al.*, 2003; Cayouette *et al.*, 2004; Estacion *et al.*, 2004; Shi *et al.*, 2004; Estacion *et al.*, 2006; Bousquet *et al.*, 2010). It has been suggested that a regulated exocytosis pathway is involved in the activation of TRPC6; co-immunoprecipitation studies showed that the surface expression of TRPC6 (indicated by degree of co-immunoprecipitation with caveolin-1) was enhanced following Gq-coupled receptor stimulation in HEK-TRPC6 cells (Cayouette *et al.*, 2004). In native cells, Gq-coupled receptor activation by platelet-activating factor has been shown to activate TRPC6-like currents in primary human lung macrophages (Finney-Hayward *et al.*, 2010), arginine-vasopresin (AVP) activated the channel in A7r5 smooth muscle cells (Jung *et al.*, 2002), and ADP activation of $P2Y_1$ GqPCRs has been reported to stimulate TRPC6-like currents in primary mouse megakaryocytes (Carter *et al.*, 2006).

TRPC6 channels undergo complex regulation by Ca^{2+}, along with protein serine and tyrosine phosphorylation (Dietrich & Gudermann, 2007). Both activation and inactivation of carbachol- and OAG- induced TRPC6 currents in HEK-TRPC6 cells were accelerated in the presence of extracellular Ca^{2+} compared with its absence (Shi *et al.*, 2004). Pre-treatment of these cells with a calmodulin (CaM) antagonist attenuated TRPC6 activation by carbachol or OAG; current density was also reduced by CaM kinase II inhibition and when ATP was not present in the patch pipette. These results suggest that phosphorlyation by CaM kinase II is required for TRPC6 activation (Shi *et al.*, 2004). PKC contributes to TRPC6 inactivation by the phosphorylation of a key serine residue on the channel; PMA inhibited carbachol- and OAG- evoked hTRPC6 currents in HEK-293 cells (Estacion *et al.*, 2004), and a PKC inhibitory peptide increased the time-course of inactivation (Shi *et al.*, 2004). Recent mutagenesis studies of mTRPC6 revealed that serine 488 is the target for PKC phosphorylation, which mediates TRPC6 inactivation (Bousquet *et al.*, 2010). Whilst PKC-mediated phosphorylation causes TRPC6 inactivation, Fyn, a Src family protein tyrosine kinase, has been shown to increase TRPC6 channel activity (Dietrich & Gudermann, 2007). Immunoprecipitation experiments in COS-7 cells expressing TRPC6 showed that epidermal growth factor (EGF) receptor stimulation gives rise to tyrosine phosphorylation of TRPC6, and that Fyn and TRPC6 physically interact (Hisatsune *et al.*, 2004). The addition of Fyn kinase to OAG-stimulated cells also enhanced TRPC6 currents (Hisatsune *et al.*, 2004). A recent study showed that FcεRI- but not thapsigargin-evoked Ca^{2+} entry was impaired in Fyn-deficient mouse bone marrow-derived mast cells (see figure 1.12). This Ca^{2+} entry was sensitive to Gd^{3+}, a commonly-used inhibitor of TRPC channels. Immunoprecipitation experiments confirmed that Fyn kinase and TRPC6 interact in mast cells; the authors concluded that TRPC6 channels are likely to contribute to receptor-operated Ca^{2+} entry downstream of FcεRI, and that Fyn kinase contributes to their activation (Sanchez-Miranda *et al.*, 2010).

There is growing evidence to suggest that TRPC6 has an important role in a number of physiological processes (Dietrich & Gudermann, 2007). TRPC6 is abundantly expressed in smooth muscle cells (SMCs), and has been shown using biophysical characterisation and gene suppression to be the α_1-adrenoceptor-activated cation channel in vascular SMCs (Inoue *et al.*, 2001). TRPC6 is also thought to be responsible for vasopressin-evoked Ca^{2+} currents in an aortic SMC line, A7r5 (Jung *et al.*, 2002). Whilst these results suggest that TRPC6 channels could be important for cardiovascular function, TRPC6-deficient mice have increased artery contractility (Dietrich *et al.*, 2005c). These conflicting results are likely to be due to compensatory up-regulation of constitutively active TRPC3 channels in the absence of TRPC6, giving rise to increased SMC contractility (Dietrich *et al.*, 2005a). Gain-of-function mutations in TRPC6 are associated with the kidney disease focal segmental glomerulosclerosis (FSGS), which is characterised by proteinuria and progressive loss of kidney function (Reiser *et al.*, 2005; Winn *et al.*, 2006). It is thought that the mutations are associated with disrupted podocyte function, where TRPC6 is normally organised into a signalling complex with nephrin and podocin (Dietrich & Gudermann, 2007).

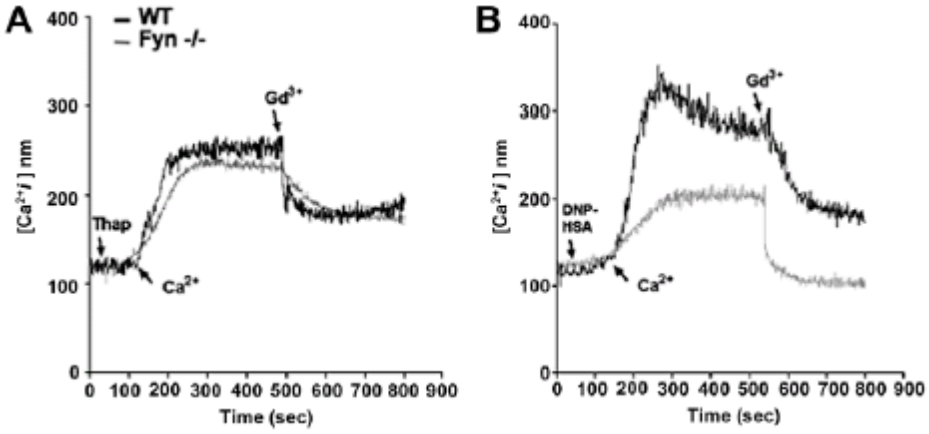

Figure 1.12. Ca^{2+} entry evoked by FcεRI, but not thapsigargin, is impaired in mast cells from Fyn-deficient mice.

A: Thapsigargin (thap)-evoked Ca^{2+} entry was of similar amplitude in bone marrow-derived mast cells from wild-type (black trace) and Fyn-deficient (grey trace) mice.

B: DNP-HSA was used to cross-link IgE anti-NP bound to FcεRI; Ca^{2+} entry was significantly reduced in mast cells from Fyn-deficient mice (grey trace) compared with wild-type mice (black trace). Ca^{2+} entry was sensitive to Gd^{3+} (100μM), a commonly-used inhibitor of TRPC channels.

Reproduced with permission from (Sanchez-Miranda *et al.*, 2010)

There are also emerging roles for TRPC6 channels in immune cells; in addition to their possible role in FcεRI-dependent Ca^{2+} entry in mast cells (discussed above), immunohistochemistry experiments revealed TRPC6 expression in human lung neutrophils (Li *et al.*, 2005). TRPC6 mRNA has also been detected in macrophages isolated from the alveolar space and lung tissues of patients with chronic obstructive pulmonary disease (COPD) and smokers (Li *et al.*, 2005), and recent electrophysiological studies confirmed the functional expression of TRPC6 channels in human lung macrophages (Finney-Hayward *et al.*, 2010). Of the TRPC channels, TRPC6 in particular is highly expressed in the lung compared with other organs (Li *et al.*, 2005). Together these data suggest that TRPC6 channels could contribute to lung inflammation in COPD. TRPC6 has also been implicated in the migration of immune cells; bone marrow-derived neutrophil granulocytes isolated from TRPC6-deficient mice showed impaired migration and Ca^{2+} entry in response to Gq-coupled chemokine receptors (Damann *et al.*, 2009), suggesting the importance of TRPC6 for neutrophil chemotaxis.

1.3.2.8.3 TRPC7

TRPC7 was the last TRPC channel to be discovered; it was cloned from mouse brain using a TRPC2 cDNA probe to identify homologous sequences (Okada *et al.*, 1999). Sequence comparison with TRPC1–6 cDNA revealed a novel TRPC homologue, which was designated mTRPC7 (Okada *et al.*, 1999). hTRPC7 was isolated from human brain in 2002 as part of a screening programme to identify novel ion channels (Riccio *et al.*, 2002); it shares 98% sequence

homology with mTRPC7 (Numaga *et al.*, 2007). Two splice variants of mTRPC7 have been reported, both with exon deletions (Okada *et al.*, 1999).

TRPC7 is a non-selective Ca^{2+}-permeable cation channel like its relatives TRPC3 and TRPC6; the I/V relationship for homomeric TRPC7 is almost linear with some flattening around the reversal potential (see figure 1.11). Ion substitution experiments suggested that TRPC7 has permeability ratio of Cs:Na:Ca^{2+}:Ba^{2+} of 1:1.1:5.9:5.0 (Okada *et al.*, 1999). Like TRPC3, TRPC7 has high constitutive activity (see grey trace in figure 1.11), and activity is enhanced by DAG independently of PKC (Okada *et al.*, 1999). Physiologically it is thought to be activated by DAG produced downstream of PLC-coupled receptor stimulation; GPCR stimulation by carbachol (Riccio *et al.*, 2002; Shi *et al.*, 2004) and ATP (Okada *et al.*, 1999) has been shown to activate the channel in heterologous expression systems.

In contrast to the complex regulation of TRPC6 channels by Ca^{2+}, mTRPC7 is only inhibited by elevated concentrations of Ca^{2+}; increasing extracellular Ca^{2+} to 1mM reduced the current density of carbachol-activated currents in HEK-TRPC7 cells, and vigorous buffering of intracellular Ca^{2+} accelerated activation by carbachol (Shi *et al.*, 2004). Negative regulation of TRPC7 channels by Ca^{2+} was inhibited by the CaM antagonist calmidazolium, indicating that Ca^{2+}-CaM negatively regulates the channel (Shi *et al.*, 2004). Like TRPC3 and TRPC6 channels, TRPC7 is negatively regulated by PKC; pre-treatment with PMA inhibited OAG-induced Mn^{2+}influx in HEK-mTRPC6 cells (Okada *et al.*, 1999), and TRPC7 current inactivation was delayed by a PKC inhibitory peptide (Shi *et al.*, 2004). Shown in figure 1.13 are experimental results obtained by Shi *et al.* (2004) illustrating the negative regulation of carbachol-activated TRPC6 and TRPC7 channels expressed in HEK-293 cells.

Relatively few physiological roles have been identified for TRPC7, compared with TRPC3 and TRPC6 (Dietrich *et al.*, 2005b). It is expressed in the heart, lung and eye at high levels, with lower expression in the brain, spleen and testis (Okada *et al.*, 1999). Due to its constitutive activity and expression patterns, it has been suggested that TRPC7 is involved in background currents such as pacemaking activity of sinoatrial node cells, and in the regulation of resting membrane potential in SMCs (Dietrich & Gudermann, 2007).

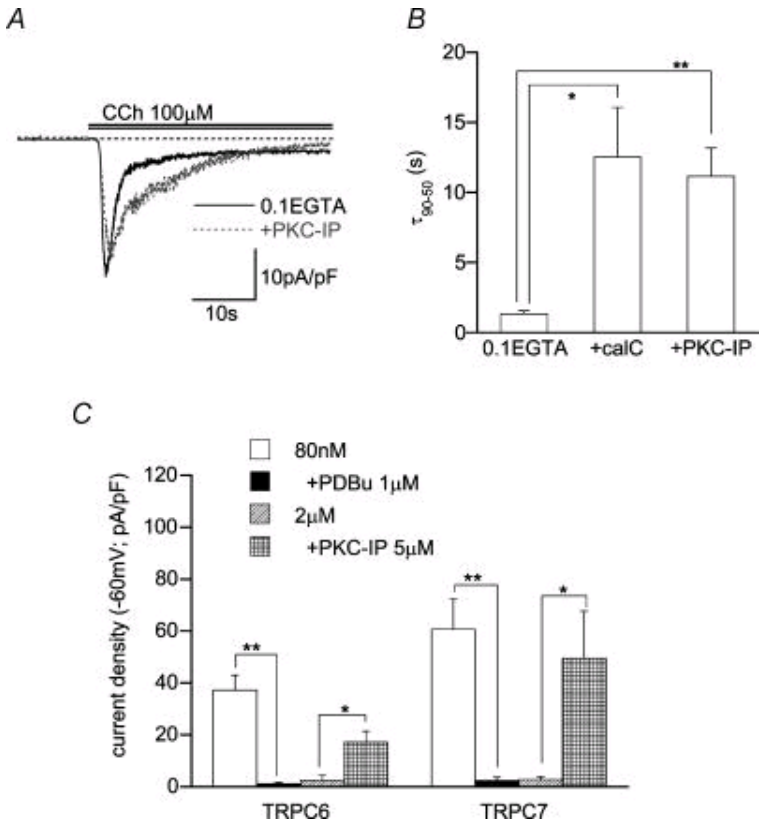

Figure 1.13. PKC mediates inactivation of TRPC6 and TRPC7 channels

A: Carbachol-evoked currents in HEK-TRPC6 cells in the presence (grey) or absence (black, "0.1 EGTA") of a PKC inhibitory peptide.

B: Bar graph comparing the effects of PKC inhibitors on the time-course of inactivation of TRPC6. Time-course was significantly increased following pre-incubation with calphostin C (calC) or when PKC inhibitory peptide was applied intracellularly (PKC-IP), compared with control (0.1 EGTA internal solution).

C: Bar graph comparing TRPC6 (left) and TRPC7 (right) current density at two different concentrations of intracellular Ca^{2+} (80nM, white, and 2μM, grey). Elevated concentrations of intracellular Ca^{2+} significantly caused a reduction in current density. The presence of the PKC activator PDBu significantly reduced both TRPC6 and TRPC7 current density, and it was increased by PKC inhibitory peptide. Together these results show that PKC, and intracellular Ca^{2+}, negatively regulate TRPC6 and TRPC7 channels.

Reproduced with permission from (Shi *et al.*, 2004)

1.3.2.8.4 Pharmacology of the DAG-regulated TRPC channels

As discussed above, the membrane-permeable DAG analogue OAG is frequently used to study the direct activation of TRPC3/6/7 channels, and they can be activated by the stimulation of Gq-coupled receptors with ligands including carbachol, histamine and ADP.

There are no selective pharmacological inhibitors of TRPC3/6/7 channels, but non-selective inhibitors including lanthanides, 2-APB, flufenamate and SKF-96365 have been used extensively to characterise the channels. 2-APB has been shown to inhibit metacholine-induced Ca^{2+} entry in HEK-TRPC3 cells in a concentration-dependent manner, with maximal (but not complete)

inhibition occurring at 30μM. This concentration of 2-APB also caused partial inhibition (~50%) of OAG- and receptor- activated Ba^{2+} entry in HEK cells expressing TRPC6 or TRPC7 channels (Lievremont *et al.*, 2005). It is not known why 2-APB only induces partial block of TRPC3/6/7 channels whilst completely inhibiting SOCE at the same concentrations; inhibition is thought to occur by different mechanisms for the two channel types (Lievremont *et al.*, 2005). The partial block suggests that 2-APB inhibits TRPC3/6/7 channels allosterically and not simply by pore occlusion.

SKF-96365 was initially characterised as an inhibitor of receptor-operated Ca^{2+} entry, attenuating ADP-evoked Ca^{2+} entry in platelets with an IC_{50} of 8.5μM (Merritt *et al.*, 1990). SKF-96365 has been shown to inhibit heterologously expressed TRPC6 channels with an IC_{50} of 4.2μM (Inoue *et al.*, 2001), and receptor- activated TRPC6 currents in rabbit portal vein smooth muscle with an IC_{50} of 5.1μM (Inoue *et al.*, 2001). More recently, 10μM SKF-96365 has been reported to abolish OAG-induced TRPC6 currents in human epithelial breast cancer cells (Guilbert *et al.*, 2008), and 100μM SKF-96365 inhibited receptor-operated TRPC6 currents in human lung macrophages (Finney-Hayward *et al.*, 2010). An IC_{50} of 8μM was reported for the inhibition of TRPC3 channels expressed in CHO cells (Halaszovich *et al.*, 2000). The mechanism by which SKF-96365 inhibits TRPC channels is largely unknown, but it is known not to compete with Ca^{2+} (Merritt *et al.*, 1990).

Lanthanides ($La^{3+}$and Gd^{3+}) are commonly used to inhibit TRPC channels. Gd^{3+} has been shown to block heterologously expressed TRPC3 and TRPC6 channels with IC_{50} values of 2.5μM and 2.3μM, respectively (Inoue *et al.*, 2001; Dietrich *et al.*, 2005b), and 100μM Gd^{3+} has been reported to completely inhibit receptor-operated Sr^{2+} entry in A7r5 smooth muscle cells (Broad *et al.*, 1999). The sensitivity of TRPC3 channels to blockade by lanthanides has been extensively analysed in different systems and found to be highly variable. 250μM La^{3+} was required to inhibit Ca^{2+} entry through TRPC3 channels in COS-M6 cells by 40% (Zhu *et al.*, 1996), but 150μM caused complete inhibition of TRPC3 channels expressed in HEK cells (Zhu *et al.*, 1998). 200μM Gd^{3+} has been reported to abolish TRPC3 currents in HEK cells (Zhu *et al.*, 1998), but in Chinese Hamster Ovary (CHO) cells, Gd^{3+} inhibited TRPC3 currents with an IC_{50} of 0.1μM; complete inhibition was achieved by 10μM (Halaszovich *et al.*, 2000). It has been suggested based on inside-out patch-clamp experiments that lanthanides act on TRPC channels from the intracellular side of the membrane, and that the concentration required to block the channel is dependent upon cell type-specific lanthanide uptake rates (Halaszovich *et al.*, 2000). These observations highlight the importance of establishing an appropriate concentration of Gd^{3+} for TRPC channel inhibition in a particular cell type. Experiments in DT40 chicken lymphocytes showed that the addition of Gd^{3+} causes rapid inhibition of fully-developed hTRPC3-mediated Ca^{2+} entry, suggesting that the lanthanide directly blocks the channel (Trebak *et al.*, 2002).

The non-steroidal anti-inflammatory agent flufenamic acid (FFA) is a non-selective cation channel

blocker (Tu *et al.*, 2009a) with complex effects on the TRPC subfamily. Whilst FFA inhibits TRPC3- and TRPC7-mediated currents when the channels are expressed in HEK-293 cells and activated by carbachol (Inoue *et al.*, 2001), it has been shown to potentiate mTRPC6 channel activity at 100-500μM in these cells (Inoue *et al.*, 2001). Potentiation of agonist-activated currents by FFA, along with current properties, has been used as a diagnostic tool for TRPC6 currents in a number of systems, including A7r5 smooth muscle cells (Jung *et al.*, 2002), primary megakaryocytes (Carter *et al.*, 2006) and cortical neurons (Tu *et al.*, 2009b). It has recently been shown in human podocytes that 200μM FFA stimulates 2-APB and SKF-96365- sensitive Ca^{2+} entry, which is abolished by dominant negative TRPC6 expression; the authors concluded that FFA is a tool to selectively activate TRPC6 channels and study them in native cells (Foster *et al.*, 2009).

1.3.2.9 DAG-independent TRPC channels: TRPC1, 4 and 5

TRPC1, 4 and 5 form a structurally-related subfamily of channels. Like TRPC3/6/7 channels they are activated downstream of PLC, but their activation is independent of DAG and less well-defined than that for the TRPC3/6/7 subgroup. There is growing evidence to suggest that channels from the TRPC1/4/5 subgroup are activated by store depletion; this will be discussed in section 1.3.2.11. Described in this section are the properties of TRPC1, 4 and 5 channels, along with the genes and discovery.

1.3.2.9.1 TRPC1

TRPC1 was the first member of the mammalian TRP family to be discovered; it was identified in a screen of the Genbank database for homologues of *Drosophila* TRP channels and cloned from foetal human brain cDNA (Zhu *et al.*, 1995). The TRPC1 protein was later expressed in CHO-K1 cells and gave rise to non-selective currents activated by store depletion (Zitt *et al.*, 1996). There are two splice variants of hTRPC1, TRPC1 and TRPC1A (Zitt *et al.*, 1996); whilst four splice variants exist in mouse, two of these are highly truncated and thought to be non-functional (Sakura & Ashcroft, 1997; Rychkov & Barritt, 2007). In the TRPC1 N-terminal region, three ankyrin repeats have been identified, along with a binding site for caveolin-1. Calmodulin and $InsP_3$ receptor binding sites at the C-terminal region have also been found (Rychkov & Barritt, 2007). A number of studies employing immunofluorescence techniques have investigated the intracellular localisation of TRPC1. The channels have been shown, in heterologous expression systems and in native cells, to be present at both the plasma membrane, where they co-localise with cholesterol-rich lipid rafts (Lockwich *et al.*, 2001), and at intracellular sites including the ER and Golgi membranes. (Wang *et al.*, 1999; Xu & Beech, 2001; Uehara, 2005).

Of the TRPC channels, the structure and pore region have been most extensively investigated for TRPC1. The membrane topology has been investigated using truncation mutants of TRPC1 channels expressed in HEK-293 cells. Whilst TRPC1 contains 8 hydrophobic regions (HRs) that could potentially span the membrane, only 6 form membrane-spanning subunits. HR 3 is thought to sit outside the membrane on the cytosolic side, whereas HR7 is suggested to reside in the membrane but not span it (Dohke *et al.*, 2004). Figure 1.14 indicates the predicted membrane topology of TRPC1. Neutralisation of negatively charged residues in the TM5-TM6 region of TRPC1 gave rise to reduced Ca^{2+} currents when the mutants were expressed in HEK-293 cells (Liu *et al.*, 2003). Taken together with the more extensive studies into voltage-gated K^+ and Ca^{2+} channels, which are used as models for the structure and topology of TRP channels (Rychkov & Barritt, 2007), the results obtained by Liu *et al.* (2003) suggest that negatively charged residues located close to the TM5-TM6 pore regulate ion flow thorough TRPC1 channels.

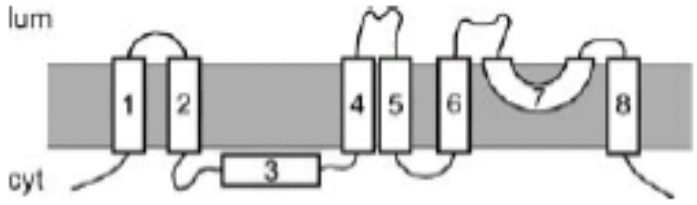

Figure 1.14. Predicted membrane topology of TRPC1 channels

Whilst TRPC1 is predicted to have 8 hydrophobic segments, only 6 are thought to span the membrane. Figure reproduced from (Dohke *et al.*, 2004); copyright permission not required from the *Journal of Biological Chemistry*.

In the initial characterisation of TRPC1, it was found to produce a linear, non-selective cation channel with a reversal potential close to 0mV and an estimated single channel conductance of 16 picosiemens when expressed in CHO-K1 cells (Zitt *et al.*, 1996). Currents with similar properties were recorded in Sf9 insect cells transfected with TRPC1 (Sinkins *et al.*, 1998). The activation of TRPC1 by Ca^{2+} store depletion is discussed below in section 1.3.2.11. In addition to this mode of activation, TRPC1 channels have been suggested as components of a store depletion-independent channel activated by mechanical stretch, called mechanosensitive cation channel (MscCa), in *Xenopus laevis* oocytes (Maroto *et al.*, 2005).

TRPC1-mediated Ca^{2+} entry has been suggested to have an important physiological role in replenishing depleted intracellular Ca^{2+} stores (Rychkov & Barritt, 2007). As they are also permeable to Na^{+}, TRPC1 channels have also been proposed to have a role in Na^{+} entry in excitable cells, leading to membrane depolarisation and the activation of transporters and exchangers (Eder *et al.*, 2005). In contrast to some TRPC channels, TRPC1 is widely expressed in many animal tissues, including brain, heart, lung, smooth muscle, salivary gland and liver (Wu *et al.*, 2010); this extensive expression suggests that the channel may serve a range of functions in different cell types. TRPC1-deficient mice have been reported to show increased weight (Dietrich *et al.*, 2007) and impaired salivary gland secretion (Liu *et al.*, 2007) due to defects in SOCE. In line with this observation, TRPC1-deficient human salivary gland (HSG) cells exhibit impaired Ca^{2+} entry (Cheng *et al.*, 2011), providing further evidence for the involvement of TRPC1 channels in salivary gland function. Ca^{2+} entry through TRPC1 is also thought to have a role in the regulation of nerve growth cone movement downstream of netrin-1 receptor activation and store depletion (Wang & Poo, 2005).

The function of TRPC1 channels in immune cells has not been extensively characterised, but TRPC1 mRNA has been detected in human skin mast cells (Bradding *et al.*, 2003), B lymphoblasts (Roedding *et al.*, 2006) and the human T-cell line HPB-ALL (Rao & Kaminski, 2006). A recent study in mouse bone marrow-derived mast cells showed that siRNA knock-down of TRPC1 channels caused defects in Ca^{2+} influx and degranulation downstream of FcεRI cross-

linking (Suzuki *et al.*, 2010). Given its expression in the lung, it is reasonable to hypothesise that TRPC1 channels could also be expressed in HLMCs and have a role in the essential Ca^{2+} entry required for mediator release.

1.3.2.9.2 TRPC4

TRPC4 cDNA was initially cloned from bovine adrenal gland as a store-operated, Ca^{2+} and Ba^{2+}-permeable cation channel (Philipp *et al.*, 1996); the human homologue was cloned from a kidney cDNA library (McKay *et al.*, 2000). Like the other TRPC channels, TRPC4 contains N-terminal ankyrin repeats, the TRP box and a CaM binding site (Cavalie, 2007). Uniquely to TRPC4 and TRPC5, however, it contains a PDZ-binding site (Tang *et al.*, 2001). PDZ domains are protein-protein interaction sites involved in the organisation of signalling complexes. The PDZ binding domain is known to be important for the assembly of TRPC4 channels in signalling complexes at the plasma membrane; TRPC4 mutants lacking the PDZ binding domain have reduced surface expression (Mery *et al.*, 2002).

Homomeric TRPC4 and TRPC5 channels have a unique s-shaped current-voltage relationship (shown in figure 1.15), which is often described as "doubly-rectifying", and a reversal potential close to 0mV. The factors contributing to the unique I/V relationship have been studied in more depth for TRPC5 (section 1.3.2.9.3) than TRPC4 so will be discussed below. In most studies investigating homomeric TRPC4 channels they have been activated downstream of GPCRs using carbachol as a ligand (Philipp *et al.*, 1996; Schaefer *et al.*, 2000; Plant & Schaefer, 2003). Like the related TRPC1 and TRPC5 channels, they are thought to be activated by store depletion; this is discussed below in section 1.3.2.11.

TRPC4-deficient mice exhibit reduced Ca^{2+} entry in aortic endothelial cells and acetylcholine-induced vasorelaxation of aortic rings, suggesting that TRPC4 channels have a role in vascular function (Freichel *et al.*, 2001). Ca^{2+} entry in lung vascular endothelial cells in response to thrombin stimulation was also reduced in these mice. TRPC4-deficient mice have also been used to reveal a role for the channel in the brain; 5-hydroxytryptamine (5-HT)-coupled Ca^{2+} entry leading to GABA release in thalamic relay neurons was shown to be defective (Munsch *et al.*, 2003). Studies in chromaffin and PC12 cells have shown that TRPC4-mediated Ca^{2+} entry can trigger a secretory response (Obukhov & Nowycky, 2002); TRPC4 has also been suggested to have a role in the depolarisation of neurons and smooth muscle cells (Cavalie, 2007). TRPC4 is thus likely to have a number of physiological roles in excitable cells; there are no reports of its expression or functional roles in cells of the immune system.

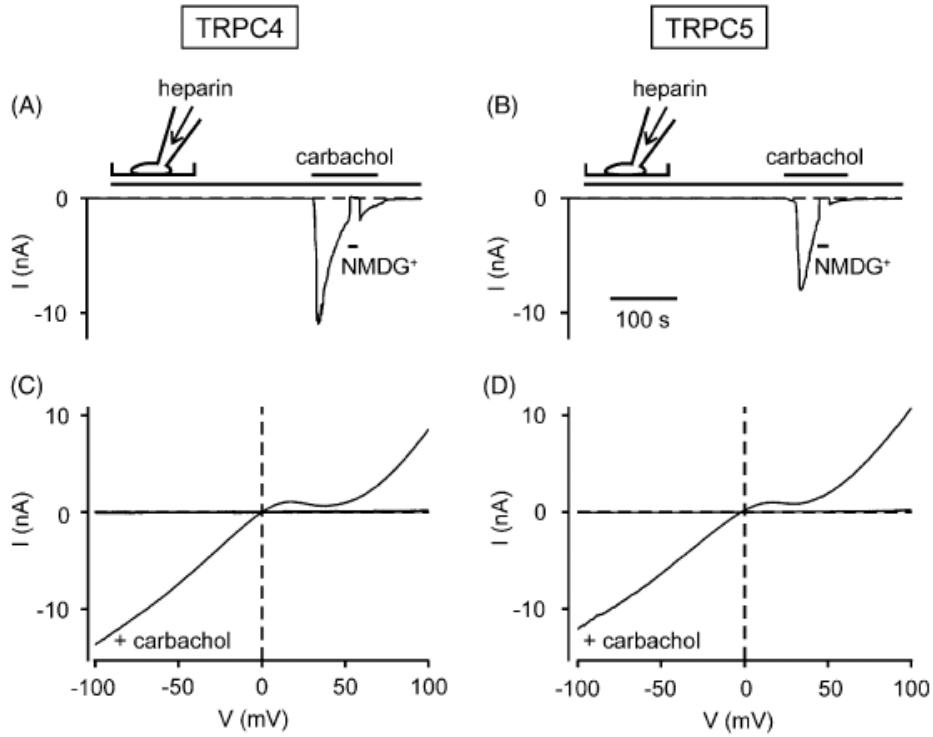

Figure 1.15. TRPC4 and TRPC5 currents activated by carbachol

Carbachol was applied to HEK293 cells expressing mTRPC4 (A,C) or mTRPC5 (B,D). A and B show the time-course of current activation; I/V relationships are shown in C and D. Note the characteristic s-shaped I/V relationship of these channels.

Reproduced with permission from (Plant & Schaefer, 2003)

1.3.2.9.3 TRPC5

TRPC5 was initially cloned from mouse brain (Okada *et al.*, 1998); human TRPC5 (hTRPC5) was cloned as part of a screen of the X chromosome for genes involved in non-syndromic mental retardation (Sossey-Alaoui *et al.*, 1999). Like the other TRP channels, TRPC5 is believed to have six membrane-spanning regions with intracellular N- and C-termini. Similarly to TRPC4, homomeric TRPC5 channels in heterologous expression systems have a characteristic s-shaped, doubly-rectifying I/V relationship, which is shown in figure 1.15. The unique I/V relationship of TRPC5 is thought to be due in part to its voltage-dependence; whilst the channel is not voltage-gated, it can be modulated by voltage once switched on by another mechanism (Beech, 2007). Hyperpolarisation has been suggested to enhance opening of the channel, giving rise to the inwardly-rectifying component (Beech, 2007). TRPC5 has an estimated single channel conductance of 41 picosiemens (Jung *et al.*, 2003) and is permeable to Ca^{2+}, Ba^{2+}, Mn^{2+} and Sr^{2+}, as well as monovalent cations including Na^{+} (Okada *et al.*, 1999; Schaefer *et al.*, 2000; Venkatachalam *et al.*, 2003; Beech, 2007). As described for TRPC1, amino acids between TM5 and TM6 are likely to form the selectivity filter for TRPC5; mutation of the leucine-phenylalanine-tryptophan sequence to alanine-alanine-alanine gives rise to a dominant negative TRPC5 mutant with damaged ion flux (Strubing *et al.*, 2003).

TRPC5 is known to be activated by a multiplicity of signals. In addition to activation by store depletion, which is described in section 1.3.2.11, store-independent receptor activation is known to take place. Carbachol-evoked Ca^{2+} entry in HEK-293 cells expressing TRPC5 (HEK-TRPC5 cells) was reduced, but not inhibited by thapsigargin pre-treatment (Zeng *et al.*, 2004), indicating that the channel is involved in both store-dependent and –independent Ca^{2+} entry downstream of receptor activation. Receptor activation of TRPC5 has been described following carbachol application to CHO-K1 cells expressing mTRPC5 (Schaefer *et al.*, 2000), prostaglandin E2 stimulation of *Xenopus laevis* oocytes (Tabata *et al.*, 2002), and B cell receptor cross-linking in DT40 B cells (Venkatachalam *et al.*, 2003). DAG is not involved in the activation of TRPC5 channels following receptor stimulation; application of OAG or elevation of DAG concentration by a DAG lipase inhibitor inhibited the activation of TRPC5. This inhibition was relieved in the presence of a PKC inhibitor, indicating that the inhibitory action of DAG on TRPC5 occurs via PKC (Venkatachalam *et al.*, 2003). This is in contrast to the stimulatory action of DAG on TRPC3/6/7 channels, which is PKC-independent (Hofmann *et al.*, 1999).

Another mechanism of action for TRPC5 channels is external ionic activation. Whilst lanthanides such as Gd^{3+} potentiate mTRPC5 and inhibit TRPC1, 3, 6 and 7, hTRPC5 is activated by Gd^{3+} in the absence of any other stimuli (Zeng *et al.*, 2004). This striking feature of hTRPC5 was demonstrated using HEK-TRPC5 cells; it was shown that 100μM Gd^{3+} gave rise to Ca^{2+} entry and whole-cell currents that were not inhibited by GDP-β-S, indicating the lack of involvement of G proteins (Zeng *et al.*, 2004). The stimulatory effect of lanthanides on TRPC5 channels was investigated in more detail in HEK-mTRPC5 cells, where it was shown that at concentrations greater than 1μM, Gd^{3+} and La^{3+} potentiated TRPC5 currents in a concentration-dependent manner. Inhibition of the currents occurred at millimolar concentrations of lanthanide. Shown in figure 1.16 are the effects of lanthanides on TRPC5 channels, compared with TRPC6 channels. Neutralisation of negatively charged amino acids (glutamic acid 543, 595 and 598) situated extracellularly and close to the putative pore-forming loop of TRPC5 gave rise to a loss of La^{3+} potentiation (Jung *et al.*, 2003), indicating that these residues are responsible for the stimulatory effects of lanthanides. Identical amino acids are present at corresponding sties in TRPC4, which is also potentiated by lanthanides, but not in TRPC3/6/7 (Jung *et al.*, 2003). Activation by lanthanides thus provides a way to selectively study TRPC4 and TRPC5 channels whilst inhibiting the other TRPCs.

5–10mM extracellular Ca^{2+} has also been reported to stimulate hTRPC5 channels expressed in HEK-293 cells. The steep concentration-response curve and rapid desensitisation resembled the response to Gd^{3+} (Zeng *et al.*, 2004), and the authors suggested that both ions act at a common extracellular site to mediate external ionic activation of TRPC5 channels.

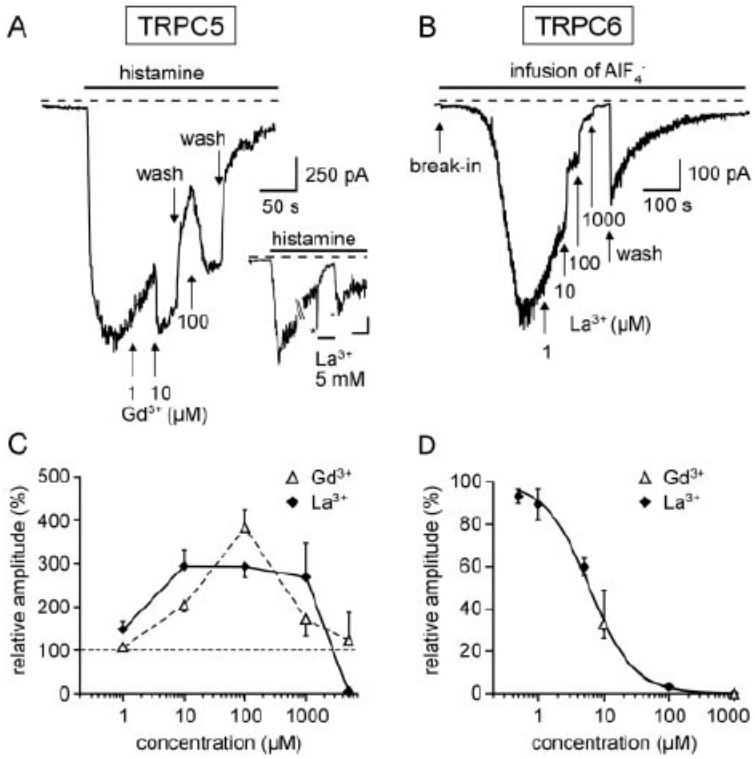

Figure 1.16. The effects of lanthanides of mTRPC5 and mTRPC6 channels expressed in HEK293 cells

A: Dual effects of lanthanides on histamine-activated TRPC5 currents; graph shows whole-cell currents recorded at -60mV. μM concentrations of Gd^{3+} caused potentiation. 5mM La^{3+} (inset) inhibited TRPC5 currents. B: Inhibition of receptor-operated TRPC6 currents by increasing concentrations of La^{3+}. C: Concentration-dependent effects of lanthanides on TRPC5 channels. D: Concentration-dependent effects of lanthanides on TRPC6 channels.

Reproduced from (Jung *et al.*, 2003); copyright permission not required from the *Journal of Biological Chemistry*.

Sphingosine-1-phosphate has been identified as an activator of TRPC5 channels in a screen of potential lipid regulators using HEK-TRPC5 cells (Xu *et al.*, 2006b). It was reported to give rise to Ca^{2+} entry in TRPC5-expressing, but not non-expressing, cells in a concentration-dependent manner. S1P was also shown to activate TRPC1-TRPC5 heteromeric assemblies expressed in HEK cells, but not TRPC1 channels alone (Xu *et al.*, 2006b). When applied to human saphenous vein SMCs, S1P gave rise to Ca^{2+} entry that had two phases, both of which were sensitive to the inhibitory TRPC5 antibody T5E3. The mechanisms of action of S1P on TRPC5 channels were further investigated in HEK-TRPC5 cells; treatment with pertussis toxin or the PLC inhibitor U73122 inhibited S1P-evoked Ca^{2+} entry, indicating the respective involvement of Gi/o-coupled receptors and PLC. A recent study suggested that group 6 phospholipase A2 (PLA_2) enzymes, which release the fatty acids lysophosphatidylcholine (LPC) and arachidonic acid (AA) from glycerol, are involved in the activation of TRPC5 by extracellular S1P (Al-Shawaf *et al.*, 2011). An intracellular mechanism of action of S1P has also been suggested; it was reported to elicit single-

channel events in inside-out patch clamp experiments of HEK-TRPC5 cells (Xu *et al.*, 2006b). As S1P can be transported across the membrane or accumulate intracellularly following activation of S1P receptors (Saba & Hla, 2004), it was concluded that TRPC5 can be activated by S1P by two different mechanisms; TRPC5 can act as an ionotropic receptor for intracellular S1P, or become activated downstream of PLC production following S1P receptor stimulation (Xu *et al.*, 2006b). S1P is a complex signalling molecule, regulating many physiological processes through binding its receptors ($S1P_{1-5}$) and by intracellular mechanisms (Strub *et al.*, 2010). In mast cells $S1P_1$ is important for chemotaxis and $S1P_2$ contributes to degranulation (Jolly *et al.*, 2004). This highlights the potential importance of TRPC5 in mediating inflammatory cell activation. Interestingly, S1P has been found at increased levels in the airways of asthmatic patients compared with non-asthmatics (Ammit *et al.*, 2001); S1P in the lung may therefore represent an important mechanism for mast cell activation in asthma.

Reduced thioredoxin has also been shown to activate TRPC5 channels expressed in HEK-293 cells, along with TRPC5-like currents in fibroblast-like synovial cells taken from patients with rheumatoid arthritis (Xu *et al.*, 2008). TRPC5 is thus activated by a range of different agonists, indicating that it is a versatile sensor with the potential to mediate Ca^{2+} entry in response to different stimuli.

Despite extensive research into the activation and properties of heterologously expressed TRPC5 channels, its physiological roles have not been thoroughly characterised. TRPC5-deficient mice have no obvious defects, although they have been reported to show less anxiety-like behaviour (Riccio *et al.*, 2009). TRPC5 has been implicated in the regulation of neuronal growth cone extension; expression of dominant negative TRPC5 in hippocampal neurones led to enhanced growth cone extension (Greka *et al.*, 2003). A TRPC5-like current activated by muscarinic receptor stimulation has been reported in stomach SMCs, suggesting that the channel could be involved in acetylcholine-induced SMC depolarisation (Lee *et al.*, 2003b). S1P-evoked SMC motility was inhibited by an inhibitory TRPC5 antibody, the non-selective TRPC5 inhibitor 2-APB and dominant negative TRPC5, suggesting that S1P sensing by TRPC5 causes SMC motility. The physiological role of TRPC5 channels has not been extensively characterised in the immune system, but one study (discussed below in section 1.3.2.11) showed that TRPC5 could contribute to FcεRI-evoked degranulation in RBL-2H3 cells (Ma *et al.*, 2008).

1.3.2.9.4 Pharmacology of TRPC1/4/5 channels

As with TRPC3/6/7 channels, there are no selective inhibitors of TRPC1, 4 and 5. The lanthanide Gd^{3+}, whilst activating TRPC4 and 5 in the micromolar range, has been used extensively to inhibit TRPC1 channels (Rychkov & Barritt, 2007); 10μM Gd^{3+} inhibits TRPC1 channels expressed in CHO-K1 cells (Zitt *et al.*, 1996). Lanthanides at millimolar concentrations can be used to inhibit TRPC4 and TRPC5 channels; 5mM La^{3+} and Gd^{3+} were shown to inhibit histamine-activated TRPC5 channels expressed in HEK-293 cells (Jung *et al.*, 2003). 100μM 2-APB has been shown to

inhibit TRPC1 channels expressed in HEK-293 cells (Zagranichnaya *et al.*, 2005). TRPC5 is inhibited by 2-APB with an IC_{50} of 20μM in HEK-TRPC5 cells (Xu *et al.*, 2005a). Outside-out patch clamp recordings revealed that 2-APB inhibits TRPC5 channels from the extracellular side of the membrane, and mild voltage-dependence of inhibition occurred, indicating that 2-APB may interfere with channel gating (Xu *et al.*, 2005a). The non-selective TRPC channel blocker SKF-96365 has been shown to inhibit receptor-activated TRPC5 and store-operated TRPC1 expressed in HEK-293 cells (Okada *et al.*, 1998; Zagranichnaya *et al.*, 2005). FFA has been shown to inhibit TRPC5-like currents in mouse SMCs at a concentration of 100μM (Lee *et al.*, 2003b). The lack of selective pharmacological inhibitors of TRPC channels means that they are very difficult to study in native cells. However, when used in combination with electrophysiological studies to analyse the properties of currents stimulated with known activators of the channels, pharmacological inhibitors can provide useful information on the channels present. Inhibition of a TRPC-like current by 10μM Gd^{3+}, for example, would indicate that TRPC4 and TRPC5 channels are not involved.

1.3.2.10 Heteromultimerisation potential of TRPC channels

A number of experimental approaches were employed by Hofmann *et al.* (2002) to determine the heteromultimerisation potential of TRPC channels. Cellular co-trafficking experiments revealed that wild-type TRPC3 and TRPC6 could traffick a targeting-deficient TRPC6 mutant to the cell membrane, and that TRPC4 could target a defective TRPC1. A dominant-negative TRPC6 mutant was shown to suppress TRPC3 and TRPC6 currents, but not those mediated by TRPC4 or TRPC5. Fluorescence resonance energy transfer (FRET) experiments showed that TRPC channels can can assemble into homo- or hetero-tetramers within the confines of the TRPC1/4/5 and TRPC3/6/7 subfamilies; immunoprecipitation experiments of c-myc tagged TRPC subunits confirmed these observations (Hofmann *et al.*, 2002). Co-immunoprecipitation studies in rat brain synaptosomes were in accordance with these results, showing that interactions can occur within, but not between, TRPC channel subgroups. More recently, novel interactions between TRPC1 plus TRPC4 or TRPC5 with TRPC6 have been reported in the rat embryonic brain but not in adult brain (Strubing *et al.*, 2003). This suggests that novel TRPC channel complexes between the two subgroups may play a role in neuronal development. Novel interactions between the subgroups have also been suggested based on co-immunopreciptation studies of TRPC subunits expressed in HEK-293 cells; TRPC3 was precipitated with TRPC1 in the presence of STIM1, and TRPC6 with TRPC4 (Yuan *et al.*, 2007).

In some cases, the I/V relationship can be analysed to assess whether a homomeric or heteromeric TRPC current is present in native cell types. For example, whilst homomeric TRPC5 channels have a characteristic s-shaped I/V relationship, TRPC5-TRPC1 heteromeric assemblies expressed in HEK-293 cells give rise to a more outwardly-rectifying relationship, without inflection near 0mV (Xu *et al.*, 2006b).

To summarise, a large body of experimental evidence supports the heteromeric assembly of TRPC channels within subgroups. There is, however, emerging evidence to suggest that novel assemblies across subgroups may occur, which could extend the functional diversity of TRPC channels.

1.3.2.11 TRPC channels and store-operated Ca^{2+} entry

TRPC channels were originally proposed to be the molecular determinants of I_{CRAC} when they were identified as PLC-activated channels in *Drosophila* photoreceptors (Hardie & Minke, 1992). Electrophysiological evidence later revealed that TRPC channels do not possess the same biophysical properties as I_{CRAC} and have larger conductance than Orai1 channels (Parekh & Putney, 2005; Ma & Beaven, 2011); TRPC channels also lack the Ca^{2+} selectivity of I_{CRAC}, conducting other divalent ions such as Ba^{2+} and Sr^{2+} (Ma *et al.*, 2008). As SOCE channels are thought to encompass a family of channels with distinct properties (Parekh & Putney, 2005), it has been proposed that TRPC channels form another type of SOCE channel, distinct from I_{CRAC} and sometimes referred to as I_{SOC} (Parekh & Putney, 2005; Cheng *et al.*, 2011).

A number of reports have suggested that TRPC channels, especially from the TRPC1/4/5 subgroup, are regulated by STIM1; in the first studies it was shown that STIM1 co-immunoprecipitates with TRPC1, 4 and 5 but not with TRPC3, 6 and 7 in HEK-293 cells (Huang *et al.*, 2006). The same study revealed that STIM1 gates TRPC1 via the STIM1 cytoplasmic ERM domain; this was extended to other TRPC channels to show that TRPC1, 3, 4, 5 and 6 are gated by STIM1 (Yuan *et al.*, 2007). This study showed that STIM1 regulates TRPC1, 4 and 5 by direct interaction, and indirectly regulates TRPC3 and 6 by mediating their interaction with TRPC1 and 4, respectively. The authors proposed that SOCE channels are those that are regulated by STIM1 and require store depletion-dependent STIM1 clustering; all TRPCs except TRPC7 function as SOCE channels by this definition (Yuan *et al.*, 2007). In contrast, one study reported that TRPC channel activity is not affected by STIM1 knock-down, and co-expression of STIM1 does not enhance the activity of TRPC channels transiently expressed in HEK-293 cells (DeHaven *et al.*, 2009). However, there is a large body of evidence from a number of different laboratories supporting the regulation of TRPC channels by STIM1. In addition to the data discussed above, TRPC1 and STIM1 were shown to co-immunoprecipitate in mouse pancreatic acinar cells; store depletion with thapsigargin enhanced their interaction (Hong *et al.*, 2011). Similar results were obtained using co-immunoprecipitation in mouse pulmonary artery smooth muscle cells and human saphenous vein smooth muscle cells (Li *et al.*, 2008; Ng *et al.*, 2009), indicating the association of STIM1 and TRPC1 in native cells. Mutagenesis studies revealed that the gating of TRPC1, but not Orai1, involves electrostatic interactions between two negatively charged aspartate residues in the TRP box region of TRPC1 (residues 639 and 640) and two positively charged lysine residues (684 and 685) in the STIM1 ERM domain (Zeng *et al.*, 2008). Mutation of these positively charged residues to negatively charged glutamic acid residues ($^{684}EE^{685}$) produces a STIM1 mutant that lacks the ability to gate TRPC1; expression of STIM1$^{684}EE^{685}$ in

human salivary gland (HSG) cells suppressed thapsigargin-evoked SOCE (Cheng *et al.*, 2011). As the TRP box is conserved across the TRPC channels, it has been suggested that electrostatic interactions also mediate contacts between STIM1 and other TRPC channels (Lee *et al.*, 2010).

As suggested by Yuan *et al*. (2007), regulation by STIM1 can be used to define TRPC channels as SOCE channels. A number of other approaches have also been taken to demonstrate the involvement of TRPC channels, especially TRPC1, in SOCE in a number of different cell types. TRPC1 was first implicated as a SOCE channel based on heterologous expression studies in Chinese hamster ovary (CHO) cells; TRPC1 expression enhanced Ca^{2+} entry following store depletion and gave rise to $InsP_3$- and thapsigargin-induced non-selective currents in whole-cell patch clamp studies (Zitt *et al.*, 1996). The role of native TRPC1 channels in SOCE has been extensively investigated in salivary gland cells, where RNA knock-down of TRPC1 has been shown to attenuate SOCE in mouse and human (Liu *et al.*, 2007; Ong *et al.*, 2007). Over-expression of TRPC1 increased SOCE, and the expression of TRPC1 with a mutated putative pore region (TRPC1 Δ567-793) reduced thapsigargin- and carbachol-evoked SOCE in human salivary gland (HSG) cells (Liu *et al.*, 2003; Ong *et al.*, 2007). Suppression of TRPC1 currents by shRNA or the expression of a STIM1 mutant lacking TRPC1 gating was reported to reveal store-operated I_{CRAC} currents, which are masked by the larger TRPC1 currents in HSG cells when both channels are activated following store depletion (Cheng *et al.*, 2011). Together, these data indicate that TRPC1 is a functional component of SOCE in salivary gland cells. Genetic knock-down of TRPC1 has been shown to attenuate thapsigargin-evoked SOCE in B lymphocytes (Mori *et al.*, 2002); inhibition of the channel with an inhibitory TRPC1 antibody (T1E3) reduced SOCE in human arterial smooth muscle cells (Xu & Beech, 2001). In the human liver HL-7702 cell line, over-expression of STIM1 and TRPC1 gave rise to a 2.5-fold increase in thapsigargin-induced SOCE (Zhang *et al.*, 2010b). In HEK-293 cells, over-expression of TRPC1 has been reported to increase SOCE and thapsigargin-induced non-selective cation currents (Cheng *et al.*, 2008), and enhance Ba^{2+} entry following thapsigargin application (Wu *et al.*, 2000).

A number of reports have suggested that Orai1 is functionally required for store-operated TRPC1 channels. In human platelets, TRPC1 and Orai1 were reported to co-immunoprecipitate; this interaction was prevented by an antibody to the Orai1 C-terminus that inhibits STIM1-Orai1 interaction (Jardin *et al.*, 2008). The authors concluded that Orai1 is required for the interaction of STIM1 and TRPC1, and that STIM1 interacts with TRPC1 and Orai1 channels in a complex following store depletion. The concept of a STIM1-Orai1-TRPC1 ternary complex was supported by immunocytochemistry data showing that TRPC1 and Orai1 channels strongly co-localise in the plasma membrane in HSG cells; co-localisation of STIM1 and TRPC1 as well as STIM1 and Orai1 was enhanced by thapsigargin pre-treatment (Ong *et al.*, 2007). TRPC1 and Orai1 were also shown to interact by co-immunoprecipitation in HSG cells; interaction was found to increase following store depletion (Ong *et al.*, 2007). The authors suggested that a STIM1-Orai1-TRPC1 ternary complex is involved in SOCE, and that all three proteins are essential for SOCE. It has

been reported that a complex of STIM-1, Orai1 and TRPC1 can be co-immunoprecipitated from HEK cells expressing the three proteins, and treating HEK cells with TRPC1 siRNA has been shown to reduce STIM1-Orai1 interaction (Ong *et al.*, 2007; Kim *et al.*, 2009b). Additionally, Orai1 siRNA was reported to reduce STIM1-TRPC1 interaction, suggesting that the interaction of TRPC1 and Orai1 with STIM1 is enhanced by the presence of both channels (Kim *et al.*, 2009b). The expression of Orai1 in TRPC1-expressing HEK cells has also been shown to enhance SOCE (Liao *et al.*, 2009). Whilst all these experiments suggest that store-operated TRPC1 channels are functionally dependent on Orai1 channels, co-immunoprecipitation and siRNA studies do not provide evidence for the direct interaction of TRPC1 and Orai1 channels.

It has recently been proposed that the surface expression of TRPC1 is affected by Orai1-mediated SOCE, but that the channels do not form a heteromeric assembly (Cheng *et al.*, 2011). The authors showed that Orai1-mediated I_{CRAC} currents, detected by the characteristic inwardly-rectifying I/V relationship, are present when TRPC1 is knocked-down by shRNA in HSG cells. Similar results were obtained when a STIM1 mutant lacking TRPC1 gating was expressed; it was concluded that SOCE in HSG cells is composed of a large TRPC1 current and a separate smaller I_{CRAC} current mediated by Orai1. Plasma membrane insertion of TRPC1, which is enhanced by thapsigargin treatment, was shown to be partially dependent on Orai1; expression of the dominant negative Orai1 mutant E106Q reduced the surface expression of TRPC1 following store depletion (Cheng *et al.*, 2011). TRPC1 trafficking was not affected by the expression of a STIM1 mutant defective in TRPC1 gating, but channel activation was suppressed under these conditions. Novel experiments revealed that TRPC1 and Orai1 co-immunoprecipitate following store depletion, but this was inhibited in the presence of STIM1 siRNA. The authors concluded that STIM1 is required for the activity of TRPC1 following store depletion, but Orai1-mediated SOCE is required for its surface expression. A model was proposed where TRPC1 is present in recycling vesicles; following store depletion STIM1 interacts with TRPC1 to retain the vesicles at the cell surface, and recruits Orai1 to the same plasma membrane microdomains. Ca^{2+} entry via Orai1 was proposed to cause plasma membrane insertion of TRPC1 channels and subsequent gating of TRPC1 by STIM1. This model of TRPC1 and Orai1 functional dependence is illustrated in figure 1.17; it accounts for previous observations that TRPC1 and Orai1 co-localise (Ong *et al.*, 2007; Jardin *et al.*, 2008), that this interaction is enhanced by store depletion (Ong *et al.*, 2007), and that TRPC1-STIM1 interactions are inhibited by Orai1 siRNA (Kim *et al.*, 2009a). It therefore represents a likely scenario for the dependence of TRPC1 channels on Orai1-mediated SOCE in other cell types.

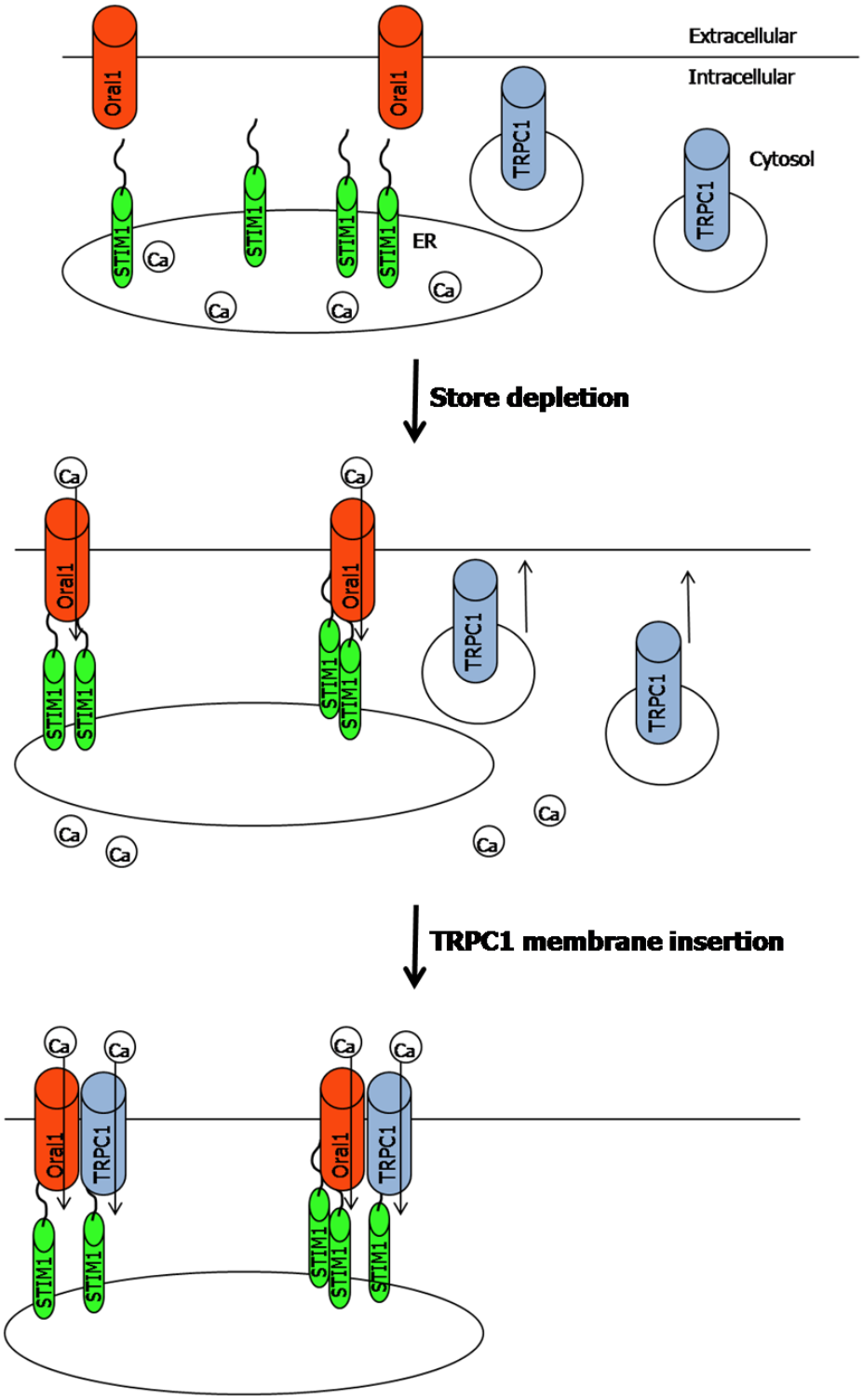

Figure 1.17. Model for TRPC1 activation by store depletion

STIM1 is located in the ER membrane, and Orai1 in the plasma membrane. TRPC1 is hypothesized to be localised in vesicles. Following store depletion, STIM1 aggregates and translocates to the plasma membrane, activating Orai1 channels. Orai1-mediated Ca^{2+} entry enhances TRPC1 insertion into the plasma membrane where it is gated by STIM1 to cause further SOCE.

Adapted from (Cheng *et al.*, 2011)

The plasma membrane localisation of TRPC1 and Orai1 channels is controlled by cholesterol- and sphingomyelin- rich regions called lipid rafts (Lingwood & Simons, 2010). Caveolin 1 has been shown to regulate the localisation of TRPC1 (Brazer *et al.*, 2003), and STIM1-Orai1 association has recently been shown to be controlled by the ordering of lipids. The association of the two proteins is enhanced by ordered PtdIns(4,5)P_2 and reduced by disordered PtdIns(4,5)P_2; the balance is determined by different isoforms of PIP5 kinase (Calloway *et al.*, 2011). PIP5 kinase-β enhances the ordering of PtdIns(4,5)P2 and the association of STIM1 and Orai1, whereas PIP5 kinase-γ negatively regulates these processes (Calloway *et al.*, 2011). Proteins are also crucially involved in determining plasma membrane structure and lipid order, and interactions between proteins and lipids bring about complexity in membrane structure (Lingwood & Simons, 2010). Interestingly, it has been shown in HEK-293 cells that TRPC1 associates into plasma membrane lipid rafts only when STIM1 is co-expressed; total internal reflection fluorescence (TIRF) microscopy experiments revealed that TRPC1-caveolin co-localisation was observed in 76% of cells when STIM1 was present, but only 11% when STIM1 was not present. Disruption of lipid rafts using the cholesterol-sequestering agent methyl-β-cyclodextrin (MβCD) in this study reduced thapsigargin-induced TRPC1 currents by 80%, suggesting that lipid raft assembly is essential for the store-operated behaviour of TRPC1 (Alicia *et al.*, 2008). Another study showed that TRPC1 and STIM1 co-localisation in lipid rafts was inhibited by MβCD in HEK-293 and HSG cells; this inhibition was reversed by replenishing membrane cholesterol (Pani *et al.*, 2008). Thapsigargin-evoked Ca^{2+} entry in HSG cells was also impaired following cholesterol disruption with either MβCD or filipin (Pani *et al.*, 2008). Together these important studies highlight the significance of plasma membrane microdomains in the store-operated behaviour of TRPC1 channels. In the model shown above, the close proximity of Orai1 and TRPC channels in lipid raft microdomains is important to mediate STIM1-dependent TRPC1 gating.

Whilst a large body of evidence indicates that TRPC1 is activated by store depletion and is dependent on Orai1 channel activity, some studies suggest that TRPC1 is not activated by store depletion. DeHaven *et al.* (2009) showed that no carbachol-induced SOCE occurred in HEK cells transfected with TRPC1 in the presence of 5μM Gd^{3+}. The inclusion of 5μM Gd^{3+} in this study was intended to inhibit endogenous Orai1 channels and reveal the contribution of TRPC channels to SOCE (DeHaven *et al.*, 2009). It is possible that TRPC1-mediated SOCE did not occur in the presence of 5μM Gd^{3+} due to the dependence of store-operated TRPC1 channels on Orai1-mediated Ca^{2+} entry, as depicted above in figure 1.17. Whilst 5μM Gd^{3+} does not inhibit TRPC channels *per se* (Broad *et al.*, 1999; DeHaven *et al.*, 2009), it does inhibit Orai1-mediated SOCE, which could compromise the ability of TRPC1 channels to insert into the plasma membrane in lipid raft microdomains and become activated by STIM1. It has also been suggested that the store-dependent or –independent nature of TRPC1 is determined by STIM1 (Yuan *et al.*, 2007; Alicia *et al.*, 2008). It has been shown in HEK-293 cells that STIM1 levels are crucial to the store-operated behaviour of TRPC1; when TRPC1 was expressed without STIM1 in HEK-293 cells, it was not activated by thapsigargin. The size of thapsigargin-induced TRPC1 currents became

larger with increasing levels of STIM1 expression, showing that STIM1 association with TRPC1 converts it from a receptor-operated to a store-operated channel (Alicia *et al.*, 2008). It has also been shown that TRPC6, whilst not typically activated by store depletion, can interact with TRPC4 in a STIM1-dependent manner to produce a store-operated heteromultimeric channel (Yuan *et al.*, 2007). This study supports the theory that TRPC channels can be activated by STIM1 to confer store-operated behaviour, or act as STIM1-independent non-store operated channels. It is possible that STIM1 expression levels were lower in the study by DeHaven *et al.* (2009) compared with other studies showing that TRPC1 channels are SOCE channels in HEK-293 cells, giving rise to store-independent behaviour in that study. It is also known that TRPC1 channel assemblies at the plasma membrane following store depletion are the result of complex interactions involving lipid rafts, STIM1, Orai1-mediated Ca^{2+} entry, vesicle fusion and possibly interaction with other TRPC channels (Yuan *et al.*, 2007; Alicia *et al.*, 2008; Lee *et al.*, 2010; Lingwood & Simons, 2010; Calloway *et al.*, 2011; Cheng *et al.*, 2011); differences in these factors between experimental systems could account for the apparent non-store-operated behaviour of TRPC1 channels in the study by DeHaven *et al.* (2009).

Discrepancies have also been reported regarding the store-operated behaviour of TRPC1 in platelets. Whilst studies using an inhibitory antibody suggested that TRPC1 mediates SOCE in human platelets (Rosado *et al.*, 2002), normal SOCE was observed in platelets derived from TRPC1-deficient mice (Varga-Szabo *et al.*, 2008). The authors suggested that the antibody used in the study by Rosado *et al.* (2002) was non-specific and that TRPC1 is not a store-operated channel in platelets. Species-dependent differences and the platelet isolation methods used have been suggested as possible reasons for the conflicting results (Salido *et al.*, 2009); it is also possible that species- or cell- dependent variations in other factors such as STIM1 and Orai1, as discussed above, gave rise to conflicting results. Variation in the expression level of channels in different studies has also been suggested to account for confounding results (Vazquez *et al.*, 2003; Salido *et al.*, 2009). It has been shown in DT40 chicken B-lymphocytes that when expressed at low levels, TRPC3 can be activated by thapsigargin-evoked store depletion, but when expressed at higher levels it could only be activated by PLC-coupled muscarinic receptors (Vazquez *et al.*, 2003). The authors concluded that at low expression levels, TRPC3 channels could stoichiometrically associate with other proteins to confer store-operated behaviour; for example, association with TRPC1 allows interaction with STIM1 (Yuan *et al.*, 2007). At elevated expression levels, however, it is likely that TRPC3 channels were present at much higher levels than the native proteins in DT40 cells, so could not associate with the interacting partners required to confer store-operated behaviour (Vazquez *et al.*, 2003). It is possible that varying levels of channel expression, giving rise to altered interactions with other proteins, could account for discrepancies in results using heterologous expression systems to determine the store-operated behaviour of TRPC channels. To summarise, although some studies suggest that TRPC1 is not activated by store depletion, a number of factors could account for inconsistent results,

and a large body of evidence indicates that TRPC1 is a STIM1-regulated, Orai1-dependent, store-operated Ca^{2+} channel.

In addition to TRPC1, the related TRPC4 and TRPC5 channels have also been proposed as store-operated channels. As discussed above, STIM1 has been shown to interact with both channels (Yuan *et al.*, 2007), and the conserved TRP box structure suggests that TRPC4 and 5, like TRPC1, may be gated by electrostatic interactions between negatively charged aspartate residues in the channel and positively charged lysine residues in STIM1 (Zeng *et al.*, 2008). Endothelial cells from TRPC4-deficient mice display reduced $InsP_3$-induced currents compared with those from wild-type mice (Freichel *et al.*, 2001). Expression of TRPC4 in CHO and RBL-2H3 cells gave rise to thapsigargin- and $InsP_3$- evoked currents that could be recorded in the presence of extracellular Ca^{2+} or Ba^{2+} (Warnat *et al.*, 1999). Thapsigargin-evoked Ba^{2+} and Ca^{2+} entry was enhanced in HEK-293 cells expressing human TRPC5 compared with cells not expressing the channel, and TRPC5 expression gave rise to CPA-induced currents (Zeng *et al.*, 2004). In arteriolar smooth muscle cells, application of the T5E3 TRPC5-blocking antibody inhibited CPA-induced currents with the biophysical properties corresponding to TRPC1-TRPC5 heteromeric channels (Xu *et al.*, 2006a); these data suggest that TRPC1-TRPC5 heteromers are also SOCE channels. However, there are some conflicting data concerning TRPC4 and TRPC5 as SOCE channels; Schaefer *et al.* (2000) failed to observe store-operated currents activated by $InsP_3$ in HEK-293 cells expressing mouse TRPC4 or TRPC5. Receptor-mediated mTRPC5 activation was shown to be unaffected by $InsP_3$ receptor inhibition in HEK-293 cells (Plant & Schaefer, 2003); these results apparently contradict those described previously suggesting that TRPC4 and 5 are SOCE channels. As discussed previously in the context of TRPC1, it is possible that the availability of STIM1 in different systems, or the expression level of heterologously expressed channels, could account for contrasting results. Experiments questioning the role of TRPC4 and TRPC5 in SOCE were all carried out using mouse channels expressed in HEK cells; it is possible that species-dependent variations in the channels, or interacting partners, could also be responsible for discrepancies.

In the only study investigating the store-operated behaviour of TRPC channels in mast cells, Ma *et al.* (2008) showed that Sr^{2+} and Ca^{2+} entry occur following FcεRI cross-linking or store depletion with thapsigargin in Ca^{2+} free solution, indicating that the non-selective TRPC channels are involved. Divalent entry following store depletion with thapsigargin was substantially impaired when TRPC5 channels were knocked-down using shRNA in RBL-2H3 cells. These results are illustrated in figure 1.18. STIM1 and Orai1 knock-down also suppressed thapsigargin-evoked Sr^{2+} and Ca^{2+} entry, and over-expression of TRPC5 and STIM1 enhanced divalent ion entry (Ma *et al.*, 2008). Based on the knowledge that Orai1 channels are highly Ca^{2+}-selective and do not conduct other divalent ions such as Sr^{2+} (Hoth & Penner, 1992; Lis *et al.*, 2007), the authors proposed that TRPC5 channels are activated by STIM1 following store depletion and that TRPC5, STIM1 and Orai1 are functionally dependent (Ma *et al.*, 2008).

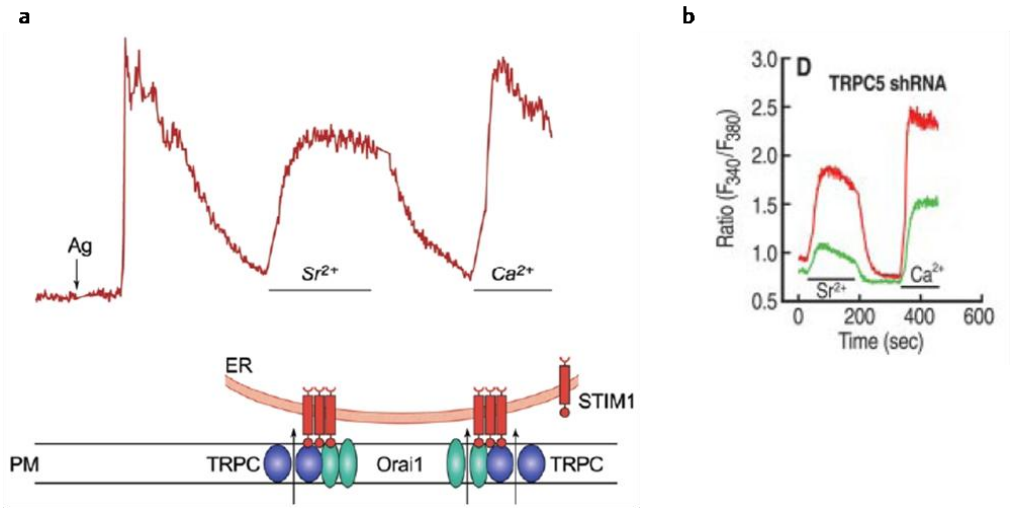

Figure 1.18. TRPC5-mediated SOCE in RBL-2H3 cells

a: Sr^{2+} and Ca^{2+} entry were assessed following FcεRI cross-linking in RBL-2H3 cells. The trace reflects Ca^{2+} release from stores (1st peak), entry of Sr^{2+} (2nd peak, TRPC-mediated) and entry of Ca^{2+} (3rd peak, TRPC and Orai-mediated). Reproduced with permission from (Ma & Beaven, 2011)

b: Divalent ion entry following store depletion with thapsigargin in RBL-2H3 cells transfected with TRPC5 shRNA (green trace) and in control cells (red trace). The entry of both divalent ions was impaired in the absence of TRPC5, suggesting that this channel mediates SOCE in RBL-2H3 cells.

Reproduced with permission from (Ma *et al.*, 2008). Copyright 2008. The American Association of Immunologists, Inc.

These results are in accordance with the model proposed for the STIM1- and Orai1-dependent activation of TRPC1 in figure 1.17; SOCE through Orai1 channels could promote the association of TRPC5 channels into lipid raft domains where they are gated by STIM1 to give rise to TRPC5-mediated SOCE. Similar studies to those carried out for TRPC1 are required to elucidate whether TRPC4 and TRPC5 channels co-localise with STIM1, and whether store depletion enhances their interaction. Whilst further investigation is required, this study investigating TRPC5 channels in RBL-2H3 cells suggests that store-operated TRPC channels are activated by STIM1 in mast cells and are functionally dependent on Orai1, as described for HSG cells in figure 1.17.

TRPC3, 6 and 7 are considered as DAG-regulated channels activated downstream of receptor stimulation, but the possibility that these channels are also activated by store depletion cannot be excluded. As described above, TRPC3 and TRPC6 have been shown to interact indirectly with STIM1 via interactions with TRPC1 and TRPC4, respectively (Yuan *et al.*, 2007), suggesting that they could function as store-operated channels under some conditions. When TRPC3 was originally cloned it was reported to form thapsigargin-activated Ca^{2+} channels when expressed in HEK-293 cells (Zhu *et al.*, 1996). However, when constitutive TRPC3-mediated Ca^{2+} entry was subtracted from that induced by thapsigargin and carbachol, it was concluded that TRPC3 is sensitive to receptor activation but not store depletion (Zhu *et al.*, 1998). Association with other channels could account for the apparent store-operated behaviour of TRPC3 in some studies;

whilst it was previously thought to interact only with TRPC6 and TRPC7, it has recently been proposed that TRPC3 interacts with TRPC1, based on studies in HEK-293 (Yuan *et al.*, 2007) and HSG cells (Liu *et al.*, 2005). It was reported that thapsigargin and OAG evoke currents with similar properties in HSG cells, and that the two agonists do not have an additive effect. TRPC1 and TRPC3 co-immunoprecipitated in these cells, and were shown by yeast two-hybrid analysis to interact via their N-terminal regions; knock-down of TRPC1 or TRPC3 gave rise to a reduction in OAG- and thapsigargin- evoked currents (Liu *et al.*, 2005). The authors concluded that TRPC3 can form a store-operated channel when interacting with TRPC1 that can also be activated by agonist stimulation; such novel channel assemblies may increase the diversity of store-operated Ca^{2+} channels in different cell types. As discussed above, TRPC3 has been shown to form store-operated channels when expressed at low levels and store-independent DAG-activated channels when expressed at higher levels; it is likely that interaction with other channels such as TRPC1 at low expression levels could give rise to store-operated TRPC3 channels in some cell types (Vazquez *et al.*, 2003). Store-operated behaviour of TRPC3 channels independently of other channels has not been demonstrated in any cell type, and they are generally considered to be receptor-operated channels activated by DAG (Trebak *et al.*, 2003).

TRPC6 is not thought to be activated by store depletion; when the channel was first cloned it was demonstrated that thapsigargin-evoked Ca^{2+} entry was not increased by the expression of TRPC6 in HEK-293 cells (Boulay *et al.*, 1997). Electrophysiological characterisation of hTRPC6 expressed in CHO-K1 cells revealed that the channel is not activated by $InsP_3$, or store depletion by thapsigargin (Hofmann *et al.*, 1999). It has, however, recently been shown that TRPC6 channel density at the plasma membrane is increased by store depletion as well as receptor activation (Cayouette *et al.*, 2004); the authors speculate that an increase in cytosolic Ca^{2+} caused by store depletion may cause TRPC6 translocation. The localisation of TRPC6 channels at discrete plasma membrane microdomains along with TRPC4 and STIM1 proteins and interaction with the same accessory proteins could account for their co-immunoprecipitation reported in HEK-293 cells (Yuan *et al.*, 2007).

Whilst TRPC7 was not reported to interact with STIM1 in the study by Yuan *et al.* (2007) in HEK-293 cells, Lievremont *et al.* (2004) reported enhanced Ba^{2+} entry following thapsigargin stimulation of HEK-293 cells when TRPC7 was expressed. However, the same group later reported that knock-down of STIM1 and Orai1 did not affect TRPC7-mediated Ba^{2+} entry, and currents were not observed following $InsP_3$-mediated store depletion in HEK cells expressing TRPC7 (DeHaven *et al.*, 2009). The authors concluded that TRPC7 is not a store-operated channel, and that previously observed activation by thapsigargin could be as a result of SERCA inhibition *per se* and not due to store depletion. To summarise, there is a lack of conclusive evidence implicating TRPC3, 6 and 7 channels in SOCE, whereas a number of studies suggest that TRPC1, 4 and 5 are STIM1-regulated SOCE channels.

1.3.2.12 Methods to study store-operated TRPC channels

Difficulties arise in studying contribution of TRPC channels to store-operated Ca^{2+} entry due to the lack of selective pharmacological inhibitors. Methods used to activate store-activated TRPC channels, such as thapsigargin-mediated inhibition of the SERCA pump, also activate Orai1 channels; it is important to distinguish between the two channels in order to establish their relative contributions to SOCE. This is possible by examination of the I/V relationships of the two channels; as discussed above, I_{CRAC} has an inwardly-rectifying I/V relationship with a positive reversal potential, whereas TRPC channels have outwardly-rectifying relationships with a reversal potential close to 0mV (compare figures 1.8, 1.11 and 1.15). The selective I_{CRAC} inhibitor synta 66 can also be used in conjunction with activators of SOCE, in order to determine the contribution of TRPC channels. Another important property that can be used to distinguish the two channels is Ca^{2+} permeability; whilst Orai1 is highly selective for Ca^{2+}, many studies have demonstrated that TRPC channels can readily permeate Ba^{2+} ions, including but not limited to (Trebak *et al.*, 2002; Ma *et al.*, 2008; DeHaven *et al.*, 2009; Tu *et al.*, 2009b; Bousquet *et al.*). I_{CRAC} currents mediated by Orai1, 2, and 3 channels are abolished when Ba^{2+} is the sole charge carrier (Lis *et al.*, 2007); glutamate residues in the transmembrane regions of Orai channels are thought to be responsible for their Ca^{2+} selectivity (Vig *et al.*, 2006a).As many Ca^{2+} indicator dyes can bind to both Ca^{2+} and Ba^{2+}, it is possible to employ Ca^{2+} imaging techniques to determine the Ba^{2+} permeability of SOCE channels to assess the involvement of TRPC channels.

1.4 TRPC channels in mast cells

Given the crucial importance of Ca^{2+} in mast cell activation and inflammatory mediator release, characterisation of the ion channels responsible for Ca^{2+} entry is important as they provide potential therapeutic targets for mast cell modulation in allergic diseases such as asthma. Studies carried out in RBL cells (Ma *et al.*, 2008; Sanchez-Miranda *et al.*, 2010) indicate that TRPC channels could be important for Ca^{2+} entry mediating mast cell degranulation, and results from an affymetrix mRNA screen indicate that TRPC1 channels may be functionally expressed in primary human mast cells (Bradding *et al.*, 2003). This study aimed to characterise the functional expression of TRPC channels in human mast cells using the LAD 2 cell line and primary HLMCs, to investigate their role in SOCE in these cells, and to assess whether they have a role in human mast cell mediator release.

The experimental tools that can be used to study TRPC channels that have been discussed in this chapter are summarised in table 1.4.

DAG-sensitive TRPCs	**Activators**		**Inhibitors**
TRPC3	DAG analogues: OAG, SAG GPCR agonists: ADP, carbachol, histamine		Gd^{3+}/La^{3+} (10–100μM) SKF-96365 (10μM) 2-APB (10–100μM)
TRPC6		100μM FFA	
TRPC7			
Store-operated TRPCs			
TRPC1	Store-depletion: thapsigargin, CPA, activation downstream of receptor stimulation. To distinguish from I_{CRAC}: store depletion in the presence of synta 66, Ba^{2+} entry following store depletion.		Gd^{3+}/La^{3+} (10μM) SKF-96365 (10μM) 2-APB (10–100μM)
TRPC4		100μM Gd^{3+}/La^{3+}	Gd^{3+}/La^{3+} (>5mM) SKF-96365 (10μM) 2-APB (10–100μM)
TRPC5		100μM Gd^{3+}/La^{3+} 10μM S1P thioredoxin	

Table 1.4. Summary of pharmacological methods to study TRPC channels

Experimental use of these tools is discussed in the text above.

Chapter 2: Materials and methods

2.1 HEK 293 cell lines over-expressing TRPC channels

2.1.1 HEK-TRPC5 cells

Generation of the cell line

The tetracycline-inducible HEK-TRPC5 cell line used in this study was a generous gift from Professor David Beech. To generate the cell line, human TRPC5 cDNA was cloned from two plasmids containing overlapping TRPC5 fragments. Primers were used to amplify the C-terminal region of TRPC5 from plasmid 2B11 and the N-terminal region from plasmid 6A1; further amplification reactions were used to generate full-length TRPC5 cDNA. HEK-293 cells stably expressing Tet repressor (T-Rex 293 cell line) were transfected with hTRPC5/pcDNA4 using lipofectamine 2000 reagent (Zeng *et al.*, 2004).

HEK-TRPC5 cell culture

HEK-TRPC5 cells were grown in 25cm^2 Nunclon™Δ surface tissue culture flasks and incubated at 37^{o}C in a 5% CO_2 humidified atmosphere. Cells were cultured in Dulbecco's modified Eagle's medium (DMEM)-F12 media supplemented with 10% foetal calf serum (FCS); those stably expressing TRPC5 were selected for using 400µg/ml zeocin and 5µg/ml blasticidin ("TRPC5 selective media"). Blasticidin powder was dissolved in H_2O as 10mg/ml stock, filter sterilised and stored at -20^{o}C. Zeocin was purchased as a 100mg/ml stock solution. Cells were split twice per week; cell dissociation solution (CDS) was used to harvest the cells, which were then centrifuged at 1000rpm for 4 minutes. Following resuspension, HEK-TRPC5 cells were split 1 in 5 or 1 in 8, depending on density. Cells were plated onto coverslips and incubated with 1µg/ml tetracycline in TRPC5 selective media for 24 hours when required to induce TRPC5 expression. Tetracycline powder was dissolved in H_2O as a 1mg/ml stock, filter sterilised and stored at -20^{o}C.

To freeze HEK-TRPC5 cells, 2 million cells in 1ml FCS + 10% DMSO in a cryovial were placed in a "Mr Frosty" cryo 1^{o}C freezing container and kept at -80^{o}C overnight. Vials of cells were then transferred to liquid nitrogen for long-term storage. To thaw cells, vials were placed in a 37^{o}C water bath upon removal from liquid nitrogen. The FCS + 10% DMSO cell suspension was transferred to 5ml of DMEM-F12 and washed twice by centrifugation at 1000rpm for 4 minutes followed by resuspension in DMEM-F12. After the final wash, cells were resuspended in 5ml HEK-TRPC5 selective media for culture.

2.1.2 HEK-TRPC6 cells

Generation of the cell line

The stable HEK-TRPC6 cell line was a generous gift from Professor Guylain Boulay. TRPC6 was cloned from mouse brain RNA using a PCR reaction, and specific primers were used to amplify mouse TRPC6 (mTRPC6). To create the stable cell line, HEK-293 cells were transfected with mTRPC6-pcDNA3 using a calcium phosphate-based protocol. Transfected cells were grown in the presence of G418 to select for resistance, which is conferred by pcDNA3. G418-resistant cells were expanded to produce the HEK-TRPC6 cell line (Boulay *et al.*, 1997).

HEK-TRPC6 Cell culture

HEK-TRPC6 cells were grown in DMEM containing 10% FCS and 400µg/ml G418 to select for TRPC6 expression ("TRPC6 selective media") and were incubated at 37°C in a 5% CO_2 humidified atmosphere. G418 powder was dissolved as a 50mg/ml stock in H_2O and stored at 4°C. Cells were split twice per week, using CDS to harvest them followed by centrifugation at 1000rpm for 4 minutes. Following resuspension, they were split 1 in 5 or 1 in 8, depending on density. Cells were plated onto coverslips in HEK-TRPC6 selective media when required for experiments.

HEK-TRPC6 cells were frozen and thawed as described above for HEK-TRPC5 cells. However, immediately following thawing, the cells do not stick properly to standard tissue culture flasks (L. Wilson, unpublished observation); for this reason they were grown on poly-D-lysine-coated 25cm^2 tissue culture flasks for one week after thawing. At all other times they were cultured in 25cm^2 Nunclon™Δ surface tissue culture flasks.

2.2 The LAD 2 human mast cell line

2.2.1 Derivation of the cell line

As described in chapter 1.1.3, LAD 2 cells were generated in the Laboratory of Allergic Diseases (LAD), from bone marrow aspirates taken from a patient with mast cell sarcoma/leukaemia. These cells express CD117 and are dependent on SCF for growth.

2.2.2 LAD 2 cell culture

The LAD 2 cell line used in this study was a kind gift from Dr Dean Metcalfe, Laboratory of Allergic Diseases, National Institutes of Health, USA. Cells were cultured in serum-free StemPro-34 media supplemented with StemPro-34 nutrient supplement and 2mM L-glutamine ("complete LAD 2 media"). 100ng/ml rhSCF was added to the media weekly upon use from frozen aliquots of a 100µg/ml solution in PBS + 0.1% bovine serum albumin (BSA). Cells were maintained at a density of 200 000 to 500 000 cells per ml of media in 25cm^2 Nunclon™Δ surface tissue culture flasks; they were counted weekly and fed or diluted as appropriate. Cells were incubated at 37°C in a 5% CO_2 humidified atmosphere.

To obtain frozen stocks of LAD 2 cells, 10 million cells were suspended in 1.5ml non-FCS, non-DMSO containing PZerve cryopreservative supplemented with 200ng/ml rhSCF as described previously (Kirshenbaum *et al.*, 2003). Vials of cells were placed in a "Mr Frosty" cryo 1°C freezing container and incubated for 30 minutes at 25°C, 1 hour at -20°C and 1 hour at -70°C. Vials were then placed in liquid nitrogen for long-term storage. For thawing, cells were slowly equilibrated to room temperature and added to 1.5ml complete LAD 2 media supplemented with 100ng/ml rhSCF. Cells were agitated at room temperature in 12.5cm^2 flasks for 6 hours, followed by incubation at 37°C in 5% CO_2 for 24 hours. Cells were then transferred to a 25cm^2 tissue culture flask and 3ml of complete LAD 2 media with 100ng/ml SCF was added.

2.3 Isolation, purification and long-term culture of primary human lung mast cells (HLMCs)

Mast cells were isolated from human lung tissue obtained from surgical resections in collaboration with Dr Peter Peachell, Department of Infection and Immunity, University of Sheffield. All patients donating tissue gave informed written consent, and the study was approved by the Local Research Ethics Committee.

2.3.1 HLMC Isolation

HLMCs were obtained from macroscopically normal lung tissue taken from patients undergoing resection for lung cancer as described previously (Sanmugalingam *et al.*, 2000). All steps were carried out aseptically. Large bronchi were removed if necessary and lung tissue was cut into strips 0.5cm wide using scissors. Using tweezers and scissors, strips of tissue were cut into small squares and put into a funnel lined with 100µm gauze. Tissue was washed with DMEM + 2% FCS before being transferred to a straight-sided jar and chopped to a fine pulp using two pairs of scissors. Tissue pulp was washed twice in a funnel lined with 100µm gauze using DMEM + 2% FCS before being placed in a sterile screw top pot for overnight storage. 4ml of DMEM + 10% FCS + 1% antibiotic/antimycotic solution (A/A; contains 10 units/ml penicillin, 10 units/ml streptomycin and 25µg/ml amphotericin B) + 1% MEM non-essential amino acids (NEAA) per 1g of tissue was added to the tissue pulp, and the tissue was stored at 4°C overnight. Overnight storage in antibiotics was done to help prevent the growth of infectious micro-organisms.

The following day, lung tissue was digested using 37.5mg hyaluronidase and 50mg collagenase type 1A per 10g tissue for 90 minutes at 37°C with stirring. To liberate cells from connective tissue the pulp was forced through a 50ml syringe 30 times and was filtered through a 100µm gauze with DMEM + 2% FCS three times. Dispersed cells were then washed twice in DMEM + 2% FCS by centrifuging at 1200rpm for 8 minutes. After the final wash, cells were resuspended in 10ml DMEM + 2% FCS and were counted on a haemocytometer using Kimura stain in a 1:10

mast cell:stain ratio. Mast cells appear cerise in colour when stained with Kimura, so can be identified in a mixed cell population.

2.3.2 HLMC purification

Mast cells were purified using immunomagnetic affinity selection as described previously (Okayama *et al.*, 1994). Anti-mouse IgG1 Dynabeads® coated with mouse anti-c-kit antibody (mAb YB5.B8, see section 2.3.4 "Coating of magnetic beads with anti-CD117 antibody") were used to positively select CD117-expressing HLMCs. Figure 2.1 illustrates the HLMC purification procedure.

Cells were centrifuged at 1200rpm for 8 minutes at 4°C, resuspended in 4ml HBSS/FCS-protein and incubated at 4°C for 30 minutes under continuous rotation. This blocking stage prevents nonspecific binding during purification. After incubation, cells were added to 10ml of cold HBSS + 2% FCS, passed through a 100µm cell strainer, and centrifuged at 1200rpm for 8 minutes at 4°C. The appropriate volume of anti-CD117-coated Dynabeads® was washed (see section 2.3.4 for details); the Dynabead:mast cell ratio is 5:1 so the appropriate volume could be calculated from the cell count performed earlier. Following centrifugation, the cells were resuspended in 1ml HBSS/protein containing the appropriate amount of beads and incubated in a cryotube at 4°C for 90 minutes under continuous rotation.

After the incubation, cells were transferred to a larger 15ml tube and resuspended in 10ml HBSS + 2% FCS. The tube was placed in a Dynal® MPC™-1 magnetic field for 3 minutes and the supernatant was removed. This was repeated two further times; after the final wash, cells were resuspended in 1ml DMEM + 10% FCS + A/A + NEAA and a final count was performed.

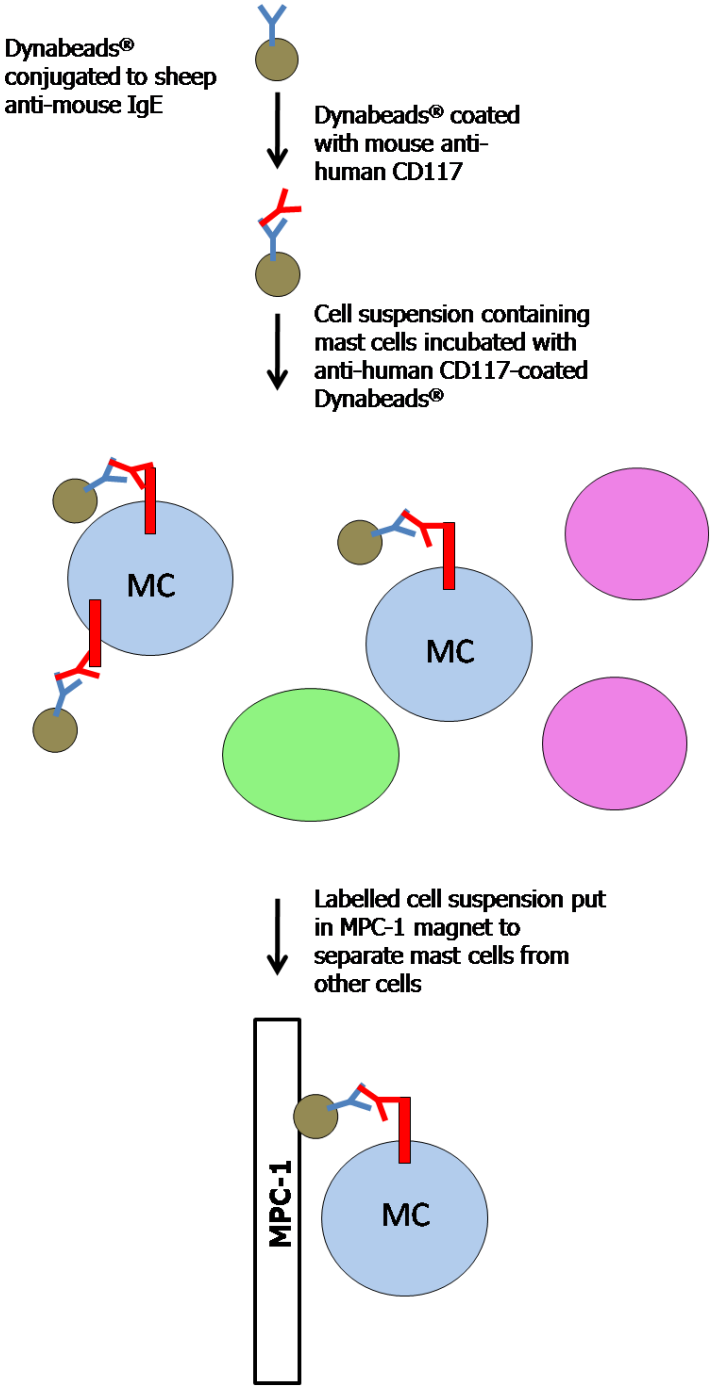

Figure 2.1. Schematic diagram representing mast cell purification using Dynabeads®.
Dynabeads® conjugated to sheep anti-mouse IgG are coated with mouse anti-human CD117. The mixed cell population is incubated with coated Dynabeads®, which stick to CD117 on the surface of mast cells (MC, blue). Only mast cells attached to Dynabeads® remain attached to the magnet, isolating them from other cells.
Adapted with permission from K. Wareham PhD thesis, 2010.

2.3.3 HLMC culture

HLMCs were maintained at a density of 200 000 to 500 000 cells per ml in DMEM + 10% FCS + A/A + NEAA supplemented with 100ng/ml SCF, 50ng/ml IL-6 and 10ng/ml IL-10. Cytokines were added to the media when required from frozen stocks of 100µg/ml SCF, 50µg/ml IL-6 and 10µg/ml IL-10 in sterile PBS + 0.1% BSA. Cells were counted weekly and fed or diluted as appropriate. HLMCs were maintained at 37^{o}C in a 5% CO_2 humidified atmosphere, in 12.5cm^2 BD Falcon^{TM} cell culture flasks or 12-well cell culture plates as appropriate.

2.3.4 Coating of beads with anti-CD117 antibody

Magnetic Dynabeads® conjugated to sheep anti-mouse IgG were coated with mouse anti-human CD117 antibody by the following procedure.

1. To wash the beads, 100µl beads were added to 15ml HBSS + 2% FCS in a 15ml tube. The tube was placed in an MPC-1 magnetic field for 3 minutes and the supernatant was removed, followed by resuspension in 15ml HBSS + 2% FCS.
2. Beads were washed three times; after the final wash beads were resuspended in 400µl HBSS/protein solution.
3. Anti-human CD117 antibody was added to the bead suspension at an antibody:bead ratio of 1:12.5 The mix was incubated at 4^{o}C for 2 hours under continuous rotation.
4. The beads were washed (as in step 1) three times; after the final wash they were resuspended in 100µl HBSS/protein with 1% NaN_3 and stored at 4^{o}C.
5. Immediately before use, anti-CD117-coated beads were washed to remove toxic NaN_3. The appropriate amount of beads was added to 15ml HBSS + 2% FCS and washed as in step 1. After the final wash, beads were resuspended in 1ml HBSS/protein to use for purification.

2.3.5 Buffers for HLMC preparation

The following recipes were used to prepare the solutions required for HLMC isolation.

1. DMEM + 10% FCS + A/A + NEAA: DMEM with HEPES and glutamax with 10% FCS, 1% A/A solution and 1% NEAA.
2. HBSS/protein: HBSS + 2% FCS + 10% horse serum + 1% BSA, stored at -20^{o}C
3. Collagenase type 1A: Powder dissolved as 75mg/ml stock in phosphate buffered saline (PBS), stored at -20^{o}C.
4. Hyaluronidase: Powder dissolved as 37.5mg/ml stock in PBS, stored at -20^{o}C.
5. Kimura stain: 11ml of 0.05% toluidine blue solution, 0.8ml of 0.03% light green, 0.5ml saponin saturated in 50% ethanol, 5ml phosphate buffer at pH 6.4.
6. Phosphate buffer: 0.067M Na_2HPO_4 (0.59g in 50ml H_2O) and 0.067M KH_2PO_4 (0.449g in 50ml H_2O); titrate pH of KH_2PO_4 to 6.4 with Na_2HPO_4.
7. 0.05% toluidine blue: 0.05g toluidine blue dissolved in 50ml 1.8% NaCl. Add 22ml ethanol and make up to 100ml with H_2O.

2.3.6 Isolation of impure HLMCs for secretion assays

As sufficient numbers of pure HLMCs were not able to be obtained using the method above for mediator release assays, impure preparations of cells isolated in the laboratory of Dr P. Peachell were used for such studies. The cells were isolated from macroscopically normal lung tissue, as described previously (Havard *et al.*, 2011). Lung tissue was chopped vigorously using scissors and the chopped tissue washed over a 100µm pore size nylon mesh using PBS. Tissue was digested in 35mg collagenase per 10g of tissue at 37^{o}C under constant agitation. Following digestion, tissue was disrupted using a syringe and washed over nylon gauze using PBS + 10% FCS. The filtrates were centrifuged at 480g, 10 min, 25^{o}C, and pellets were resuspended in PBS + 10% FCS. This wash was repeated three times, and mast cells were counted; typically 3–13% of all cells were mast cells. Mediator release assays were performed the day after cell isolation following overnight incubation in RPMI 1640 buffer with 10 units/ml penicillin, 10mg/ml streptomycin and 50mg/ml gentamicin. HLMC isolation was not carried out aseptically and cells could not be maintained long-term in culture.

2.4 Coverslip preparation

For electrophysiology and Ca^{2+} imaging experiments cells were plated onto 1.5mm thick glass coverslips (VWR). Coverslips were washed in 95% ethanol + 5% acetic acid for 6 hours, rinsed with water and autoclaved. HEK-TRPC5 and HEK-TRPC6 cells were plated directly onto sterile washed coverslips at a 1 in 5 or 1 in 8 dilution from a confluent 25cm^2 tissue culture flask. After 30 minutes at 37^{o}C, cells were flooded with selective media.

Non-adherent LAD 2 cells and HLMCs were plated onto coverslips coated with 0.1% poly-L-lysine hydrobromide. Poly-L-lysine was dissolved in sterile H_2O; 70µl was applied to 13mm coverslips, and 150µl was applied to 16mm coverslips. Following a 30 minute incubation at 37^{o}C, coverslips were rinsed with sterile H_2O and dried under sterile conditions. Cells were placed on the coverslip and incubated for 30 minutes at 37^{o}C to allow attachment, before flooding with culture medium.

2.5 Ca^{2+} Imaging

Fluorescent Ca^{2+} imaging was used in this study to quantify changes in intracellular Ca^{2+}. Fluorescence, defined as the emission of light by a molecule that has absorbed light, is caused when an electron returns to its ground state by emitting a photon of light after being excited to a higher energy level. Figure 2.2 illustrates the energy changes in fluorescence. The emitted photon has energy equivalent to the difference between the lowest excited state and the ground state so has less energy than the absorbed photon. This difference, called the Stokes shift, allows fluorescence to be visualised because emitted light has a longer wavelength than absorbed light.

2.5.1 Calcium indicator dyes

Ca^{2+} indicators have altered fluorescent properties when they bind Ca^{2+} (Paredes *et al.*, 2008) so can be used to monitor changes in intracellular Ca^{2+} levels. They are derivatives of Ca^{2+} chelators such as EGTA and BAPTA (Tsien, 1980), and many dyes are now available for the detection of intracellular Ca^{2+} over a range of concentrations and in different organelles (Paredes *et al.*, 2008). They can broadly be classed into single wavelength and ratiometric dyes; single wavelength dyes such as fluo-4 are usually bright and used for Ca^{2+} detection when more than one indicator is present. Ratiometric indicators such as fura-2 are advantageous as they reduce the problems of photobleaching, uneven dye loading and leakage commonly associated with fluorescent indicators (Paredes *et al.*, 2008).

Fura-2 was used in this study as it is a ratiometric dye, and it was appropriate to use with the available detection methods. Fura-2 is a dual excitation, UV light-excitable Ca^{2+} indicator. The peak absorbance is 380nm when Ca^{2+} is not bound, shifting to 340nm when Ca^{2+} is bound. This shift can be observed by measuring emission at 510nm (see figure 2.3).

In addition to Ca^{2+}, fura-2 can be used as an indicator of other divalent ions including Ba^{2+} and Sr^{2+}. The dissociation constant (Kd) of fura-2 is 236nM for Ca^{2+}, 780nM for Ba^{2+} and 2.62μM for Sr^{2+}. The acetoxymethyl (AM) ester form of fura-2 was used in this study to facilitate loading of the cells. AM esters are engineered onto Ca^{2+} dyes as they are sufficiently hydrophobic to cross the cell membrane; once inside the cell, esterases cleave the AM group and the dye remains inside the cell (Paredes *et al.*, 2008).

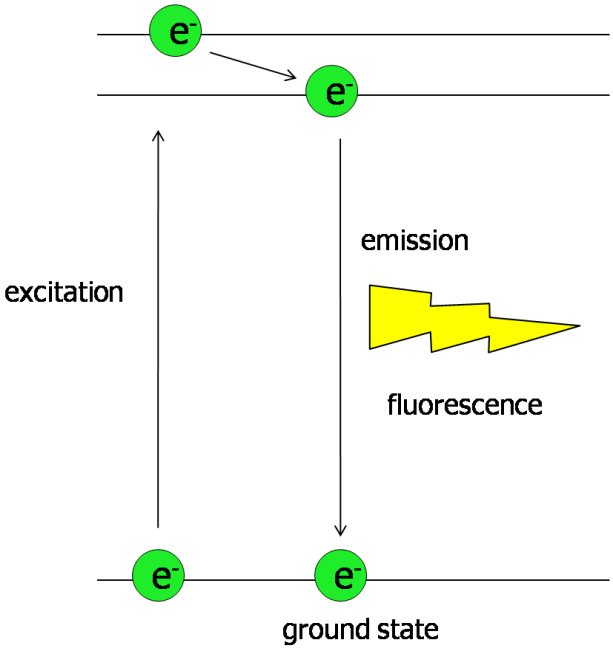

Figure 2.2. Energy level changes in fluorescence

When energy, such as light energy, is absorbed, an electron (green, e-) moves to a higher energy state. A small amount of energy is lost as heat or through molecular collisions and the electron drops to a lower excited state. To re-enter the ground state the electron emits a photon of light (seen as fluorescence) in order to lose its energy.

Adapted from *The Molecular Probes® Handbook—A Guide to Fluorescent Probes and Labeling Technologies edited by Iain Johnson and Michelle Spence*

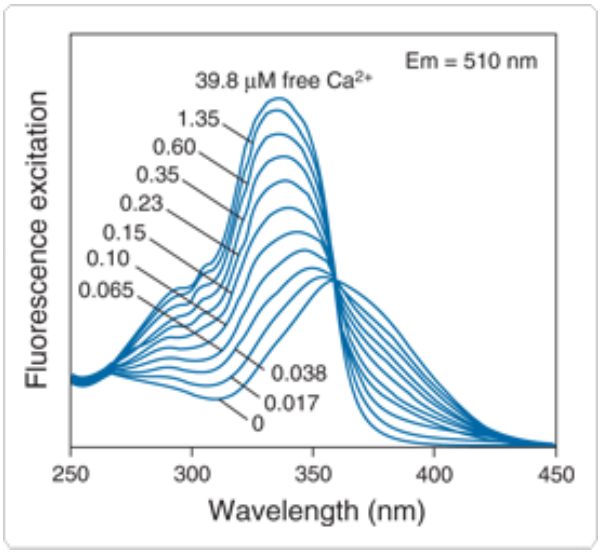

Figure 2.3. Fluorescence excitation spectra of fura-2

A higher concentration of bound Ca^{2+} gives rise to a higher absorbance at 340nm and a lower absorbance at 380nm. Emission is monitored at 510nm.

Image reproduced from http://www.invitrogen.com/site/us/en/home/References/Molecular-Probes-The-Handbook.html with permission from Life Technologies Ltd.

2.5.2 Calcium imaging experiments

2.5.2.1 Loading of cells with Fura-2-AM

Cells were plated onto 16mm coverslips as described in section 2.4. Cells were loaded with 1μM fura-2 AM at 37^{o}C for 30 minutes. HEK-293 cells and HLMCs were loaded in DMEM + 10% FCS + 0.1% BSA; LAD 2 cells were loaded in StemPro-34 media + 0.1% BSA. Antibiotics were not present in the media when cells were loaded. Cells were then washed for 15 minutes in the appropriate media at 37^{o}C, followed by a 15 minute wash in standard imaging solution. Cells were protected from light at all stages.

2.5.2.2 Calcium imaging apparatus

Coverslips were placed in a superfusion chamber and mounted on an inverted microscope (Axiovert S100 TV, Zeiss) equipped with a 40X oil immersion objective (NA 1.3, Zeiss). Cells were alternately illuminated at 340 and 380nm with a 20ms exposure time using a monochromator (Polychrome IV, TILL Photonice LPS-150). The shutter was closed between exposures to reduce the exposure of fura-2-loaded cells to UV light. Emitted light was passed through a 510nm band pass filter and collected by a 512B CCD camera (Roper Scientific, Photometrics UK). Images were acquired at a rate of 1 frame every 2 seconds using Metamorph® Meta imaging software. The intensifier gain was set at 3500 and the linear gain at 1x for all experiments.

The recording chamber was continually superfused with standard imaging solution at a rate of approximately 1.5ml/minute. Syringes on a perfusion rack were used to apply solutions to cells, as illustrated in figure 2.4. Bungs with plastic tubing in the centre were placed in all containers of solution to ensure a constant flow rate. The outflow tube was connected to a peristaltic pump (Watson Marlow SciQ 323) to transfer solution into a waste bottle. The time taken for solutions to reach the bath was measured at 40 seconds; solutions were fully equilibrated after another 30 seconds. Bars showing the application of solutions in figures have been corrected for this delay.

Experiments were carried out at room temperature unless otherwise stated. When heating was required, tubes containing solutions were passed through a heating block before application to cells, and a thermometer was placed in the perfusion chamber to check the required temperature was reached. Cotton wool was wrapped around the tube to retain heat. A maximum temperature of 35^{o}C was able to be reached using this method.

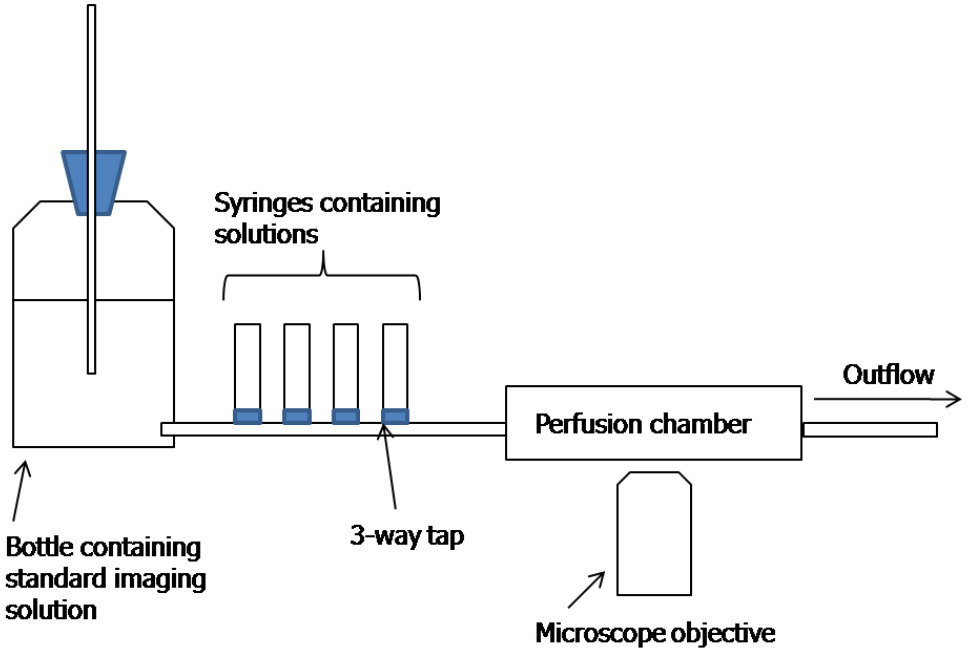

Figure 2.4. Schematic diagram of the Ca^{2+} imaging perfusion system

Standard imaging solution in a 1 litre bottle continually superfused cells on a coverslip in the recording chamber. Syringes on a perfusion rack were used to apply additional solutions to cells; the outflow tube was connected to a peristaltic pump.

2.5.2.3 Recording solutions

Unless indicated otherwise, standard imaging solution was perfused onto cells prior to the addition of other solutions. Standard imaging solution contained (in mM): 147 NaCl, 10 HEPES, 16 glucose, 2 KCl, 2 $CaCl_2$, 1 $MgCl_2$ and 0.1% BSA. Ca^{2+}-free solution contained (in mM): 147 NaCl, 10 HEPES, 16 glucose, 2 KCl, 3$MgCl_2$ and 0.1% BSA. Ba^{2+}-containing solution contained (in mM): 147 NaCl, 10 HEPES, 16 glucose, 2 KCl, 2 $BaCl_2$, 1 $MgCl_2$ and 0.1% BSA. The solution was titrated to pH7.3 using NaOH, and the osmolarity was approximately 307mOsm/litre.

2.5.2.4 HLMC staining

When Ca^{2+} imaging experiments were carried out on primary HLMCs, cells were incubated with a phycoerythrin (PE)-tagged anti-CD117 IgG1 antibody for 10 minutes to assess the purity of the cells following experimental protocols. Antibody-labelled cells were excited at 488nm and an image was taken after the light was passed through a 520nm emission filter; HLMCs were stained as shown in figure 2.5. Incubation for 10 minutes with an IgG1 isotype control antibody did not give rise to fluorescence when cells were excited at 488nm. HLMCs on coverslips were found to be >98% pure by this method.

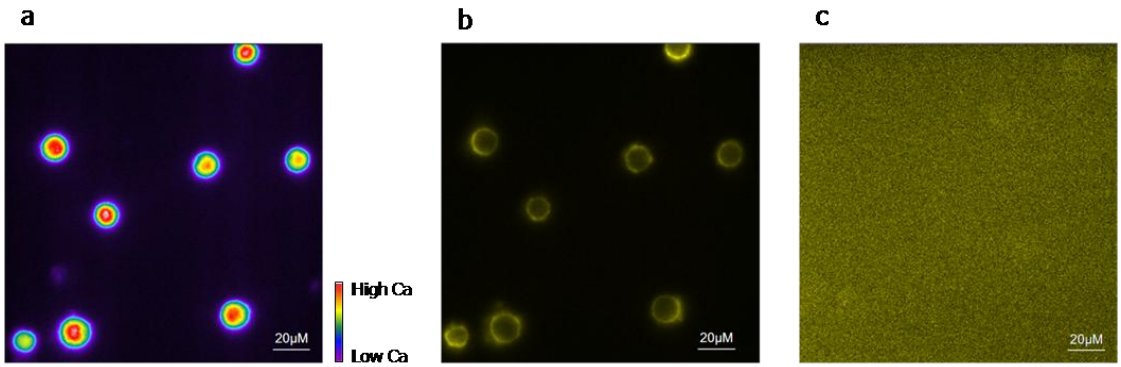

Figure 2.5. HLMCs loaded with fura-2 and stained with anti-CD117

a: Image of fura 2- loaded HLMCs excited at 340nm.

b (i): Image of same coverslip of HLMCs as in part (a) incubated with PE-tagged anti-CD117 for 10 minutes and excited at 488 nm. (ii): HLMCs were incubated with PE-tagged mouse IgG1 isotype control and excited at 488nm.

2.5.2.5 Ca^{2+} imaging data analysis

Metamorph® Meta imaging software was used to analyse all Ca^{2+} imaging experiments. A region of interest (ROI) was placed over each cell in the field of view on the 340nm and 380nm images and raw fluorescence values were exported to a Microsoft Excel spreadsheet, along with background fluorescence values for each wavelength. Using the spreadsheet, background fluorescence corresponding to the same frame was subtracted from the fluorescence value for each cell, for both the 340nm and 380nm signals. The background-subtracted 340nm fluorescence values were then divided by the background-subtracted 380nm fluorescence values to give "$F_{340/380}$". To work out the amplitude of Ca^{2+} entry following the application of a particular agonist, the mean $F_{340/380}$ of the 5 frames prior to agonist application was calculated. This value was subtracted from the maximum $F_{340/380}$ in the presence of agonist to give change in $F_{340/380}$, or $\Delta F_{340/380}$. When calculating the percentage of cells responding to a particular agonist, "responders" were classed as cells where the fluorescence ratio in the presence of agonist rose by more than 10 standard deviations above the baseline fluorescence.

Data were then copied into OriginPro 8.5 for graphing and further analyses. When concentration response curves were constructed, data were fitted using the Hill equation: y= Vmax*x^n/(k^n+x^n). Ca^{2+} imaging figures are displayed in this thesis as 5 representative individual cells, indicated by different coloured traces, and the mean ± standard error of the mean (SEM) of all cells, unless otherwise stated. Concentration-response curves are plotted as concentration of solution against mean $\Delta F_{340/380}$. GraphPad Prism 5 was used for all statistical analyses. Student's T test or one-way ANOVA was used as appropriate; log transformations of percentage data were carried out before statistical analysis.

2.6 Electrophysiology

2.6.1 Development of the patch clamp technique

The patch clamp technique was first used by Neher and Sakmann to record currents through acetylcholine-activated channels in frog skeletal muscle (Neher & Sakmann, 1976). The technique was developed from early voltage clamp studies of the squid giant axon (Hodgkin *et al.*, 1952); this method measures the flow of ions across a cell membrane as electric current, whilst the voltage of the membrane is controlled with a feedback amplifier. The patch clamp method was subsequently refined to enable high current resolution, and the giga seal was discovered; it was found that a fire-polished clean pipette could form a seal of more than 10GΩ with a clean cell membrane when suction was applied (Hamill *et al.*, 1981).The principle of patch clamping is that a patch of membrane is electrically isolated from the external solution and current flowing in the patch is recorded. A fire-polished glass pipette filled with an electrolyte solution is pushed against the cell surface and suction is applied to form a seal. A high-resistance seal is required to electrically isolate the patch of membrane and to reduce the current noise of the recording. When a gigaseal is achieved, a number of different patch clamp recording configurations can be used (figure 2.6). These configurations allow the recording of membrane currents when the cell is voltage-clamped by the amplifier. The composition of intracellular and extracellular solutions can be varied in order to investigate the physiological role of ion channels in electrically excitable and non-excitable cells.

2.6.2 Recording configurations

Illustrated in figure 2.6 are the different patch clamp recording configurations that can be achieved after the formation of a giga-seal. The cell-attached configuration is used for single-channel recordings. The inside-out patch clamp configuration is obtained by pulling the membrane patch from the cell into the bath solution; the inside of the cell is in contact with the extracellular solution. When further suction is applied to a cell attached patch, the whole-cell recording configuration is achieved. The inside of the cell is in contact with the pipette solution and can be voltage-clamped or current-clamped. In the whole-cell recording configuration the contents of the cell equilibrate with the pipette solution over time (Fenwick *et al.*, 1982); the intracellular solution can therefore be controlled to record currents through different ion channels. From the whole-cell mode, the pipette can be pulled away from the cell, allowing the membrane to reseal and giving rise to the outside-out patch configuration. The intracellular face of the membrane is in contact with the extracellular solution in this configuration.

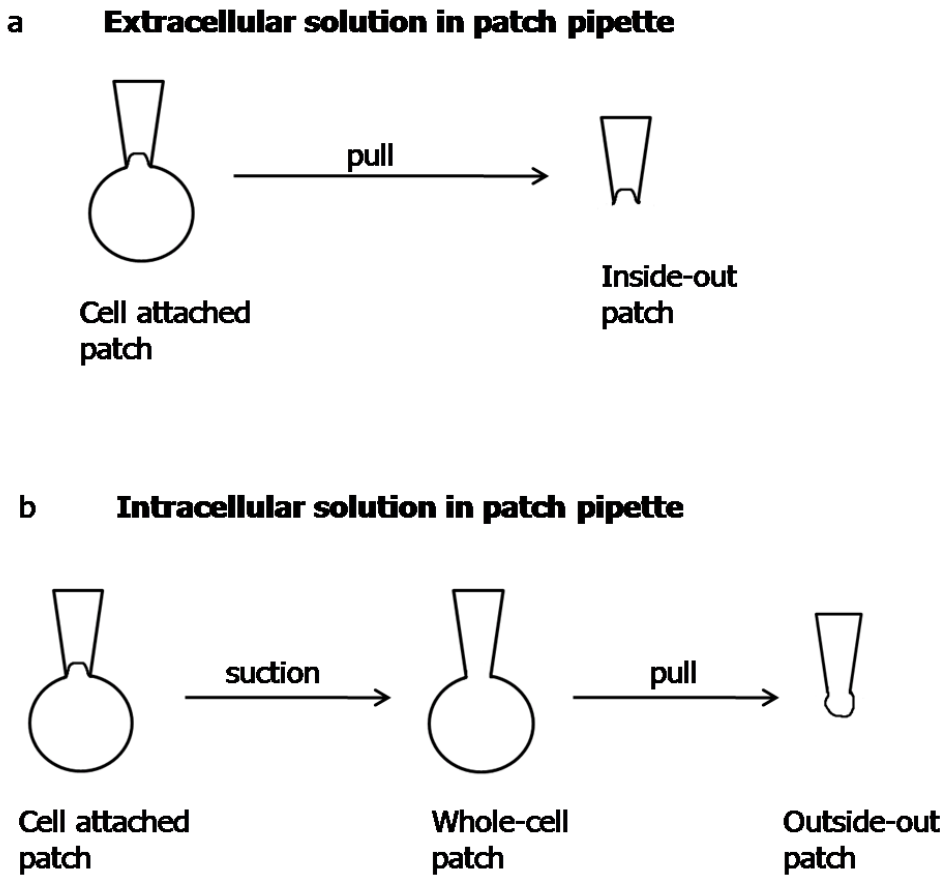

Figure 2.6. Patch clamp recording configurations

Modified from Ogden, D. 1994. Microelectrode Techniques: The Plymouth Workshop handbook.

In the whole-cell recording configuration, the cell contents are in equilibrium with the pipette solution; depending on the pipette tip width and the length of the recording, intracellular signalling molecules can dialyse into the pipette. This can be problematic if important cellular components are lost, such as second messengers. To avoid such problems, the perforated patch configuration can be used; instead of rupturing the membrane to gain access to the inside of the cell, small pores are created by the inclusion of gramicidin (Rhee *et al.*, 1994) or amphotericin (Rae *et al.*, 1991) in the patch pipette. This technique maintains a more complete intracellular environment than the whole-cell configuration, but is difficult to implement because pore-forming agents can interfere with seal formation.

2.6.3 Patch clamp experiments

LAD 2 cells and HLMCs were plated onto 13mm coverslips coated with 0.1% poly-L-lysine for patch clamp experiments. HEK-TRPC5 and HEK-TRPC6 cells were plated onto non-coated coverslips. The whole-cell recording configuration was used for patch-clamp experiments in this study.

2.6.4 Patch clamp apparatus

Patch clamp experiments were carried out using an EPC-10 amplifier (HEKA, Lambrecht, Germany). The patch clamp amplifier is a current-to-voltage converter with a high gain, allowing small currents to be recorded using a silver chloride-coated wire electrode inside the patch pipette (see figure 2.7). The voltage measured by this electrode is compared with that measured by a reference electrode in contact with the extracellular solution. The amplifier can be used to control the voltage inside the patch pipette (voltage clamp); this can be kept constant, or changed in a step-wise or ramp-wise fashion. Alternatively, the amplifier can be used to current clamp the cell and record changes in voltage.

2.6.5 Pipette preparation

Patch pipettes were produced from filamented boroscillate glass (World Precision Instruments Inc.) using a DMZ universal puller, and fire-polished using a heated wire mounted on the stage of a compound microscope (Narishige). Polished pipettes had a resistance of 2–5MΩ when filled with internal solution.

2.6.6 Superfusion system

The superfusion system on the patch clamp rig was similar to that for the Ca^{2+} imaging rig shown in figure 2.4. Coverslips with cells attached were placed in a superfusion bath above an inverted microscope (Axiovert 100, Zeiss) and viewed at a magnification of 10x or 40x to allow visualisation of single cells. The bath was continuously superfused with standard external solution at a rate of approximately 2ml/minute, and the outflow tube was connected to a peristaltic pump, as described above for Ca^{2+} imaging experiments. A "bubble trap" was created, consisting of a syringe with a bung and needle, through which the outflow solution passed to reduce perfusion-related noise.

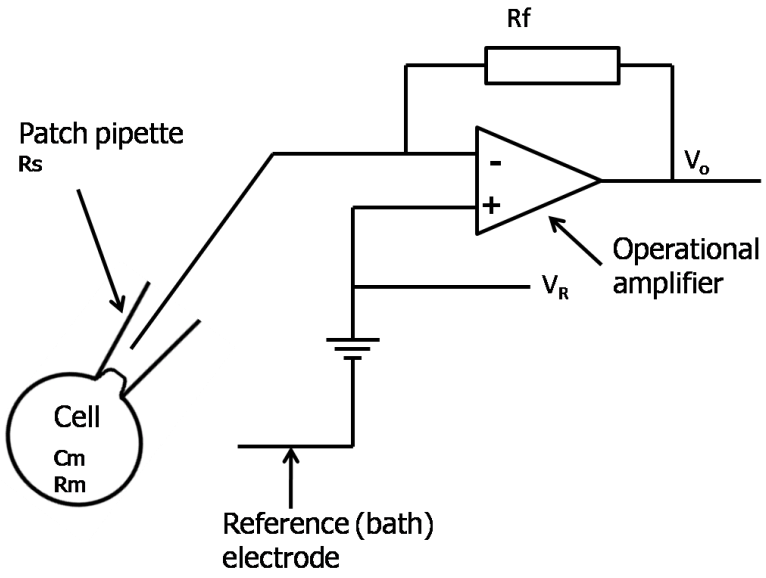

Figure 2.7. Schematic diagram of the patch clamp amplifier.

Simplified diagram of a voltage clamp amplifier. The cell membrane acts as a capacitor (Cm, storing charge) and a resistor (Rm, impeding the movement of ions). The access resistance (or series resistance, Rs) is created mainly by the opening of the patch pipette. The operational amplifier is a current-to-voltage converter with a feedback resistor (Rf), which gives the amplifier high gain, allowing small currents to be recorded. The amplifier measures the voltage inside the patch pipette relative to that recorded by the reference electrode. Amplifier correctional circuits for the cancellation of pipette and cell capacitance are not shown.

Modified from Ogden, D. 1994. Microelectrode Techniques: The Plymouth Workshop handbook.

2.6.7 Fast-flow system

A fast-flow system was used to apply solutions rapidly and accurately to a cell of interest. Syringes containing solutions were connected to silicone tubing, which was inserted into four fine glass capillary tubes in the superfusion chamber (see figure 2.8). The flow through each tube was controlled by a rapid solution chamber system (RSC 160, BioLogic Science Instruments); a valve system controlled solution flow through each tube. In all experiments, one tube (tube 4) contained standard external solution and was aligned with the cell of interest; agonists and antagonists were placed in the other tubes. The capillary tubes were carefully aligned on a barrel, which rotated to allow focal application of the different solutions to the cell of interest. Every time the system was set up, the capillary tubes were carefully aligned by eye to ensure correct positioning and focal drug application upon rotation of the barrel. The correct alignment was tested experimentally by focal application of 5mM ATP to LAD 2 cells; it has previously been shown in our laboratory that 5mM ATP gives rise to $P2X_7$ currents with rapid onset and current amplitude in the nA range (Wareham *et al.*, 2009). This was done to ensure that a $P2X_7$ current with similar amplitude and kinetics was produced from each tube, confirming the correct alignment of the tubes. Figure 2.9 shows $P2X_7$-mediated currents in a representative LAD 2 cell.

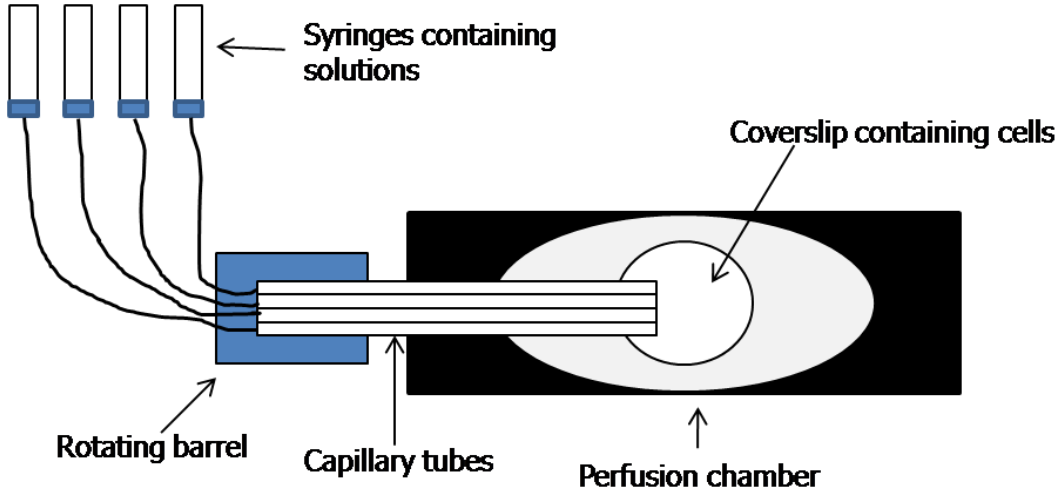

Figure 2.8. Schematic representation of the fast flow system

Syringes containing solutions were connected to glass capillary tubes attached to a rotating barrel to rapidly apply solutions to cells of interest.

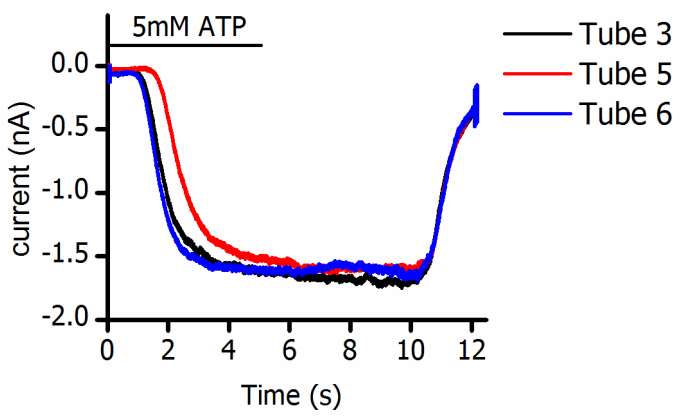

Figure 2.9. $P2X_7$ currents in LAD 2 cells

Superimposed current-time trace showing P2X7 currents in a single LAD 2 cell in response to 5mM ATP applied for 5 seconds at 30 second intervals. Each coloured trace represents a different fast flow tube; tube 4 contained standard external solution and did not generate a current when applied to the cell. The currents generated from each tube were similar in size and kinetics, indicating good alignment of the tubes.

2.6.8 Recording solutions

Standard extracellular recording solution contained (in mM): 147 NaCl, 10 HEPES, 16 glucose, 2 KCl, 2 $CaCl_2$, 1 $MgCl_2$. The solution was titrated to pH7.3 using NaOH, and the osmolarity was approximately 307mOsm/litre. Agonists and antagonists to be applied to cells were made up in standard extracellular solution. An internal solution recipe previously used for the recording of TRPC3, 5, 6 and 7 channels expressed in HEK-293 cells (Yuan *et al.*, 2007) was used for all voltage-clamp experiments in this study, unless otherwise stated, containing (in mM): 140 CsCl, 2 $MgCl_2$, 5 EGTA, 10 HEPES, 1.5 $CaCl_2$, 1 Na-ATP. The estimated cytoplasmic free Ca^{2+} concentration was 70nM. CsOH was used to titrate the pH to 7.3, and the osmolarity was approximately 300mOsm/litre. For current-clamp experiments a KCl-based internal solution was used, containing (in mM): K+ glutamate 125, NaCl 8mM, EGTA 10, HEPES 10, $CaCl_2$ 3.6, $MgCl_2$ 6. KOH was used to titrate the pH to 7.3, and the osmolarity was approximately 307mOsm/litre.

2.6.9 Experimental protocols

2.6.9.1 Whole-cell recordings

The whole-cell recording configuration was used for the majority of electrophysiology experiments in this study (unless otherwise stated), and experiments were carried out at room temperature. Pipettes were filled with internal solution following filtering of the solution through a nylon mesh with 0.2µm pore diameter; tips were filled via glass filament action. The filled pipette was secured into the electrode holder, and positive pressure was applied to avoid blocking of the pipette tip prior to forming a seal. A seal test was performed to calculate pipette resistance; a +5mV pulse of 5ms duration was applied, and the current was displayed in the oscilloscope window of the amplifier software. Figure 2.10 depicts changes in the oscilloscope window as the pipette enters the bath, through to whole-cell recording. The pipette tip was aligned above the cell of interest, using a coarse manipulator (Newport 360 90, Newport Spectra-Physics Ltd), under 10x magnification. The objective was switched to 40x magnification, positive pressure removed, and a micromanipulator (Burleigh PZ-301, EXFO) was used to gently lower the pipette tip onto the cell membrane. A deflection in the current trace displayed in the oscilloscope window and an increase in pipette resistance were indicative of cell contact. Gentle continuous suction was applied to form a gigaseal (>1GΩ), and pipette capacitance was cancelled using the amplifier correction circuitry. Short applications of suction were then used to rupture the patch of membrane in the pipette whilst maintaining a gigaseal; entry into whole-cell configuration was indicated by an increase in amplitude and a widening of the transients due to contributions from the cell membrane capacitance and access resistance. These transients were cancelled using the amplifier correction circuitry, and cells were voltage-clamped at -60mV for recordings (all recordings were carried out in voltage-clamp mode unless otherwise stated). Recordings were started 1 minute after the whole-cell configuration was achieved, to allow time for solution equilibration.

1 second ramps ranging from -100mV to +100mV were applied to cells every 2 seconds for the examination of agonist-induced currents. Resting currents were recorded by applying ramps to cells in the absence of the agonist; these recordings were subtracted from those in the presence of agonist to produce an agonist-activated I/V relationship, which can be used to assess which channels are active. In order to verify that the intended membrane potential was achieved within the time over which the ramp was applied, 1 second voltage steps ranging from -100mV to +100mV in 20mV increments were applied to LAD 2 cells in the whole-cell recording configuration. The I/V relationship constructed from the application of voltage steps was then compared with the I/V relationship resulting from ramp application; as shown in figure 2.11 the traces overlay, indicating that the required membrane potential was achieved when ramps were applied.

2.6.9.2 Perforated patch recordings

For perforated patch clamp recordings, standard internal solution was used, with 350µg/ml gramicidin added. The solution was not filtered prior to pipette filling. Experiments were carried out as described above for whole-cell recordings until a gigaseal was obtained (cell-attached mode). The pipette capacitance was cancelled using the amplifier correction circuitry and time was allowed for gramicidin to form pores in the membrane. Pore formation was monitored by observing a decrease in access resistance and an increase in amplitude of the capacitance transients when the test pulse was applied. When equilibrium between gramicidin in the pipette and the membrane was reached, the transients stopped changing and the access resistance remained constant; this process took around 30–45 minutes. The membrane capacitance and access resistance transients were cancelled using the correction circuitry, and recordings commenced.

2.6.9.3 Current-clamp recordings

Current-clamp recordings were carried out using the perforated patch configuration to determine the resting membrane potential of LAD 2 cells, and to investigate whether depolarisation occurs following FcεRI cross-linking. Following gramicidin pore formation and the achievement of equilibrium (described above in section 2.6.9.2), the amplifier was switched into current-clamp mode; current was set to 0 and the voltage was measured. In these experiments, cells were incubated overnight with 300ng/ml IgE and stimulated with 3µg/ml anti-IgE, which was focally applied. All cells had a negative resting membrane potential, ranging from -0.12mV to -20.21mV. The average resting potential was measured at -12.66mV ± 5.51 (n=6); 66% of cells showed depolarisation upon anti-IgE application, when "depolarisation" was classed as a voltage change of >10mV. Results are shown in figure 2.12. For all further voltage clamp experiments, cells were held at -60mV as described previously for TRPC channel recordings (Xu *et al.*, 2005a).

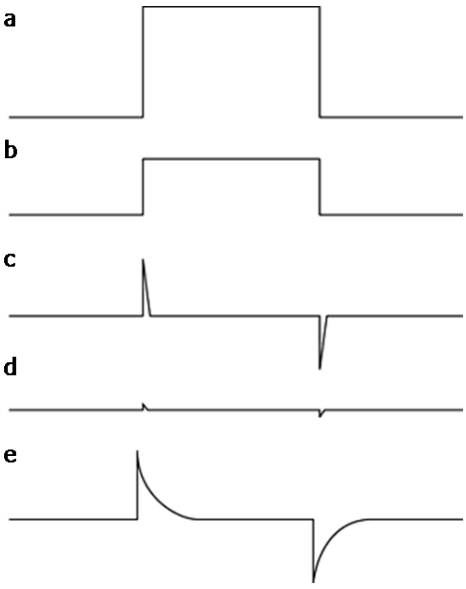

Figure 2.10. Schematic diagram showing the stages involved in reaching whole-cell configuration.

a: Patch pipette in bath, seal test applied (5mV, 5ms). b: Deflection in the current trace as the pipette touches the cell membrane. c: Gigaseal formation after gentle continuous suction. d: Pipette capacitance cancelled using amplifier correction circuitry. e: Membrane ruptured by short application of suction to establish whole-cell patch clamp recording configuration. Cell capacitance then cancelled using amplifier correction circuitry.

Reproduced with permission from Yuan, Y. and Atchison, W. D. 2003. Electrophysiological Studies of Neurotoxicants on Central Synaptic Transmission in Acutely Isolated Brain Slices. Current Protocols in Toxicology. 17:11.11.1–11.11.38

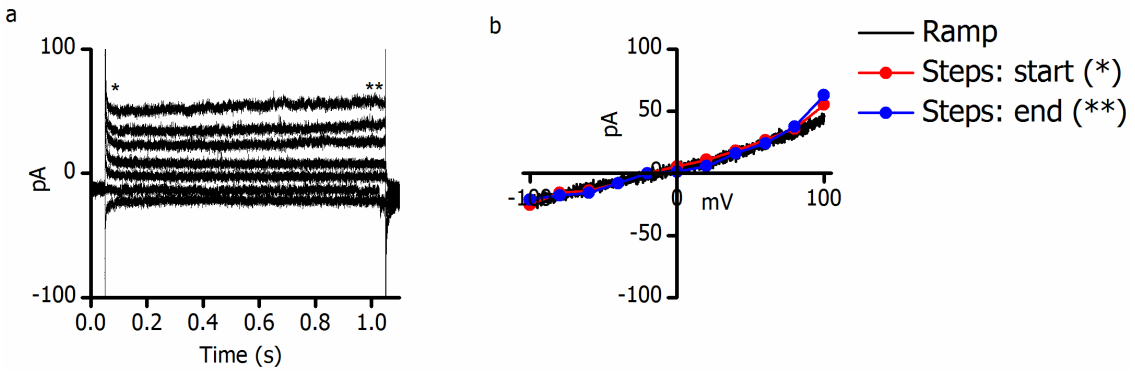

Figure 2.11. Current-voltage relationships recorded in LAD 2 cells

a: 1 second voltage steps were applied to LAD 2 cells in 20mV increments. Traces are shown for steps at -100mV, -60mV, -20mV, 20mV, 60mV, 80mV and 100mV.

b: I/V relationships resulting from application of steps and ramps in LAD 2 cells. Black trace shows resulting current when a 1 second ramp from -100mV to +100mV was applied. Red and blue traces show I/V relationships taken from the start and end voltage steps shown in (a), respectively (shown as * and ** on traces in (a)).

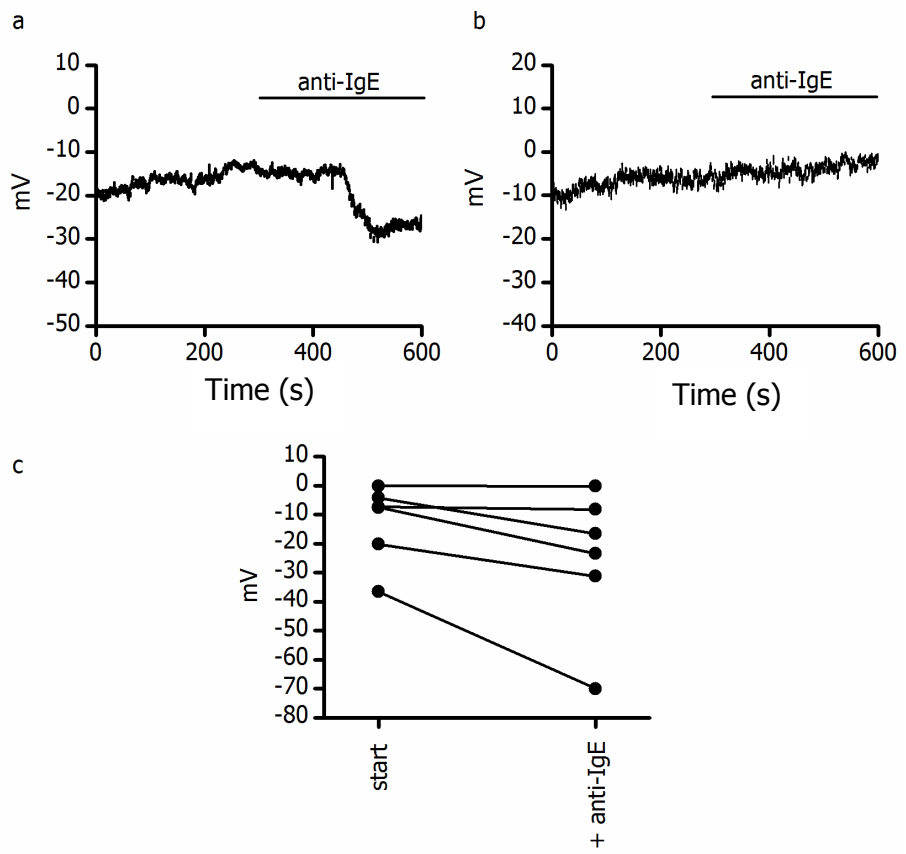

Figure 2.12. Voltage changes in LAD 2 cells stimulated with anti-IgE

Perforated patch current clamp recordings of LAD 2 cells incubated overnight with 300ng/ml IgE and stimulated with 3µg/ml anti-IgE as indicated by the horizontal bars. a: example voltage trace of a cell that depolarised in response to anti-IgE application; this occurred in 66% of cells (4/6). A cell was classed as showing deplolarisation when the voltage changed by >10mV when anti-IgE was applied. b:example voltage trace of a cell that did not depolarise in response to anti-IgE, as occurred in 34% of cells (2/6). c: line series graph showing voltage recorded at the start of the recording ("start") and peak voltage during anti-IgE application for each cell ("+anti-IgE").

2.6.10 Capacitance and series resistance

Capacitance is the ability to store charge. There are many sources of stray capacitance in patch clamp recordings; these must be charged when the voltage is changed in a patch clamp experiment, so ideally should be kept to a minimum. A major source of capacitance is the pipette; capacitance arises across the pipette wall, and is called fast capacitance (Cf). This can be seen in the oscilloscope display as sharp transients at the beginning and end of the seal test when a gigaseal is formed (see figure 2.10c), due to charging and discharging of the pipette wall as the voltage is changed. To reduce pipette capacitance, pipettes were coated with Sylgard®, an inert, hydrophobic resin that thickens the pipette wall and prevents the bath solution creeping up the pipette. Maintaining a low bath volume also reduces the length of pipette in contact with the solution, reducing the area of capacitance coupling.

Series resistance, or access resistance (Rs), acts as a barrier to current flow in the patch clamp circuit. This is mainly created by resistance in the pipette tip; a high series resistance can be indicative of a blocked tip. The cell capacitance and series resistance affect how quickly and accurately the membrane potential reflects the command potential; current injected to change the holding potential of the cell must first charge the capacitors and overcome series resistance. This can be a problem if rapid changes in membrane potential are required, as the potential of the membrane may not reach the desired value in time. The amplifier can be used to compensate for capacitance and series resistance if necessary by adding a voltage signal to the command potential. Cs and Rs values were cancelled in this study but not compensated for; figure 2.11 shows that the desired potential was reached in time when ramps were applied.

2.6.11 Data analysis

All recordings were examined using Patchmaster software; relevant ramps were exported as *.asc* files and opened in OriginPro 8.5 for graphing and further analysis. Current-time series were imported into OriginPro 8.5 as *.dat* files. All current values were divided by the cell capacitance value and displayed as pA/pF, so that currents were normalised to cell size. When concentration response curves were constructed, data were fitted using the Hill equation: y= Vmax*x^n/(k^n+x^n).

When analysing agonist-induced I/V relationships, the resting I/V was subtracted from that in the presence of agonist. To compare currents in the presence of agonist and solvent or antagonist, the peak current in the presence of solution of interest (measured at +100 and -100mV) was subtracted from the resting current (measured at +100 and -100mV) to give change in current, or ΔpA/pF. Current-time graphs for one representative cell are typically shown in this thesis; I/V curves are typically shown as mean ± SEM. Statistical analyses were carried out using GraphPad Prism 5.

When investigating transient and sustained currents, a current was classed as "sustained" if more than 50% of current remained 2 minutes after cessation of drug application.

2.7 Polymerase chain reaction (PCR)

2.7.1 RNA extraction and cDNA production

Total RNA was extracted from approximately 3 million LAD 2 cells using a Qiagen® RNeasy kit, according to manufacturers' instructions. For HLMCs, due to limited cell numbers, a Qiagen® RNA micro kit was used to extract total RNA from 10 000 cells that were 97–100% pure, as determined by staining with Kimura stain and counting using a haemocytometer. RNA was converted to cDNA using an iScript™ cDNA synthesis kit in a reaction volume of 20µl. As a negative control for each reaction, reverse transcriptase was replaced with an equivalent volume of H_2O (-RT sample). The reverse transcription reaction was carried out using a Mycycler thermo cycler (Bio Rad), and the protocol was as follows; 25°C for 5 min, 42°C for 30 min, 85°C for 5 min, 4°C for 5 min, 85°C for 5 min, hold at room temperature. cDNA was stored at -20°C for use in PCR reactions. PCR reactions were carried out using beta actin primers (positive control) with each cDNA sample to verify its integrity before primers for TRPC channels were tested.

2.7.2 Primers

To assess the expression of TRPC channel mRNA in LAD 2 cells and HLMCs, previously published primers were used. The primers were designed based on human gene sequences; products were verified by DNA sequencing (Wang *et al.*, 2003). Primer sequences are shown in table 2.1. Primers were dissolved as a stock concentration of 2pmol/µl for use in PCR reactions.

2.7.3 PCR reaction

For the PCR reaction, a mastermix was made containing the following ingredients (volumes given per sample):

- 2.5µl 10x PCR buffer
- 2.5µl dNTPs
- 4µl MgCl2
- 9.5µl H2O
- 0.5µl Taq DNA polymerase

To each reaction, 19µl mastermix was added, along with 1µl cDNA (or –RT sample from cDNA reaction) and 2.5µl of each primer. For positive controls, total human brain cDNA was used.

PCR reactions were performed using a Mycycler thermo cycler (Bio Rad); the following cycles were used:

- Stage 1: 94oC 5 min
- Stage 2 (50 cycles):
  94°C 1 min
  58°C for TRPC1, 3, 4 and 6; 55°C for TRPC5; 53°C for TRPC7; 1 min
  72°C 1min
- Stage 3: 72°C 7 min

Gene	GenBank Accession no	Forward primer sequence (5'–3')	Reverse primer sequence (5'–3')	Product size (base pairs)	Location in sequence (nucleotides)
TRPC1	U31110	CAAGATTTTGGAAAA TTTCTTG	TTTGTCTTCATGATTT GCTAT	372	2238–2709
TRPC3	Y13758	TGACTTCCGTTGTGC TCAAATATG	TCTGAAGCCTTCTCC TTCTGC	317	2316–2633
TRPC4	X90697	TCTGCAGATATCTCT GGGAAGGATGC	AAGCTTTGTTCGAGC AAATTTCCATTC	415	1–415
TRPC5	AF054568	ACCTCTCATCAGAAC CATGCCA	TGCATGAGCAAGTCA CAAGCCT	444	3351–3794
TRPC6	U49069	AAAGATATCTTCAAA TTCATGGTC	CACGTCCGCATCATC CTCAATTTC	327	2181–2507
TRPC7	AF139923	TGTAACGCTGCACAA CGTCTCA	AATTCCTCATGCCAG CCTGGTA	767	1621–2387
β-actin	M10277	GACGGGGTCACCCA CACTGTGCCCATCTA	CTAGAAGCATTTGCG GTGGACGATGGAGG	661	2134–3000

Table 2.1. PCR primer information

Primer sequences were taken from (Wang *et al.*, 2003)

2.7.4 Gel electrophoresis

PCR products were run on 1% agarose gel containing 0.005% ethidium bromide, made up in TRIS-acetate-EDTA (TAE) buffer. Loading dye (New England Biolabs) was added to the samples and they were run at 100V alongside a wide range DNA molecular weight marker (New England Biolabs), using a consort E844 power supply. TAE buffer contained (in mM): 40 Tris base, 1.14 acetic acid and 1 EDTA. Following electrophoresis, gels were visualised using a BioDoc-it imaging system (UVP BioImaging Systems).

2.8 Mediator release assays

The release of granule-associated mediators including histamine and β-hexosaminidase from both LAD 2 cells and HLMCs can be measured experimentally.

2.8.1 β-hexosaminidase release assays

2.8.1.1 LAD 2 cells

β-hexosaminidase release is commonly assayed as a marker of rat mast cell degranulation, and LAD 2 cells have been shown to release it following FcεRI cross-linking (Kirshenbaum *et al.*, 2003). β-hexosaminidase is an enzyme whose substrate, *p*-nitrophenyl-N-acetyl-β-D-glucosaminidase, is converted to the chromogenic product *p*-nitrophenol. The reaction can be measured by light absorbance at 405nm, indicating how much β-hexosaminidase is released.

The method for measuring β-hexosaminidase release from LAD 2 cells was adapted from that used to assess release from adherent RBL-2H3 cells (Ramkumar *et al.*, 1993). To assess β-hexosaminidase from LAD 2 cells following FcεRI cross-linking, cells were incubated overnight

with 300ng/ml human IgE at 37°C and 5% CO_2. The following day, they were centrifuged at 1000rpm for 4 minutes, resuspended in standard imaging solution and placed in a V-bottomed 96-well plate at a concentration of 50 000 cells per well. If required, antagonists were added and the plate was incubated for 5 minutes at 37°C, 5% CO^2. Agonists (3µg/ml anti-IgE for FcεRI cross-linking experiments) were diluted in standard imaging solution and added to each well. The plate was incubated for 30 minutes at 37°C, 5% CO^2, followed by centrifugation at 1500rpm for 10 minutes. 40µl supernatant from each well was added to 40µl *p*-nitrophenyl-N-acetyl-β-D-glucosaminidase (at a concentration of 2mM diluted in 0.2M citrate buffer) in another 96 well plate. The substrate plate was incubated for 2.5 hours at 37°C, 5% CO^2, and the reaction was stopped by adding 90µl 1M Tris HCl, pH 9.0. The plate absorbance at 405nm was measured using an Expert Plus microplate reader (Biochrom Ltd) with Digiread software. Spontaneous release was determined by the addition of imaging solution only to cells; total release was determined by lysis of cells with 0.1% Triton-X-100. Background absorbance readings were determined from wells containing imaging solution and *p*-nitrophenyl-N-acetyl-β-D-glucosaminidase only. Experiments were carried out in duplicate on a single plate.

2.8.1.2 β-hexosaminidase release assays: HLMCs

β-hexosaminidase release was not able to be carried out on HLMCs using the method described above for LAD 2 cells, because sufficient numbers of pure cells were not able to be obtained in our laboratory due to the limited availability of lung tissue. HLMC release assays were carried out in collaboration with Dr Peter Peachell, using impure suspensions of HLMCs isolated using the method described in section 2.3.6. Release assays were carried out one day after cell isolation. The number of HLMCs in a suspension was counted using Kimura stain. Cells were centrifuged at 1000rpm for 4 minutes, resuspended in standard imaging solution, and 50 000 HLMCs per condition were placed into 15ml centrifuge tubes. If required, antagonists were added and the tubes were incubated for 5 minutes at 37°C, 5% CO_2. Agonists (3µg/ml anti-IgE for FcεRI cross-linking experiments) were diluted in standard imaging solution and added to each tube; tubes were incubated for 30 minutes at 37°C, 5% CO_2. Tubes were then centrifuged at 1000 rpm for 4 minutes, and 40µl supernatant was assayed for β-hexosaminidase release as described above for LAD 2 cells. The remainder of the supernatant was stored at -20°C and assayed for histamine content.

2.8.1.3 Data analysis: β-hexosaminidase assays

Absorbance readings were imported into Microsoft Excel. Average background values were subtracted from all values, and average spontaneous release values were then subtracted from all other readings. Release was calculated as a percentage of total release, determined by Triton-X-100 lysis. Percentage release values were imported into OriginPro 8.5 for graphing, and statistical analyses were carried out using Graphpad Prism 5. Results are displayed as mean ± SEM; N numbers refer to the number of wells. Experiments were typically carried out in duplicate

on one plate and repeated three times for LAD 2 cells. For HLMCs, the number of donors used is indicated in the figure legend.

2.8.2 Histamine release assays

2.8.2.1 Protocol: histamine release assays in HLMCs

Impure HLMCs were stimulated and centrifuged as described above for β-hexosaminidase release (section 2.8.1); supernatant was stored at -20^{o}C and histamine release was measured in the laboratory of Dr P. Peachell, using a fluorimetric method described previously (Siraganian, 1974). An automated sampler dispensed reference histamine solutions of known concentration, water, and the samples into the system. Histamine was extracted into butanol, followed by a wash with NaOH, and back-extraction of histamine into HCl in the presence of heptane. The aqueous phase was mixed with *o*-phthaldialdehyde (OPT) in the presence of NaOH. OPT is commonly used to quantify protein concentrations as it reacts with amino groups to form a fluorescent moiety. The reaction was stopped by the addition of HCl; the resulting fluorescence was detected with a fluorometer and recorded using a chart recorder. A pump with calibrated tubes allowed precise volumes of the different reagents to be delivered into the system. Histamine release was measured as a percentage of total release for each donor, determined by lysis with 0.5% perchloric acid.

2.8.2.2 Data analysis: histamine assays

Peaks on the chart recorder were measured with a pencil and ruler, and the values put into Microsoft Excel. Average spontaneous release values were subtracted from all readings, and release was calculated as a percentage of total release, determined by lysis with perchloric acid. Percentage release values were imported into OriginPro 8.5 for graphing, and statistical analyses were carried out using Graphpad Prism 5. Results are displayed as mean ± SEM; N numbers refer to the number of sample. Experiments were typically carried out in duplicate on each donor; the number of donors for each experiment is stated in the figure legend.

2.8.3 Release assay solutions

Cells were suspended in standard imaging solution for the assessment of mediator release, to allow comparisons to be made between results. *p*-nitrophenyl-N-acetyl-β-D-glucosaminidase was used at 2mM, diluted in citrate buffer; 2.34g citric acid and 2.588g sodium citrate in 100ml H_2O, pH adjusted to 4.5 with HCl. 1M Tris HCl was dissolved in H_2O and the pH adjusted to 9.0 using NaOH.

2.9 Mast cell motility assays

Motility assays were carried out using a method previously published for HLMCs (Brightling *et al.*, 2005) using transwells with 8μM fibronectin-coated inserts in 24 well plates (BD Biosciences). 50 000 LAD 2 cells were placed onto each insert and 500μl agonist was added to wells below the inserts. Following a three hour incubation at 37°C and 5% CO_2, wells were photographed and the number of cells in a defined central region were counted.

2.10 Reagents

2.10.1 Cell culture reagents

DMEM, DMEM-F12, FCS, zeocin, blasticidin, cell dissociation solution, G418, tetracycline, StempPro-34, nutrient supplement, L-glutamine, HBSS, antibiotic/antimycotic solution, MEM non-essential amino acids and Dynabeads® were obtained from Invitrogen Life Technologies (Paisley, UK). Stem cell factor, IL-6 and IL-10 were obtained from R&D Systems (Abingdon, UK). DMSO, collagenase type 1A, hyaluronidase and poly-L-lysine hydrobromide were obtained from Sigma Aldrich (Poole, UK); mouse anti-human CD117 was obtained from BD Pharmingen™, BD Biosciences (Oxford, UK).

2.10.2 Antibodies and PCR reagents

PE-tagged anti-CD117 was obtained from Miltenyi Biotech (Surrey, UK). PCR mastermix ingredients and DNA ladders were from New England Biolabs (Hitchin, UK). Custom-made primers were from Invitrogen Life Technologies (Paisley, UK).

2.10.3 All other reagents

Compounds were dissolved in sterile H_2O and stored at -20°C unless otherwise stated. Anti-IgE, ATP, SKF-96365, $GdCl_3$, ADP, carbachol, UTP, PMA (dissolved in DMSO), ionomycin (dissolved in DMSO), flufenamic acid (dissolved in 95% ethanol) and *p*-nitrophenyl-N-acetyl-β-D-glucosaminidase (dissolved in DMSO) were from Sigma Aldrich (Poole, UK). Fibronectin was from BD Biosciences (Oxford, UK). Synta 66 (dissolved in DMSO) was a generous gift from GSK Stevenage. OAG, S1P and thapsigargin (all in DMSO) and MRS2179 were from Tocris Bioscience (Bristol, UK). Ro-31-8425 (dissolved in DMSO) and human IgE myeloma (dissolved in NaCl) were from Merck Bioscience (Middlesex, UK). NP-BSA (dissolved in PBS) was from Biosearch Technologies, Inc. (Novato, USA), and human IgE anti-NP (stored at 4°C) was from ABD Serotec (Kidlington, UK).

Chapter 3: Human mast cell activation

Initial studies into human mast cell activation aimed to investigate whether FcεRI-mediated allergic activation and stimulation by GPCRs could be quantified in human mast cells using Ca^{2+} imaging and secretion assays. The entry of Ba^{2+} ions following intracellular Ca^{2+} store depletion was assessed in order to obtain preliminary data on which ion channels may be responsible for store-operated Ca^{2+} entry in human mast cells. Finally, mRNA expression for the six human TRPC channels was characterised using RT-PCR.

3.1 Assessment of different IgE/anti-IgE combinations to activate LAD 2 cells

Activation of mast cells by anti-IgE cross-linking of IgE bound to FcεRI (Cochrane & Douglas, 1974) is the best-studied mechanism of mast cell activation, and represents physiological activation by allergens (Metz & Maurer, 2007). Thus, it was firstly important to verify that LAD 2 cells do indeed secrete in response to FcεRI cross-linking as reported (Kirshenbaum *et al.*, 2003), and secondly to establish a combination of IgE/anti-IgE that reliably activates the cells. LAD 2 cells were incubated overnight with various concentrations of human IgE (0.1–3µg/ml) and stimulated with various concentrations of anti-human IgE (0.3–100µg/ml); β-hexosaminidase release was measured as described in chapter 2.8. As shown in figure 3.1a (i), anti-IgE gave rise to concentration-dependent secretion of β-hexosaminidase. Concentrations above 100µg/ml were not tested as this involved a 1 in 5 dilution from the stock solution and likely would have led to non-specific solvent effects; moreover, higher concentrations would have required un-economical amounts of anti-IgE. Increasing the concentration of IgE alone did not appear to have an effect on secretion, suggesting that FcεRI receptors are fully occupied at the lowest concentration of IgE tested. 300ng/ml human IgE was used for all future experiments.

Calbiochem anti-human IgE was then compared with Sigma anti-human IgE (used by (Shim *et al.*, 2003)); see figure 3.1a (ii). As shown, both types of anti-IgE effectively stimulated concentration-dependent β-hexosaminidase release from LAD 2 cells; with Sigma anti-IgE the curve reached a plateau at concentrations above 10µg/ml, whereas the Calbiochem anti-IgE did not appear to cause maximal release even at 100µg/ml. For this reason, and because Calbiochem anti-IgE contains 0.1% sodium azide not present in the Sigma product, Sigma anti-human IgE was used for future experiments. The sub-maximal concentration of 3µg/ml was selected for use in future studies.

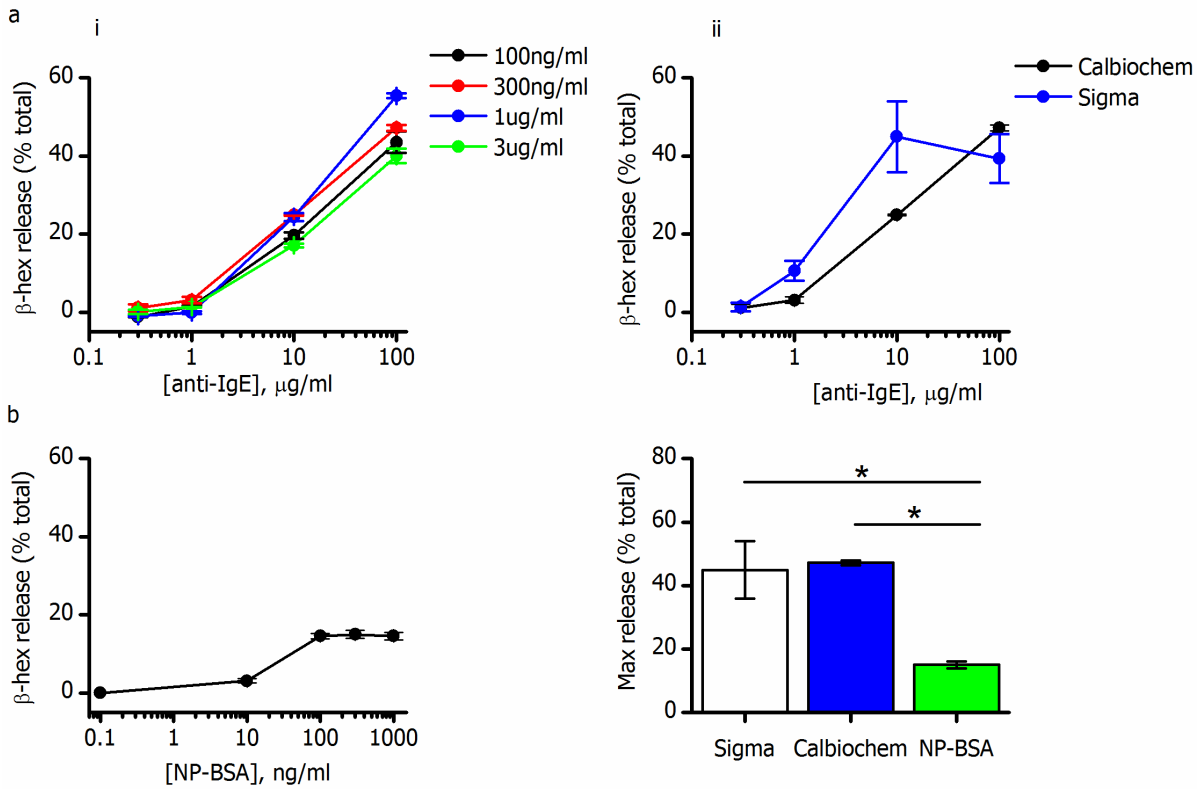

Figure 3.1. IgE-mediated β-hexosaminidase secretion in LAD 2 cells

a (i): Cells were sensitised overnight with different concentrations of human IgE (indicated by coloured lines; see legend) and stimulated with Calbiochem anti-human IgE at the concentrations shown (N=4 for 300ng/ml IgE, N=2 for all other concentrations). In (ii), cells were incubated overnight with 300ng/ml IgE and stimulated with various concentrations of Calbiochem (black) and Sigma (blue) anti-IgE (N=4). B-hexosaminidase release was measured, and is expressed as "% total"; total release was determined by lysis with 0.5% Triton X-100.

b (i): Cells were sensitised overnight with 300ng/ml human IgE anti-NP and stimulated with varying concentrations of NP-BSA, as shown. The bar chart in (ii) compares the maximal release in response to Sigma (clear bar) and Calbiochem (blue bar) anti-human IgE, and NP-BSA (green bar, N=4). *: means were significantly different, $p<0.05$, one-way ANOVA with Tukey post-test.

Experiments in part (a) were carried out by Kathryn Wareham

When the LAD 2 cell line was originally characterised, it was shown that the cells released β-hexosaminidase in response to NP-BSA cross-linking of anti-NP IgE bound to FcεRI, with a maximal release of around 40% (Kirshenbaum *et al.*, 2003). This method of stimulation was carried out in our laboratory; LAD 2 cells were incubated overnight with 300ng/ml anti-NP IgE and stimulated with various concentrations of NP-BSA before assaying for β-hexosaminidase release. As shown in figure 3.1b (i), NP-BSA elicited concentration-dependent secretion from LAD 2 cells, with maximal release of around 20%. Compared in figure 3.1b (ii) is maximal β-hexosaminidase release elicited by Calbiochem or Sigma anti-IgE, and NP-BSA. The maximal

release stimulated by NP-BSA in LAD 2 cells was approximately half of that measured in response to anti-IgE and the 40% maximal release reported previously for NP-BSA stimulation (Kirshenbaum *et al.*, 2003). For this reason, the IgE anti-NP/NP-BSA combination was not used further.

3.2 Cytosolic Ca^{2+} fluxes upon receptor activation

Cytosolic Ca^{2+} entry is an essential prerequisite for mast cell mediator secretion following FcεRI cross-linking (Cochrane & Douglas, 1974); typically this consists of Ca^{2+} release from intracellular stores, followed by entry from outside the cell across the plasma membrane (Vig & Kinet, 2009). In order to assess the contribution of different ion channels to this Ca^{2+} entry, it was investigated whether human mast cell activation led to quantifiable increases in cytosolic Ca^{2+}. LAD 2 cells were loaded with fura-2-AM, and fluorescent imaging was used as detailed in chapter 2.5 to investigate the Ca^{2+} signalling that occurs downstream of FcεRI cross-linking. Shown in Figure 3.2a (i) is Ca^{2+} entry in LAD 2 cells incubated overnight with 300ng/ml IgE and stimulated with 3µg/ml anti-IgE in the presence of extracellular Ca^{2+}; 96% of cells responded to anti-IgE application, where "responders" were classed as cells where the fluorescence ratio in the presence of anti-IgE rose by more than 10 standard deviations above the baseline fluorescence. In part (ii) no Ca^{2+} was present in the recording solution, and 81% of cells responded to anti-IgE application. Similar observations were made in three separate experiments. Figure 3.2a (iii) shows the mean Ca^{2+} entry in LAD 2 cells in the presence and absence of extracellular Ca^{2+}; when Ca^{2+} was present, LAD 2 cells showed a sustained Ca^{2+} entry phase in response to FcεRI cross-linking. In the absence of extracellular Ca^{2+}, a transient release of Ca^{2+} from intracellular stores can be seen.

This experiment was repeated on primary HLMCs; as shown in figure 3.2b, following anti-IgE application a rapid, transient Ca^{2+} release could be seen in 88% of cells in the absence of extracellular Ca^{2+}, when the same criteria to classify responding cells were used as described for LAD 2 cells. In one donor tested (donor 411), 100% of cells (n=4) responded to anti-IgE application in the absence of extracellular Ca^{2+}; 82% of cells responded in donor 410 (n=11). When extracellular Ca^{2+} was present, prolonged Ca^{2+} entry in HLMCs occurred in 100% of cells tested, corresponding to influx through plasma membrane ion channels. As similar results were obtained from two separate donors, the average traces in 3.2b (iii) were calculated using data from both donors The change in fluorescence corresponding to the size of Ca^{2+} release from stores was significantly larger in HLMCs than in LAD 2 cells (0.44±0.1 and 0.11±0.02, respectively; $p<0.0001$, unpaired Student's T-test). The reasons for this will be discussed in section 3.5.

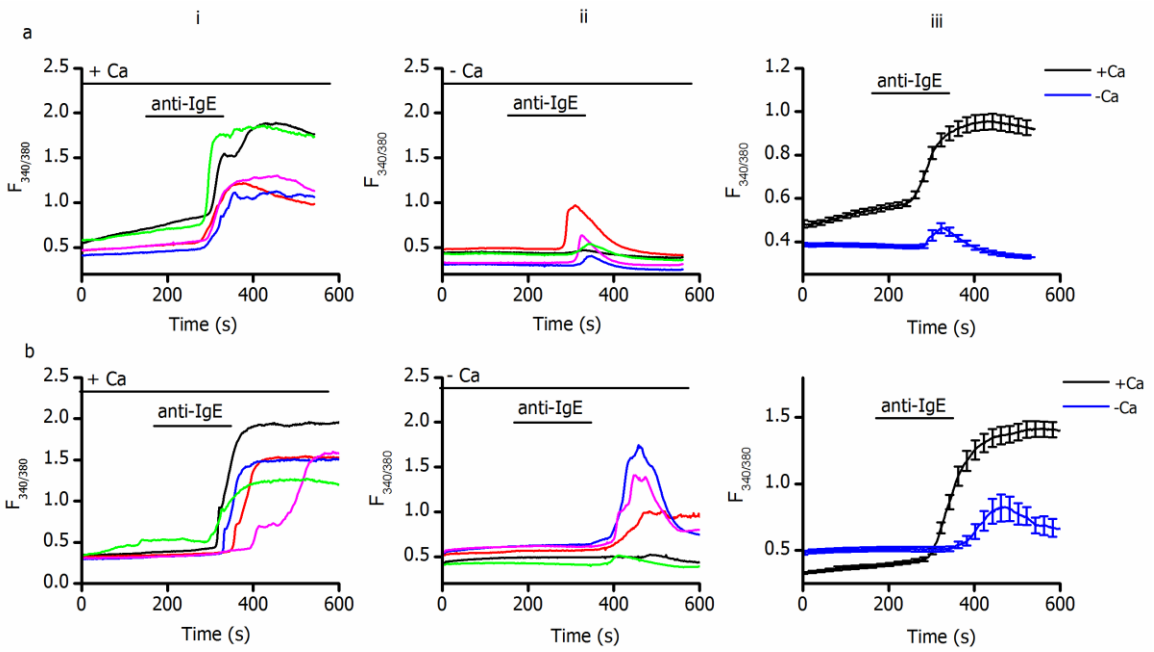

Figure 3.2. IgE-induced Ca^{2+} signals in LAD 2 cells and HLMCs

Fura 2-loaded cells sensitised overnight with 300ng/ml IgE were stimulated with 1/300 anti-IgE, which was bath applied as indicated by the horizontal bars.

a: IgE-mediated Ca^{2+} entry in LAD 2 cells, shown by $F_{340/380}$, in the presence (i) or absence (ii) of 2mM extracellular Ca^{2+}. Traces in (i) and (ii) show individual representative cells. Part (iii) shows mean ± SEM in the presence (black trace; n=75 cells, N=3 individual experiments, 96% of cells responded) or absence (blue trace; n=32, N=3, 81% of cells responded) of extracellular Ca^{2+}.

b: Experiments were carried out in HLMCs as in (a); n=30, N=4, 100% of cells responded in the presence of extracellular Ca^{2+}. n=15, N=3, 88% of cells responded in the absence of extracellular Ca^{2+}. Results are representative of 2 separate donors.

Whilst IgE-mediated signalling is an important mechanism for mast cell activation, ligands for other receptors are likely to be present *in vivo* at sites of mast cell activation. ATP is present at high concentrations at sites of inflammation and is degraded to produce ADP, AMP and adenosine (Bulanova & Bulfone-Paus, 2010). ADP has been shown to stimulate histamine release from mouse mast cells (Saito *et al.*, 1991) so could be an important stimulator of human mast cells. Of the ADP receptors $P2Y_1$, $P2Y_{12}$ and $P2Y_{13}$, the Gq-coupled $P2Y_1$ has been reported to be expressed in HLMCs (Schulman *et al.*, 1999); whilst FcεRI is coupled to PLCγ (Park *et al.*, 1991), $P2Y_1$ activation leads to PLCβ stimulation (Gilfillan & Tkaczyk, 2006). In order to explore the potential for differential coupling between receptors and Ca^{2+} signalling pathways, Ca^{2+} responses through $P2Y_1$ receptors were then investigated. Because these receptors are coupled to PLCβ, it can be hypothesised that their stimulation could lead to store-released Ca^{2+} and the downstream activation of plasma membrane Ca^{2+} channels such as TRPC channels.

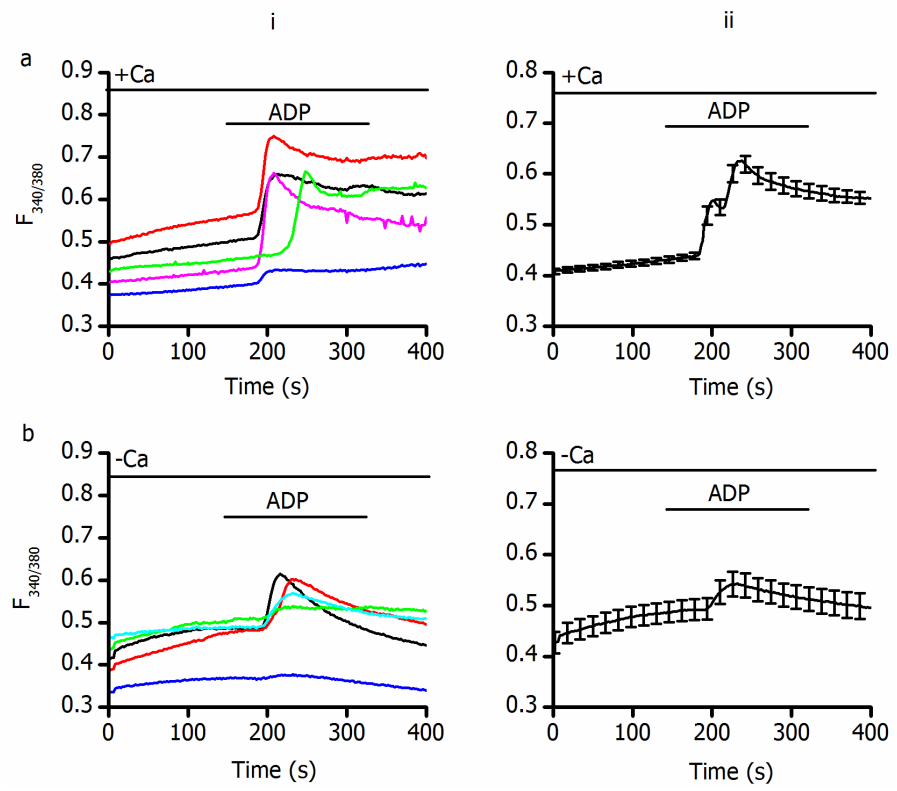

Figure 3.3. ADP-induced Ca^{2+} signals in HLMCs

Fura-2-loaded cells were stimulated with 100μM ADP in the presence (a) and absence (b) of 2mM extracellular Ca^{2+}. (i) shows individual representative cell traces. (ii) shows mean ± SEM; n=53 cells, N=8 experiments, representative of 4 donors in part (a). N=9, N=3, representative of 2 donors in part (b). 100% of cells responded to ADP application in both parts.

As shown in figure 3.3a, HLMCs show sustained Ca^{2+} entry in response to ADP stimulation of P2Y receptors when extracellular Ca^{2+} is present, corresponding to intracellular store depletion followed by prolonged influx across the cell membrane. Figure 3.3b shows Ca^{2+} fluxes in the absence of extracellular Ca^{2+}; as with IgE-mediated stimulation, HLMCs show a transient release of Ca^{2+} from intracellular stores following activation with ADP. 100% of cells responded to ADP application in the presence and absence of extracellular Ca^{2+}, when using the same criteria to classify "responders" as described above for IgE-mediated responses in LAD 2 cells and HLMCs. It is evident that there was some variability between cells in the time course of ADP responses; as shown in figure 3.3a (i), some cells displayed a rise in Ca^{2+} before others. Figure 3.3a (ii) shows mean data taken from HLMCs from four separate donors; each donor was then analysed individually to determine whether the variability was donor-dependent. Shown in figure 3.4 are ADP responses in the four different donors, represented by different coloured lines.

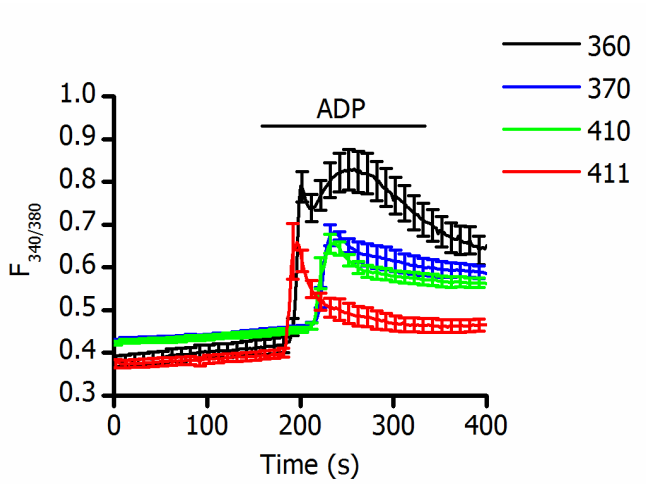

Figure 3.4. Comparison of ADP responses in HLMCs from different donors.
Data shown in figure 3.3a (ADP responses in the presence of extracellular Ca^{2+}) were separated into different donors, and average $F_{340/380}$ was calculated. Data from different donors (indicated by numbers in legend) are shown by different coloured lines; traces show mean ± SEM. n numbers are as follows: 11 for 360, 10 for 370, 15 for 410, 12 for 411.

As shown above, whilst 100% of HLMCs tested responded to ADP, there was donor-dependent variability in the size and time course of the responses. Cells from donors 370 and 410 (blue and green traces, respectively) showed a similar time-course of response, with an initial rise in intracellular Ca^{2+} followed by a small drop and a plateau phase. HLMCs from donor 360 displayed a larger initial Ca^{2+} entry peak, followed by a gradual decrease; cells from donor 411 showed an initial peak in Ca^{2+}, with a rapid decline followed by a plateau. These data demonstrate that there is donor-dependent variability in HLMC responses to ADP; this could be due to the complement of ADP receptors present, or the expression of different plasma membrane ion channels activated downstream of PLCβ. These possibilities will be explored in section 3.5.

When comparing IgE- and ADP-dependent Ca^{2+} entry in HLMCs (compare figure 3.3a with figure 3.2b), it is evident that the change in fluorescence was greater following IgE-mediated stimulation. Figure 3.5 illustrates this difference; as shown, both Ca^{2+} release from stores and Ca^{2+} influx across the membrane were significantly higher with IgE-mediated stimulation compared to ADP activation of P2Y receptors. This difference could be due to differential coupling to downstream signalling pathways and will be discussed in section 3.5.

To summarise, whilst there were differences in the Ca^{2+} signalling occurring downstream of FcεRI- and P2Y receptor-mediated HLMC activation, both mechanisms of stimulation led to store-dependent Ca^{2+} release and Ca^{2+} entry in HLMCs. The data obtained show that Ca^{2+} imaging can be used as a tool to investigate the ion channels activated downstream of receptor signalling in human mast cells; this was used later in the study to identify whether TRPC channels may be coupled to FcεRI- and P2Y- mediated signalling.

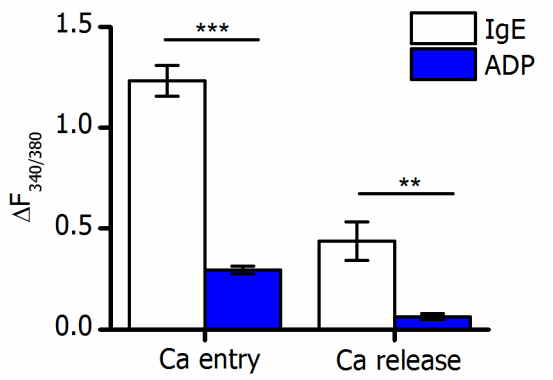

Figure 3.5. Comparison of IgE- and ADP- mediated Ca^{2+} signalling in HLMCs
Bar graph comparing IgE (white)- and ADP (blue)- stimulated Ca^{2+} entry ($\Delta F_{340/380}$ in the presence of extracellular Ca^{2+}) and release from stores ($\Delta F_{340/380}$ in the absence of extracellular Ca^{2+}). Means were significantly different, $p<0.0001$ (***) or $p<0.001$ (**), unpaired student's T-test.

3.3 $Ba^{2+}$and Ca^{2+} ion entry following store depletion in human mast cells

Having established that fura-2 imaging can be used to visualise Ca^{2+} release from intracellular stores and influx across the plasma membrane, it was possible to use a protocol of store depletion in the absence of extracellular Ca^{2+} followed by divalent ion addition, to assess the selectivity of plasma membrane channels contributing to Ca^{2+} influx. It is known that the Ca^{2+} release-activated Ca^{2+} current I_{CRAC} (Hoth & Penner, 1993) activated downstream of store depletion is mediated by Ca^{2+}- selective Orai1 channels (Feske *et al.*, 2006; Prakriya *et al.*, 2006; Vig *et al.*, 2006b); there is also strong evidence to suggest that TRPC channels, which are permeable to Ba^{2+} as well as other cations (Ma *et al.*, 2008), are activated downstream of store depletion. Ba^{2+} can be used as an experimental tool to evaluate whether channels other than Orai1, such as TRPC channels, may be activated downstream of Ca^{2+} store depletion in human mast cells. The entry of Ba^{2+} and Ca^{2+}, which can both bind to fura-2 (Schilling *et al.*, 1989), was assessed following depletion of intracellular stores by three different methods; firstly, thapsigargin was used to passively deplete intracellular stores by inhibiting Ca^{2+} re-uptake via the SERCA pump (Lytton *et al.*, 1991). Secondly, anti-IgE was used to cross-link FcεRI following overnight incubation with IgE, and finally ADP was applied to stimulate P2Y receptors, leading to downstream store depletion. Results obtained in LAD 2 cells are shown in figure 3.6; when the stores were depleted by thapsigargin, anti-IgE or ADP, a small transient rise in fluorescence could be seen, corresponding to Ca^{2+} store release. This was followed by further increases in fluorescence when Ba^{2+} or Ca^{2+} ions were added back to the external solution, showing entry of these divalent ions from the extracellular solution. When thapsigargin was used to deplete stores, 94% of cells showed an increase in fluorescence corresponding to Ba^{2+} entry; 100% responded to Ca^{2+} ion re-addition. Following FcεRI cross-linking, Ba^{2+} entry occurred in 95% of

cells and Ca^{2+} entry in 83% of cells. Interestingly, cells not responding to Ba^{2+} ion addition following FcεRI cross-linking did respond to Ca^{2+} application; this suggests that different cells may express a distinct complement of channels. Following P2Y stimulation with ADP, Ba^{2+} entry occurred in 86% of cells and Ca^{2+} entry in 96% of cells. Ca^{2+} entry occurred in 85% of the cells that did not show Ba^{2+} entry following P2Y receptor stimulation, again suggesting that the expression of TRPC and Orai channels activated downstream of store depletion may vary from cell to cell.

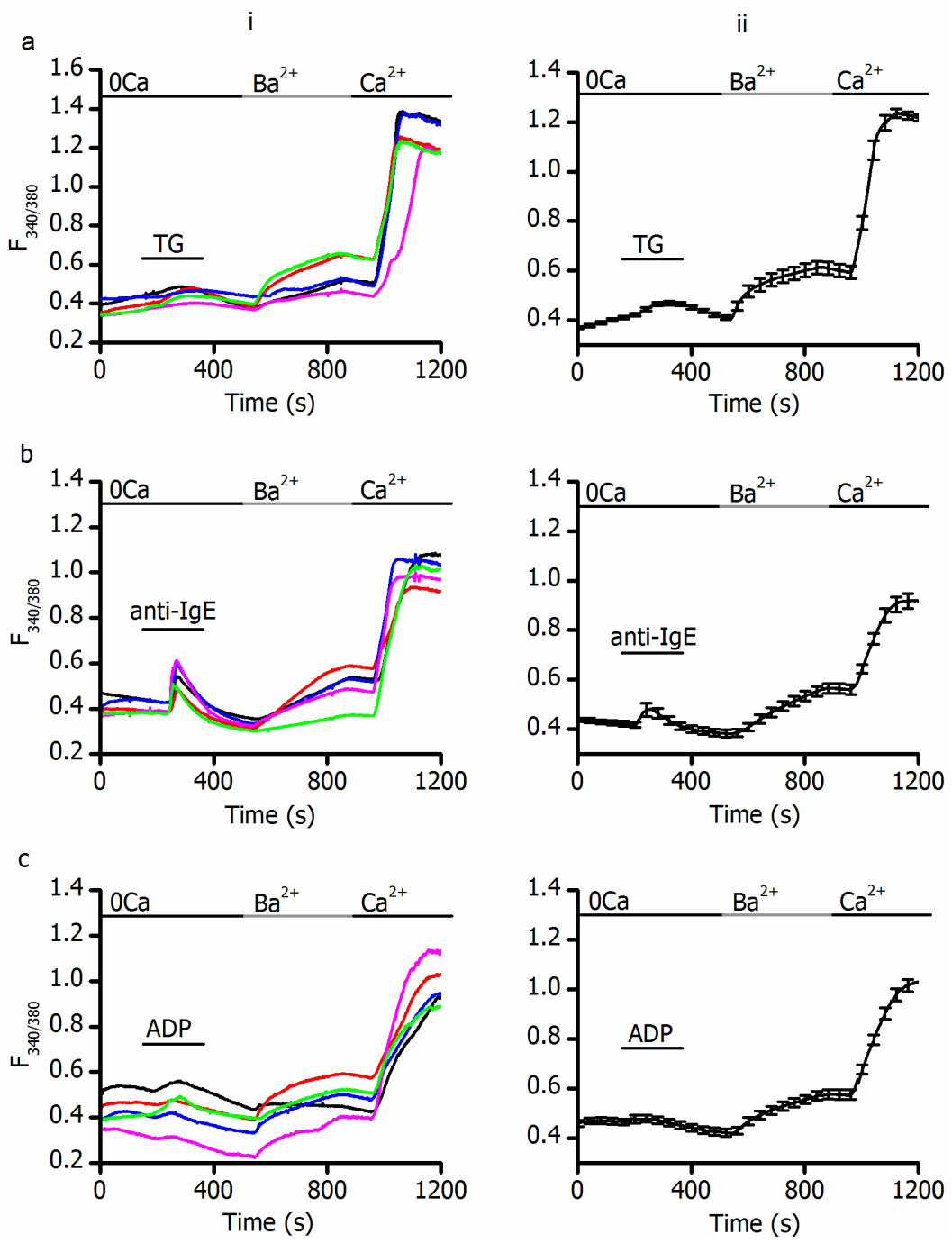

Figure 3.6. Ba^{2+} and Ca^{2+} ions enter LAD 2 cells following store depletion

Fura-2-loaded LAD 2 cells were superfused with Ca^{2+}-free external solution and stimulated with (a) 2μM thapsigargin (TG), (b) 3μg/ml anti-IgE, following overnight incubation with 300ng/ml IgE, or (c) 100μM ADP, to stimulate P2Y purinoceptors. Solutions containing 2mM Ba^{2+} or Ca^{2+} were bath-applied as indicated by the horizontal bars. In all parts, (i) shows example individual cell traces and (ii) shows mean ± SEM. n numbers are as follows; (a): n=36 cells, N=4 experiments. (b): n=40, N=4. (c): n=57 N=4.

$Ba^{2+}$and Ca^{2+}entry following intracellular store depletion was also assessed in primary HLMCs, to give an indication of which channels may be involved in SOCE in these cells. Results are shown in figure 3.7; as with LAD 2 cells, a transient Ca^{2+} entry could be seen in the absence of extracellular Ca^{2+} when the stores were depleted by thapsigargin, or by downstream signalling of FcεRI and P2Y receptors. Ba^{2+} and Ca^{2+} entry could then be observed when the ions were added to the extracellular solution. The percentage of cells where Ba^{2+} and Ca^{2+} entry occurred following store depletion was assessed in the donors tested; results are summarised in table 3.2. As with previous data, cells were classed as "responders" when the fluorescence ratio increased by more than 10 standard deviations above the baseline fluorescence when Ba^{2+} and Ca^{2+} ions were added to the solution following store depletion. In both LAD 2 cells and HLMCs, it should be noted that the time course for internal store release differed in both cell types depending on the agent used to deplete the stores; this is expected given their different modes of action, and will be discussed in section 3.5.

In both cell types, the amplitude of the Ba^{2+} component is similar under all conditions and smaller than Ca^{2+} entry; it is known that fura-2 has a lower affinity for Ba^{2+} than Ca^{2+} (K_d values of 780 and 236 , respectively) (Schilling *et al.*, 1989), meaning that fura-2 is approximately 3.3 fold more sensitive for Ca^{2+}. The change in fluorescence corresponding to Ba^{2+} and Ca^{2+} entry was assessed and the results are shown in table 3.1. In LAD 2 cells, the size of Ca^{2+} entry was around 3.5 times larger than Ba^{2+} entry following all three methods of stimulation; given the K_d values, this indicates that the size of Ba^{2+} entry was similar to Ca^{2+} entry following store depletion in LAD 2 cells. In HLMCs, however, the size of Ba^{2+} entry was similar following store depletion by the different mechanisms, but the size of Ca^{2+} entry varied. Ca^{2+} entry was less than 3.3 times greater than Ba^{2+} entry in all conditions, indicating that Ba^{2+} entry could have been greater than Ca^{2+} entry in HLMCs. It is likely that divalent ion influx through the Ba^{2+}-permeable channels represents a small component of the influx through all Ca^{2+}-permeable channels; Ba^{2+} entry would be expected to occur through TRPC channels activated downstream of store depletion only, whereas Ca^{2+} influx could occur through TRPC channels and Ca^{2+}-selective Orai channels. Ba^{2+} entry may appear greater than Ca^{2+} entry in HLMCs because Ca^{2+} is a negative regulator of both TRPC (Singh *et al.*, 2002; Shi *et al.*, 2004) and Orai (DeHaven *et al.*, 2007) channels; Ba^{2+} is a poor substrate for Ca^{2+} regulatory sites (Uvelius *et al.*, 1974; Ohya *et al.*, 1988) so cannot cause channel inhibition. This, along with the contributions of the different channels, is discussed in more detail in section 3.5.

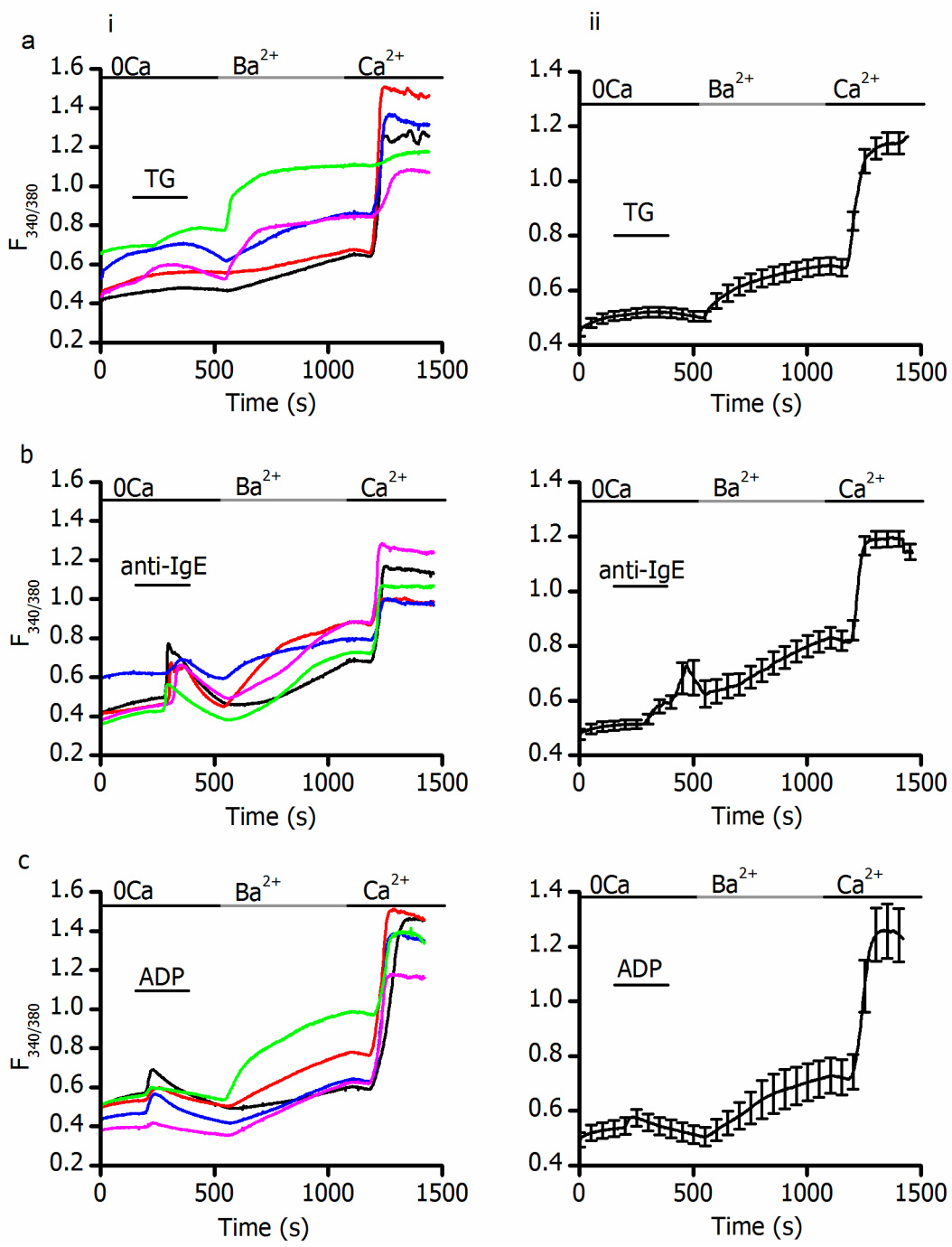

Figure 3.7. Ba^{2+} and Ca^{2+} ions enter HLMCs following store depletion

Fura 2-loaded HLMCs were superfused with Ca^{2+}-free external solution and stimulated with (a) 2μM thapsigargin (TG), (b) 1/300 anti-IgE, following overnight incubation with 300ng/ml IgE, or (c) 100μM ADP, to stimulate P2Y purinoceptors. Solutions containing 2mM Ba^{2+} or Ca^{2+} were bath-applied as indicated by the horizontal bars. In all parts, (i) shows example individual cell traces and part (ii) shows mean ± SEM. n numbers are as follows; (a): n=33 cells, N=4 experiments from 2 donors. (b): n=30, N=4, N=2 donors (c): n=9 N=3, N=2 donors.

	LAD 2 $\Delta F_{340/380}$			HLMC $\Delta F_{340/380}$		
	Ba^{2+}	Ca^{2+}	Ca^{2+}/Ba^{2+}	Ba^{2+}	Ca^{2+}	Ca^{2+}/Ba^{2+}
TG	0.186 ± 0.02	0.659 ± 0.04	3.54	0.189 ± 0.02	0.499 ± 0.05	2.64
IgE	0.142 ± 0.01	0.520 ± 0.02	3.67	0.230 ± 0.02	0.399 ± 0.03	1.73
ADP	0.146 ± 0.02	0.500 ± 0.02	3.42	0.209 ± 0.04	0.547 ± 0.04	2.62

Table 3.1. Comparison of Ba^{2+} and Ca^{2+} entry following store depletion in LAD 2 cells and HLMCs

Baseline fluorescence was subtracted from peak fluorescence in the presence of Ba^{2+} or Ca^{2+}, to give "$\Delta F_{340/380}$" corresponding to the entry of each divalent ion. $\Delta F_{340/380}$ corresponding to Ca^{2+} entry was then divided by that for Ba^{2+} entry to calculate"Ca^{2+}/Ba^{2+}" . There was no significant difference in the mean divalent ion entry elicited by the different mechanisms of store depletion in both cell types (one-way ANOVA with Tukey post-test).

	Ba^{2+} entry			Ca^{2+} entry		
	Total % responders	D1 response (%)	D2 response (%)	Total % responders	D1 response (%)	D2 response (%)
TG	88	100	79	100	100	100
IgE	80	93	69	97	93	100
ADP	89	100	80	100	100	100

Table 3.2. Ba^{2+} and Ca^{2+} entry in HLMCs following store depletion

The percentage of cells displaying Ba^{2+} or Ca^{2+} entry was assessed in HLMCs following store depletion with thapsigargin ("TG"), anti-IgE ("IgE") and ADP. D1: donor 1 (410). D2: donor 2 (411)

Following the demonstration that Ba^{2+} ions can enter both LAD 2 cells and primary HLMCs after store depletion, it was investigated whether divalent ions other than Ca^{2+}could also support human mast cells functionally. It has previously been shown that Ba^{2+} and Sr^{2+}, as well as other divalent ions, can support degranulation in RBL-2H3 cells (Hide & Beaven, 1991; Ma *et al.*, 2008), and has been suggested that TRPC channels are the carriers of these divalent ions (Ma *et al.*, 2008). The ability of different divalent ions to support degranulation has not been investigated in human mast cells; therefore, β-hexosaminidase release from LAD 2 cells stimulated via FcεRI was measured in the presence of Ca^{2+}, Ba^{2+} and Sr^{2+} ions in the extracellular solution. The results (figure 3.8) show that these divalent ions can support degranulation in LAD 2 cells stimulated via FcεRI; β-hexosaminidase release elicited by 300ng/ml NP-BSA was not significantly different in the presence of the different divalent ions. NP-BSA was used to cross-link human IgE anti-NP in this experiment as it was carried out before the comparison of IgE/anti-IgE combinations shown in figure 3.1.

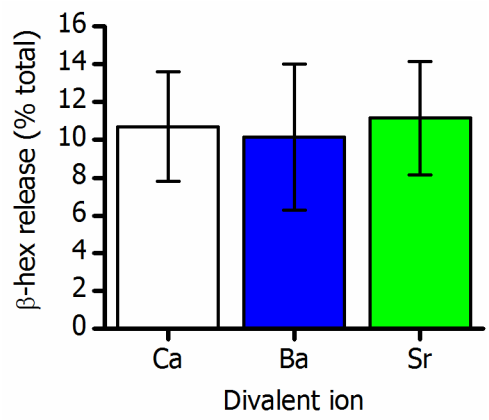

Figure 3.8. Ba^{2+} and Sr^{2+} ions can support degranulation in LAD 2 cells

LAD 2 cells incubated overnight with 300ng/ml human IgE anti-NP were stimulated with 300ng/ml NP-BSA. β-hexosaminidase release was measured and expressed as % total, which was determined by lysis with 0.5% Triton X-100. There was no significant difference in the mean β-hexosaminidase release supported by the different divalent ions (one-way ANOVA, N=4).

The observation that divalent ions other than Ca^{2+} can enter human mast cells following store depletion and support degranulation suggest that non-selective cation channels, such as TRPC channels, may contribute to Ca^{2+} entry brought about by these stimuli *in vivo*. It was therefore necessary to assess which TRPC family members are present in human mast cells.

3.4 mRNA expression for TRPC channels in human mast cells

RT-PCR was used to characterise mRNA expression of the six human TRPC channels in LAD 2 cells and HLMCs using the primers and methods detailed in chapter 2.7. As shown in figure 3.9a, it was found that LAD 2 cells express mRNA transcripts for TRPC1, 3, 5, 6 and 7, but not TRPC4. Total human brain cDNA was used as a positive control for the TRPC4 primers. Expression of some of the different TRPC channels in HLMCs varied between donors. An example band pattern for TRPC mRNA expression in one donor tested is shown in figure 3.9b; the results taken from three HLMC donors (A387, A410 and A411) are shown in table 3.3. TRPC1 and TRPC6 mRNA transcripts were found to be present in HLMCs from all donors tested; TRPC5 and 7 transcripts were present in one donor only (A387 and A410, respectively). mRNA transcripts for TRPC3 and 4 were not present in any donor tested. These results confirm that TRPC channels are expressed in human mast cells, suggesting that they could have a role in mediating the divalent ion entry reported earlier in this chapter.

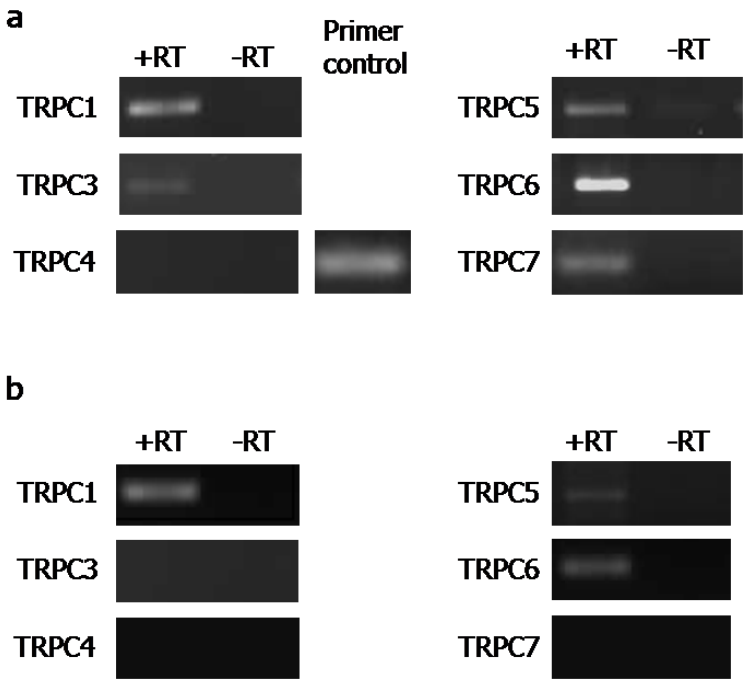

Figure 3.9. TRPC channel mRNA expression in human mast cells

RT-PCR was carried out on total RNA isolated from LAD 2 cells and HLMCs.

a: LAD 2 cells expressed mRNA for TRPC1,3, 5, 6 and 7, with band sizes corresponding to their expected size as detailed in chapter 2. "+RT" and "-RT" indicate the presence and absence of reverse transcriptase in the reaction to produce cDNA. The positive control for TRPC4 primers was total human brain cDNA.

b: Example band pattern for TRPC channel mRNA expression in one donor of HLMCs tested, expressing TRPC1, 5 and 6 mRNA.

The housekeeping gene β-actin was used as a positive control to test the integrity of all cDNA samples before PCR was carried out for the TRPC channels.

TRPC channel	mRNA expression (number of donors)
TRPC1	3/3
TRPC3	0/3
TRPC4	0/3
TRPC5	1/3
TRPC6	3/3
TRPC7	1/3

Table 3.3. Summary of TRPC mRNA expression in HLMCs

RT-PCR was carried out on samples taken from three HLMC donors (A387, A410 and A411); the table shows how many donors mRNA for each TRPC channel was expressed in.

3.5 Discussion

In the allergic response, for example in the airways of asthma sufferers, mast cells are activated by anti-IgE cross-linking of IgE bound to FcεRI (Segal *et al.*, 1977). At the time that this work was done, LAD 2 cells were the only human mast cell line reported to degranulate in response to FcεRI cross-linking (Kirshenbaum *et al.*, 2003) and were therefore a potentially good model to study IgE-mediated human mast cell activation. This preliminary part of the study aimed firstly to verify that LAD 2 cells secreted β-hexosaminidase in response to IgE receptor cross-linking, and to establish a combination of IgE/anti-IgE that reliably activates the cells. Following overnight incubation with IgE, the cells were found to secrete β-hexosaminidase in a concentration-dependent manner in response to Calbiochem anti-IgE (figure 3.1a). These data are in accordance with results obtained by Kirshenbaum *et al*. (2003) showing that LAD 2 cells released β-hexosaminidase in response to NP-BSA cross-linking of anti-NP IgE bound to FcεRI in a concentration-dependent manner, with maximal release of approximately 40%. Following FcεRI cross-linking, a complex series of intracellular signalling events leads to downstream mediator release. These signalling cascades are discussed in detail in chapter 1.2, but importantly for the release of pre-formed mediators by degranulation, the FcεRI-proximal signalling complex activates PLCγ; degranulation follows the cleavage of $PtdInsP_2$ by PLCγ to generate $InsP_3$ and DAG, which cause Ca^{2+} release from stores and PKC activation, respectively. In addition, P13K, which is activated downstream of Fyn phosphorylation, is also thought to be required for optimal degranulation (Gilfillan & Tkaczyk, 2006). As β-hexosaminidase is a marker for mast cell degranulation (Schwartz *et al.*, 1979), the results obtained in this study confirm that IgE-mediated activation of LAD 2 cells stimulates this complex signalling cascade, leading to degranulation.

Whilst LAD 2 cells degranulated in response to anti-IgE application in a concentration-dependent manner, the concentration of IgE that was used to incubate the cells overnight had little effect on the subsequent amount of β-hexosaminidase secretion. The α subunit of FcεRI is responsible for binding IgE with high affinity, and it is believed that IgE/FcεRI interaction occurs with 1:1 stoichiometry (Kinet, 1999). This, along with the previous observation that mouse serum containing low titres of IgE antibodies is able to sensitise rat mast cells (Prouvost-Danon *et al.*, 1975), suggests that low concentrations of IgE are able to sufficiently sensitise FcεRI. Additionally, it has been shown that only a fraction of FcεRI must be cross-linked to allow optimal degranulation in RBL-2H3 cells (Ortega *et al.*, 1988). Therefore, it is likely that in this study, sufficient numbers of FcεRI receptors were occupied with IgE at all concentrations tested.

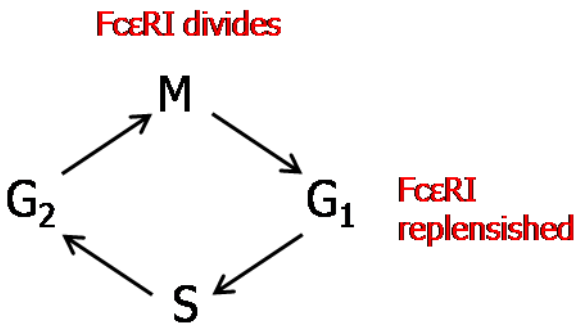

Figure 3.10. FcεRI variation in the cell cycle

Receptors are equally divided between daughter cells in mitosis (M), resulting in a 50% decrease in the number of receptors per cell. Receptors are then replenished in G_1 phase, the gap that occurs before DNA synthesis (S phase). Levels then remain constant through gap 2 (G_2), until they are halved again at M phase (Furuichi *et al.*, 1985).

It has previously been shown using RBL-2H3 cells that FcεRI stability on the mast cell surface is dependent on the binding of IgE. In the absence of IgE, receptors are divided between daughter cells during mitosis, and are replenished in the G_1 stage of the cell cycle (Furuichi *et al.*, 1985); figure 3.10 illustrates this process. When cells are not dividing, however, FcεRI receptors are rapidly lost from the cell surface. In the presence of IgE this loss does not occur (Furuichi *et al.*, 1985); this is thought to be due to the protection of FcεRI degradation by bound IgE (Kinet, 1999). Whilst it has not been investigated whether this IgE-mediated increase of FcεRI surface expression is concentration-dependent, it is reasonable to conclude that all concentrations of IgE tested in this study were sufficient to bind FcεRI on the surface of LAD 2 cells, protecting the receptors from degradation and allowing cross-linking when the cells were stimulated with anti-IgE.

Anti-human IgE from Calbiochem was then compared with Sigma anti-human IgE, which has previously been used to stimulate histamine release from basophils at a concentration of 2μM (Shim *et al.*, 2003), in order to select the most appropriate to use in future experiments. When looking at the concentration-response curves (figure 3.1a (ii)), it appears that the Calbiochem anti-IgE curve is shifted to the right when compared with the Sigma version; this could be because the latter has a higher affinity for IgE, therefore lower concentrations were required to achieve β-hexosaminidase release compared to the Calbiochem version. The bell-shaped concentration response curve seen in response to Sigma anti-IgE is consistent with results obtained previously using the LAD 2 cell line (Kirshenbaum *et al.*, 2003) and mouse mast cells (Gimborn *et al.*, 2005). The phosphatase SHIP has been implicated in the reduction of IgE-dependent secretion at supra-optimal concentrations of anti-IgE; BMMCs from SHIP-deficient mice have been reported to be more susceptible to antigen-induced degranulation than those from WT mice (Huber *et al.*, 1998), and basophils from hyper-allergic patients contain lower

levels of SHIP than those from healthy individuals (Vonakis *et al.*, 2001). It has been suggested that SHIP is weakly activated at optimal mast cell stimulation levels, whereas at supra-optimal concentrations of anti-IgE it is more strongly activated, thus is able to negatively regulate degranulation. In support of this theory, SHIP1 has been reported to be more strongly phosphorylated following supra-optimal activation, compared to optimal stimulation (Gimborn *et al.*, 2005). In this study, it is possible that when 10µg/ml Sigma anti-IgE was used to cause maximal degranulation, SHIP was weakly activated; when the concentration of anti-IgE was increased to 100µg/ml, however, this could have resulted in SHIP becoming more strongly activated and the concomitant small reduction in degranulation. If the concentration of anti-IgE was increased above 100µg/ml in this study, degranulation would be expected to decrease further due to SHIP and other negative regulators such as the actin cytoskeleton (Gimborn *et al.*, 2005) becoming more strongly activated; although beyond the remit of this study, this would be an interesting avenue for further investigation.

Another difference between the two types of anti-IgE tested was that Calbiochem anti-IgE contained ≤0.1% sodium azide. Although this is a very low concentration, sodium azide is known to cause cell death (Sato *et al.*, 2008), therefore might be expected to have toxic effects when applied to cells. For this reason, and because the concentration-response curve did not reach a plateau with Calbiochem anti-IgE, Sigma anti-human IgE was chosen as the ligand.

In the initial characterisation of the LAD 2 cell line, NP-BSA was used to crosslink human IgE anti-NP bound to FcεRI and stimulate β-hexosaminidase release, with a maximal release of approximately 40% (Kirshenbaum *et al.*, 2003). However, the maximal release measured in this study in response to NP-BSA was around 20%, compared with 40% reported previously (Kirshenbaum *et al.*, 2003). Release observed in this study could be lower than that obtained by Kirshenbaum *et al.* (2003) due to phenotypic variation. It has previously been reported that LAD 2 cells have an unstable phenotype in culture compared to terminally differentiated primary mast cells (Laidlaw *et al.*, 2011); for example, c-kit expression is down-regulated in response to IL-4 in LAD 2 cells, whereas its expression is stable in mature skin mast cells (Thienemann *et al.*, 2004). In addition, FcεRI expression is known to vary in a cell-cycle dependent manner, as discussed above and shown in figure 3.10. It has been shown that RBL-2H3 cells tightly regulate I_{CRAC} currents as they progress through the cell cycle; currents are up-regulated in S phase during chromatin duplication, and strongly suppressed during mitosis (Tani *et al.*, 2007). It is possible that similar cell cycle-dependent variations in I_{CRAC} and other currents could occur in LAD 2 cells. It is therefore possible that cell cycle- or passage number-dependent down-regulation of FcεRI, ion channels or other components of the signalling cascade could have occurred in the LAD 2 cells used in this study compared with those used by Kirshenbaum *et al.* (2003); this would account for the reduced β-hexosaminidase secretion.
It is also evident that spontaneous release, which was subtracted from all values, was higher in this study; this was measured at an average of 14% in this study (n=6), whereas Kirshenbaum

et al. (2003) report very low spontaneous release (2-3%). Technical differences in the assay conditions could account for the higher spontaneous release observed in our laboratory. For example, although in both laboratories a HEPES-buffered NaCl- based assay buffer was used, there were differences in composition. Whilst the buffer used in our laboratory contained 2mM $CaCl_2$ and 1mM $MgCl_2$, that used by Kirshenbaum *et al*. (2003) had 1.8mM $CaCl_2$ and 1.3mM $MgSO_4$ (Woolhiser *et al.*, 2001). Therefore, minor experimental differences or passage number-dependent phenotypic changes may have been responsible for the higher spontaneous release in our laboratory; subtracting higher values would thus result in reduced secretion levels in response to NP-BSA.

When comparing the results obtained in this study (summarised in figure 3.1b (ii)), it is apparent that the maximal release in response to anti-IgE was approximately double that elicited by NP-BSA. These assays were carried out using the same protocol and similar passage numbers of LAD 2 cells, therefore differences cannot be explained by differences in procedure or phenotypic changes. The difference in secretion seen between the two ligands is likely to be due to their mechanisms of action. Whilst the anti-IgE used in this study is an IgG antibody produced in goat to specifically react with the heavy chain of IgE antibodies, NP-BSA is a synthetic hapten-protein conjugate. The use of hapten-protein conjugates to study immunology was pioneered in the early 20th century by Karl Landsteiner, who showed that small molecules can elicit an immune response in rabbits when attached to larger proteins (Landsteiner & Simms, 1923). Hapten-protein conjugates have different cross-linking potentials depending on a number of factors, including valency between hapten and carrier protein, avidity of bonds, number of hapten molecules attached per carrier and size of carrier protein (Oda *et al.*, 2004). In addition, hapten-protein conjugates are a mixture of molecules with different numbers of haptens per carrier, resulting in a heterogeneous mix (Oda *et al.*, 2009). The NP-BSA used in this study had an average of 16 NP molecules per BSA (NP_{16}-BSA); a previous study reported that NP_{19}-BSA has an avidity of 1.4×10^8 for interaction with antibody when interactions were measured using surface plasmon resonance with an immobilised antibody, and analysed using a Scatchard plot (Oda *et al.*, 2009). Whilst caution should be applied due to the heterogeneity of NP-BSA molecules in suspension, it is likely that the NP-BSA used in this study had a similar avidity value to that reported by Oda *et al*. (2009). Whilst data is not available regarding the avidity of the Anti-IgE used in our laboratory, a higher value could account for its increased propensity to induce degranulation. The heterogeneous nature of NP-BSA could also account for the differences in results obtained in this study and those reported by Kirshenbaum *et al*. (2003) where NP-BSA was the stimulus for LAD 2 degranulation.

Having established an appropriate combination of IgE/anti-IgE to activate human mast cells, Ca^{2+} imaging was then used to demonstrate that quantifiable changes in intracellular Ca^{2+} could be measured following FcεRI cross-linking. Whilst the signalling events that occur immediately after receptor cross-linking are common for all types of mediators, those further downstream

diverge to regulate the release of different mediators (Gilfillan & Tkaczyk, 2006). The signalling pathways are detailed in chapter 1.2; importantly for Ca^{2+} entry, cross-linked FcεRI receptors aggregate into lipid raft microdomains in the plasma membrane (Field *et al.*, 1999), where the formation of macromolecular signalling complexes occurs, which trigger downstream release of different mediators. Importantly for granule-associated mediators, PLCγ is activated (Zhang *et al.*, 2000), which catalyses the production of DAG and $InsP_3$ from PtdIns(4,5)P_2 (Gilfillan & Tkaczyk, 2006); $InsP_3$ binds its receptor in the endoplasmic reticulum and causes transient Ca^{2+} release from intracellular stores. This could be seen in fura-2-loaded LAD 2 cells and HLMCs in this study; IgE receptor cross-linking led to a small rise in fura-2 fluorescence in the absence of extracellular Ca^{2+}, corresponding to release from intracellular stores (figure 3.2a (ii) and b (ii)).

Ca^{2+} release from stores is sensed by STIM1 (Stathopulos *et al.*, 2006); the activation of plasma membrane Ca^{2+} channels then follows, leading to a sustained increase in cytosolic Ca^{2+} (Hoth & Penner, 1992), which is essential for mast cell degranulation (Cochrane & Douglas, 1974). Ca^{2+} entry could be seen in fura-2-loaded LAD 2 cells and HLMCs in this study; FcεRI cross-linking in the presence of extracellular Ca^{2+} led to a sustained increase in fluorescence, indicative of Ca^{2+} entry from outside the cell. It has recently been shown that Orai1 mediates I_{CRAC}, the first identified and most well-characterised store-operated Ca^{2+} current (Feske *et al.*, 2006; Prakriya *et al.*, 2006; Vig *et al.*, 2006b); studies using knock-out mice have shown that Orai1 is essential for FcεRI-induced mast cell degranulation, cytokine production and lipid mediator release (Vig *et al.*, 2008). Other work, detailed in chapter 1.3.2, suggests that plasma membrane TRPC channels are activated downstream of intracellular store depletion. Therefore, store-operated Ca^{2+} entry in human mast cells following FcεRI cross-linking may be occurring through a combination of Orai1 channels and store-operated TRPC channels; this hypothesis is explored later in this chapter, and in chapter 5.

In addition to the store-operated Ca^{2+} channels activated following the Lyn-LAT-PLCγ cascade, evidence exists for the requirement of an initial Ca^{2+} influx that is not controlled by store depletion for full mast cell activation (Lee & Oliver, 1995). BMMCs from Fyn-deficient mice are unable to fully degranulate, an effect that is restored by the Ca^{2+} ionophore A23187 (Parravicini *et al.*, 2002; Sanchez-Miranda *et al.*, 2010); these cells also exhibit defective Ca^{2+} entry in response to FcεRI cross-linking but not thapsigargin (Sanchez-Miranda *et al.*, 2010), suggesting that SOCE is unaffected by Fyn knockout, but receptor-operated Ca^{2+} entry is reduced. As the Fyn- controlled channels were sensitive to 2-APB, and TRPC3/6/7 channels were shown to associate with Fyn in WT BMMCs, the authors concluded that non store-operated TRPC channels from the TRPC3/6/7 subfamily are activated downstream of FcεRI cross-linking via Fyn kinase, to provide Ca^{2+} influx necessary for optimal degranulation. The Fyn-dependent complementary activation pathway has not yet been evaluated in human mast cells; it would be insightful to investigate whether Fyn knock-out has similar effects as those observed in mouse BMMCs. It is also possible that the DAG-operated TRPC channels could be activated downstream of the LYN-

LAT-PLCγ signalling cascade described above following FcεRI cross-linking, as DAG is produced by PLCγ. The contribution of TRPC3/6/7 channels to Ca^{2+} entry and mediator release downstream of FcεRI cross-linking was assessed later in this study and is discussed in chapter 6.

It is evident that both Ca^{2+} store release and entry are bigger in HLMCs than in LAD 2 cells; as discussed previously, this could be due to lower levels of FcεRI present in LAD 2 cells due to cell cycle-dependent regulation. It has been reported that tryptase and chymase expression in mast cells is dependent on the level of differentiation; terminally differentiated skin mast cells contained higher levels of these enzymes than the less mature LAD 2 cells (Guhl *et al.*, 2010). It is possible that LAD 2 cells contain lower levels of FcεRI than those present in terminally differentiated HLMCs, which could account for activation of downstream signalling molecules to a lesser degree, and reduced Ca^{2+} release and entry as a result. It has been reported that B cells exhibit maturation stage-dependent differences in Ca^{2+} signalling downstream of B cell antigen receptor activation at various stages of the signalling cascade, including Lyn phosphorylation, PLCγ levels and phosphorylation of adaptor proteins (Benschop *et al.*, 2001). Reduced levels of the signalling molecules activated downstream of FcεRI in LAD 2 cells compared to HLMCs would account for the decreased Ca^{2+} entry seen in figure 3.2. It is also possible that different ion channels account for the Ca^{2+} entry in the two different cell types; different combinations of the six human TRPC channels and the three isoforms of Orai would lead to channels with altered conductance. Orai1-mediated currents have an estimated single channel conductance of around 30 femtosiemens (Hogan *et al.*, 2010) compared with 16 picosiemens for TRPC1 (Rychkov & Barritt, 2007) and 28-37 picosiemens for TRPC6 (Dietrich & Gudermann, 2007); therefore TRPC channels activated downstream of FcεRI would be expected to effect greater Ca^{2+} entry than Orai channels. RT-PCR results (figure 3.9) in this study showed that TRPC channel expression varies between LAD 2 cells and HLMCs; for example, mRNA for TRPC3 was expressed in LAD 2 cells but was not present in HLMCs. It is therefore possible that a different complement of channels mediates FcεRI-induced Ca^{2+} entry in the two different cell types, resulting in different levels of Ca^{2+} entry.

In summary, the results obtained using fura-2 imaging showed that Ca^{2+} entry can be measured in human mast cells following FcεRI cross-linking. It is likely that a variety of ion channels, possibly including TRPC channels, are activated downstream of IgE-mediated stimulation. In order to explore the potential for differential coupling between receptors and Ca^{2+} signalling in HLMCs, Ca^{2+} responses downstream of PLCβ-coupled GqPCRs were then investigated using ADP stimulation of $P2Y_1$ receptors. ADP application stimulated Ca^{2+} entry; this is in agreement with previous results showing that $P2Y_1$ receptors are expressed in HLMCs (Schulman *et al.*, 1999). In contrast to FcεRI signalling, stimulation of GPCRs promotes the exchange of GDP bound to G_α subunits of trimeric G proteins ($G_{\alpha\beta\gamma}$) for GTP, which results in the activation of G_α and $G_{\beta\gamma}$ subunits. These activated G protein components then activate downstream signalling in mast cells (Bansal *et al.*, 2008). Whilst GPCR signalling in mast cells is not as well characterised as that

occurring downstream of FcεRI, it is known that $P2Y_1$ receptors are coupled to PLCβ and the generation of $InsP_3$ (Gilfillan & Tkaczyk, 2006). $InsP_3$ production leads to Ca^{2+} release from stores and subsequent entry from outside the cell (Communi *et al.*, 2000); in this study Ca^{2+} release from stores could be seen when ADP was applied in the absence of extracellular Ca^{2+} (figure 3.3b), and influx through plasma membrane ion channels occurred when extracellular Ca^{2+} was present (figure 3.3a). These data are in accordance with a previous study showing that ADP stimulates Ca^{2+} influx in cord blood-derived human mast cells (Feng *et al.*, 2004). Whether the combination of ion channels regulating Ca^{2+} influx following GPCR activation and FcεRI remains to be determined.

When looking at the size and time-course of ADP-induced Ca^{2+} entry in HLMCs, it is evident that there was donor-dependent variability. HLMCs from donors 370 and 410 showed a similar time-course of response, with an initial rise in intracellular Ca^{2+} followed by a plateau; the plateau is likely to represent Ca^{2+} entry across the plasma membrane downstream of $P2Y_1$ and PLCβ activation. The time-course of Ca^{2+} entry in donors 370 and 410 was similar to that reported by Feng *et al.* (2004) in human cord blood-derived mast cells, where $P2Y_1$ receptors were shown to be responsible. In donors 360 and 411, a larger initial Ca^{2+} peak could be seen; this could be due to $P2X_1$ receptor activation. $P2X_1$ receptors are Ca^{2+}-permeable ligand-gated ion channels with characteristic fast opening and rapid declining of the current in the presence of agonist in a process called desensitisation (North & Surprenant, 2000). ADP has been suggested to activate $P2X_1$ receptors, which are functionally expressed in HLMCs (Wareham *et al.*, 2009), with an EC_{50} of 30μM (Evans *et al.*, 1995; North & Surprenant, 2000); a concentration of 100μM ADP might therefore be expected to activate these receptors. A more recent study reported that $P2X_1$ receptors in megakaryocytes are activated by commercially obtained ADP at a concentration of 10μM, but not by purified ADP at concentrations up to 100μM (Mahaut-Smith *et al.*, 2000). The authors suggest that contamination by ATP is responsible for the activation of $P2X_1$ receptors by commercial samples of ADP. As the ADP used in this study is certified to be ≥95% pure, it is possible that contaminating ATP, which activates $P2X_1$ receptors with an EC_{50} of around 1μM (North & Surprenant, 2000),was present at a sufficient concentration to activate these receptors in this study. It is possible that donor-dependent expression of $P2X_1$ receptors was responsible for the more rapid Ca^{2+} entry seen in donors 360 and 411 compared with those from donors 370 and 410.

Differential expression of P2Y receptors could also account for the donor-dependent variability in ADP-induced Ca^{2+} entry shown in figure 3.4. ADP is able to activate $P2Y_1$,$P2Y_{12}$ and $P2Y_{13}$ (von Kugelgen, 2006); whilst $P2Y_1$ couples to Gq proteins and PLCβ, $P2Y_{12}$ and $P2Y_{13}$ are coupled to Gi proteins (Communi *et al.*, 2001; Nicholas, 2001), causing downstream inhibition of cyclic adenosine monophosphate (cAMP) production. Therefore, donor-dependent expression of the different ADP-sensitive P2Y receptors could elicit distinct downstream responses, giving rise to the differences observed in Ca^{2+} signalling.

As discussed above in relation to FcεRI-induced Ca^{2+} signalling, the complement of ion channels activated downstream of P2Y receptor stimulation may also vary between donors. It is known that the levels of $InsP_3$ fall quickly following elevation downstream of P2Y receptors, because P2Y receptors rapidly desensitise (Chang *et al.*, 2007). Ca^{2+} influx through $InsP_3$-regulated channels, including Orai1 (Feske *et al.*, 2006; Prakriya *et al.*, 2006; Vig *et al.*, 2006b) and possibly store-operated TRPC channels (Ong *et al.*, 2007; Liao *et al.*, 2008; Ma *et al.*, 2008), is likely to be transient because incoming Ca^{2+} is taken up into ER stores and not released again in the absence of $InsP_3$ (Chang *et al.*, 2007). Ca^{2+} entry through ion channels that are not dependent on $InsP_3$, for example the DAG-activated TRPC3/6/7 channels, could be more sustained; differential ion channel expression between donors could therefore account for the differences in the size and time course of Ca^{2+} entry seen downstream of ADP stimulation. Previous studies carried out in RBL-2H3 cells have suggested that Orai1-mediated I_{CRAC} activated downstream of receptor stimulation is an all-or-nothing event in single cells; increasing agonist concentration was reported to increase the number of responding cells and not the size of Ca^{2+} entry, giving rise to a graded response in the population of cells (Chang *et al.*, 2007). It is possible that I_{CRAC} activation downstream of P2Y receptor stimulation in this study occurred in a greater number of HLMCs from some donors compared with others, causing the differences in amplitude and time course of the Ca^{2+} signals shown in figure 3.4. Whilst outside the aims of this project, investigation of the all-or-nothing nature of I_{CRAC} currents in human mast cells would provide insightful information on the channels activated downstream of P2Y receptor activation.

It is evident that both Ca^{2+} store release and entry are larger in HLMCs following FcεRI cross-linking than following ADP stimulation (see figure 3.5). This is likely to be due to differential downstream coupling of the two classes of receptor. Following GqPCR activation, soluble PLCβ enzymes are attracted to $PtdIns(4,5)P_2$ in the membrane by their phosphoinositide binding domain and by activated G_{α}-GTP (Falkenburger *et al.*, 2010); PLCγ is regulated by key tyrosine residues in LAT, which is activated following FcεRI cross-linking (Saito *et al.*, 1991). Additional Src homology domains in PLCγ that are not present in PLCβ mediate its interaction with phosphorylated tyrosine residues (Wilde & Watson, 2001). Different phosphoinositides are maintained in distinct membrane compartments by the subcellular distribution of kinases and phosphatases; for example, $PtdIns(4,5)P_2$ is maintained by high PIP 5-kinase activity, which preserves its phosphorylated state (Mao & Yin, 2007). Two isoforms of PIP 5-kinase have been shown to synthesise distinct pools of $PtdIns(4,5)P_2$ in the membrane, which have separate roles in SOCE and $InsP_3$ generation (Vasudevan *et al.*, 2009). The pools of $PtdIns(4,5)P_2$ are thought to be spatially segregated by membrane heterogeneity and the degree of lipid order (Calloway *et al.*, 2011). It is possible that these distinct pools of $PtdIns(4,5)P_2$ react with PLCβ and PLCγ, thus targeting them to different regions of the membrane where they can regulate specific Ca^{2+} channels. Ca^{2+} channels are located at discrete regions of the plasma membrane within specialised lipid raft microdomains; for example TRPC1 interacts directly with caveolin 1, which regulates its plasma membrane localisation (Brazer *et al.*, 2003). Many other Ca^{2+} channels,

including the other TRPC channels, Orai1 channels and voltage-gated Ca^{2+} channels (Pani & Singh, 2009), have been shown to localise in distinct plasma membrane regions. It has recently been shown that PtdIns(4,5)P_2 in ordered lipid membrane regions promotes STIM1-Orai1 association, whereas PtdIns(4,5)P_2 in disordered lipid regions inhibits this association (Calloway *et al.*, 2011). It is therefore likely that PLCβ and PLCγ are targeted to specific regions of the membrane, where they act on discrete pools of PtdIns(4,5)P_2 to activate distinct channels, giving rise to the differences in Ca^{2+} signalling seen following FcεRI- or ADP- mediated activation.

Distinct downstream regulatory mechanisms could also account for the larger Ca^{2+} release and entry seen in FcεRI-stimulated HLMCs compared with ADP-mediated activation. Regulator of G protein signalling (RGS) proteins are expressed in mast cells and impair G protein signalling by accelerating GTPase activity and the deactivation of G proteins; RGS13 has been shown to be particularly important in restricting GPCR-mediated Ca^{2+} entry in HMC-1 cells (Bansal *et al.*, 2008). FcεRI-mediated mast cell activation is known to be negatively regulated by NTAL (Zhu *et al.*, 2004) and LYN (Gilfillan & Tkaczyk, 2006). These distinct regulatory mechanisms could account for the reduction in Ca^{2+} store release and entry seen in response to P2Y activation compared with that observed downstream of FcεRI.

In summary, fura-2 Ca^{2+} imaging can be used to measure ADP- and FcεRI-mediated Ca^{2+} release and entry in human mast cells. Due to the distinct downstream coupling of the two receptors as a result of spatial regulation in the plasma membrane, it is likely that different ion channels are activated as a result of P2Y and FcεRI stimulation.

In order to gain further insight into which ion channels may be involved in store-operated Ca^{2+} entry in human mast cells, a protocol of Ca^{2+} store depletion in the absence of extracellular Ca^{2+}, followed by divalent ion re-addition, was employed. Following passive store depletion by thapsigargin (Lytton *et al.*, 1991), FcεRI cross-linking and ADP stimulation of P2Y receptors in this study, Ba^{2+} and Ca^{2+} ions entered LAD 2 cells and HLMCs (figures 3.6 and 3.7). It is apparent that the time course for internal store release differed depending on the agent used to deplete the stores in both LAD 2 cells and HLMCs. This is expected given the different mechanisms of action of the agents used. In both cell types, thapsigargin application resulted in a small, slow Ca^{2+} release from stores; this agent works by inhibiting Ca^{2+} re-uptake into stores through the SERCA pump (Lytton *et al.*, 1991). Stores are therefore prevented from re-filling as opposed to being actively depleted; as a result the time-course for depletion is slow, as seen in figures 3.6a and 3.7a. Anti-IgE, on the other hand, resulted in a more transient, quick release from stores; this is consistent with the activation of PLCγ (Park *et al.*, 1991), production of $InsP_3$, and depletion of stores by $InsP_3$ receptor binding (Gilfillan & Tkaczyk, 2006). ADP-induced Ca^{2+} store release was quicker in onset than that induced by thapsigargin; this is likely to be due to the activation of PLCβ (Gilfillan & Tkaczyk, 2006) and the resulting production of $InsP_3$ causing store release. The size of Ca^{2+} release downstream of P2Y receptor stimulation was smaller than

that caused by FcεRI cross-linking; this is likely to be due to the differential coupling of the two types of receptor and resulting differences in downstream signalling, as discussed above. $InsP_3$ generation depends on the availability of PtdIns(4,5)P_2, which is generated primarily by the phosphorylation of phosphatidylinositol-4-phosphate (PI4P) by the lipid kinase phosphatidylinositol 4-phosphate 5-kinase (PIP5 kinase) (Wang *et al.*, 2008). PtdIns(4,5)P_2 levels are therefore regulated by a number of factors; different levels of this enzyme at particular regions of the membrane targeted by PLCβ and PLCγ could result in differential production of $InsP_3$ depending on the isoform of PLC that is active, causing store depletion to a greater degree with FcεRI-mediated PLCγ stimulation than P2Y-mediated PLCβ activation, for example.

It is also possible that human mast cells contain greater levels of PLCγ than PLCβ, which could result in the production of more $InsP_3$ and causing greater levels of store depletion. It has previously been reported that different isoforms of PLCγ and PLCβ in bovine parathyroid gland are expressed at varying levels (Dare *et al.*, 1998); human mast cells express two isoforms of PLCγ, with PLCγ_1 believed to be the main active form (Wilde & Watson, 2001; Tkaczyk *et al.*, 2003). The expression of PLCβ isoforms in mast cells has not been investigated, but it can be hypothesised that differential expression of PLCβ and PLCγ isoforms with different catalytic abilities for the generation of $InsP_3$ would lead to differing levels of store depletion dependent on the isoforms present. An assessment of the levels of different PLC enzymes in HLMCs using quantitative PCR, for example, would be an interesting avenue of investigation to gain insight into the mechanisms of store depletion occurring following GPCR and receptor tyrosine kinase activation.

Despite the differences seen in the time-course of initial Ca^{2+} store release, there was no significant difference in the size of divalent ion entry in both cell types when different methods of activation were used, suggesting that store depletion was the primary factor controlling channel activation. The results obtained in this study are in agreement with a previous study showing that Sr^{2+}ions were able to enter RBL-2H3 cells following store depletion (Ma *et al.*, 2008). The authors reported that shRNA-mediated knockdown of TRPC5 impaired Sr^{2+} entry following store depletion with thapsigargin, concluding that TRPC5 is likely to be a component of store-operated Ca^{2+} channels in RBL-2H3 cells. The results obtained in this study suggest that channels other than Ca^{2+}-selective Orai1 channels may be involved in SOCE, such as the non-selective TRPC channels. Results from previous studies recording I_{CRAC} currents in RBL cells and Jurkat T cells challenge the view that Orai channels cannot permeate Ba^{2+} ions, showing that equimolar replacement of Ca^{2+} ions with Ba^{2+} in the extracellular recording solution leads to a reduction, but not complete inhibition, of the I_{CRAC} current (Hoth, 1995; Zweifach & Lewis, 1995). However, these results were obtained in solutions where both Na^+ and Ba^{2+} were present; a recent study showed that replacement of Ca^{2+} with Ba^{2+} ions when Na^+ ions were replaced with TEA caused abolition of I_{CRAC} currents mediated by Orai1, 2 and 3 in HEK-293 cells (Lis *et al.*, 2007). The authors re-examined Ba^{2+} permeation of I_{CRAC} in Jurkat T cells in the presence and absence of

Na^+, reporting that currents are inhibited in the absence of Na^+. It was concluded that I_{CRAC} currents are abolished when Ba^{2+} is the sole charge carrier, and that Na^+ ions carry the current observed in the absence of Ca^{2+} previously thought to be mediated by Ba^{2+}(Lis *et al.*, 2007). Many studies have demonstrated that TRPC channels can readily permeate Ba^{2+} ions, including but not limited to (Trebak *et al.*, 2002; Ma *et al.*, 2008; DeHaven *et al.*, 2009; Tu *et al.*, 2009b; Bousquet *et al.*). Therefore, the Ba^{2+} entry seen in this study is unlikely to be through Orai channels, suggesting a role for the nonselective TRPC channels in SOCE.

It is also unlikely that TRP channels other than those from the TRPC family contribute to Ba^{2+} entry in this study, although TRPV (Bradding *et al.*, 2003) and TRPM (Bradding *et al.*, 2003; Wykes *et al.*, 2007) channel mRNA transcripts are expressed in HLMCs. Most other TRP channels would not be activated downstream of Ca^{2+} store depletion; for example, TRPV channels are activated by heat and capsaicin (Pingle *et al.*, 2007) and TRPA channels are sensitive to irritants and pungent compounds (Garcia-Anoveros & Nagata, 2007). TRPV6 can be constitutively active, but is highly Ca^{2+} selective and does not permeate Ba^{2+} or Sr^{2+} so would be unable to mediate Ba^{2+} entry downstream of Ca^{2+} store depletion (Wissenbach & Niemeyer, 2007). There have been reports suggesting that TRPM3 is activated by store depletion, for example a small increase in Ca^{2+} entry through human TRPM3 channels following store depletion has been described under some conditions (Lee *et al.*, 2003a). However, it has been shown that the expression of TRPM3 in HEK-293 cells did not enhance Mn^{2+} entry in response to thapsigargin or GPCR stimulation (Grimm *et al.*, 2003), and store depletion does not affect D-erythro-sphingosine-mediated activation of TRPM3 (Grimm *et al.*, 2005). Therefore, TRPM3 has not convincingly been shown to be activated by store depletion (Oberwinkler & Phillipp, 2007). Finally, TRPM5 is activated downstream of GPCR stimulation and PLCβ-mediated $InsP_3$ generation, but it is only permeable to the monovalent cations Na^+, K^+ and Cs^+ and does not permeate divalent ions (Liman, 2007). The contribution of TRP channels from subfamilies other than TRPC channels to Ba^{2+} entry downstream of intracellular store depletion can therefore be excluded.

As PLCβ and PLCγ are respectively activated downstream of FcεRI and GqPCRs, it is important to consider the contribution of PLC to divalent ion entry following store depletion by the different mechanisms. In contrast to the other stimuli used, it has previously been shown in RBL-2H3 cells that thapsigargin stimulates PLC only minimally (Cissel *et al.*, 1998). Caution should be applied due to these results being obtained in rat; there are distinct functional differences between rat and human mast cells including receptor expression and mediator release (Bischoff, 2007). However, whilst they have not been investigated in human mast cells, the basic principles of thapsigargin and receptor signalling are likely to be similar to those in RBL-2H3 cells. Therefore, because divalent ion entry was observed downstream of thapsigargin stimulation, which does not activate PLC, it could be suggested that store depletion *per se* was able to activate the Ba^{2+}-permeable channels in this study, as opposed to channels only becoming active as a result of PLC signalling. Repeating these experiments in the presence of a PLC inhibitor would

demonstrate the relative contributions of store depletion and PLC-mediated signalling to Ba^{2+}-permeable channel activation following the different mechanisms of activation.

It is important to consider that different channels could be activated following the different methods of store depletion; for example, passive store depletion by thapsigargin may trigger activation of the TRPC1/4/5 subgroup, whereas PLC activation downstream of P2Y receptor signalling might be expected to activate TRPC3/6/7 channels through DAG production. As discussed previously, the coupling of PLCβ and PLCγ to distinct regions in the plasma membrane could mean that ADP and FcεRI-mediated store depletion leads to the activation of different channels. However, the size of Ba^{2+} entry in both LAD 2 cells and HLMCs was not significantly different when different methods of store depletion were used, suggesting the involvement of the same channels. It must be noted that Ba^{2+} has a lower affinity for fura-2 than Ca^{2+}(K_d values of 780 and 236nM, respectively) (Schilling *et al.*, 1989); therefore if the size of Ba^{2+} and Ca^{2+} entry was the same, it would be expected that the change in fura-2 fluorescence occurring due to Ba^{2+} entry would be approximately 3.3. fold smaller than that corresponding to Ca^{2+} entry. The ratio of Ca^{2+} to Ba^{2+} entry was calculated and is shown in table 3.1. In LAD 2 cells, the change in fura-2 fluorescence indicating Ca^{2+} entry was around 3.5 fold higher than that for Ba^{2+} entry; given the K_d values, this suggests that the size of Ba^{2+} and Ca^{2+} entry was similar following all mechanisms of activation. This was unexpected, as divalent entry through Ba^{2+}-permeable channels (i.e. TRPC channels) was expected to represent a small proportion of the entry through Ca^{2+}-permeable channels (i.e. a combination of TRPC and Orai channels).

If Ba^{2+} entry represents TRPC channel activation only, and Ca^{2+} entry reflects the combined activation of TRPC and Orai channels as expected, the apparently similar size of Ba^{2+} and Ca^{2+} entry must be accounted for. Cytosolic Ca^{2+} concentration is not only affected by Ca^{2+} entry through plasma membrane channels, but also the rate of removal. Re-uptake into ER stores by the SERCA pump, mitochondrial sequestration and plasma membrane transporters are all responsible for the removal of Ca^{2+} from the cytoplasm; Ba^{2+} is not a substrate for Ca^{2+} transporters so cannot be extruded from the cytosplasm in the same way as Ca^{2+}(Parekh & Putney, 2005). Fura-2 fluorescence when bound to Ba^{2+} is therefore an indicator of unidirectional Ba^{2+} entry, whereas that bound to Ca^{2+} reflects Ca^{2+} entry into and removal from the cytoplasm (Chang *et al.*, 2007). Ca^{2+} entry could therefore be larger than Ba^{2+} entry but appear smaller due to its removal from the cytoplasm; as expected, Ca^{2+} entry could then reflect the action of a greater number of channels than Ba^{2+} entry.

In HLMCs, the ratio of Ca^{2+}- to Ba^{2+}-bound fura-2 fluorescence was more variable than that calculated for LAD 2 cells; with all mechanisms of store depletion it was lower than 3.3 (see table 3.1). As the K_d value for fura-2 bound to Ba^{2+} is 3.3 fold higher than that for Ca^{2+}, these results suggest that Ba^{2+} entry is greater than Ca^{2+} entry in HLMCs. However, as discussed above, Ba^{2+} fura-2 fluorescence does not reflect removal from the cytoplasm, so Ca^{2+} entry could in fact be

greater than Ba^{2+} entry but have lower fura-2 fluorescence due to sequestration in intracellular stores and removal from the cell. Whilst the ratio of Ca^{2+} to Ba^{2+}-bound fura-2 did not show much variation in LAD 2 cells following the different mechanisms of activation, it was much lower in HLMCs when IgE was used to deplete stores (1.73), compared with thapsigargin and ADP (2.64 and 2.62, respectively). In agreement with this variability in primary cells, it has previously been described that primary rat peritoneal mast cells show extremely diverse calcium signals following FcεRI crosslinking compared with RBL-2H3 cells (Chang *et al.*, 2007). The different ratios of Ca^{2+} to Ba^{2+} entry seen in this study could reflect the activation of distinct plasma membrane channels following the different mechanisms of store depletion. As discussed above, the activation of PLCγ downstream of FcεRI and PLCβ following ADP stimulation may couple to distinct signalling cascades in different regions of the membrane, activating separate ion channels.

Having determined that Ba^{2+} ions can enter LAD 2 cells and HLMCs following store depletion, which suggests the involvement of the non-selective TRPC cation channels in mediating their entry, it was demonstrated that $Ba^{2+}$and Sr^{2+} were able to support degranulation in LAD 2 cells. These data are in agreement with previous results showing that Ba^{2+}, Sr^{2+} and other divalent ions can support degranulation in RBL-2H3 cells (Hide & Beaven, 1991; Ma *et al.*, 2008), and suggest that TRPC channels may be the carriers of the divalent ions. Ma *et al*. (2008) reported that TRPC5 knock-down using shRNA impaired degranulation in RBL-2H3 cells, concluding that TRPC5, along with Orai1 and STIM1, is required for degranulation (Ma *et al.*, 2008). Sanchez-Miranda *et al.* (2010) showed that BMMCs from Fyn-deficient mice exhibit impaired IgE-mediated degranulation, and suggest that TRPC3/6/7 channels provide a Ca^{2+} signal for optimal mediator release. The preliminary results obtained in this study do not disagree with these interpretations, and suggest that non-selective TRPC channels may also contribute to human mast cell degranulation; this idea was explored further and is discussed in chapters 5 and 6.

As the preliminary results obtained in this chapter suggest that TRPC channels may be involved in Ca^{2+} entry in human mast cells following different methods of stimulation, and could have a role in degranulation, it was then assessed which TRPC family members were expressed in human mast cells. RT-PCR showed that mRNA transcripts for TRPC1, 3, 5, 6 and 7 were expressed in LAD 2 cells; expression in HLMCs was donor-dependent for TRPC5 and TRPC7; mRNA for TRPC1 and TRPC6 were present in all three donors tested. These data contradict previous results, where GeneChip microarrays did not reveal TRPC channel mRNA in HLMCs; only TRPC1 was found to be present in human skin mast cells (Bradding *et al.*, 2003). The differences seen between this study and that by Bradding *et al*. (2003) could be explained by donor variability; an example of donor variability is shown by the variable expression of TRPC5 in this study. It is possible that HLMCs from the donors tested in the GeneChip study did not express mRNA for any of the TRPC channels. However, given the non-redundant functions of TRPC channels in other systems as detailed in chapter 1.3.2, it is unlikely that some donors would not

express mRNA for any TRPC channels at all when others do express the channels. There are a number of problems with GeneChip arrays; importantly, the technology has sensitivity limits, and genes can be classed as absent when they are on the threshold of detection (Tadesse & Ibrahim, 2004). The technique relies on hybridisation of gene-specific probes, and software is used to calculate whether the target sequence is present. Hybridisation assays can be unreliable, so a transcript may be classed as absent because the hybridisation has not worked, as opposed to the gene not being present (Tadesse & Ibrahim, 2004). It is therefore probable that the mRNA for some TRPC channels was present in the donors screened by Bradding *et al*. (2003), but could have been missed due to the GeneChip method used for detection. Inconsistencies have been observed between the results obtained by Bradding *et al*. (2003) and other studies; $P2X_7$ mRNA was found to be absent from HLMCs using the GeneChip array (Bradding *et al*., 2003), but Wareham *et al*. (2009) reported strong $P2X_7$ receptor mRNA expression in three donors of HLMCs detected using RT-PCR. This highlights that caution is required when interpreting GeneChip array results, and supports the theory that TRPC channel mRNA could have been present but not detected in the GeneChip array (Bradding *et al*., 2003).

In conclusion, the initial studies into human mast cell activation carried out in this chapter show that mast cell activation by IgE receptor signalling and by GPCR stimulation can be measured using Ca^{2+} imaging and secretion assays. The entry of Ba^{2+} ions into LAD 2 cells and HLMCs following intracellular store depletion suggests the involvement of non-selective TRPC cation channels; mRNA for TRPC channels was found to be expressed in both cell types. These preliminary data indicate the possible involvement of TRPC channels in human mast cell Ca^{2+} signalling; this was then investigated in the remainder of the study.

Chapter 4: Characterisation of TRPC channels in HEK cell lines

The preliminary results obtained in chapter 3 suggest that non-selective TRPC cation channels, the mRNA for which is expressed in human mast cells, may have a role in mediating Ca^{2+} entry following FcεRI- or P2Y- mediated activation, and downstream of intracellular store depletion. In order to investigate the functional expression of TRPC channels in human mast cells further, it was necessary to develop the protocols and tools required to study their biophysical properties. A HEK-293 cell line stably expressing TRPC6 (HEK-TRPC6) (Boulay *et al.*, 1997) was used as a model to study the second messenger-regulated TRPC3/6/7 subgroup. Similarly, a HEK-293 cell line with inducible TRPC5 expression (HEK-TRPC5) (Zeng *et al.*, 2004) was used to test activation mechanisms for TRPC5 channels.

4.1 Characterisation of TRPC6 channels in HEK cells

The second messenger-regulated TRPC3/6/7 channels are activated by the lipid DAG (Hofmann *et al.*, 1999). Its membrane-permeable analogue, OAG, is commonly used to activate TRPC6 channels experimentally, and has been shown to activate TRPC6-mediated Ca^{2+} entry and currents in HEK-TRPC6 cells (Estacion *et al.*, 2006) as well as in native cells including A7r5 smooth muscle cells (Jung *et al.*, 2002) and primary mouse cortical neurons (Tu *et al.*, 2009b). To verify that OAG could be used to activate TRPC6 channels in our laboratory, fura-2 Ca^{2+} imaging was employed to investigate OAG-induced Ca^{2+} fluxes in HEK-TRPC6 cells. Results are shown in figure 4.1; OAG elicited concentration-dependent Ca^{2+} entry in HEK-TRPC6 cells with an EC_{50} of 0.38μM. As shown in figure 4.1c, 100μM OAG caused maximal activation of TRPC6; this concentration was used for all future experiments.

Whole-cell patch clamp recordings were then carried out in HEK-TRPC6 cells as detailed in chapter 2.6.9 to investigate the biophysical properties of the OAG-induced TRPC6 currents. It has previously been shown that TRPC6 channels expressed in HEK cells give rise to a typical outwardly-rectifying current with a reversal potential near 0mV when stimulated with OAG (Estacion *et al.*, 2006). Cells were clamped at -60mV and 1 second voltage ramps from -100mV to +100mV were applied every 2 seconds. Results are shown in figure 4.2; a (i) and (ii) show two example current-time plots of OAG-induced whole-cell currents in HEK-TRPC6 cells. Currents were measured at +100mV (i.e. outward cation current) and -100mV (i.e. inward cation current).

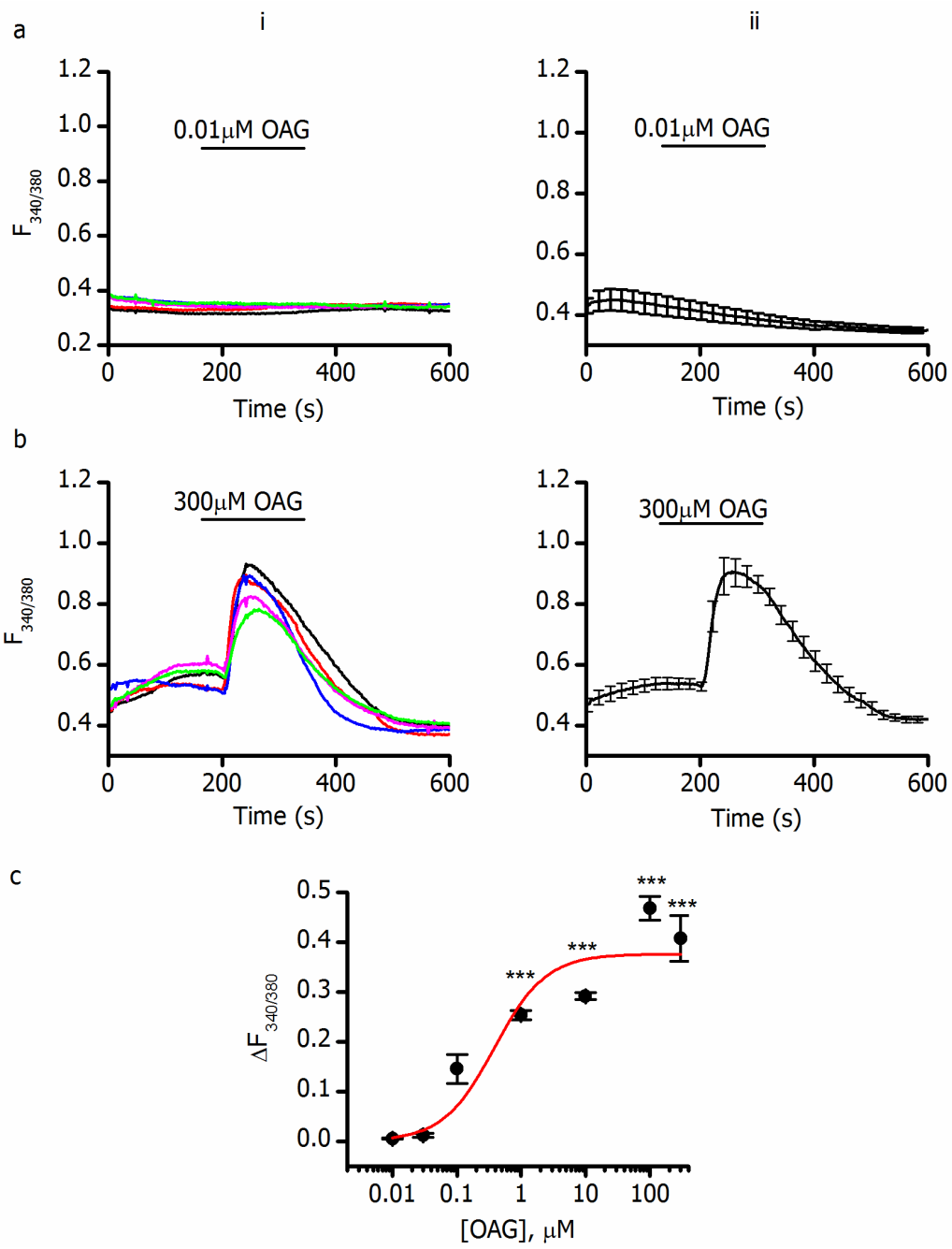

Figure 4.1. OAG-induced Ca^{2+} entry in HEK-TRPC6 cells.

a: Ca^{2+} fluxes, indicated by $F_{340/380}$, when HEK-TRPC6 cells were perfused in standard external solution and 0.01μM OAG was applied as indicated by the horizontal bar. (i) shows individual cell traces; (ii) shows mean ± SEM (n=14).b: Experiments as in (a), where 300μM OAG was applied to cells. c: Concentration-response curve for OAG-activated changes in fluorescence ($\Delta F_{340/380}$). Estimated EC_{50}= 0.38μM. n numbers are as follows: 5 for 0.01μM, 12 for 0.03μM, 19 for 0.1μM, 81 for 1μM, 102 for 10μM, 37 for 100μM, 14 for 300μM. ***: mean OAG-induced $\Delta F_{340/380}$ was significantly different from that induced by DMSO at 1/333 dilution (vehicle for OAG at its minimal dilution, n=56, N=2), $p<0.0001$, one-way ANOVA with Tukey post-test.

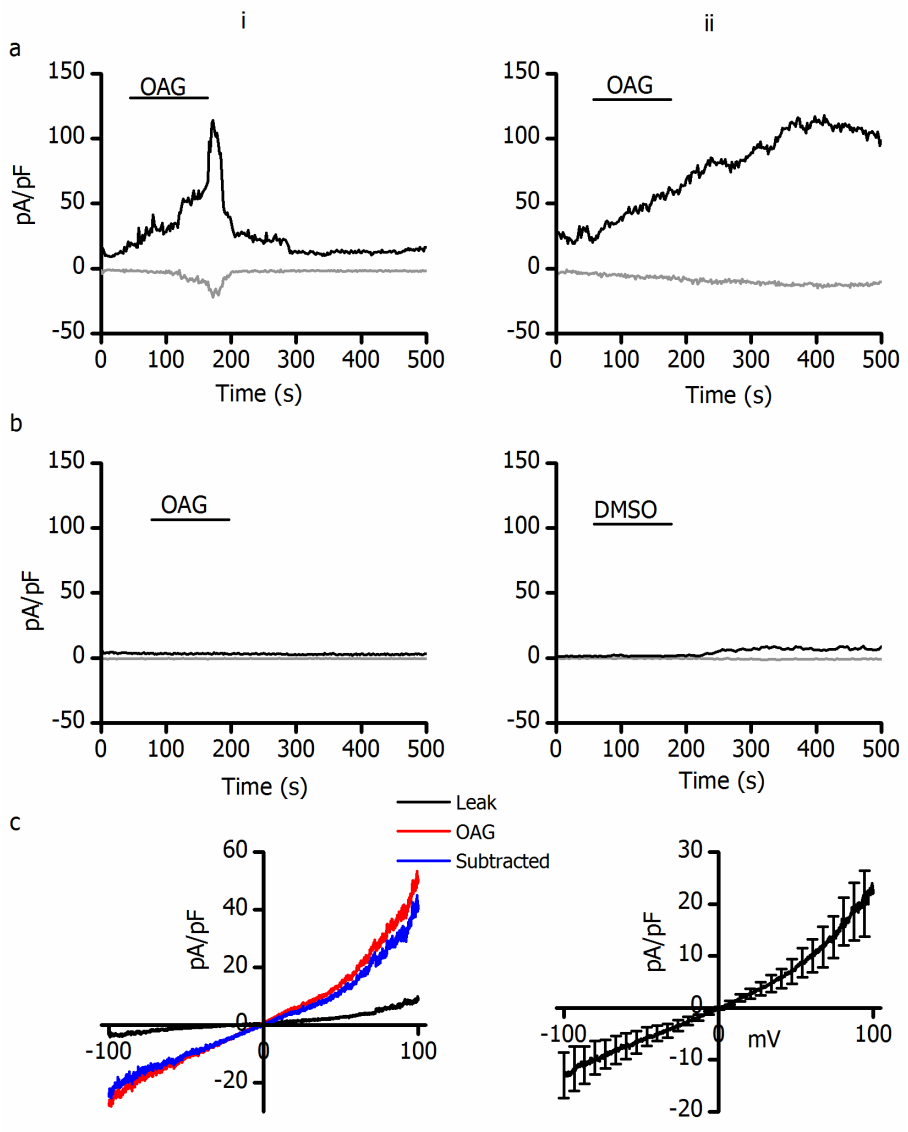

Figure 4.2. OAG-induced whole-cell currents in HEK cells stably expressing TRPC6.

a (i) and (ii): Diary plot of inward and outward currents measured at -100mV (grey trace) and +100mV (black trace) before and after focal application of 100μM OAG. Time of drug application indicated by solid bar above the trace. (i) shows an example of a transient current activated by OAG, as observed in 50% (4/8) cells. (ii) shows an example of OAG-induced current that remained after washout; this was seen in 50% (4/8) cells.

b (i): Example current-time trace when OAG was focally applied to a HEK cell not expressing TRPC6; similar results were obtained in 3 other cells. (ii) shows an example current-time trace when DMSO at 1/1000 dilution (vehicle for OAG) was focally applied to a HEK-TRPC6 cell; similar results were obtained in 2 other cells.

c (i): Current-voltage (I/V) relationship from a single cell before OAG stimulation (black, "leak") and at the peak current in the presence of OAG (red, "OAG"). The "leak" I/V relationship was subtracted from the peak ("OAG") I/V relationship to give a subtracted I/V (blue, "subtracted"). (ii) shows the mean ± SEM subtracted I/V relationship (n=8) OAG-induced current had a mean reversal potential of 0.06 ± 0.31mV (n=8).

Two kinetically distinct current responses were observed; 50% (4/8) of HEK-TRPC6 cells showed a transient current in response to OAG activation, whereas 50% exhibited a sustained current that remained after washout. Currents were classed as "sustained" when more than 50% of current remained at 2 minutes after the end of drug application. Unless otherwise stated, these criteria will be used to classify responses for the remainder of this report.The mean peak current amplitude in cells with a transient response to OAG was 69.37pA/pF ± 18.40 (n=4) at +100mV, and 17.51pA/pF ± 4.88 (n=4) at -100mV. That in cells with a sustained response to OAG was measured at 108.70pA/pF ± 56.78 (n=4) at +100mV, and 19.95pA/pF ± 10.48 (n=4) at -100mV. There was no significant difference between peak currents (either inward or outward) in cells showing a transient response compared with those showing a sustained response (unpaired Student's T-test), suggesting that current amplitude is not related to time-course. Application of OAG to HEK cells not expressing TRPC6 did not result in a current (figure 4.2b (i)), and application of DMSO, the vehicle for OAG, did not elicit currents in HEK-TRPC6 cells; see figure 4.2b (ii).

To calculate the current-voltage (I/V) relationship for each cell, the "leak" I/V relationship, taken before OAG application, was subtracted from the I/V relationship taken when the current was maximal in the presence of OAG. Leak and maximal I/V relationships are shown in figure 4.2c (i) in black and red, respectively. The blue trace shows the leak-subtracted I/V curve (i.e. only current induced by OAG); for all future experiments, subtracted I/V curves are shown. The subtracted I/V relationship was calculated for each individual cell, and the mean was calculated; the mean ± SEM (n=8) I/V relationship for OAG-induced currents is shown in figure 4.2c (ii). As expected, OAG stimulation of TRPC6 channels resulted in an outwardly-rectifying current with a reversal potential close to 0mV; this was measured at 0.06 ± 0.31mV (n=8). The "rectification index" was calculated for each cell using the formula:
rectification index = current at +100mV/current at -100mV.
The rectification index therefore shows how outwardly-rectifying the current is; a greater rectification index value means that there is a larger contribution from the outward current. The mean rectification index in cells with a transient response to OAG was 4.78 ± 1.21 (n=4) (i.e. the outward current was approximately 5-fold larger than the inward current); that in cells with a sustained response to OAG was 6.86 ± 1.23 (n=4). There was no significant difference between the rectification index for cells with a transient response and that for cells with a sustained response, suggesting that the kinetics and rectification of OAG-induced currents are not linked. The mean rectification index for all cells combined was 5.82 ± 0.89 (n=8).

To summarise, in whole-cell patch clamp recordings, OAG activated outwardly-rectifying currents with the expected biophysical properties of TRPC6 channels. These experiments show that in our hands, OAG can be used to activate TRPC6-containing channels and can therefore be used as a tool to investigate functional expression of DAG-regulated TRPC3/6/7 channels in native cells.

It was then investigated why OAG-induced currents observed in some HEK-TRPC6 cells were transient and those in others were more sustained. The possibility that PKC could be switching off the channels was considered; 100μM OAG is known to switch on PKC (Venkatachalam *et al.*, 2003), which has been shown to negatively regulate TRPC6 channels. Bousquet *et al.* (2010) showed, using the same HEK-TRPC6 cell line used in this study, that OAG- and carbachol-induced Ca^{2+} entry was potentiated and more sustained in the presence of a PKC inhibitor. To investigate whether such a mechanism regulated the kinetics of OAG-evoked currents in HEK-TRPC6 cells used in this study, the effects of the selective PKC inhibitor, Ro-31-8425 (Wilkinson *et al.*, 1993), were assessed. To verify that the PKC inhibitor was functional and determine the appropriate concentration to use when investigating OAG-induced currents, a β-hexosaminidase secretion assay in LAD 2 cells was used, as it has previously been shown that PKC is required for mast cell secretion (Mazurek *et al.*, 1987). A combination of 100nM PMA + 1μM ionomycin was used to induce maximal secretion of LAD 2 cells; this stimulus was used following a 5 minute incubation with various concentrations of Ro-31-8425, and β-hexosaminidase release from LAD 2 cells was quantified as described in chapter 2.8. It was found that Ro-31-8425 caused concentration-dependent inhibition of PMA + ionomycin-induced secretion with an IC_{50} of 0.87μM (figure 4.3a). DMSO (vehicle for Ro-31-8425) at the minimal dilution did not cause inhibition of secretion (figure 4.3b). These results show that Ro-31-8425 can be used to effectively inhibit PKC, and could therefore be used to evaluate whether PKC is switching off OAG-induced TRPC6 currents. A concentration of 3μM Ro-31-8425 was used in subsequent experiments.

Whole-cell patch clamp experiments in HEK-TRPC6 cells like those shown in figure 4.2 were then repeated in the presence of 3μM Ro-31-8425. Control experiments were carried out on the same experimental days as those in the presence of Ro-31-8425, so data was culture-matched. Results are shown in figure 4.4; the percentage of cells displaying a sustained current was compared in the presence and absence of Ro-31-8425. It was found that when PKC was inhibited, a greater percentage of cells showed a sustained current (78% (7/9) compared with 50% (4/8) in the absence of inhibitor).

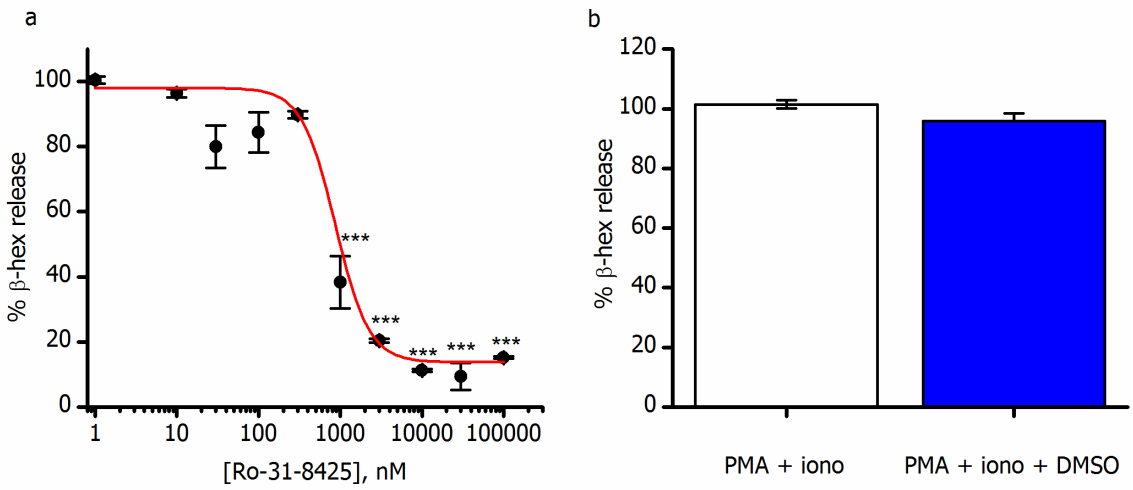

Figure 4.3. PMA and ionomcycin-induced β-hexosaminidase release in LAD 2 cells is concentration-dependently inhibited by Ro-31-8425.

a: Cells were stimulated with 100nM PMA + 1μM ionomycin following a 5 minute pre-incubation with the concentrations of Ro-31-8425 shown. β-hexosaminidase release was measured as a percentage of total, determined following lysis with 0.5% Triton X-100. Ro-31-8425 inhibited PMA + ionomycin-induced secretion in a concentration-dependent manner with an IC_{50} of 870nM. Points show mean ± SEM; N=4. ***: means were significantly different from control (no Ro-31-8425), $p<0.0001$, one-way ANOVA with Tukey post-test.

b: Bar chart showing % β-hexosaminidase release induced by PMA + ionomycin in the presence (N=4) and absence (N=4) of DMSO at 1/100 dilution (vehicle for Ro-31-8425 at minimum dilution). Means were not significantly different (unpaired Student's T-test).

The peak current was increased in the presence of Ro-31-8425 from 89.03pA/pF ± 28.61 (n=8) to 177.12pA/pF ± 47.80 (n=9) at +100mV, and from 18.73pA/pF ± 5.37 (n=8) to 43.29pA/pF ± 12.99 (n=9) at -100mV (figure 4.4b (i)). The difference in peak current amplitude was not significantly different (unpaired Student's T-test). The mean rectification index for OAG-induced currents in the presence of Ro-31-8425 was 4.19 ± 0.28 (n=9); this was not significantly different from that calculated in the absence of Ro-31-8425 (5.82 ± 0.89, n=8, unpaired Student's T-test). The rectification and amplitude of OAG-induced currents were therefore not significantly affected by the presence of Ro-31-8425. When the percentage of the maximal current remaining at two minutes after the end of drug application was calculated, only a small increase from 54.93% ± 19.31 (n=8) to 73.19% ± 8.5 (n=9) at +100mV and from 56.01% ± 14.44 (n=8) to 61.52% ± 9.79 at -100mV was seen when Ro-31-8425 was present. This increase did not reach statistical significance. Taken together, these results suggest that PKC- does regulate TRPC6 function, but that other mechanisms may also be at work to regulate inactivation of the channels, which are discussed further in section 4.3.

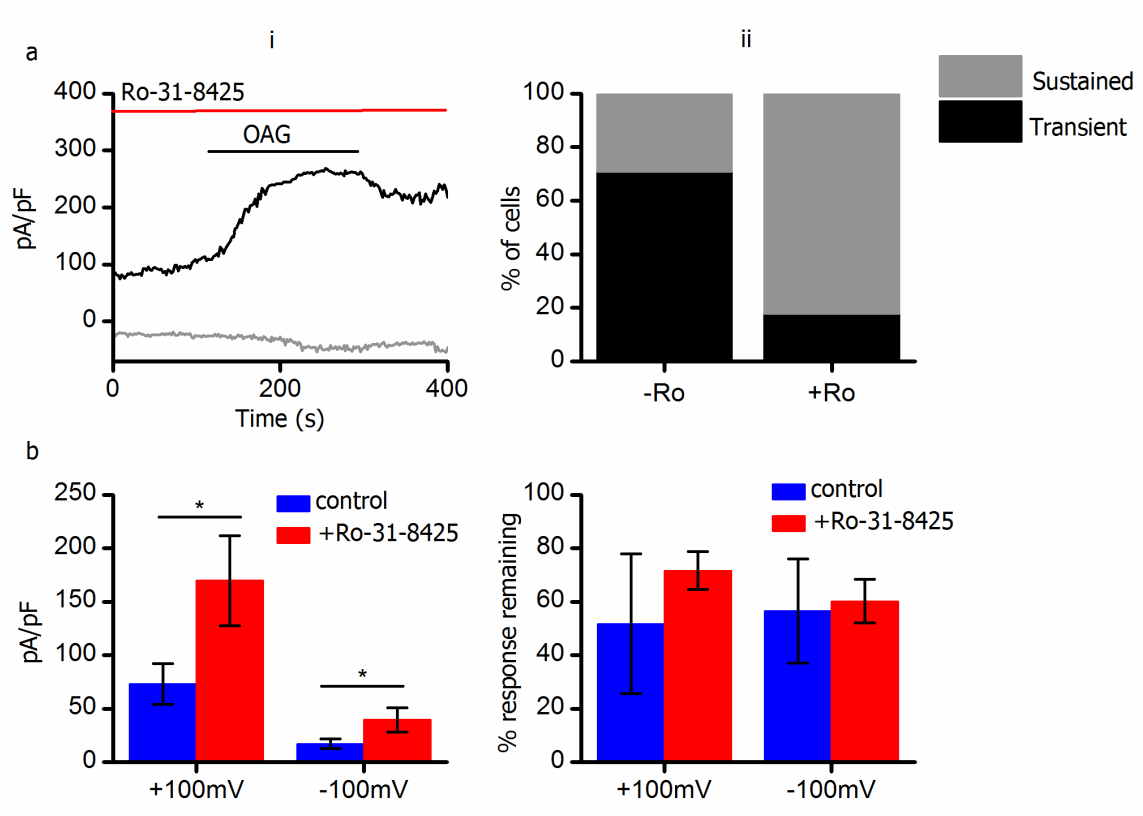

Figure 4.4. OAG-induced currents in HEK-TRPC6 cells in the presence of Ro-31-8425.
Experiments described in figure 4.2 were repeated in the presence of 3μM Ro-31-8425.
a: (i) shows a current-time plot of an example whole-cell recording; solutions containing drugs were focally applied as indicated by the horizontal bars. (ii): Bar graph showing percentage of cells with a "sustained" or "transient" response in the presence versus absence of Ro-31-8425 ("+Ro" and "-Ro", respectively). A response was classed as "sustained" when more than 50% of current remained at 2 minutes after the end of drug application.
b: (i) compares peak current at +100mV and -100mV in the presence (red) and absence (blue) of Ro-31-8425. *: means were significantly different, $p<0.05$, unpaired Student's T-test. (ii): Current remaining at 2 minutes after drug application was calculated as a percentage of peak current in the presence of OAG. Means were not significantly different. n numbers are as follows; n=9 in the presence of Ro-31-8425, n=8 in the absence of Ro-31-8425.

The results so far show that OAG can be used as a pharmacological tool to activate TRPC6 channels expressed in HEK cells with the expected biophysical properties. Receptor-mediated activation of the channel was then considered; *in vivo* DAG is produced downstream of signalling cascades initiated by ligands binding to receptors coupled to PLC. GPCRs including P2Y receptors and receptors for sphingosine, C3a and adenosine, as well as FcεRI, are present on the surface of mast cells, and regulate their activation in a physiological setting (Gilfillan & Tkaczyk, 2006). The possibility that second messenger-regulated TRPC channels could be activated downstream of receptor signalling in human mast cells was therefore explored. The HEK-TRPC6 cell line was used as a model to determine whether receptor-mediated TRPC6 activation could be measured

using electrophysiological and Ca^{2+} imaging approaches.

Firstly, it was investigated whether the stimulation of three different GPCRs led to Ca^{2+} entry in HEK-TRPC6 cells, in order to identify an appropriate method for receptor-mediated activation of TRPC6 channels. Carbachol was used to stimulate muscarinic acetylcholine receptors (mAChRs), as has been described previously using this cell line (Cayouette *et al.*, 2004). ADP was also used, which binds to Gq-coupled $P2Y_1$ as well as Gi-coupled $P2Y_{12}$ and $P2Y_{13}$ receptors (Burnstock *et al.*, 2010). UTP, which activates Gq-coupled $P2Y_4$ receptors (Burnstock *et al.*, 2010), was also applied in this study. Ca^{2+} imaging of fura-2-loaded HEK-TRPC6 cells showed that application of all three agonists resulted in an increase in fluorescence corresponding to Ca^{2+} entry (figure 4.5).

ADP was selected to investigate receptor-mediated stimulation of TRPC6 channels because it is likely to represent a physiological stimulus for human mast cells *in vivo*. Data from chapter 3 in this study showed that ADP induces Ca^{2+} entry in human lung mast cells (see figure 3.3); electrophysiological approaches were used to investigate whether this occurs through second messenger-regulated TRPC3/6/7 channels. For comparison, HEK-TRPC6 cells were also used to investigate whether ADP-induced TRPC6 currents could be measured under the recording conditions described in chapter 2.6.9

HEK-TRPC6 cells were voltage-clamped at -60mV and 1 second ramps from -100mV to +100mV were applied every 2 seconds. Focal application of ADP resulted in an outwardly-rectifying current being switched on, which had a reversal potential of 1.44 ± 0.38mV (n=5; figure 4.6) and a rectification index of 4.39 ± 1.28 (n=5). This ADP-induced current was absent from HEK cells not expressing TRPC6. The mean current amplitude at +100mV was measured at 105.48pA/pF ± 45.10 (n=5); that at -100mV was 24.75pA/pF ± 12.68 (n=5). 40% (2/5) of HEK-TRPC6 cells had a transient current in response to ADP activation; 60% (3/5) displayed a sustained current. Therefore, agonists at P2Y receptors can activate TRPC6 channels under the whole-cell patch clamp conditions used in these experiments. Table 4.1 summarises the properties of OAG- and ADP- activated currents in HEK-TRPC6 cells and in HEK cells not expressing TRPC6.

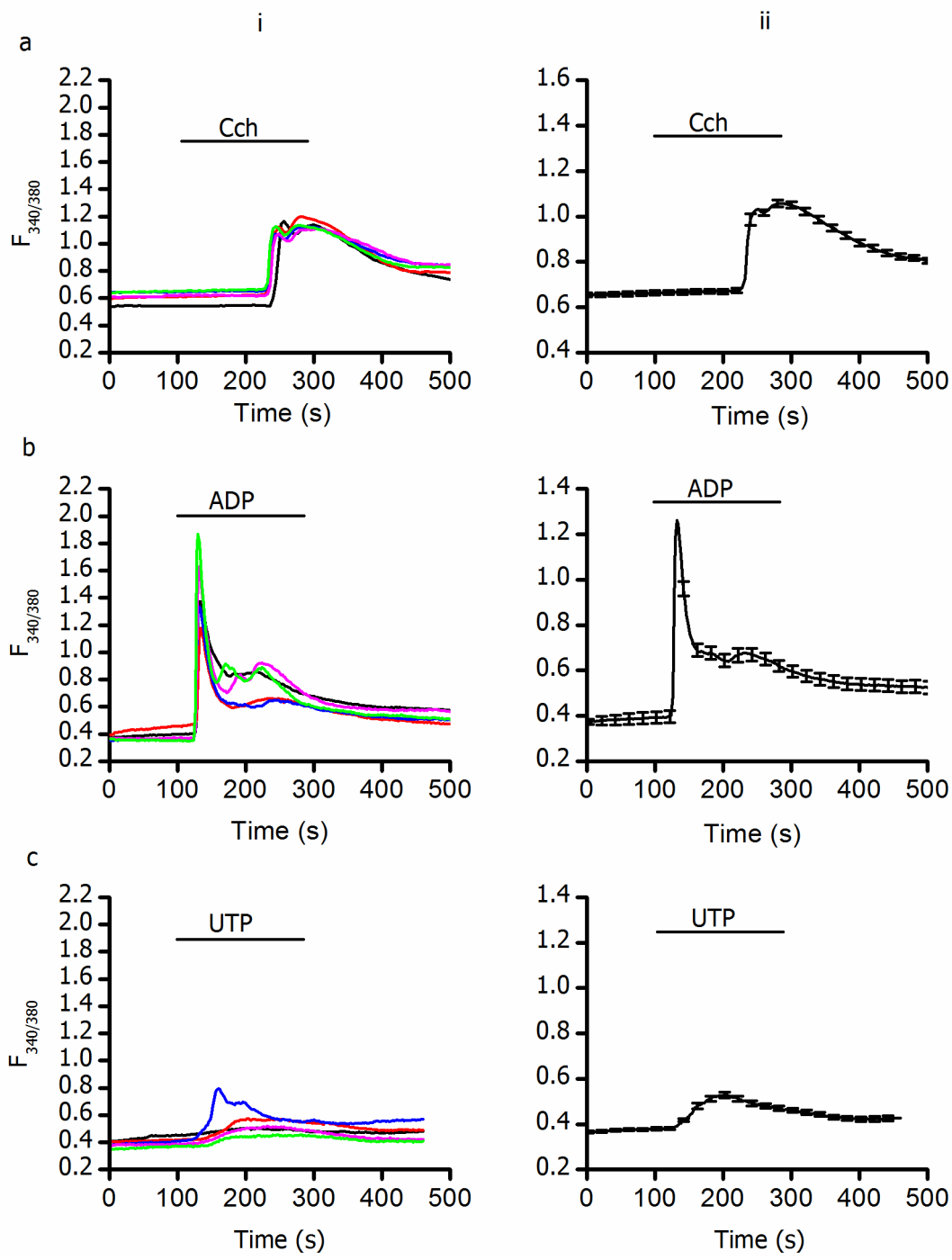

Figure 4.5. Ca^{2+} entry following GPCR stimulation in HEK-TRPC6 cells

a: Cells were perfused with standard external solution and 100μM carbachol (Cch) was bath-applied as shown. (i) shows $F_{340/380}$ in individual representative cells; (ii) shows mean ± SEM (n=30 cells, N=2 experiments)

b: Experiments as in (a), but 100μM ADP was applied (n= 24, N=2).

c: Experiments as in (a) and (b), where 100μM UTP was applied (n= 58, N=2).

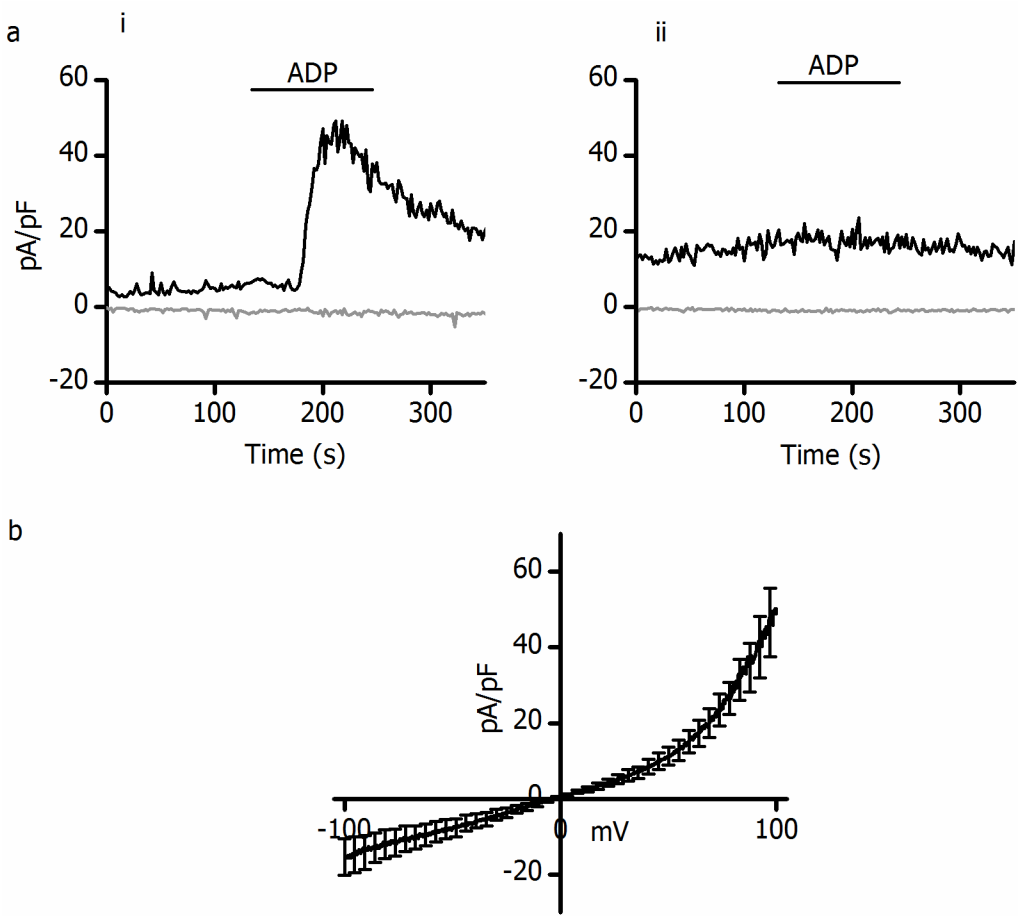

Figure 4.6. ADP-induced currents in HEK cells stably expressing TRPC6.

a: Current-time traces of whole-cell currents induced by 100μM ADP in (i) HEK-TRPC6 cells and (ii) HEK cells not overexpressing TRPC6. ADP was focally applied as indicated by horizontal bars. Current was sampled at -100mV (grey trace) and +100mV (black trace); individual representative cell traces are shown. Similar results were obtained in 4 other HEK-TRPC6 cells and 2 other HEK cells not expressing TRPC6.

b: Subtracted current-voltage relationship of ADP-induced currents in HEK-TRPC6 cells; mean ± SEM, n=5 cells. Currents had a mean reversal potential of 1.44 ± 0.38mV.

In summary, the results obtained with HEK-TRPC6 cells showed that live cell Ca^{2+} imaging and whole-cell patch clamp electrophysiology can be used to study the activation of TRPC6 channels either directly by OAG or following agonist stimulation of GqPCRs including P2Y receptors. These techniques and activation mechanisms were then applied to native human mast cells to study the functional expression of second messenger-regulated TRPC channels.

	HEK-TRPC6 OAG (n=8)	**HEK OAG** (n=3)	**HEK-TRPC6 ADP** (n=5)	**HEK ADP** (n=3)
% cells responding	100	0	100	0
Peak current +100mV (pA/pF)	89.03 ± 28.61	-2.24 ± 0.23	105.48 ± 45.10	5.63 ± 5.87
Peak current -100mV (pA/pF)	18.73 ± 5.37	1.47 ± 1.92	24.75 ± 12.68	2.99 ± 3.12
Rectification index (all cells)	5.81 ± 0.89	0.93 ± 0.75	4.39 ± 1.28	-0.13 ± 0.15
Rectification index (transient current)	4.78 ± 1.21	N/A	N/A	N/A
Rectification index (sustained current)	6.86 ± 1.23	N/A	N/A	N/A
% cells with sustained current	50	N/A	60	N/A
Reversal potential (mV)	0.06 ± 0.31	N/A	1.44 ± 0.38	N/A

Table 4.1. Properties of OAG- and ADP-evoked currents in HEK-TRPC6 cells and in HEK cells not expressing TRPC6

4.2 Activation of TRPC5 channels in HEK cells

As discussed in chapter 1.3.2, there are a number of mechanisms by which TRPC5 channels can be activated, including Gd^{3+} ions, which uniquely activate TRPC5 channels whilst inhibiting other ion channels (Zeng *et al.*, 2004), and S1P (Xu *et al.*, 2006b). In order to study the functional expression of TRPC5 in HLMCs, it was firstly verified that the TRPC5 activators Gd^{3+} and S1P could be used to activate TRPC5 channels in our laboratory. HEK-TRPC5 cells with tetracycline-inducible expression (Zeng *et al.*, 2004) were used to test carbachol, S1P and Gd^{3+} as mechanisms for TRPC5 activation. Carbachol was firstly used, in an attempt to replicate the results obtained by Zeng *et al.* (2004) when the cell line was initially characterised. As shown in figure 4.7, carbachol stimulated an increase in $F_{340/380}$, corresponding to a rise in intracellular Ca^{2+}, in Tet^{+} cells (figure 4.7a). A small rise in Ca^{2+} was also seen in response to carbachol stimulation in Tet^{-} cells, but this was abolished when the cells were pre-treated with 1μM thapsigargin for 30 minutes to deplete intracellular stores before stimulation (figure 4.7c).

It was then investigated whether whole-cell patch clamp electrophysiology could be used to record TRPC5-mediated currents activated by carbachol, as reported previously (Zeng *et al.*, 2004). Cells were voltage-clamped at -60mV and carbachol-induced currents were recorded in the whole-cell configuration. 1 second ramps from -100mV to +100mV were applied every 2 seconds. As shown in figure 4.8, carbachol application gave rise to currents in Tet^{+} HEK-TRPC5 cells, but not in non-induced cells. The mean current amplitude at +100mV (95.95pA/pF ± 19.76; n=3) and -100mV (14.71pA/pF ± 5.30; n=3) in Tet^{+} cells was significantly higher ($p<0.05$, unpaired Student's T-test) than that in Tet^{-} cells (8.83pA/pF ± 1.64, n=3 at +100mV; 1.68pA/pF ± 0.57, n=3 at -100mV). The I/V relationship of the carbachol-induced current (figure 4.8b) is typical of a TRPC5 current; it is s-shaped, outwardly-rectifying and has a reversal potential near 0mV (mean reversal potential was measured at 0.76 ± 0.24mV; n=3). The rectification index of Cch-induced currents in HEK-TRPC5 cells was measured at 7.96 ± 2.16 (n=3). Although inward and outward currents were enhanced by carbachol application, it is evident that currents were already active at the start of recordings in tetracycline-induced cells (see figure 4.8a (i)). For this reason, the I/V relationship shown in figure 4.8b has not been leak-subtracted. The reasons for this current being switched on at the start of the experiment are discussed in section 4.3.

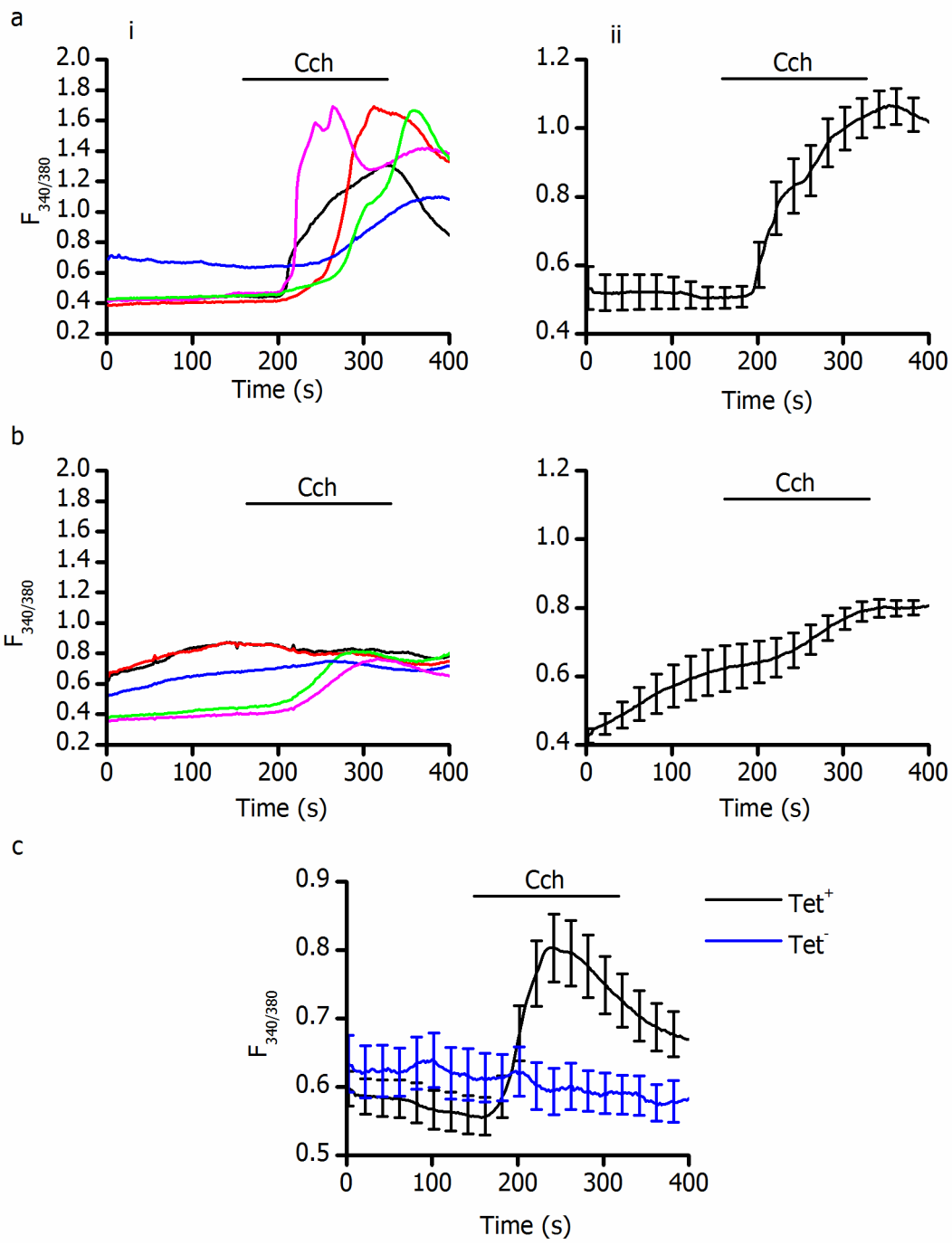

Figure 4.7. Carbachol-induced Ca^{2+} entry in HEK-TRPC5 cells.

Cells were perfused in standard external solution and 100μM carbachol (Cch) was bath-applied as indicated by the horizontal bars.

a: Ca^{2+} fluxes ($F_{340/380}$) induced by Cch in tetracycline-induced HEK-TRPC5 cells. (i) shows individual representative cells; (ii) shows mean ± SEM (n=32 cells, N=2 experiments)

b: Experiments as in (a) were carried out on non-induced (Tet-) cells (n=22, N=3)

c: Cells were pre-treated with 1μM thapsigargin to empty intracellular stores for 30 minutes, then were perfused with standard external solution and stimulated with Cch as shown. Black trace shows mean ± SEM for Tet^+ cells (n=79, N=3); blue trace shows data for Tet^- cells (n=41, N=3)

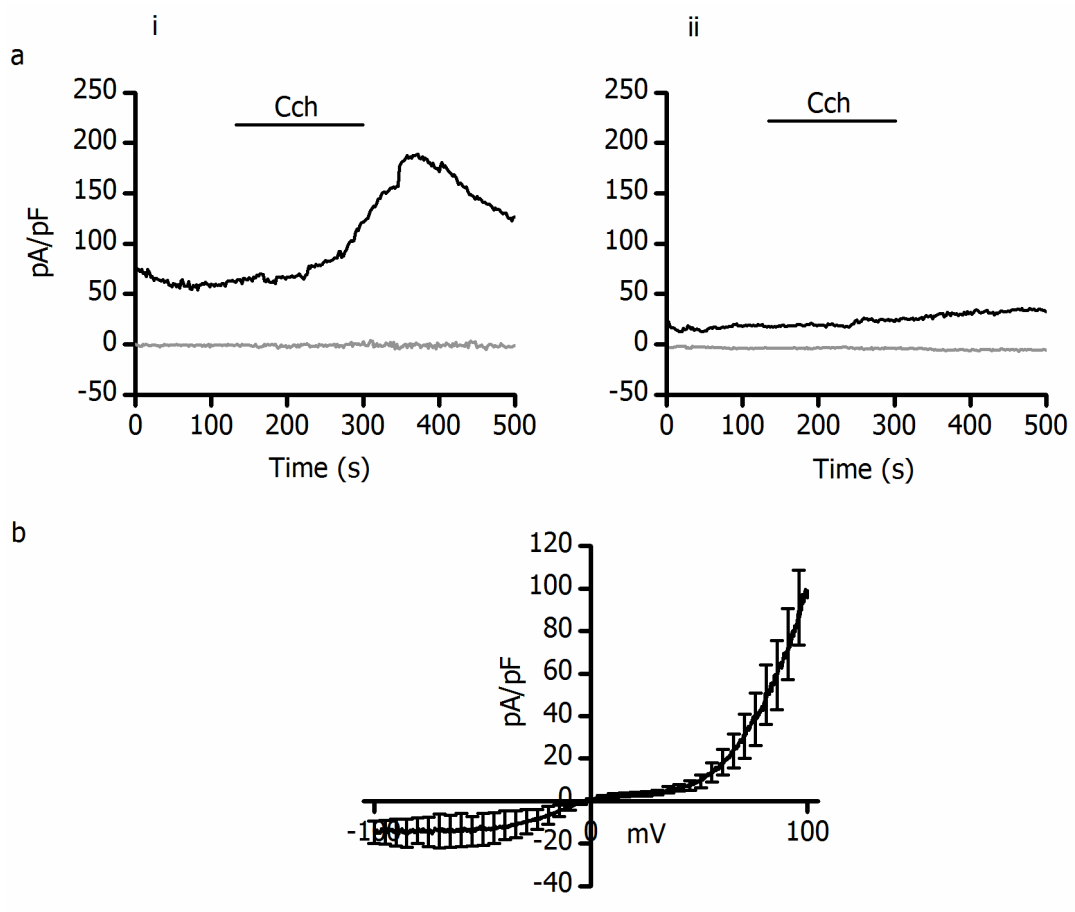

Figure 4.8. Carbachol-induced whole cell currents in HEK-TRPC5 cells.

a (i) and (ii): Current-time plots when cells were superfused with standard external solution and 100μM carbachol (Cch) was focally applied where indicated by the horizontal bars. Current was sampled at -100mV (grey trace) and +100mV (black trace). (i) shows Cch-induced current in a HEK-TRPC5 cell induced with tetracycline (tet^+); similar results were obtained in 2 other cells. (ii): example current-time plot when Cch was applied to a HEK-TRPC5 cell not induced by tetracycline (tet^-). Similar results were observed in 2 other cells.

b: Current-voltage relationship of the Cch-induced current in Tet^+ cells (n=3). The current had a mean reversal potential of 0.76 ± 0.24mV.

S1P activation of TRPC5 channels was then tested in HEK-TRPC5 cells using fura-2 Ca^{2+} imaging. As shown in figure 4.9, 10μM S1P caused Ca^{2+} influx in HEK-TRPC5 cells induced overnight by tetracycline, but not in non-induced cells. The mean $\Delta F_{340/380}$ was significantly larger ($p<0.001$, unpaired Student's T-test) in Tet^+ cells (1.28 ± 0.11; n=34, n=3) than in Tet^- cells (0.03 ± 0.01; n=85, n=3). These data confirm that S1P can be used to activate TRPC5 channels and can be used as a pharmacological tool to identify them in human mast cells. Gd^{3+} was also tested as an activator of TRPC5 in this cell line using fura-2 Ca^{2+} imaging. Since 100μM Gd^{3+} is reported to activate TRPC5 or TRPC4 channels only (Beech, 2007), whilst inhibiting other TRPC channels (Zitt *et al.*, 1996; Okada *et al.*, 1999; Inoue *et al.*, 2001; Eder *et al.*, 2007) and I_{CRAC} (Liao *et al.*, 2008), it is a useful tool to examine TRPC5 channels in native cells whilst avoiding contamination from other channels. Application of 100μM Gd^{3+} to fura-2-loaded HEK-TRPC5 cells gave rise to

Ca^{2+} influx in cells induced with tetracycline but not in non-induced cells; see figure 4.10. $\Delta F_{340/380}$ induced by Gd^{3+} was significantly higher ($p<0.001$, unpaired Student's T-test) in Tet^{+} cells than Tet^{-} cells (0.14 ± 0.04; n=37, N=3 and 0.02 ± 0.01; n=87, N=3, respectively). These results show that S1P and Gd^{3+} can be used effectively to activate TRPC5 channels, rendering these agents useful pharmacological tools to study their functional expression in human mast cells. Gd^{3+} in particular was able to be used to produce insightful results showing whether TRPC4 or 5 were present without activating other channels. It is clear that S1P gives rise to larger Ca^{2+} fluxes in induced HEK-TRPC5 cells than Gd^{3+}; this could be due to their different mechanisms of action, which will be discussed in section 4.3.

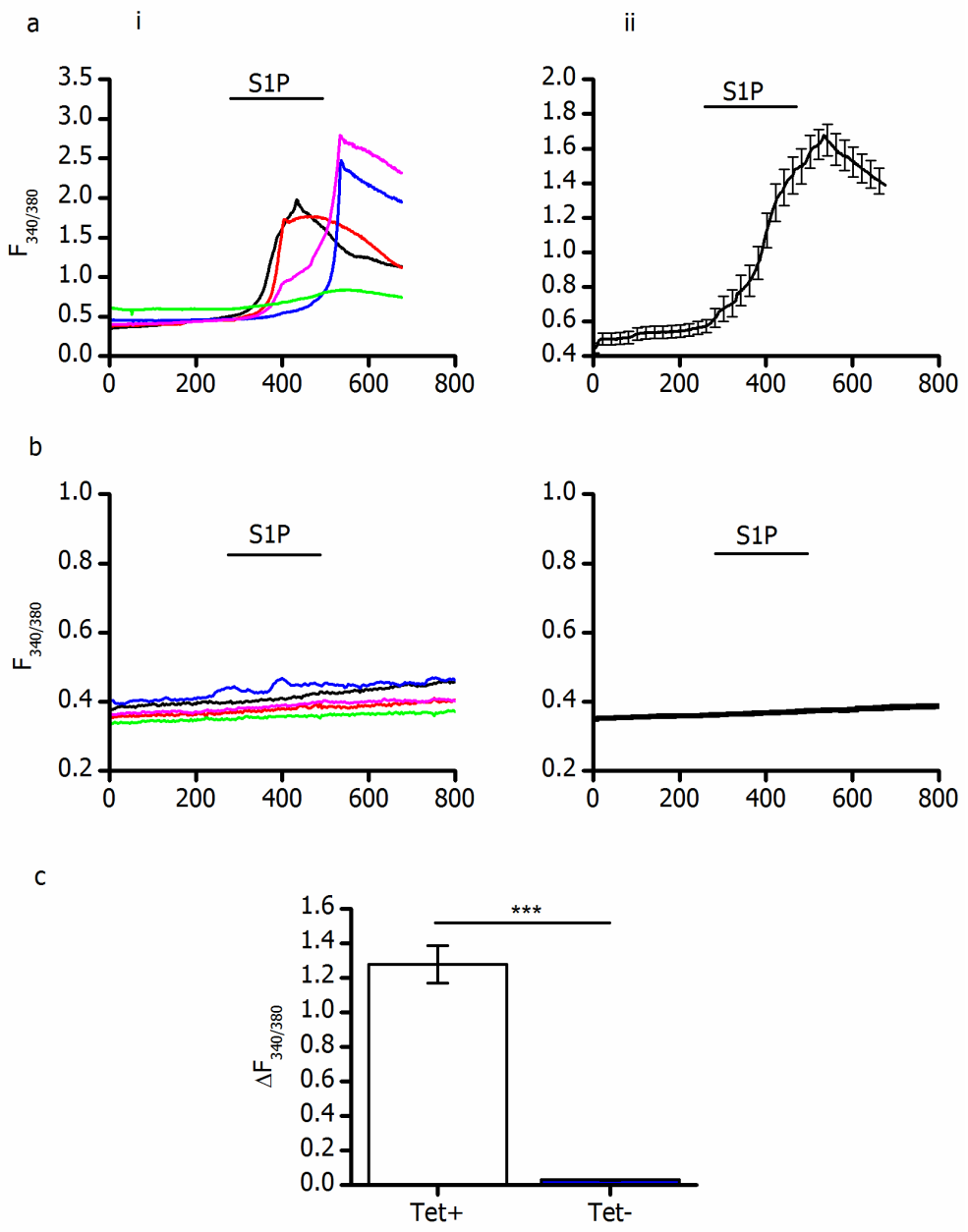

Figure 4.9. Sphingosine-1-phosphate stimulates Ca^{2+} entry in HEK-TRPC5 cells

a: TRPC5-expressing HEK cells induced overnight with tetracycline were perfused in standard external solution and 10μM S1P was bath-applied as shown. (i) shows individual cell traces; (ii) shows mean ± SEM (n=34, N=3).

b: Experiments as in (a), where cells were not induced overnight with tetracycline. n= 85, N=3.

c: Bar graph comparing size of S1P- induced Ca^{2+} entry in tetracycline-induced (Tet^+, clear bar) and non-induced (Tet^-) cells. ***: means were significantly different, $p<0.0001$, unpaired Student's T-test.

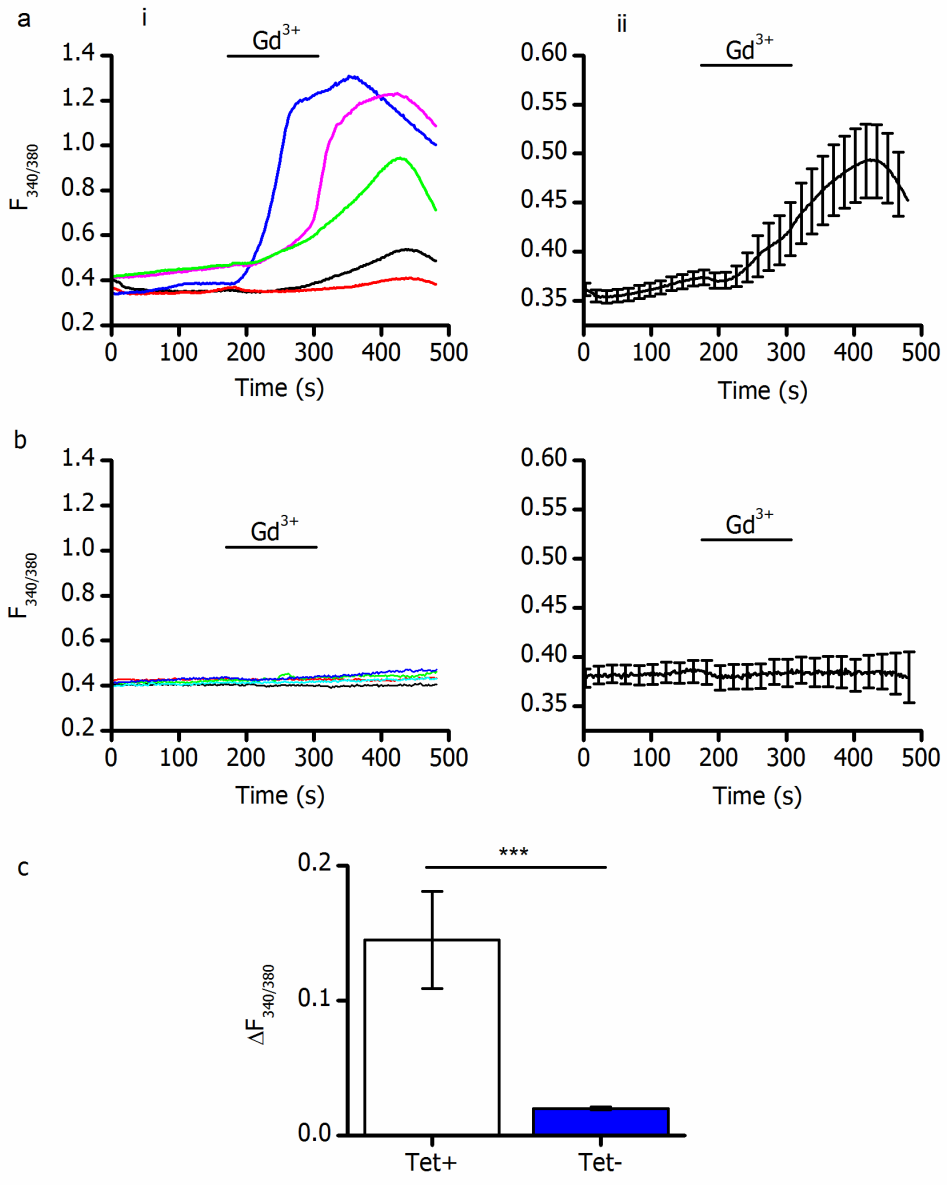

Figure 4.10. 100μM Gd^{3+} stimulates Ca^{2+} entry in HEK-TRPC5 cells

a: TRPC5-expressing HEK cells induced overnight with tetracycline were perfused in standard external solution and 100μM Gd^{3+} was bath-applied as shown. (i) shows individual cell traces; (ii) shows mean ± SEM (n=37, N=3).

b: Experiments as in (a), where cells were not induced overnight with tetracycline. n= 87, N=3.

c: Bar graph comparing size of Gd^{3+}- induced Ca^{2+} entry in tetracycline-induced (Tet^{+}) and non-induced (Tet^{-}) cells. ***: means were significantly different, $p<0.0001$, unpaired Student's T-test.

In summary, results obtained using the HEK-TRPC5 cell line have demonstrated that receptor-mediated activation of TRPC5 using carbachol gives rise to Ca^{2+} entry and the activation of currents with characteristic biophysical properties. The more selective activators for TRPC5, S1P and Gd^{3+}, were also able to stimulate Ca^{2+} entry in these cells, and may also be used to investigate the functional expression of TRPC5 in human mast cells.

4.3 Discussion

4.3.1 Characterisation of TRPC6 channels in HEK cells

This part of the study aimed firstly to characterise TRPC6 channels expressed in HEK cells and establish activation mechanisms to record TRPC6-mediated Ca^{2+} entry and currents. Fura-2 Ca^{2+} imaging experiments showed that OAG caused concentration-dependent activation of TRPC6 with an EC_{50} of 0.38μM. Maximal activation was produced by 100μM OAG, which is in agreement with results obtained by Estacion *et al.* (2004) showing that increasing OAG concentration from 100μM to 300μM produced no further increase in TRPC6 activity. A concentration of 100μM OAG was selected to use in all further experiments. Whole-cell patch clamp experiments revealed the activation of an outwardly-rectifying current by 100μM OAG with a reversal potential close to 0mV (recorded at 0.06 ± 0.31mV); these biophysical properties are typical of TRPC6 channels expressed in HEK cells (Estacion *et al.*, 2004; Shi *et al.*, 2004; Estacion *et al.*, 2006).

Interestingly, OAG-induced currents were more sustained in some HEK-TRPC6 cells than in others. There are a number of reasons why there could have been these two types of response; DAG and OAG are known to activate PKC (Bell *et al.*, 1986; Venkatachalam *et al.*, 2003), and a number of studies have shown that PKC negatively regulates TRPC6. It was hypothesised that the OAG-induced TRPC6 currents in this study could be more transient in some cells due to the activation of PKC by OAG, leading to subsequent inactivation of the channel. This hypothesis was tested using a potent and selective PKC inhibitor, Ro-31-8425; if PKC was switching off the channels, currents in HEK-TRPC6 cells should have become more sustained in the presence of Ro-31-8425. This PKC inhibitor was derived from staurosporine, which is a potent but non-selective PKC inhibitor, and bisindolylmaleimides, which are less potent but more selective inhibitors. The resulting Ro-31-8425 was able to inhibit all PKC isoforms with IC_{50} values ranging from 8–39nM (Wilkinson *et al.*, 1993). It has been used successfully in human neutrophils to inhibit PMA-induced superoxide release (Merritt *et al.*, 1997).

To verify that Ro-31-8425 was functional in our laboratory, and to determine an appropriate concentration to be used to inhibit PKC, its effects on PMA + ionomycin- induced secretion were assayed in LAD 2 cells using a β-hexosaminidase secretion assay. PKC is required for mast cell exocytosis (Mazurek *et al.*, 1987); therefore, maximal secretion was induced in LAD 2 cells using a combination of PMA and ionomycin to switch on PKC and cytosolic Ca^{2+} influx, respectively, in the presence of different concentrations of Ro-31-8425. PMA and ionomycin maximally stimulated secretion from LAD 2 cells, causing 100% β-hexosaminidase release from intracellular granules. This was inhibited by Ro-31-8425 with an IC_{50} of 870nM. The IC_{50} for PKC inhibition observed in this assay was higher than that found in other studies; this could be because LAD 2 cells contain higher levels of PKC than other cells, or that different isoforms of PKC are present. Inhibition of β-hexosaminidase release by Ro-31-8425 verified that it is an appropriate inhibitor

of PKC to use in electrophysiological studies; a sub-maximal concentration of 3μM Ro-31-8425 was selected to be used in all future experiments.

Ro-31-8425 was then used in whole-cell patch clamp studies to determine whether PKC inhibition resulted in more sustained OAG-induced currents in HEK-TRPC6 cells. It was found that 82% of cells showed a sustained current in the presence of Ro-31-8425, compared to 29% in the absence of inhibitor. The peak current measured at -100mV and +100mV was significantly increased when Ro-31-8425 was present; these results suggest that PKC, which is activated by DAG/OAG (Venkatachalam *et al.*, 2003), is switching off TRPC6 channels following OAG-mediated activation. The results found in this study are in agreement with Bousquet *et al.* (2010), who showed that PKC inhibition potentiated agonist-induced Ca^{2+} entry in HEK-TRPC6 cells, and activation of PKC with PMA reduced this Ca^{2+} entry. They concluded that PKC exerts an inhibitory effect on TRPC6 channels, and showed using mutagenesis studies that this occurs by phosphorylation of serine residue 448 on PKC(Bousquet *et al.*, 2010). Shi *et al.* (2004) found that carbachol-induced currents in HEK-TRPC6 cells were larger and had a significantly reduced time course of inactivation when PKC was inhibited. When the percentage of peak current remaining at two minutes after drug application in this study was calculated, there was a greater percentage of inward and outward current remaining when Ro-31-8425 was present, but this did not reach statistical significance. This is likely due to there being a large variation in the percentage of current remaining when PKC was not inhibited; the box and whisker plot in figure 4.11 illustrates this variation. As shown, there was much greater variation in the percentage of current remaining when PKC was not inhibited. This could be caused by differering levels of PKC between cells, for example due to cell cycle-dependent variation or dialysis up the patch pipette. The variation in percentage current remaining was greatly reduced in the presence of PKC inhibitor. This lends support to the theory that the variation seen when PKC was not inhibited was due to differing levels of PKC. The model in figure 4.12 depicts how PKC may be regulating TRPC6 channels in this study.

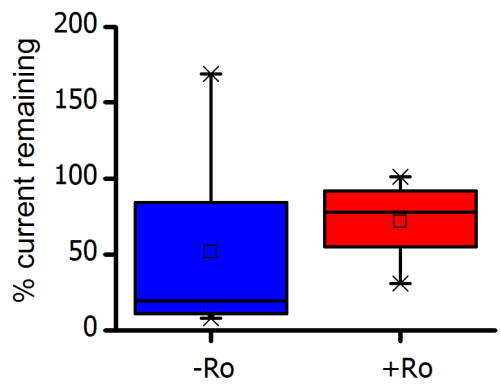

Figure 4.11. Variation in TRPC6 current remaining in the presence or absence of PKC inhibition

Box and whisker plot depicting variation in the percentage of peak current remaining at 2 minutes after drug application (data from figure 4.4b (ii)) in the presence (red box) or absence (blue box) of Ro-31-8425.

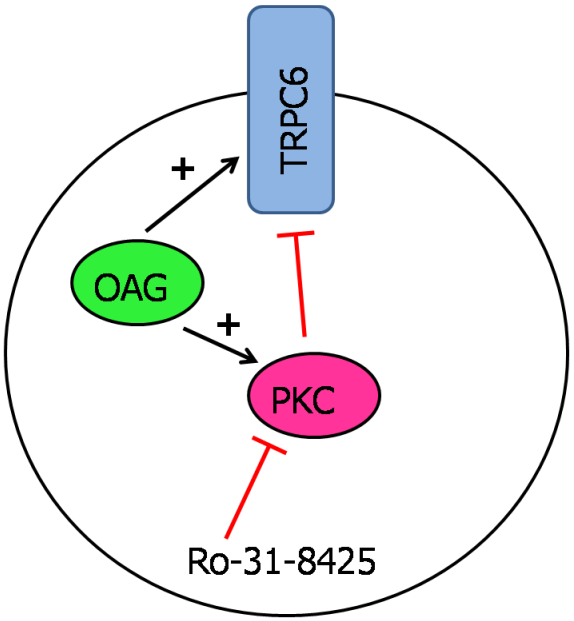

Figure 4.12. Model of TRPC6 channel regulation by PKC

OAG switches on TRPC6 channels in the plasma membrane, giving rise to currents. OAG also activates PKC, which inhibits TRPC6 channels, resulting in transient currents seen in whole-cell patch clamp recordings. Inhibition of PKC with Ro-31-8425 alleviates inhibition of TRPC6, resulting in more sustained currents

Further experiments with a PKC inhibitor thus support the notion that PKC may be regulating the time course of the currents activated by OAG in HLMCs. It is unlikely to account for the deactivation of currents alone, however, as the percentage of current remaining at 2 minutes after drug application still varied from 30 to 101% in the presence of Ro-31-8425. As electrophysiological recordings of OAG-activated currents were all done in whole-cell mode, other

important signalling molecules may have been undergoing dialysis up the patch pipette. It could be tested whether or not dialysis in the whole-cell recording mode contributes to inactivation of the currents by carrying out the recordings in the perforated patch configuration; dialysis would not be able to occur through the small pores created by gramicidin (Rhee *et al.*, 1994) or amphotericin (Rae *et al.*, 1991). If currents became more sustained in the perforated patch configuration, it would show that dialysis contributes to channel inactivation.

Another possibility is that the negative regulation of TRPC6 channels by Ca^{2+}, discussed in chapter 1.3.2, could cause some currents to be more transient. Because the Ca^{2+} regulation is complex, involving positive and negative regulation, both dependently and independently of Ca^{2+}-bound calmodulin kinase II (CaM-kinase II) (Shi *et al.*, 2004), it is possible that different cells contained varying levels of important molecules required for regulation, leading to the variation seen in the inactivation of OAG-induced currents in HEK-TRPC6 cells. Ca^{2+} regulation of the channels could be tested using extracellular solutions containing different concentrations of Ca^{2+} and using a calmodulin antagonist such as calmidazolum (Shi *et al.*, 2004). If this was carried in perforated patch and whole-cell recording configurations, Ca^{2+} regulation as well as the dialysis of signalling molecules could be investigated. In conclusion, whilst the regulatory mechanisms for TRPC6 inactivation remain somewhat elusive in this study, it is likely that PKC is playing a part as currents were found to be larger and more sustained when PKC was inhibited. In HEK-TRPC6 cells, OAG was shown to activate Ca^{2+}-permeable currents with the expected biophysical properties of TRPC6 channels; inward and outward current with outward rectification, and a reversal potential close to 0mV. Therefore, OAG was able to be used as a pharmacological tool to investigate the functional expression of second messenger-regulated TRPC3/6/7 channels in native cells.

It was also vital to consider receptor-mediated activation of TRPC6 channels; whilst DAG has been shown to directly activate TRPC3/6/7 channels (Hofmann *et al.*, 1999), *in vivo* it is produced downstream of signalling cascades switched on when ligands bind to receptors on the cell membrane. This is particularly important in mast cell biology because ligands such as ATP, ADP, C3a and adenosine are found at sites of allergic inflammation, such as the asthmatic lung. Mast cells express many GPCRs on the cell surface including and P2Y receptors (Gilfillan & Tkaczyk, 2006), therefore it was considered whether TRPC6 channels could be stimulated downstream of GPCR activation to give rise to measurable currents and Ca^{2+} entry. HEK-TRPC6 cells were used as a model for the activation of TRPC6 by GPCRs; it was shown that carbachol stimulation gave rise to Ca^{2+} entry, as reported previously for HEK-TRPC6 cells (Cayouette *et al.*, 2004; Estacion *et al.*, 2004; Estacion *et al.*, 2006). ADP, which stimulates $P2Y_1$, $P2Y_{12}$ and $P2Y_{13}$ receptors, and UTP, which activates $P2Y_4$, both induced Ca^{2+} entry in HEK-TRPC6 cells. These preliminary results indicated that the three agonists tested are appropriate to use for studies of GPCR-mediated TRPC6 activation in HEK cells.

ADP was selected to investigate GPCR-mediated stimulation of TRPC6 channels because *in vivo*, ATP and its breakdown products, ADP and AMP, are found at high concentrations at sites of allergic inflammation. ADP may represent an important mast cell stimulus in the allergic response; in mouse mast cells it was found to stimulate histamine release (Saito *et al.*, 1991). It has previously been reported that human lung mast cells express $P2Y_1$ receptors (Schulman *et al.*, 1999), and data in chapter 3 of this study demonstrates that ADP induces Ca^{2+} entry in these cells (figure 3.3). $P2Y_1$ receptors are coupled to PLCβ (Gilfillan & Tkaczyk, 2006); therefore, the downstream generation of DAG may activate TRPC3/6/7 channels. The biophysical properties of ADP-activated channels were investigated in human lung mast cells; HEK-TRPC6 cells were firstly used as a model to evaluate whether TRPC6 currents could be switched on downstream of ADP activation, and whether they could be recorded using the whole-cell patch clamp technique.

Focal application of ADP to HEK-TRPC6 cells resulted in typical outwardly-rectifying currents with a mean reversal potential of 1.44 ± 0.38mV. As observed for OAG-induced currents in HEK-TRPC6 cells, the majority of the currents stimulated by ADP were transient (83%); the reasons for this have already been discussed in the context of OAG-induced currents in this cell line and will not be explored further. The ADP-induced current was absent from HEK cells not expressing TRPC6 so is likely to be mediated by TRPC6 channels. These results show that ADP activation of P2Y receptors can be coupled to the activation of TRPC6 channels with typical biophysical properties.

In summary, the results obtained with HEK-TRPC6 cells show that fura-2 Ca^{2+} imaging and whole-cell patch clamp electrophysiology can be used to study the direct activation of TRPC6 channels by OAG, and by the more physiological method of P2Y receptor stimulation by ADP.

4.3.2 Activation of TRPC5 channels in HEK cells

HEK-TRPC5 cells with tetracycline-inducible expression (Zeng *et al.*, 2004) were used to verify that known activation mechanisms for TRPC5 could be used to activate the channels in our laboratory. Carbachol was firstly used; this has been extensively employed to study TRPC5 channels expressed in HEK cells (Zeng *et al.*, 2004; Xu *et al.*, 2005a; DeHaven *et al.*, 2009), as well as endogenously expressed TRPC5 channels (Ma *et al.*, 2008). Ca^{2+} imaging experiments showed that carbachol stimulated Ca^{2+} influx in tetracycline-induced (Tet^+) cells; a small rise in Ca^{2+} induced by carbachol was also observed in Tet^- cells, which was abolished when the cells were pre-treated with 1μM thapsigargin for 30 minutes to deplete internal Ca^{2+} stores. This indicates that the small rise in Ca^{2+} seen in Tet^- cells was due to release from intracellular stores, in agreement with results obtained previously using this cell line (Zeng *et al.*, 2004).

It is also clear that Ca^{2+} entry in Tet^+ cells was reduced in amplitude when the cells had been pre-treated with thapsigargin. There are a number of possible explanations for this; it has been shown previously that intracellular Ca^{2+} can stimulate mouse (m) TRPC5 channels in a

concentration-dependent manner (Gross *et al.*, 2009) and that 200nM can stimulate human (h) TRPC5 channels (Zeng *et al.*, 2004). The mechanism for receptor activation of TRPC5 channels is poorly defined; it has been shown using mouse TRPC5 that U73122 inhibits the response, indicating PLC involvement (Kanki *et al.*, 2001; Plant & Schaefer, 2003), and it is known that a G-protein is involved (Kanki *et al.*, 2001). It is possible that Ca^{2+} activation of the channel is partly responsible for its activation downstream of receptor stimulation. Thapsigargin pre-treatment led to elimination of the Ca^{2+} store release in these cells (figure 4.7c); this could lead to incomplete activation of TRPC5 as the elevated intracellular Ca^{2+} following store depletion was not contributing. This would result in decreased TRPC5-mediated Ca^{2+} entry, as seen in figure 4.7c. Because previous depletion of the stores did not prevent the response to carbachol, it is unlikely that intracellular Ca^{2+}-mediated activation is a major contributor to receptor stimulation of TRPC5. The results are in agreement with Zeng *et al.* (2004), who showed that pre-treatment with thapsigargin reduced but did not abolish carbachol-induced Ca^{2+} entry in Tet^{+} cells (Zeng *et al.*, 2004).

To investigate whether TRPC5 currents with the expected biophysical properties could be recorded in our laboratory, whole-cell patch clamp recordings of carbachol-activated currents in HEK-TRPC5 cells were carried out. Focal application of carbachol gave rise to currents in Tet^{+} cells, but not in non-induced cells, showing that the current recorded was mediated by TRPC5. The I/V relationship was s-shaped, outwardly-rectifying and had a reversal potential of 0.76± 0.24mV; this is typical of TRPC5 currents (Jung *et al.*, 2003; Zeng *et al.*, 2004). The characteristic s-shaped I/V curve occurs because the channel does not switch off completely at voltages between -100mV and +100mV (Beech, 2007). Whilst the inward and outward currents were enhanced by carbachol application, currents were already switched on at the beginning of the recording after the whole-cell recording configuration was established. The I/V relationship before carbachol application had all the features of a TRPC5-mediated current, and currents were not present in Tet^{-} cells; it can therefore be concluded that TRPC5 channels were already active in these recordings. Constitutive activity has been reported for mTRPC5 (Yamada *et al.*, 2000), but not hTRPC5 (Zeng *et al.*, 2004), therefore is not likely to account for pre-stimulus channel activity in this study. As discussed above, 200nM intracellular Ca^{2+} has been shown to activate hTRPC5 (Zeng *et al.*, 2004) in the absence of receptor stimulation. The estimated free Ca^{2+} concentration of the intracellular solution used in this study was 70nM; it is possible that at this concentration some activation of TRPC5 may have occurred. Whilst it is known that extracellular Ca^{2+} activates TRPC5, previous studies have shown that a concentration of 5mM is required (Zeng *et al.*, 2004); the concentration in this study was 2mM, therefore it is unlikely to have been activated by extracellular Ca^{2+}. To investigate the contribution of Ca^{2+} to the activation of TRPC5 channels prior to agonist application, it would be necessary to repeat the experiment with different intracellular Ca^{2+} concentrations. It is clear that a multiplicity of signals contributes to the activation of hTRPC5; the possibility that another, yet undiscovered, factor caused activation of the channel prior to agonist application should not be excluded. To summarise, whole-cell

patch clamp electrophysiology and Ca^{2+} imaging approaches can be successfully used to record TRPC5 channel activity, as reported previously for this cell line (Zeng *et al.*, 2004).

The activation of HEK-TRPC5 cells with the more selective activators of TRPC5, S1P and Gd^{3+}, was then tested using fura-2 Ca^{2+} imaging. Both agents gave rise to Ca^{2+} influx in Tet^{+} cells but not Tet^{-}, showing that Ca^{2+} entry is due to expression of TRPC5. Whilst lanthanides inhibit most TRP channels at micromolar concentrations (Beech, 2007), Gd^{3+} and La^{3+} potentiate mTRPC4 and 5 channels at these concentrations and cause inhibition at millimolar concentrations.

It is clear that the size of S1P-induced Ca^{2+} entry in HEK-TRPC5 cells was much larger than that induced by Gd^{3+} (compare figure 4.9a with figure 4.10a); this could be due the inhibition of endogenous ion channels by Gd^{3+}, whereas S1P would be expected only to activate channels. However, this cannot account for the difference alone, because carbachol-induced Ca^{2+} entry in these cells (figure 4.7) was also smaller in size than S1P-evoked responses, albeit larger than that induced by Gd^{3+}. This is likely to be due to the complex functions and interactions of S1P, both intracellularly and extracellularly. There are five membrane receptors for S1P ($S1PR_{1\text{-}5}$), with cell-specific expression, that couple to different G-proteins (Strub *et al.*, 2010). Whilst it has been shown in HEK-TRPC5 cells that S1P-induced Ca^{2+} entry is pertussis toxin (PTX) sensitive (Xu *et al.*, 2006b), suggesting the involvement of Gi-coupled receptors, the contribution of the other S1P receptors to TRPC5 activation has not been assessed. HEK-293 cells express $S1P_1$, $S1P_2$ and $S1P_3$ receptors (Meyer zu Heringdorf *et al.*, 2001); it is therefore possible that, in addition to the PTX-sensitive mechanism described by Xu *et al*, other G protein-coupled S1P receptors may have been activated, which could have led to a large Ca^{2+} entry when combined with direct activation of TRPC5. S1P can also act as an intracellular messenger; in addition to its effects on TRPC5 (Xu *et al.*, 2006b), caged S1P has been shown to cause Ca^{2+} rises in neuroepithelioma and hepatocellular carcinoma cell lines that do not respond to extracellular S1P. Sphingosine kinase 2 knockout mice have defective Ca^{2+} mobilisation following FcεRI crosslinking, which cannot be restored with extracellular S1P (Olivera *et al.*, 2007); this also suggests an intracellular target. These data, along with the large Ca^{2+} influx induced by S1P in this study compared to other activation mechanisms of TRPC5, highlight the complex functions of S1P. Because S1P-induced Ca^{2+} entry was absent in Tet^{-} cells, it is reasonable to conclude that its actions observed in this study were due to activation of the channel. However, when S1P was used to probe for TRPC5 activation in mast cells, it was important to consider that it is associated with complex signalling pathways and may as a result have off-target effects.

In summary, data obtained using HEK-TRPC5 cells show that receptor activation with carbachol, stimulation with S1P and external ionic activation with Gd^{3+} can be used to activate TRPC5 channels as reported previously. Gd^{3+} in particular was a useful tool to investigate TRPC5 activation in human mast cells; it only activates TRPC4 and 5 channels whilst inhibiting the others, and RT-PCR results revealed that mRNA for TRPC4 was not present in human mast cells

(figure 3.9). It could therefore be used to selectively probe for functional TRPC5 expression. As described in chapter 1.3.2, TRPC5 and TRPC6 channel activity can be distinguished by their I/V relationships. Whilst TRPC5 channels have a characteristic s-shaped I/V curve, that of TRPC6 channels is more linear with outward rectification (compare figures 4.2 and 4.8). The pharmacological profile of the channels can also be used to distinguish them in native cell types; whilst 100μM Gd^{3+} activates TRPC5 channels, as shown in figure 4.10, it inhibits TRPC6 and other channels at this concentration. OAG activates TRPC6 but not TRPC5, and S1P has only been shown to activate TRPC5. These tools were able to be used to study the functional expression of TRPC channels in human mast cells.

Chapter 5: Store-operated TRPC channels in human mast cells

As discussed in chapter 1.3.2.11, a large body of evidence exists to support the role of TRPC channels, particularly from the TRPC1/4/5 subgroup, in SOCE. A model has been proposed, based on studies in HSG cells, whereby TRPC1 channels are present in recycling vesicles, and following store depletion they are retained at the plasma membrane by STIM1. TRPC1 and Orai1, whilst not forming a heteromeric assembly, are thought to be maintained in close proximity by plasma membrane lipid raft microdomains. Ca^{2+} entry through Orai1 channels following store depletion is thought to enhance TRPC1 channel insertion in the plasma membrane, suggesting functional interactions of the three proteins. The model, recapitulated from that shown in figure 1.17, is depicted in figure 5.1.

The entry of Ba^{2+} ions following intracellular store depletion in LAD 2 cells and HLMCs (chapter 3.3) suggests that TRPC channels are involved in SOCE in human mast cells. This chapter aimed to investigate the involvement of TRPC channels in SOCE further, and the putative contribution of TRPC5 was investigated using the activators described in chapter 4.2. In the second half of this chapter, the activation of TRPC channels downstream of FcεRI cross-linking in HLMCs was investigated electrophysiologically, and the potential role of TRPC channels in IgE-mediated HLMC degranulation was assessed.

5.1 Characterisation of Synta 66 as a selective I_{CRAC} inhibitor

To assess the contribution of TRPC channels to store-operated Ca^{2+} entry, the selective I_{CRAC} inhibitor Synta 66 (3-fluoropyridine-4-carboxylic acid (2',5'-dimethoxybiphenyl-4-yl)amide) was used to inhibit the Orai1-mediated component of SOCE. Synta 66 is a recently characterised Orai1 inhibitor, blocking I_{CRAC} currents in RBL cells with reported IC_{50} values of 3μM (Ng *et al.*, 2008) and 1.4μM (Di Sabatino *et al.*, 2009), with no significant effect on other receptors, ion channels and enzymes (Di Sabatino *et al.*, 2009). Synta 66 was verified in our laboratory as an effective blocker of I_{CRAC} using HEK cells over-expressing Orai1 and STIM1 (HEK-Orai/STIM cells), and in HLMCs. Using the whole-cell patch clamp technique, 2μM $InsP_3$ and 10mM BAPTA were internally applied via the patch pipette to activate I_{CRAC} currents; divalent-free (DVF) solution was externally applied as shown in figure 5.2a to potentiate the current and facilitate recording.

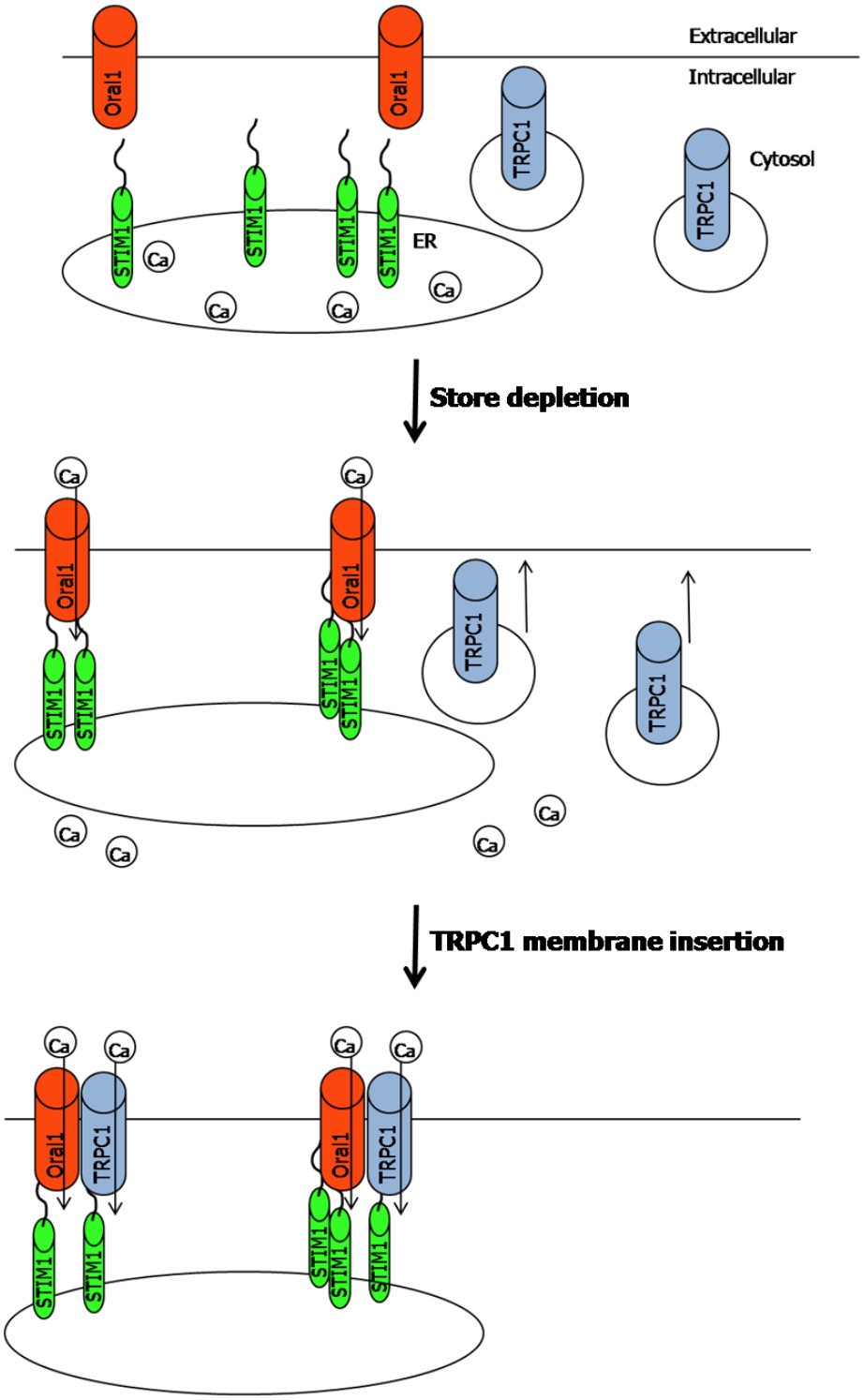

Figure 5.1. Model for TRPC1 activation by store depletion

STIM1 is located in the ER membrane, and Orai1 in the plasma membrane. TRPC1 is hypothesised to be localised in vesicles. Following store depletion, STIM1 aggregates and translocates to the plasma membrane, activating Orai1 channels. Orai1-mediated Ca^{2+} entry enhances TRPC1 insertion into the plasma membrane where it is gated by STIM1 to cause further SOCE.

N.B. Model is the same as that shown in figure 1.15

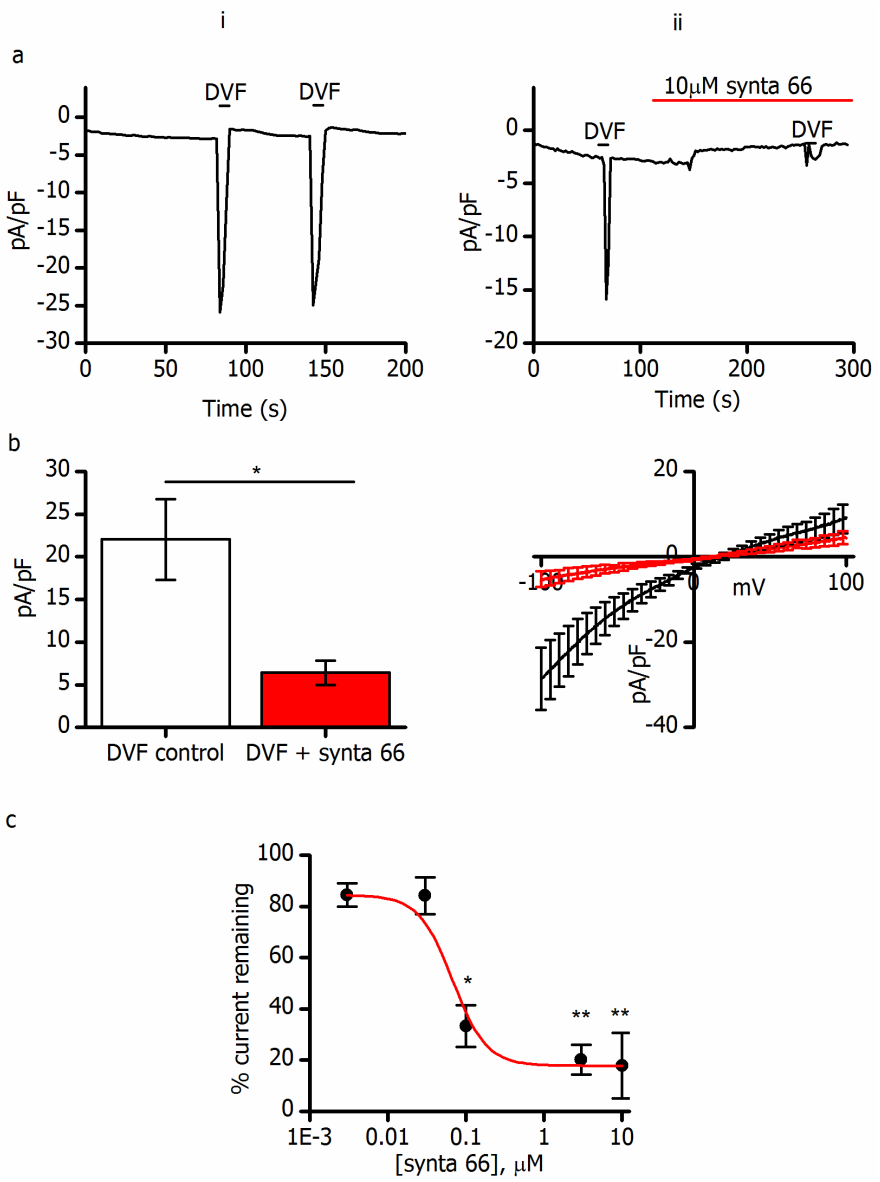

Figure 5.2. Synta 66 inhibits I_{CRAC} currents in HLMCs and HEK-Orai-STIM cells

a: Time-course of I_{CRAC} recordings in isolated primary human lung mast cells activated by internal application of 2μM IP_3 and 10mM BAPTA and perfusion of divalent free solution (DVF) to cause rapid sodium influx. (i) shows an example control recording; in (ii) 10μM synta 66 was present as indicated.

b (i): Bar graph showing mean current density recorded at -80mV in HLMCs in the presence and absence of synta 66. *: means were significantly different, $p<0.05$, unpaired Student's T-test. n=6 cells, N=1 donor. (ii): Current-voltage relationships in DVF solution in the presence (red) and absence (black) of synta 66. Ramps from -150mV to +150mV were applied every 2 seconds. Traces show mean ± SEM; n=6, N=1 donor.

c: HEK-Orai-STIM cells were held at 0mV and 2μM IP_3 and 10mM BAPTA were internally applied to activate ICRAC currents. DVF solution was applied in the presence of synta 66 at the concentrations shown; graph shows the percentage of DVF current remaining in the presence of synta 66. IC_{50} = 0.07μM. *: means were significantly different, $p<0.05$, **: $p<0.01$, one-way ANOVA of log-transformed data with Tukey post-test. Experiments were carried out by Jasmine Farrington

As shown in figure 5.2b (ii), $InsP_3$- and BAPTA-evoked currents in HLMCs recorded in the presence of DVF external solution had the characteristic properties of I_{CRAC} currents including inward rectification and a positive reversal potential. Using the same protocol in HEK-Orai/STIM cells, the inward current was measured in the presence of various concentrations of synta 66, applied externally. As shown in figure 5.2c, synta 66 gave rise to concentration-dependent inhibition of I_{CRAC} currents in HEK-Orai/STIM cells with an IC_{50} of 0.07μM. Maximal inhibition was achieved by 10μM synta 66. In HLMCs, I_{CRAC} currents were also significantly inhibited by 10μM synta 66 (figure 5.2a and b); together these data show that synta 66 is an effective inhibitor of I_{CRAC} currents in HEK-Orai/STIM cells and HLMCs. 10μM synta 66 was used for all other experiments as it caused maximal inhibition of I_{CRAC}.

Previous studies have reported that 10μM synta 66 selectively inhibits Orai1-mediated I_{CRAC} currents without affecting other targets including GABA, muscarinic receptors, P2X receptors, K^+ channels, Cl^- channels, Na^+ channels and TRPC channels (Di Sabatino *et al.*, 2009; Li *et al.*, 2011). To verify that synta 66 does not inhibit TRPC channels in our laboratory, its effects on Ca^{2+} entry in HEK-TRPC5 and HEK-TRPC6 cells were investigated. As shown in figure 5.3, there was no reduction in OAG-evoked Ca^{2+} entry in HEK-TRPC6 cells when synta 66 was present throughout the experiment; OAG-induced $\Delta F_{340/380}$ was measured at 0.44 ± 0.03 (n=31, N=3) in control cells and 0.59 ± 0.02 (n=65, N=3) in the presence of 10μM synta 66. These data show that, at a concentration causing maximal inhibition of I_{CRAC}, synta 66 does not inhibit TRPC6 channels. In Tet^+ HEK-TRPC5 cells, there was no difference in the amplitude of S1P-stimulated Ca^{2+} entry in the presence and absence of synta 66 (figure 5.4); $\Delta F_{340/380}$ in the absence of synta 66 was 1.27 ± 0.11 (n=35, N=3), and that in the presence of synta 66 was 1.24 ± 0.07 (n=108, N=3). Taken together with published data showing that synta 66 does not inhibit TRPC1/5 heteromeric assemblies (Li *et al.*, 2011), these results suggest that synta 66 can be used to inhibit Orai1 channels whilst TRPC channels remain unaffected.

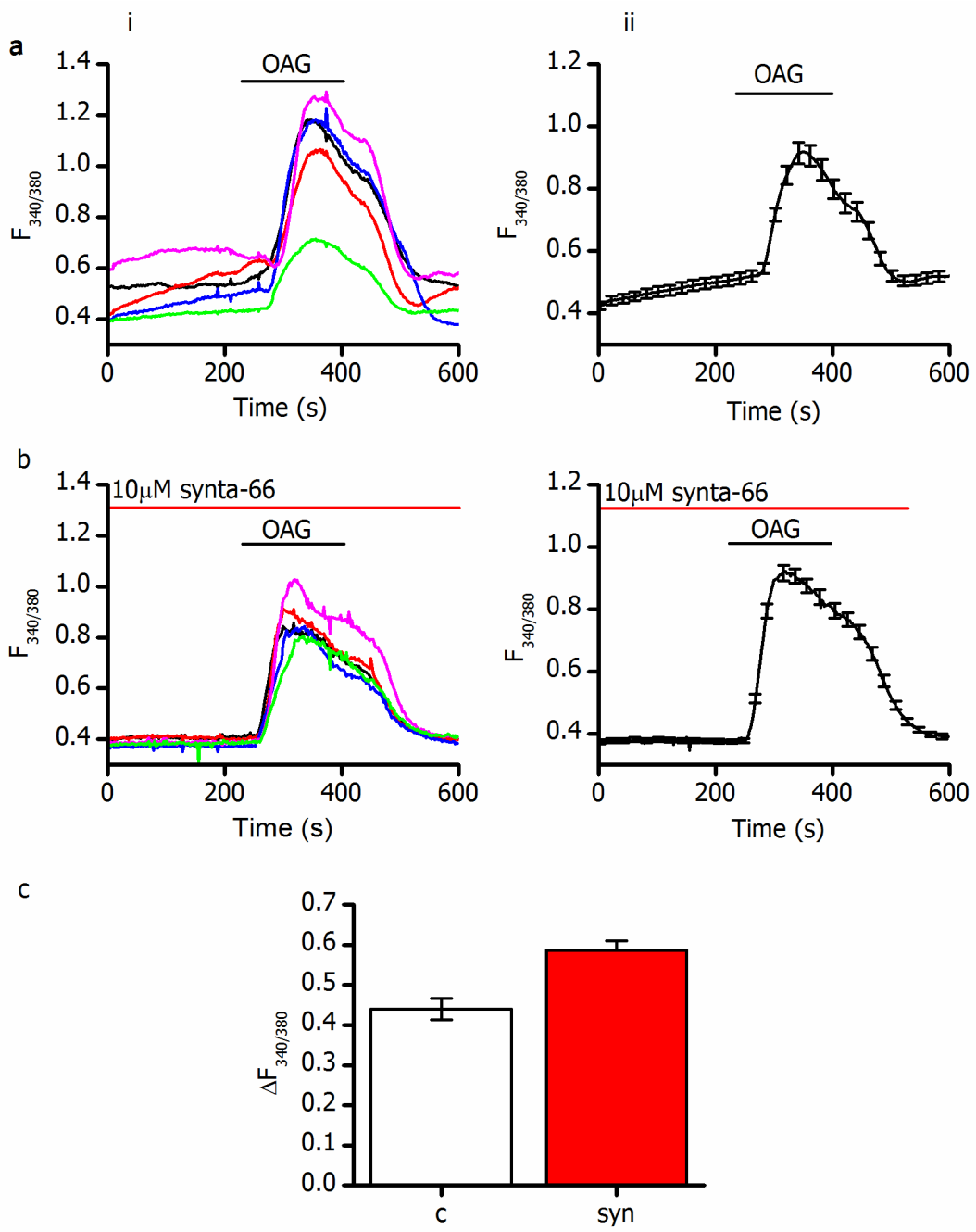

Figure 5.3. OAG-induced calcium entry in HEK-TRPC6 cells is not inhibited by Synta-66

a: Cells were perfused in standard external solution and 100μM OAG was bath-applied as shown. (i) shows individual representative cell traces; (iii) shows mean ± SEM (n=32, N=3)

b: Experiments as in (a), with 10μM Synta-66 present throughout the experiment (n= 65, N=3).

c: Bar chart showing the size of OAG-induced calcium entry ($\Delta F_{340/380}$) in control cells ("c") and in the presence of 10μM Synta-66 ("syn").

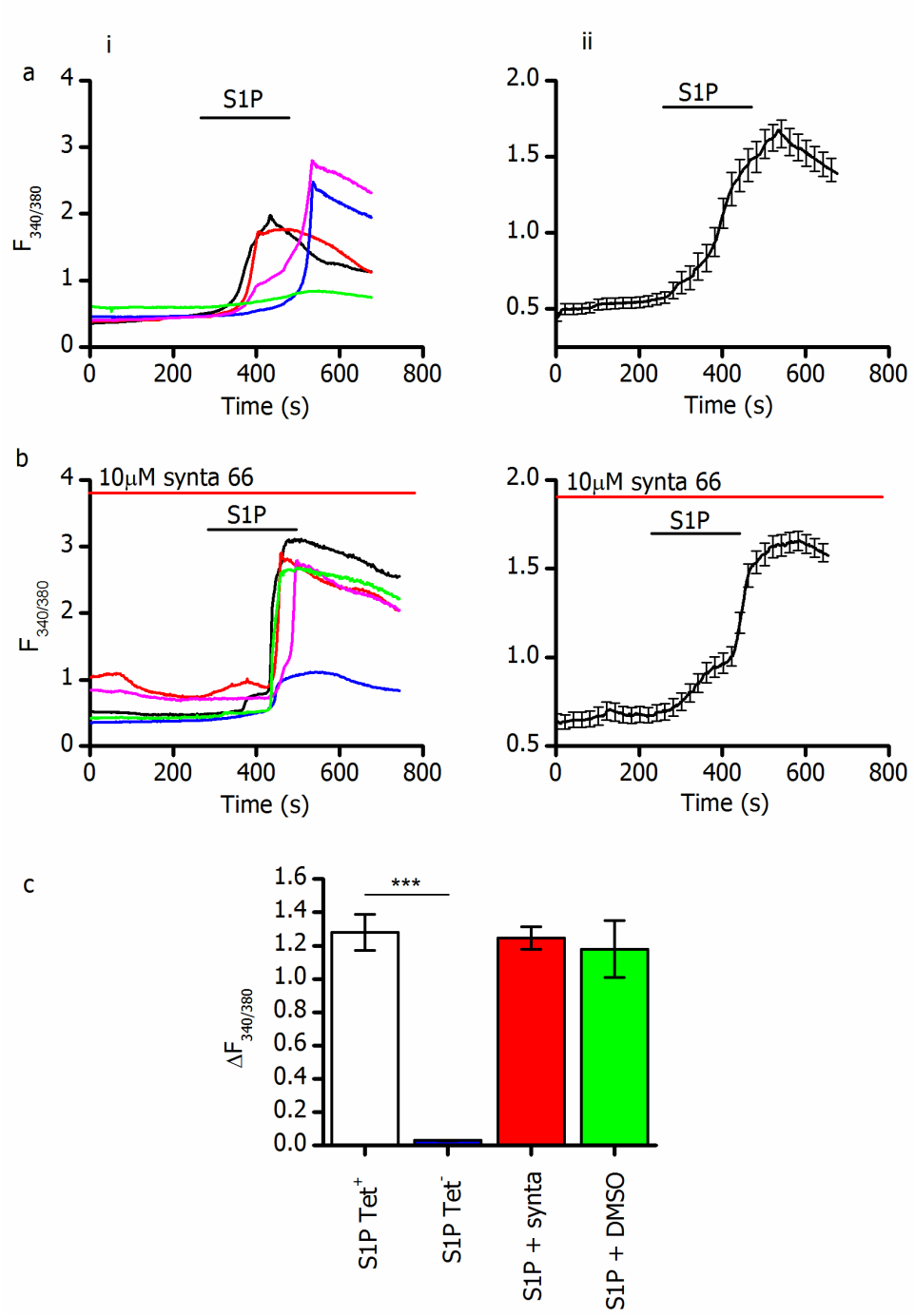

Figure 5.4. Synta-66 does not inhibit S1P-induced calcium entry in HEK-TRPC5 cells

a: TRPC5-expressing HEK cells induced overnight with tetracycline were perfused in standard external solution and 10μM S1P was bath-applied as shown. (i) shows individual cell traces; (ii) shows mean ± SEM. b: Experiments as in (a), with 10μM synta-66 present throughout the experiment.

c: Bar graph showing size of S1P-induced calcium entry in tetracycline-induced (Tet+) and non-induced (Tet-) cells, and in the presence of 10μM synta-66 or 1/1000 DMSO (solvent control for synta-66) ***: mean was significantly different from control, $p<0.001$, one-way ANOVA with Tukey post-test. Mean calcium entry in the presence of synta-66 was not significantly different from that in the absence of synta-66. n numbers are as follows: n=35 N=3 for Tet^+, n=85 N=3 for Tet^-, n=108 N=3 for synta, n=22 N=2 for DMSO.

N.B. Contol data in part (a) is the same data as shown in figure 4.8.

5.2 Store-operated Ca^{2+} entry in human mast cells

Having established that synta 66 can be used in our laboratory to inhibit I_{CRAC} currents without affecting TRPC5- or TRPC6-mediated Ca^{2+} entry, experiments assessing Ba^{2+} and Ca^{2+} entry following store depletion in LAD 2 cells and HLMCs (described in chapter 3.3) were repeated in the presence of synta 66. In LAD 2 cells (figure 5.5), the presence of 10μM synta 66 significantly reduced $\Delta F_{340/380}$ corresponding to Ba^{2+} entry following thapsigargin stimulation by 0.16 (from 0.19 to 0.03); Ca^{2+} entry was significantly reduced by 0.6 (from 0.66 to 0.06). Following FcεRI cross-linking, Ba^{2+} entry was non-significantly reduced by 0.05 (from 0.14 to 0.09) in the presence of synta 66, and Ca^{2+} entry was significantly reduced by 0.35 (from 0.53 to 0.18). When P2Y receptors were activated with ADP, Ba^{2+} entry was significantly reduced by 0.06 (from 0.15 to 0.09) in the presence of synta 66; Ca^{2+} entry was significantly reduced by 0.39 (from 0.51 to 0.12). DMSO at 1/1000 dilution (vehicle for synta 66) did not cause a significant reduction in Ba^{2+} or Ca^{2+} entry following store depletion. Synta 66-insensitive Ba^{2+} and Ca^{2+} entry occurred to a greater extent following FcεRI cross-linking and ADP activation of P2Y receptors than following thapsigargin stimulation. The size of Ca^{2+} release from intracellular stores was highly variable, as illustrated in figure 5.6, and was not significantly different in experiments where synta 66 was subsequently applied, compared with control experiments. In the context of the model shown in figure 5.1, the small inhibition of Ba^{2+} entry by synta 66 following FcεRI cross-linking and ADP stimulation of P2Y receptors could be due to the inhibition of Orai1 channels. As the activity of TRPC1 channels is thought to be enhanced by Orai1, inhibition of Orai1 with synta 66 could give rise to reduced Ca^{2+} entry through TRPC1 channels. It is evident that the synta 66-insensitive divalent ion entry is smaller when thapsigargin was used to deplete stores, compared with P2Y stimulation or FcεRI cross-linking (compare figure 5.5d (i) with 5.5d (ii) and (iii)); the possible reasons for this will be explored in section 5.6. However, synta 66-insensitive divalent ion entry occurred following Ca^{2+} store release downstream of stimulation by all three methods in LAD 2 cells, providing evidence for the involvement of TRPC channels in SOCE in these cells.

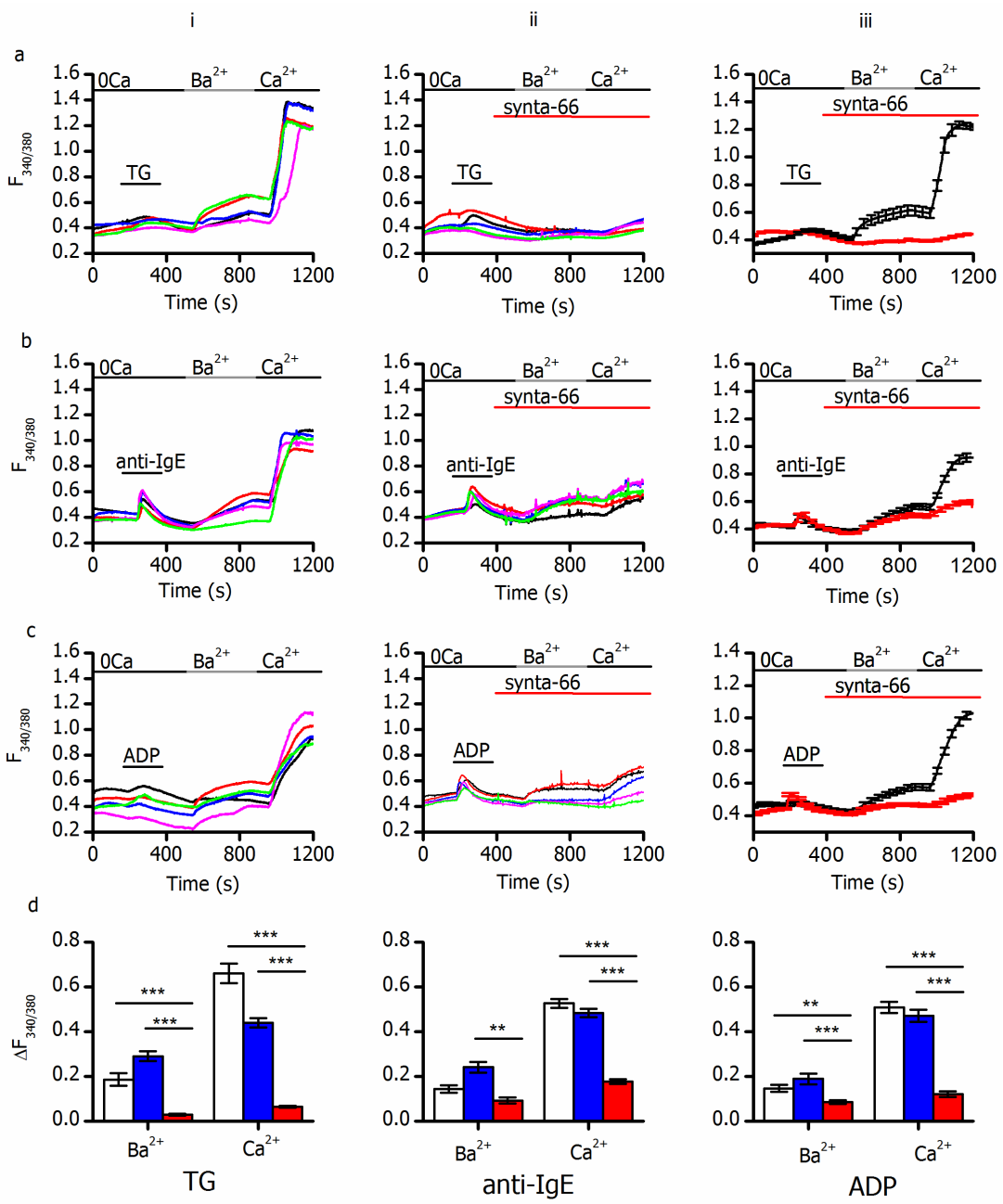

Figure 5.5. Ba^{2+} and Ca^{2+} entry into LAD 2 cells following store depletion in the presence of 10μM Synta-66.

Fura 2-loaded LAD 2 cells were superfused with Ca^{2+}-free external solution and stimulated with (a) 2μM thapsigargin (TG), (b)1/300 anti-IgE, following overnight incubation with 300ng/ml IgE, or (c) 100μM ADP. Solutions containing 2mM Ba^{2+} or Ca^{2+} were bath-applied as indicated by the horizontal bars. For (a), (b) and (c), (i) shows example individual cell traces in the absence of synta 66; (ii) shows individual cell traces in the presence of synta 66. (iii) shows mean ± SEM in the absence (black traces) and presence (red traces) of synta 66. n numbers for control data are as follows; (a): n=36 cells, N=4 experiments. (b): n=40, N=4. (c): n=57 N=4. n numbers for synta data are (a): n=48, N=3. (b): n=60, N=3. (c): n=59, N=3.

d: Bar graphs comparing size of Ba^{2+} and Ca^{2+} entry ($\Delta F_{340/380}$) following thapsigargin (i), anti-IgE (ii) or ADP (iii)-evoked Ca^{2+} store release in the presence (red) and absence (white) of synta 66, or in the presence of 1/1000 DMSO (blue, vehicle for synta-66). Bars show mean ± SEM; n numbers in the presence of DMSO are (i): n=25 N=3, (ii): n=40 N=3, (iii): n=24 N=3. ***: means were significantly different, $p<0.001$; **: $p<0.01$, one-way ANOVA with Tukey post-test.

N.B. Traces in the absence of synta 66 are the same as those shown in figure 3.6.

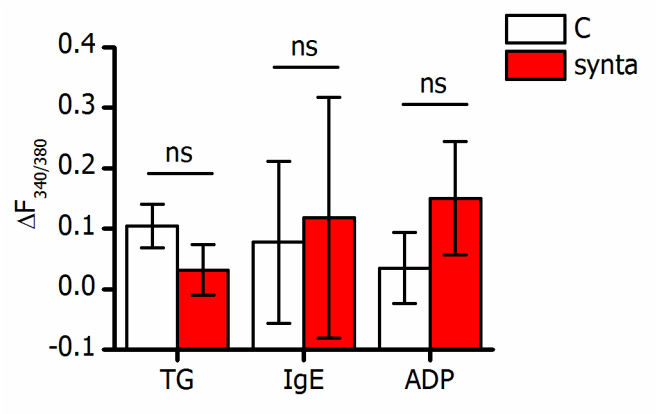

Figure 5.6. Ca^{2+} store release following LAD 2 cell stimulation

The size of Ca^{2+} released from stores in LAD 2 cells following stimulation with thapsigargin ("TG"), FcεRI cross-linking ("IgE") or ADP was compared in experiments where synta 66 was subsequently applied ("synta", red bars) and when synta 66 was not applied ("C", white bars). Error bars indicate standard deviation, to illustrate variation in results. ns: means were not significantly different, one-way ANOVA with Tukey post-test.

The Gd^{3+} sensitivity of Ba^{2+} and Ca^{2+} entry following store depletion with thapsigargin in LAD 2 cells was assessed; previous studies (Broad *et al.*, 1999; DeHaven *et al.*, 2009) have suggested that sensitivity to low μM concentrations of Gd^{3+} can be used as a further tool to distinguish I_{CRAC} from TRPC channel activity. Experiments like those shown in figure 5.5 were repeated in the presence of various concentrations of Gd^{3+}; Ba^{2+} and Ca^{2+} entry were both inhibited by Gd^{3+} at concentrations of 10μM and 30μM (figure 5.7c). No inhibition of Ba^{2+} entry occurred when Gd^{3+} was present at 1μM. Ca^{2+} entry was partially, but significantly, inhibited by 1μM Gd^{3+}, with complete inhibition occurring at 10μM. The sensitivity of Ba^{2+} and Ca^{2+} entry to 10μM Gd^{3+} provides further support for the hypothesis that TRPC channels are involved in SOCE in LAD 2 cells. The observed reduction in Ca^{2+} entry, but not Ba^{2+} entry, caused by 1μM Gd^{3+} is indicative of I_{CRAC}-mediated SOCE. It is likely that Ba^{2+} entry was not inhibited by 1μM Gd^{3+} because I_{CRAC} does not permeate Ba^{2+} (Lis *et al.*, 2007), and Gd^{3+} at this concentration inhibits I_{CRAC}, but not TRPC channels (Broad *et al.*, 1999; DeHaven *et al.*, 2009). The inhibition of Ba^{2+} entry by 10μM Gd^{3+}, but not by 1μM, provides further evidence for the involvement of TRPC channels in Ba^{2+} entry downstream of store depletion.

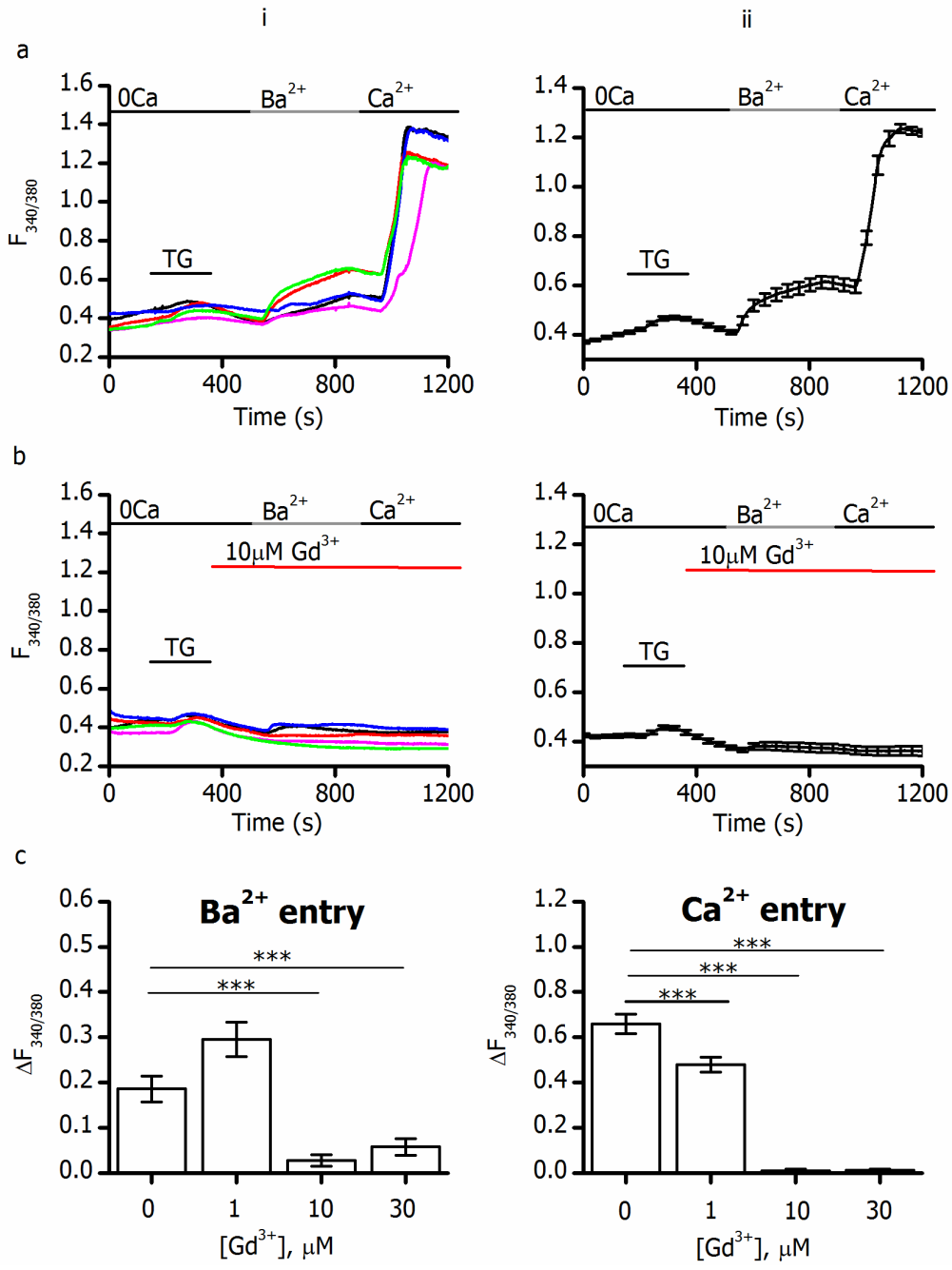

Figure 5.7. Ba^{2+} and Ca^{2+} entry into LAD 2 cells following store depletion is inhibited by Gd^{3+}.

a: Traces showing Ba^{2+} and Ca^{2+} entry in LAD 2 cells following TG-mediated store depletion in control cells; solutions were bath-applied as indicated by the horizontal bars. (i) shows individual cell traces; (ii) shows mean ± SEM (n=36 cells, N=4 experiments). b: Experiments as in (a), in the presence of 10μM Gd^{3+}. c: Bar chart showing size of Ba^{2+} (i) and Ca^{2+} (ii) entry ($\Delta F_{340/380}$) in the presence of Gd^{3+} at the concentrations shown. Bars show mean ± SEM; n numbers are as follows: 19 for 1μM, 36 for 10μM, 55 for 30μM. N= at least 2 experiments for each condition. ***: means were significantly different from control (no Gd^{3+}); $p<0.001$, one way ANOVA with Tukey post test.

N.B. Control data is the same as that shown in Figure 3.4.

In HLMCs, Ba^{2+} entry following passive store depletion with thapsigargin was unaffected by the presence of 10μM synta 66 (figure 5.8a). This result is not in accordance with that in LAD 2 cells, where Ba^{2+} entry was significantly reduced by synta 66 following thapsigargin application, suggesting that Ca^{2+} influx via Orai1 channels is not required for the stabilisation of TRPC channels at the membrane in HLMCs to the same degree as in LAD 2 cells. In HLMCs Ca^{2+} entry following thapsigargin stimulation was significantly reduced by 0.39 (from 0.50 to 0.11) in the presence of synta 66. When FcεRI cross-linking was the stimulus (figure 5.8b), a small but significant reduction in Ba^{2+} entry was observed (reduced by 0.11 from 0.23 to 0.12); Ca^{2+} entry was significantly attenuated by 0.22 (from 0.40 to 0.18). Following ADP stimulation (figure 5.8c), synta 66 reduced Ba^{2+} entry by 0.13 (from 0.21 to 0.08); this reduction was not statistically significant. Ca^{2+} entry was significantly reduced by 0.37 (from 0.55 to 0.18). As with LAD 2 cells, the size of Ca^{2+} release from stores was highly variable in HLMCs and was not significantly different in experiments where synta 66 was subsequently applied and those where synta was not applied (figure 5.9). It is evident that Ca^{2+} store release was larger when ADP and anti-IgE were used as the stimulus, compared with thapsigargin, and the time courses were different. This is expected due to the distinct mechanisms of action of the three agonists, which were explored in detail in chapter 3.5 so will not be discussed here.

In line with the model proposed for the store-operated behaviour of TRPC1 in human mast cells (figure 5.1), the partial inhibition of Ba^{2+} entry following FcεRI cross-linking and ADP stimulation of P2Y receptors is likely to be due to the blocking action of synta 66 on Orai1 causing a reduction in the gating of TRPC1 by STIM1, as discussed above for LAD 2 cells. Whilst these data are in accordance with results obtained in LAD 2 cells, data showing that Ba^{2+} entry is unaffected by synta 66 in HLMCs are not. Inhibition of thapsigargin-mediated Ba^{2+} entry by synta 66 could have occurred to a greater degree in LAD 2 cells than in HLMCs due to the differential expression of TRPC channels between the two cell types, or differences in compartmentalised signalling; these ideas will be discussed in section 5.6. The existence of synta 66-insensitive Ba^{2+} and Ca^{2+} entry provides evidence for the involvement of TRPC channels in SOCE in HLMCs; as Ca^{2+} entry is likely to represent TRPC and I_{CRAC} activation, it is probable that synta 66-insensitive Ca^{2+} entry is carried by TRPC channels.

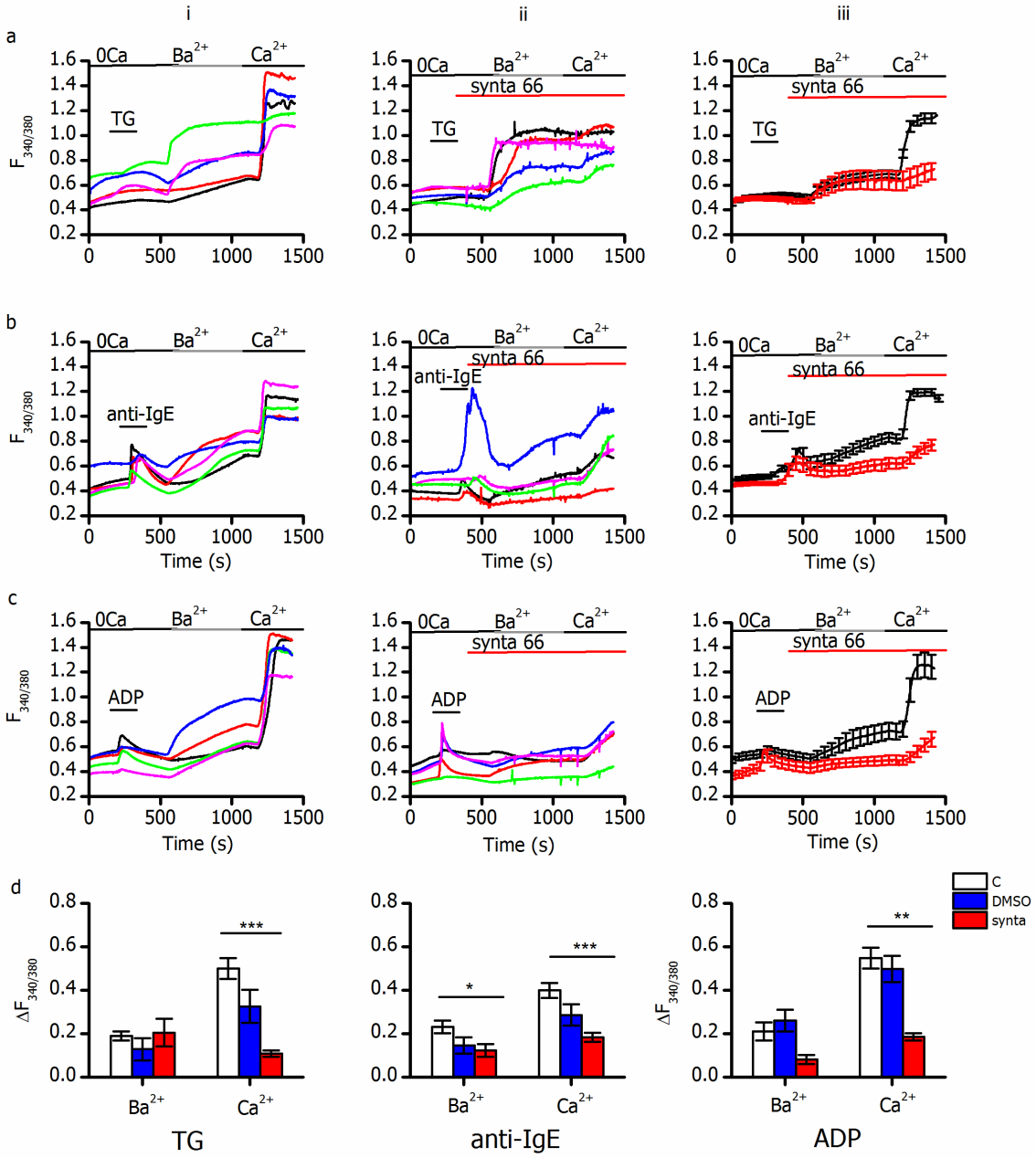

Figure 5.8. Ba^{2+} and Ca^{2+} entry into HLMCs following store depletion in the presence of 10μM Synta-66.

Fura 2-loaded HLMCs were stimulated with (a) 2μM thapsigargin (TG), (b)1/300 anti-IgE, following overnight incubation with 300ng/ml IgE or (c) 100μM ADP in the absence of extracellular calcium. Solutions containing 2mM Ba^{2+} or Ca^{2+} were bath-applied as indicated by the horizontal bars. For (a), (b) and (c), (i) shows example individual cell traces in the absence of synta 66; (ii) shows individual cell traces in the presence of synta 66. (iii) shows mean ± SEM in the absence (black traces) and presence (red traces) of synta 66. n numbers for control data are as follows; (a): n=33 cells, N=4 experiments, 2 donors. (b): n=30, N=4, 2 donors. (c): n=9, N=3, 2 donors. n numbers for synta data are (a): n=11, N=3, 1 donor. (b): n=23, N=3, 1 donor. (c): n=6, N=2, 1 donor.

d: Bar graphs comparing size of Ba^{2+} and Ca^{2+} entry ($\Delta F_{340/380}$) following thapsigargin (i), anti-IgE (ii) or ADP (iii)-evoked Ca^{2+} store release in the presence (red) and absence (white) of synta 66, or in the presence of 1/1000 DMSO (blue, vehicle for synta-66). Bars show mean ± SEM; n numbers for divalent entry in the presence of DMSO are (i): n=8, N=2, 1 donor. (ii): n=12, N=2, 1 donor. (iii): n=4, N=2, 1 donor. *: means were significantly different, $p<0.05$; **: $p<0.01$; ***: $p<0.001$, one-way ANOVA with Tukey post- test.

N.B. Control data is the same as that shown in Figure 3.7.

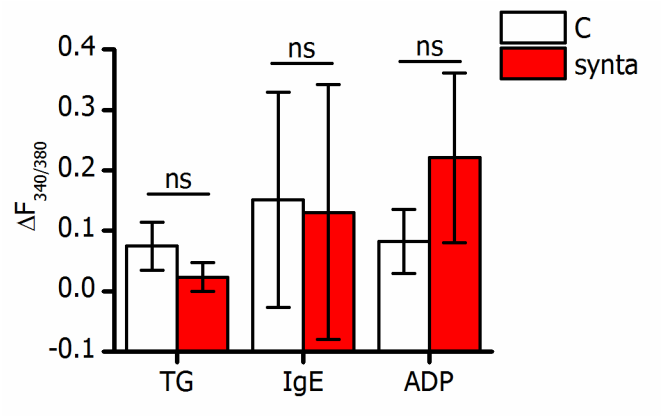

Figure 5.9. Ca^{2+} store release following HLMC stimulation

The size of Ca^{2+} release from stores in HLMCs following stimulation with thapsigargin ("TG"), FcεRI cross-linking ("IgE") or ADP was compared in experiments where synta 66 was subsequently applied ("synta", red bars) and when synta 66 was not applied ("C", white bars). Error bars indicate standard deviation, to illustrate variation in results. ns: means were not significantly different, one-way ANOVA with Tukey post-test.

Ba^{2+} and Ca^{2+} entry following passive store depletion with thapsigargin were then assessed in HLMCs in the presence of the non-selective TRPC channel inhibitor SKF-96365 (figure 5.10). $\Delta F_{340/380}$ corresponding to Ba^{2+} entry was significantly reduced by 0.12 (from 0.19 to 0.07) in the presence of SKF-96365. Taken together with data showing that store-operated Ba^{2+} and Ca^{2+} entry have synta 66-insensitive components, the sensitivity of Ba^{2+} and Ca^{2+} entry to SKF-96365 provides evidence for the involvement of TRPC channels in SOCE in HLMCs.

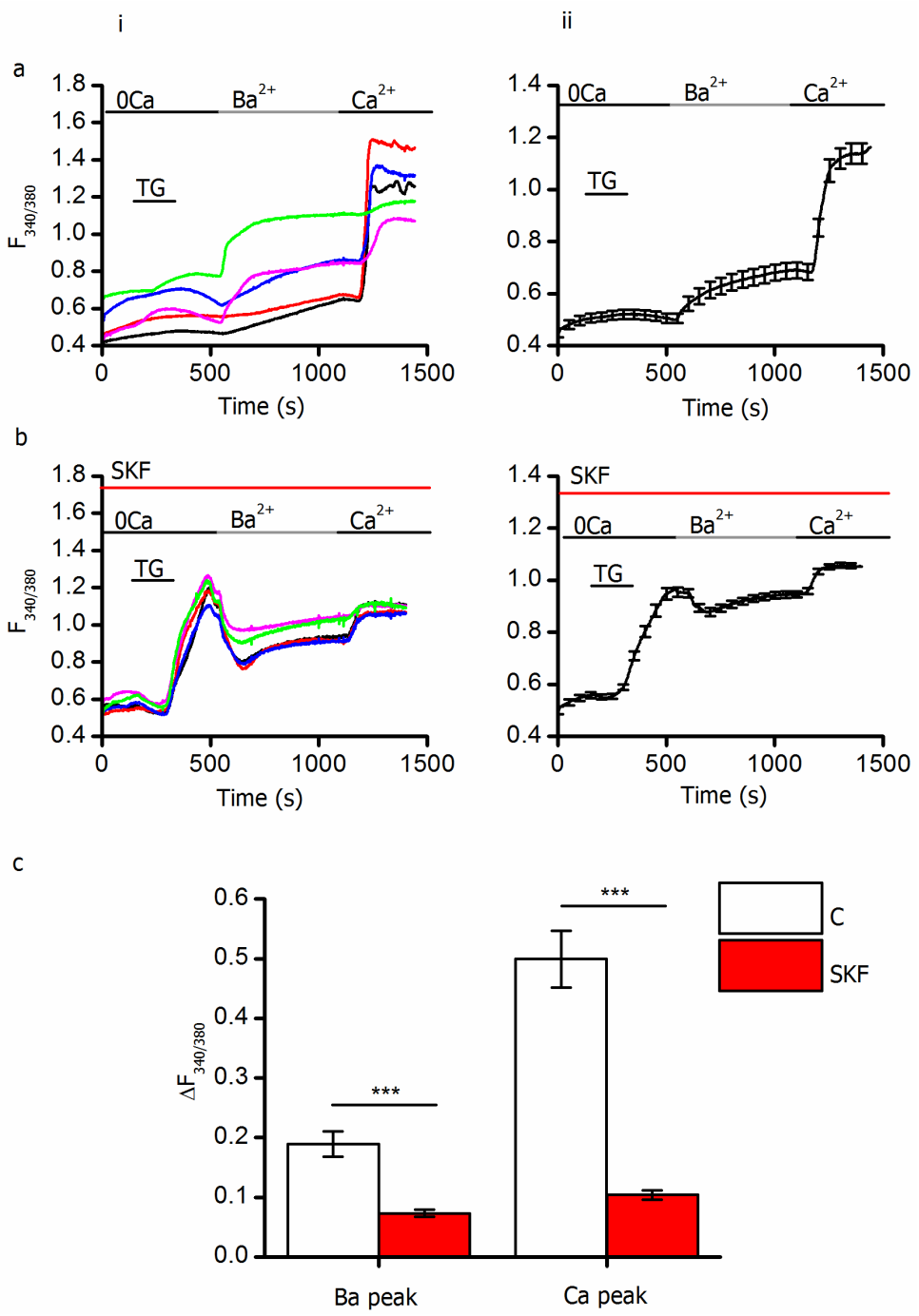

Figure 5.10. Ba^{2+} and Ca^{2+} entry following store depletion in HLMCs is sensitive to SKF-96365.

Fura 2-loaded HLMCs were stimulated with 2μM thapsigargin (TG) in the absence of extracellular calcium and solutions containing 2mM Ba^{2+} or Ca^{2+} were bath-applied as indicated by the horizontal bars in (a) and (b).

a: Divalent ion entry in the absence of SKF-96365 ("SKF"); (i) shows individual representative cell traces and (ii) shows mean ± SEM (n=33 cells, N=4 experiments, representative of 2 donors).

b: Experiments as in (a), with 10μM SKF present throughout the experiment (n=50, N=3, 1 donor).

c: Bar graph comparing size of Ba^{2+} and Ca^{2+} entry ($\Delta F_{340/380}$) in the presence (red) and absence (white) of SKF-96365. ***: means are significantly different, $p<0.001$, unpaired Student's T-test.

5.3 TRPC5 activation in LAD 2 cells and HLMCs

To determine whether TRPC5 channels are involved in Ba^{2+} and Ca^{2+} entry following store depletion in human mast cells, S1P and Gd^{3+} were used to probe for the functional expression of TRPC5 channels in both cell types. 100μM Gd^{3+} activates TRPC4 and TRPC5 channels (Jung *et al.*, 2003; Zeng *et al.*, 2004) whilst inhibiting other TRP channels (Beech, 2007). S1P activates TRPC5 homomeric channels, and TRPC5-TRPC1 heteromeric assemblies (Xu *et al.*, 2006b); data in chapter 4.2 show that these agents can be used to activate TRPC5 channels expressed in HEK-293 cells in our laboratory. As shown in figure 5.11, 10μM S1P and Gd^{3+} did not elicit Ca^{2+} entry in LAD 2 cells; the peak $F_{340/380}$ in the presence of S1P or Gd^{3+} was not significantly different from the mean baseline $F_{340/380}$ (unpaired Student's T-test). The mean $\Delta F_{340/380}$ in response to S1P application was 0.09 ± 0.03 (n=18, N=2) in LAD 2 cells, compared with 1.28 ± 0.11 (n=34, N=3) in Tet^+ HEK-TRPC5 cells. For Gd^{3+} experiments, the $\Delta F_{340/380}$ was 0.09 ± 0.03 (n=49, N=3) in LAD 2 cells and 0.14 ± 0.04 (n=37, N=3) in Tet^+ HEK-TRPC5 cells. 1μM ionomycin was applied to LAD 2 cells following S1P application to verify that Ca^{2+} signalling was functional. Taken together these data suggest that functional TRPC5 homomeric channels, or TRPC5-TRPC1 heteromeric assemblies, are not present in LAD 2 cells. It is therefore possible that synta 66-insensitive store-operated Ba^{2+} and Ca^{2+} entry in LAD 2 cells is carried by homomeric TRPC1 channels.

In HLMCs from 1 of 5 donors tested (donor 387), 10μM S1P and 100μM Gd^{3+} application gave rise to Ca^{2+} entry (figure 5.12). The maximum $F_{340/380}$ in the presence of S1P (0.53 ± 0.03; n=12) was significantly higher ($p<0.01$, unpaired Student's T-test) than the mean baseline $F_{340/380}$ (0.67 ± 0.03; n=12), and 100% of cells responded to S1P application, where "responders" were classed as cells where $F_{340/380}$ in the presence of S1P increased by more than 10 standard deviations above the mean baseline fluorescence. It is evident that two responses to S1P occurred in some cells; this is likely to be due to the two mechanisms by which S1P can activate TRPC5 channels, which will be discussed in section 5.6. Similarly, the peak $F_{340/380}$ in the presence of 100μM Gd^{3+} (0.46 ± 0.01; n=22) was significantly higher ($p<0.01$, unpaired Student's T-test) than the baseline fluorescence (0.39 ± 0.01; n=22), and 100% of cells responded to Gd^{3+} application. Taken together with RT-PCR data (chapter 3.4) showing that HLMCs from donor 387 express mRNA for TRPC1 and TRPC5, these results suggest that functional TRPC5 homomeric channels, or TRPC1-TRPC5 heteromers, are present in HLMCs from this donor. Analysis of the I/V relationships of S1P- and Gd^{3+}- evoked currents in these cells would show whether homomeric or heteromeric channels are responsible for Ca^{2+} entry; homomeric TRPC5 channels have a characteristic s-shaped I/V relationship, whereas the I/V of TRPC1-TRPC5 has greater linearity (Beech, 2007). Unfortunately, technical difficulties prevented patch clamp experiments from being carried out on HLMCs from donor 387 before the cells expired.

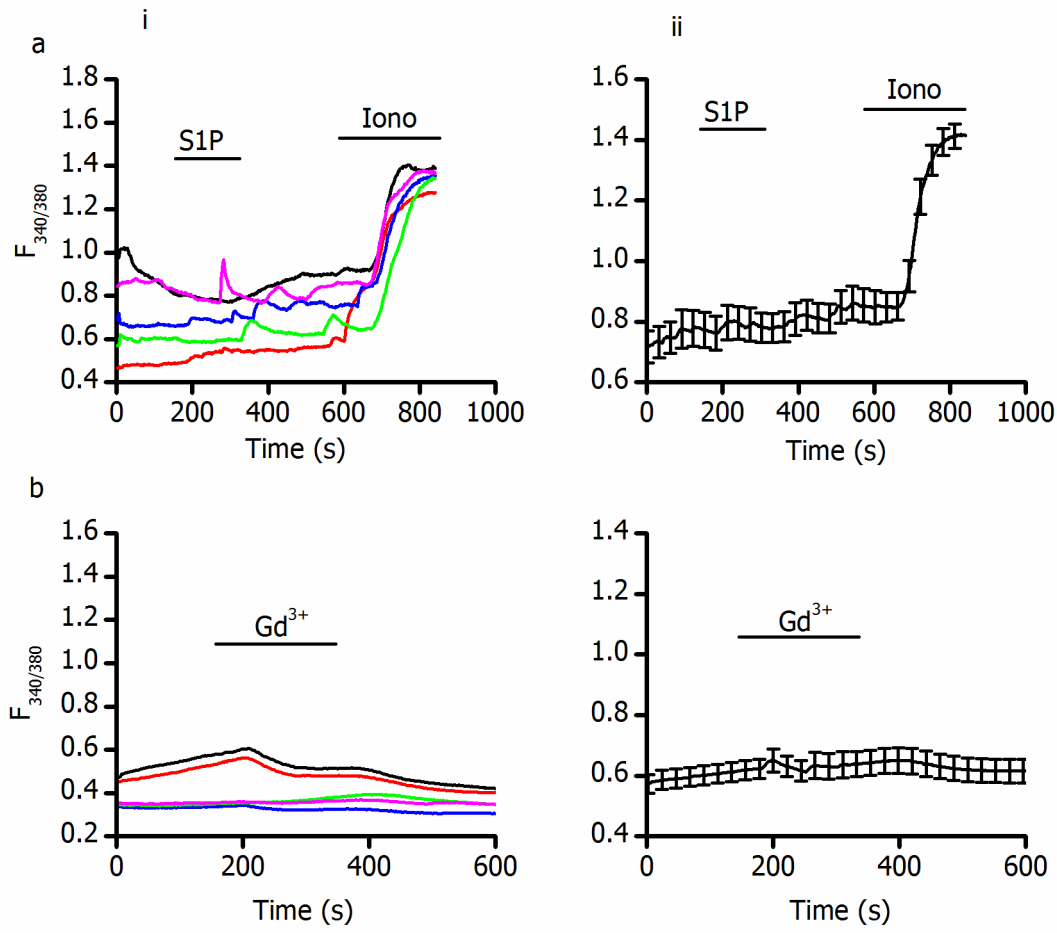

Figure 5.11. S1P and Gd^{3+} do not induce calcium entry in LAD 2 cells

a: LAD 2 cells were perfused with standard external solution and 10μM sphingosine-1-phosphate (S1P) was bath-applied as indicated. 1μM ionomycin was applied as a positive control at the end of the experiment. (i) shows individual cell traces; (ii) shows mean ± SEM of n=18 cells, N=2 experiments. b: 100μM Gd^{3+} was applied to cells as indicated; (ii) shows mean ± SEM for n=49, N=3.

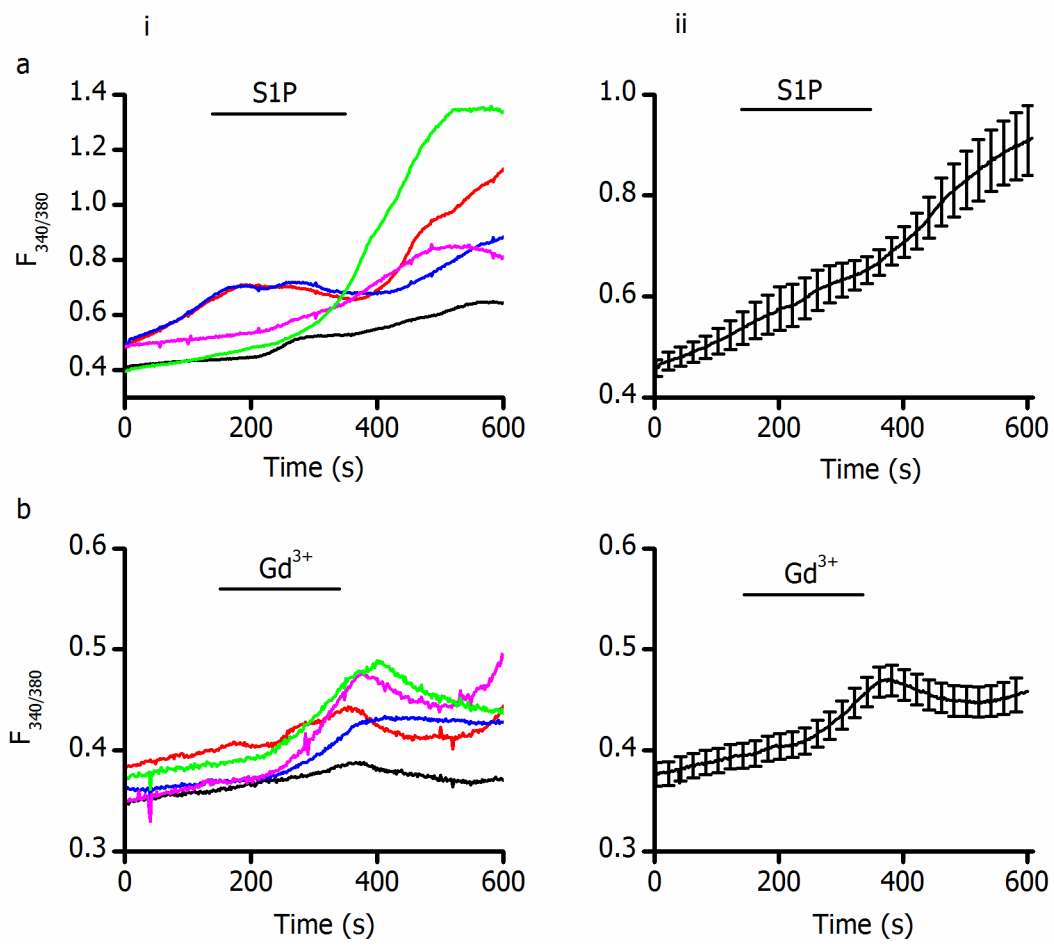

Figure 5.12. S1P and Gd^{3+} induce calcium entry in 1/5 HLMC donors

a: HLMCs (donor A387) were perfused with standard external solution and 10μM sphingosine-1-phosphate (S1P) was bath-applied as indicated. (i) shows individual cell traces; (ii) shows mean ± SEM of n=12 cells, N=2 independent experiments.

b: 100μM Gd^{3+} was applied to cells as indicated; (ii) shows mean ± SEM for n=22 cells, N=3.

HLMCs from the remaining 4/5 donors tested (360, 370, 410 and 411) did not respond to S1P and Gd^{3+} application (figure 5.13); in fura-2 Ca^{2+} imaging experiments there was no significant difference (unpaired Student's T-test) between the baseline $F_{340/380}$ and the peak $F_{340/380}$ in the presence of S1P or Gd^{3+}. In whole-cell patch clamp experiments on cells from donor 360, ΔpA/pF at +100mV following application of 10μM S1P was 0.13 ± 0.80 (n=5); that elicited by 100μM Gd^{3+} was -0.00 ± 0.37 (n=4). Peak currents measured at +100mV and -100mV in the presence of either Gd^{3+} or S1P were not significantly different from mean baseline currents (one-way ANOVA with Tukey post-test). These data indicate that TRPC5 channels are not functionally expressed in HLMCs from donors 360, 370, 410 and 411. As experiments assessing Ba^{2+} and Ca^{2+} entry following store depletion were also carried out on donors 410 and 411 (figures 5.8–5.10), the lack of TRPC5 functional expression in these cells indicates that TRPC1 alone is likely to be contributing to SOCE in these cells.

To summarise, the presence of synta 66-insensitive Ba^{2+} and Ca^{2+} entry following store depletion in LAD 2 cells and concentration-dependent attenuation by Gd^{3+} suggests that TRPC channels are involved in divalent ion entry. The lack of responsiveness to the TRPC5 activators S1P and 100µM Gd^{3+} indicates that TRPC5 channels are not functionally expressed in LAD 2 cells. Of the TRPC channels that are thought to be activated by store depletion (TRPC1, 4 and 5), it is likely that TRPC1 is responsible for the observed Ba^{2+} and Ca^{2+} entry; TRPC4 mRNA was not found to be expressed in these cells. In HLMCs from donors 410 and 411, synta-insensitive Ba^{2+} and Ca^{2+} entry following store depletion is also likely to be mediated by TRPC1; functional TRPC5 channels were not present in these donors, and TRPC4 mRNA was not detected. Although beyond the scope of this project, selective molecular knock-down of TRPC1 in both cell types is required in future studies to verify its involvement in SOCE in human mast cells.

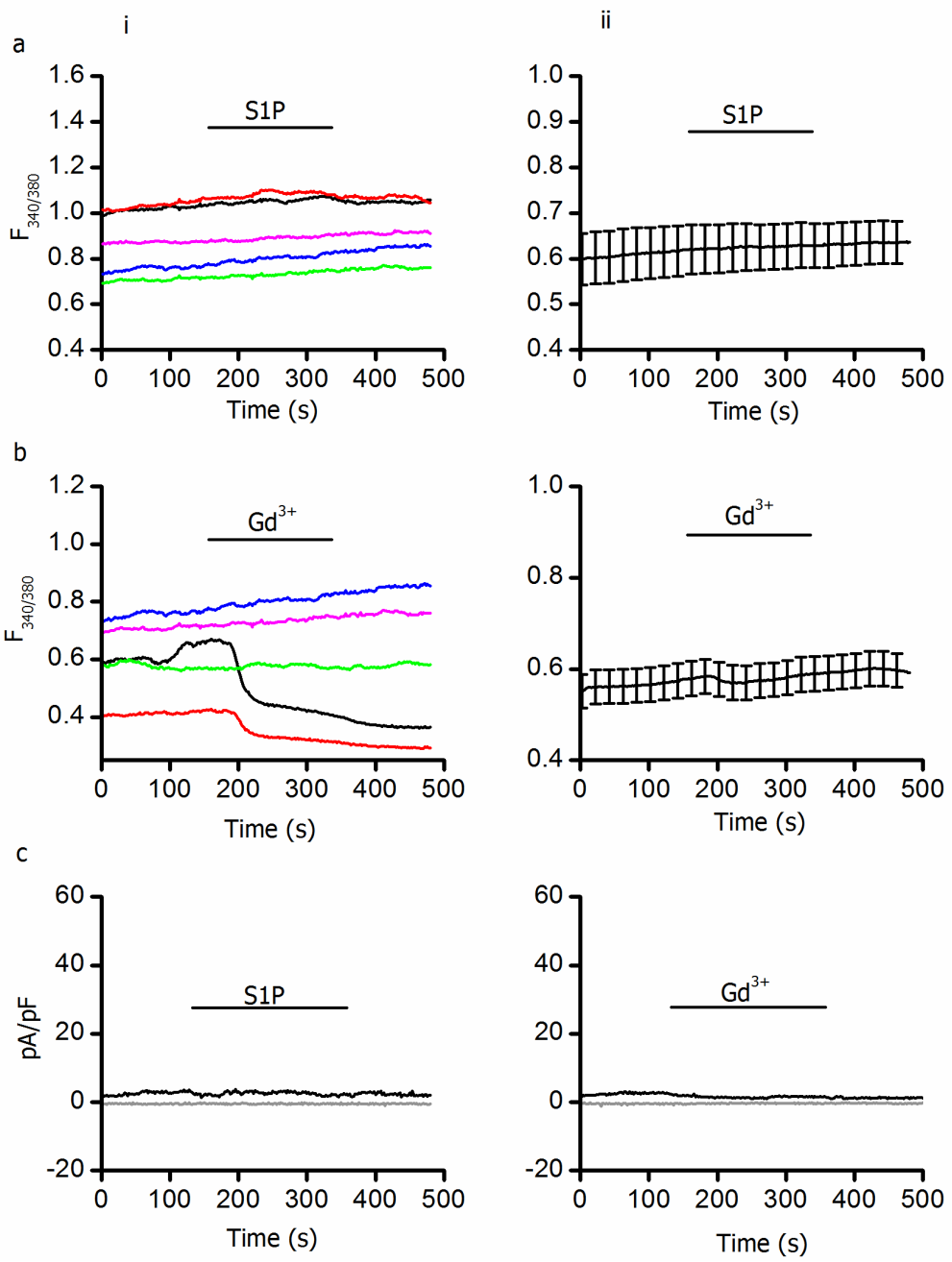

Figure 5.13. S1P and Gd^{3+} do not activate HLMCs from 4/5 donors

a: HLMCs were perfused with standard external solution and 10μM sphingosine-1-phosphate (S1P) was bath-applied as indicated. (i) shows individual cell traces; (ii) shows mean ± SEM of n=35 cells, N=8 independent experiments, representative of 4 donors.

b: 100μM Gd^{3+} was applied to cells as indicated; (ii) shows mean ± SEM for n=49 cells, N=8, 4 donors.

c: Representative whole-cell currents in HLMCs at -100mV (grey) and +100mV (black). In (i) cells were superfused with standard external solution and 10μM S1P was focally applied as indicated; similar results were obtained in 4 other cells. In (ii) 100μM Gd^{3+} was focally applied; similar results were obtained in 3 other cells.

5.4 The involvement of TRPC channels in the IgE response

Data in this chapter indicate that TRPC channels may be activated downstream of Ca^{2+} store release following FcεRI cross-linking in HLMCs. This, along with the observation that Ba^{2+} and Ca^{2+} can support degranulation in human mast cells (chapter 3.3), suggests that TRPC channels may be involved in IgE-dependent Ca^{2+} signalling. To investigate this possibility, whole-cell patch clamp experiments were carried out in HLMCs to investigate the biophysical properties of anti-IgE-induced currents. Cells were voltage-clamped at -60mV and 1 second ramps from -100mV to +100mV were applied every 2 seconds; results are shown in figure 5.14. Application of 3µg/ml anti-IgE to HLMCs incubated overnight with 300ng/ml IgE induced currents in 4/7 cells; in 3/7 cells the peak current in the presence of anti-IgE did not increase significantly above baseline (unpaired Student's T-test). Of the responding cells, 3/4 displayed an outwardly-rectifying current in response to anti-IgE application, with a rectification index of 4.46 ± 0.08 (n=3) and a mean reversal potential of 0.58 ± 0.16 (n=3); these current properties suggest TRPC channel activation. In 1/4 responding cells, an inwardly-rectifying current was activated, with a rectification index of 0.42. The I/V relationship of this current is characteristic of Ca^{2+}-selective I_{CRAC} currents, with large currents occurring at negative membrane potentials (Hoth & Penner, 1992; Feske *et al.*, 2006; Prakriya *et al.*, 2006; Scrimgeour *et al.*, 2009). Figure 5.14c (ii) summarises the current amplitude at +100mV and -100mV in cells with TRPC-like currents, I_{CRAC}-like currents, and when 0.135M NaCl (vehicle for anti-IgE) was applied. As I_{CRAC}-like currents were only observed in 1 of 7 cells tested, more experiments are required to confirm their activation downstream of FcεRI cross-linking. The conditions in this study were not optimised for the recording of I_{CRAC}-like currents; it is therefore possible that the currents were present but not detected.

To further investigate the contribution of TRPC channels to IgE-dependent Ca^{2+} signalling, the sensitivity of IgE-evoked Ca^{2+} entry in HLMCs to synta 66 was assessed. It was also examined whether synta 66-insensitive Ca^{2+} entry could be further inhibited by the non-selective TRPC channel blockers Gd^{3+} (10µM) and SKF-96365. In the presence of synta 66, $\Delta F_{340/380}$ induced by FcεRI cross-linking was significantly reduced by 0.35 (from 1.01 to 0.66); see figure 5.15. In the presence of 10µM synta 66 + 10µM Gd^{3+}, $\Delta F_{340/380}$ was reduced by 0.54 (from 1.01 to 0.47), and by 0.55 (from 1.01 to 0.46) in the presence of 10µM synta 66 + 10µM SKF-96365; this was a significant reduction from both anti-IgE alone and anti-IgE + 10µM synta 66. DMSO at 1/1000 dilution (vehicle for synta 66 its maximal concentration) did not significantly change anti-IgE-induced Ca^{2+} entry. Results are summarised in figure 5.16.

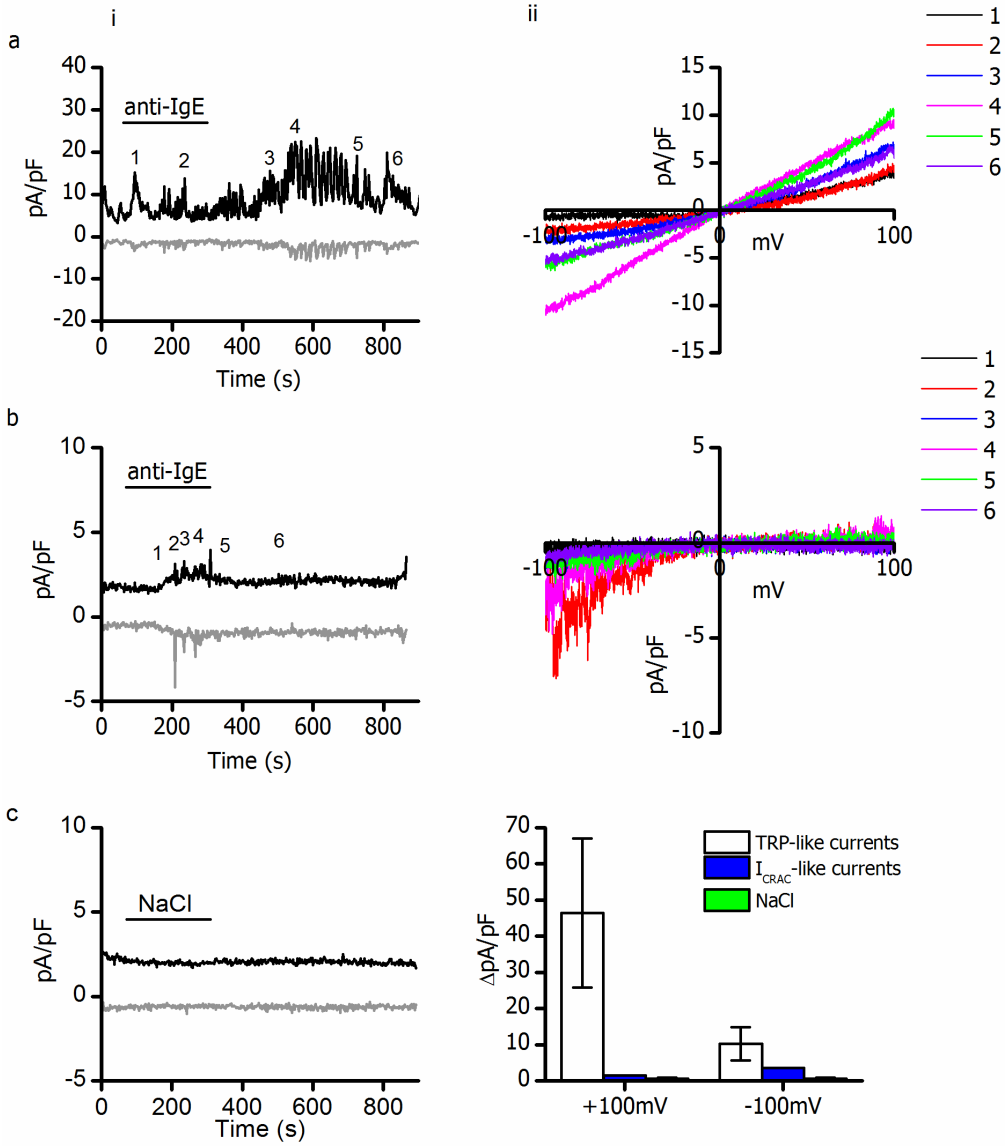

Figure 5.14. Anti-IgE-induced currents in HLMCs.

Cells incubated overnight with 300ng/ml human IgE were superfused with standard external solution and 1/300 anti- human IgE was focally applied as indicated by the horizontal bars. Anti-IgE induced a current in 4/7 cells; of these 3/4 displayed an outwardly-rectifying current with a reversal potential of 0.58 ±0.16 mV for the peak current. 1/4 responding cells displayed an inwardly-rectifying current with a reversal potential of -0.2mV for the peak current.

a: Example cell showing an outwardly-rectifying current. (i) shows a current-time graph where current was sampled at -100mV (grey trace) and +100mV (black trace). (ii) shows example I/V curves taken at points 1-6 shown in (i); see legend for trace colours.

b: Current-time graph (i) and I/V relationships taken from points 1-6 (ii) from cell displaying inwardly-rectifying current in response to anti-IgE application.

C (i): Application of 1/300 0.135M NaCl (vehicle for anti-IgE) did not give rise to a current in HLMCs. Traces show current-time plot for a single representative cell; similar results were obtained in 1 other cell. (ii): bar graph summarising the current amplitude at -100mV and +100mV for TRP-like (white) and I_{CRAC}-like (blue) currents induced by anti-IgE, when 0.135M NaCl (vehicle for anti-IgE) was applied to cells.

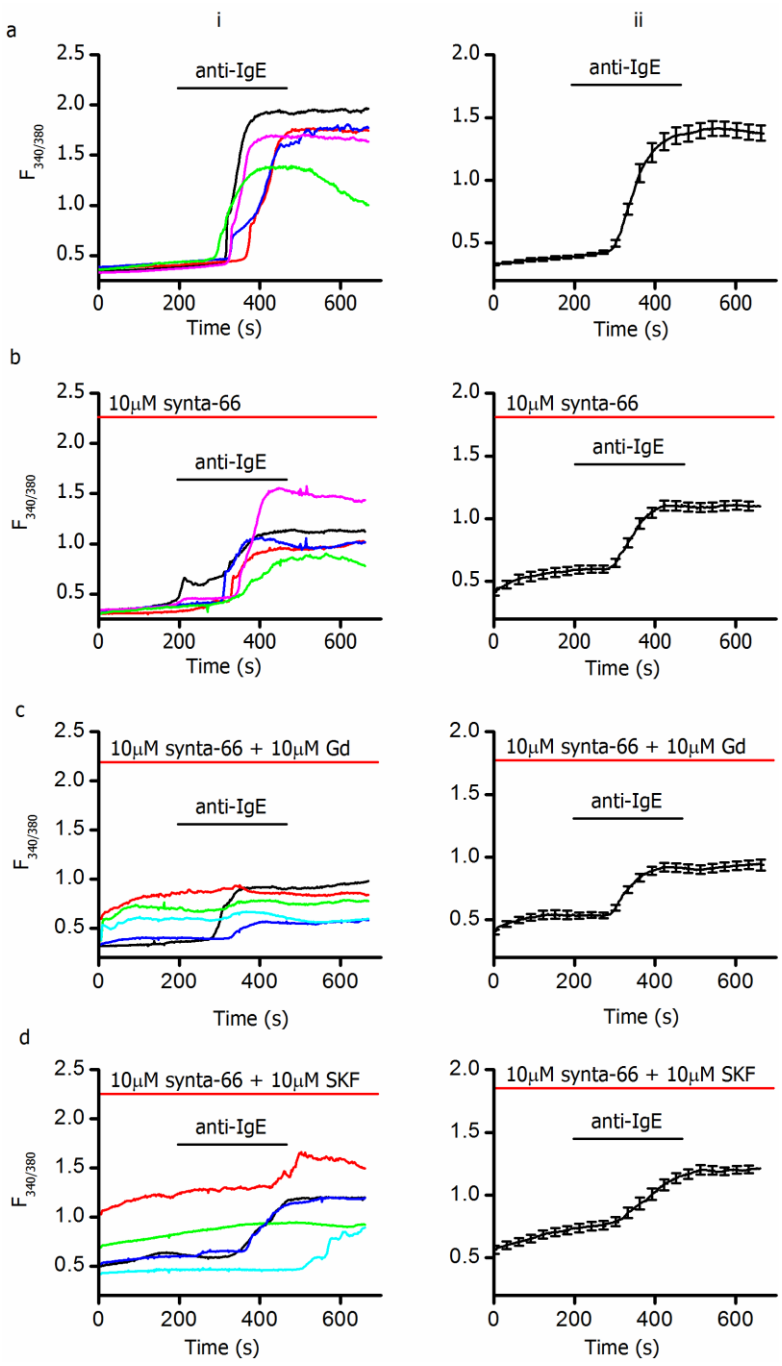

Figure 5.15. Anti-IgE- induced calcium fluxes in HLMCs are sensitive to synta-66, $GdCl_3$ and SKF-96365.

Fura 2-loaded HLMCs incubated overnight with 300ng/ml IgE were perfused in standard external solution and 1/300 anti-IgE was bath-applied where indicated by the horizontal bars. (a) shows calcium entry, indicated by $F_{340/380}$, induced by anti- IgE in control cells (no inhibitor); in all sections (i) shows traces from example cells and (ii) shows the mean ± SEM. In (a), n=30 cells, N=4 separate experiments, representative of 2 donors. (b): experiment as in (a), but 10μM synta-66 was present throughout the experiment. (ii) shows the mean response; n=68 cells, N=4 representative of 2 donors. In (c) 10μM $Gd^{3+,}$ as well as 10μM synta-66, was present throughout the experiment (n=68 cells, N=4, representative of 2 donors) and in (d) 10μM SKF-96365 was present as well as 10μM synta-66 (n=46 cells, N=4, representative of 2 donors).

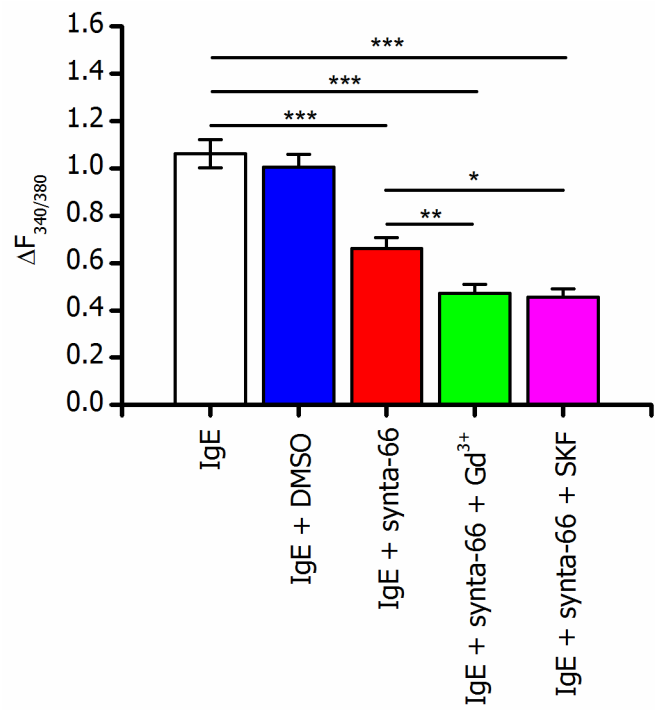

Figure 5.16. Inhibition of IgE-induced calcium entry in HLMCs

Bar graph comparing the size of IgE-induced calcium entry, calculated by subtracting the baseline $F_{340/380}$ from the maximum $F_{340/380}$ in the presence of anti-IgE to give $\Delta F_{340/380}$.

***: Means were significantly different, $p<0.001$, one-way ANOVA. **: Means were significantly different, $p<0.01$. *: Means were significantly different, $p<0.05$.

The significant reduction of anti-IgE-induced Ca^{2+} entry by 10μM synta 66 indicates that I_{CRAC} is activated downstream of FcεRI cross-linking; the presence of synta 66-insensitive Ca^{2+} entry suggests that TRPC channels may also be involved. The significant attenuation of synta 66-insensitive Ca^{2+} entry by the non-selective TRPC channel inhibitors Gd^{3+} and SKF-96365 provides further evidence for the involvement of TRPC channels in Ca^{2+} entry downstream of FcεRI cross-linking. As cytosolic Ca^{2+} influx is essential for mast cell degranulation, the possibility that TRPC channels are involved in the release of the granule markers histamine and β-hexosaminidase in human mast cells was then investigated. The release of these markers in response to FcεRI cross-linking was assessed in the presence of synta 66 and TRPC channel inhibitors. In LAD 2 cells, β-hexosaminidase release was inhibited by Gd^{3+} with an estimated IC50 of 0.95μM, and by synta 66 with an estimated IC_{50} of 2.69μM (figure 5.17).

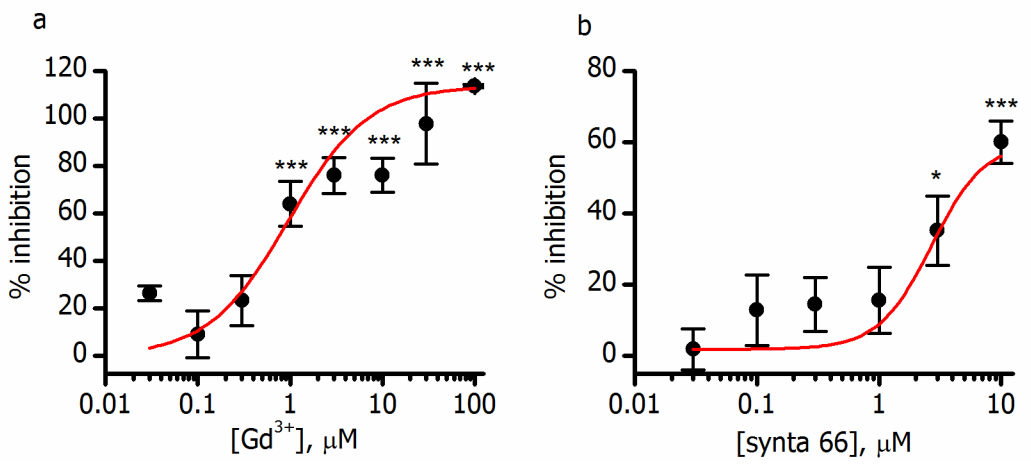

Figure 5.17. IgE-induced β-hexosaminidase release in LAD 2 cells is inhibited by Gd^{3+} and synta 66.

a: Cells were sensitised overnight with 300ng/ml IgE and stimulated with 3μg/ml anti-IgE in the presence of various concentrations of Gd^{3+}. Data are plotted as % inhibition, calculated by 100-(% of control β-hexosaminidase release remaining). N numbers are as follows: 5 for 0.03μM, 5 for 0.1μM, 5 for 0.3μM, 7 for 1μM, 7 for 3μM, 7 for 10μM, 2 for 30μM, 2 for 100μM.

b: Experiments were carried out as in (a), in the presence of various concentrations of synta 66. N=6 for all concentrations of synta 66. *: significant inhibition compared with solvent only (DMSO for synta 66, H2O for Gd^{3+}), $p<0.05$. ***: $p<0.001$, one-way ANOVA of log-transformed data with Tukey post-test.

Experiments were carried out by Oliver Houston.

At 1μM Gd^{3+}, a concentration that inhibits I_{CRAC} but not TRPC channels, β-hexosaminidase release was reduced by 64% in LAD 2 cells; 30μM Gd^{3+}, which inhibits both I_{CRAC} and TRPC channels, inhibited β-hexosaminidase release by 98%. 10μM synta 66, a concentration that has been shown to completely inhibit I_{CRAC} currents (figure 5.1 and (Ng *et al.*, 2008; Di Sabatino *et al.*, 2009; Li *et al.*, 2011)), inhibited β-hexosaminidase release in LAD 2 cells by 60%. Concentrations of synta 66 greater that 10μM were not able to be tested as the compound is insoluble at concentrations greater than 10μM (J. Farrington, unpublished observation). This partial inhibition by 10μM synta 66, along with the Gd^{3+} sensitivity profile, is indicative of the involvement of both Orai1 and TRPC channels in IgE-stimulated mediator release in LAD 2 cells.

Degranulation assays were also carried out on impure HLMC suspensions to investigate the involvement of TRPC channels in FcεRI-stimulated histamine and β-hexosaminidase release. As shown in figure 5.18, 10μM synta 66 significantly attenuated anti-IgE-evoked histamine release in HLMCs by 83% (from 39.36% to 6.72%); DMSO did not significantly reduce histamine release. This significant inhibition by synta 66 suggests that Ca^{2+} entry via I_{CRAC} channels is essential for HLMC histamine release. There was a great deal of variability in the inhibition of histamine release by synta 66 (illustrated in figure 5.18a (ii)); the percentage inhibition varied from 21.54% to 98.69%. Donors were separated into those where synta 66 inhibited IgE-dependent histamine release by >90% (complete inhibition) and those where release was inhibited by <90% (partial inhibition); 3/6 donors were in each category. Release in the donors where partial inhibition occurred was compared in the presence of synta 66, and when the non-selective TRPC channel inhibitors Gd^{3+} and SKF-96365 were applied together with synta 66. Inhibition was significantly greater when both synta 66 + Gd^{3+} or synta 66 + SKF-96365 were present, compared with synta 66 alone; see figure 5.18b (ii).

The same samples from 5 of the 6 donors used to test histamine secretion were assayed for β-hexosaminidase release; results are shown in figure 5.19. A similar pattern of results was observed as that described above; partial inhibition of β-hexosaminidase release was observed in the same 3 donors as partial inhibition of histamine release. Synta 66-insensitive β-hexosaminidase release was further inhibited by 10μM Gd^{3+} or SKF-96365, but this did not reach statistical significance. Taken together, although a greater pool of donors is required to verify these data, results are indicative of the role of both Orai1 and TRPC channels in IgE-dependent secretion in some donors. In donors where synta 66 inhibition was close to 100%, it is likely that Orai1 channels dominate in causing Ca^{2+} entry necessary for FcεRI-stimulated degranulation.

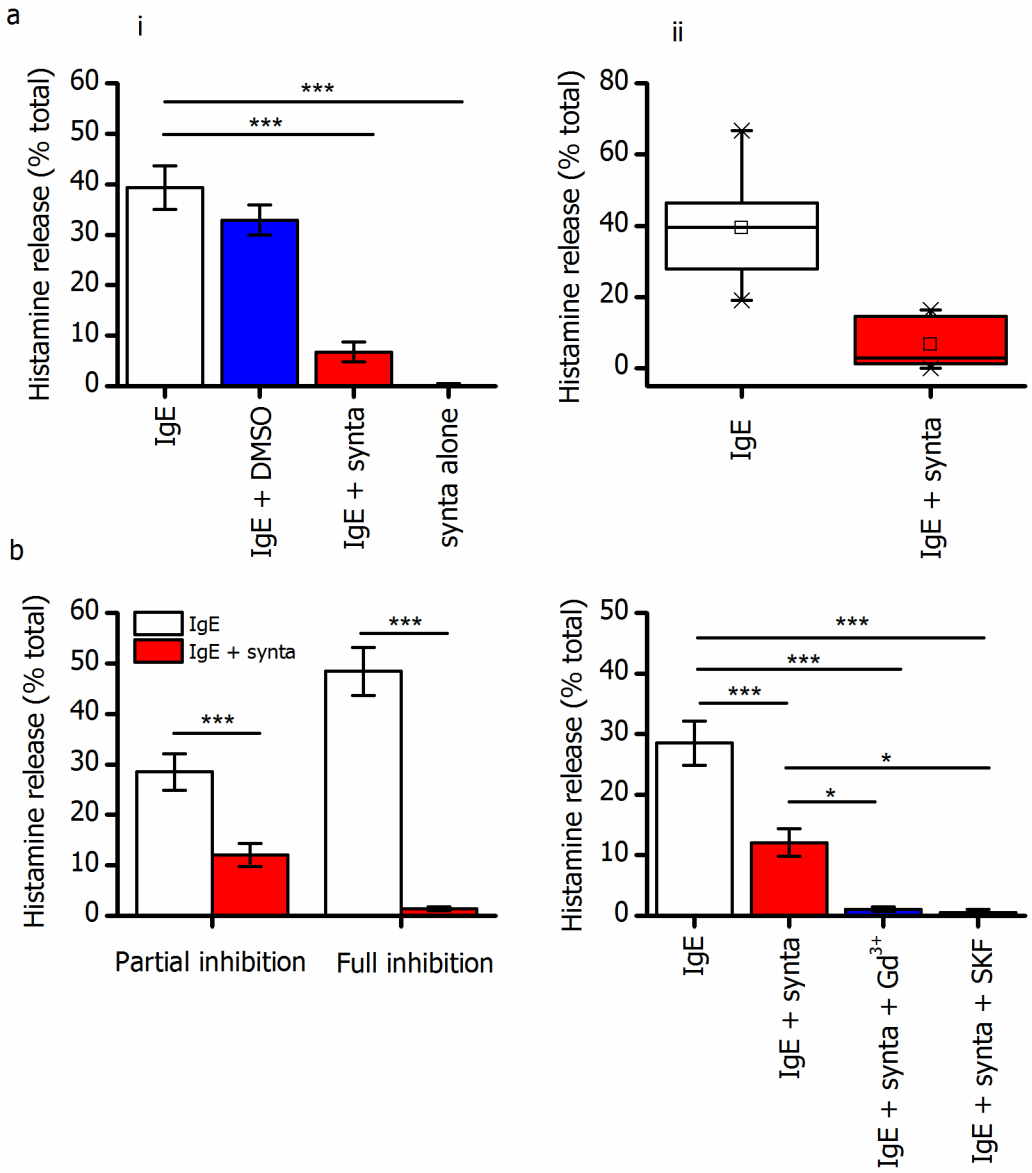

Figure 5.18. Inhibition of IgE-induced histamine release in HLMCs

Freshly isolated impure HLMCs were stimulated with anti-IgE and histamine release was measured as a % total release, determined by lysis with 0.5% perchloric acid.

a (i): Histamine release when cells were stimulated with 3µg/ml anti-IgE alone (white; N=11, 6 donors) anti-IgE in the presence of 1/1000 DMSO (blue; vehicle for synta 66) (N=6, 3 donors) or 10µM synta 66 (red; N=12, 6 donors), and with 10µM synta 66 alone (green; N=8, 4 donors). (ii): Box plot highlighting the variability in the sensitivity of anti-IgE-induced histamine release to synta 66.

b (i): Donors were separated into those where histamine release was partially inhibited by 10µM synta 66 (<90% inhibition, 3/6 donors), and those where histamine release was fully inhibited (>90% inhibition, 3/6 donors). (ii): Bar chart comparing IgE-mediated histamine release in donors with partial inhibition by synta 66 with histamine release in the presence of 10µM synta 66 + 10µM Gd^{3+} (N=4, 2 donors), or 10µM synta 66 + 10µM SKF-96365 (N=4, 2 donors).

*: means were significantly different, $p<0.05$, **: $p<0.01$, ***: $p<0.001$, one-way ANOVA with Tukey post-test.

Experiments in 1 donor (N=2) were carried out by Jasmine Farrington

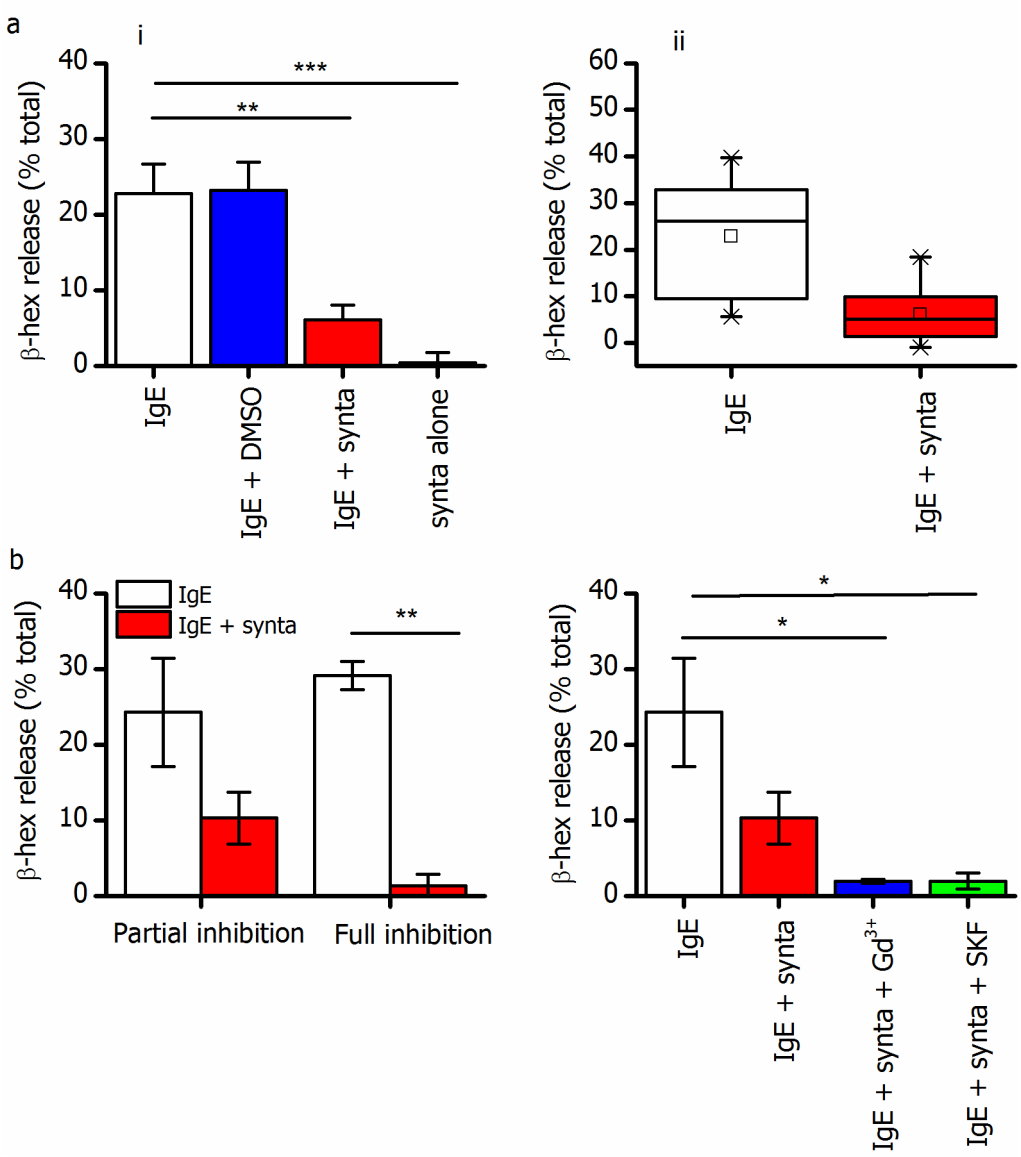

Figure 5.19. Inhibition of IgE-induced β-hexosaminidase release in HLMCs

Freshly isolated impure HLMCs from the same samples used in figure 7.7 were stimulated with anti-IgE and β-hexosaminidase release was measured as a % total release, determined by lysis with 0.5% Triton X-100.

a (i): β-hexosaminidase release when cells were stimulated with 3µg/ml anti-IgE alone (white; N=10, 5 donors) anti-IgE in the presence of 1/1000 DMSO (blue; vehicle for synta 66 and SKF-96365. N=6, 3 donors) or 10µM synta 66 (red; N=10, 5 donors), and with 10µM synta 66 alone (green; N=6, 3 donors). (ii): Box plot highlighting the variability in the sensitivity of anti-IgE-induced β-hexosaminidase release to synta 66.

b (i): Donors were separated into those where β-hexosaminidase release was partially inhibited by 10µM synta 66 (<90% inhibition, 3/5 donors), and those where histamine release was fully inhibited (>90% inhibition, 2/5 donors). (ii): Bar chart comparing IgE-mediated β-hexosaminidase release in donors with partial inhibition by synta 66 with histamine release in the presence of 10µM synta 66 + 10µM Gd^{3+} (N=4, 2 donors), or 10µM synta 66 + 10µM SKF-96365 (N=4, 2 donors).

*: means were significantly different, $p<0.05$, **: $p<0.01$, ***: $p<0.001$, one-way ANOVA with Tukey post-test.

The results obtained in mediator release assays where synta 66 caused partial inhibition of secretion are in accordance with Ca^{2+} imaging data showing that synta 66 partially inhibits Ca^{2+} entry, and synta 66-insensitive Ca^{2+} entry is inhibited further by Gd^{3+} and SKF-96365. Unfortunately, Ca^{2+} imaging and secretion assay experiments were unable to be carried out on HLMCs from the same donors, as sufficient numbers of pure HLMCs were not able to be obtained in our laboratory for secretion assays due to limited availability of lung tissue. Although only two donors were used to investigate the synta 66 sensitivity of FcεRI-stimulated Ca^{2+} entry, inhibition was partial in both donors, whereas partial inhibition of histamine secretion occurred in 50% of donors (3/6). As Ca^{2+} imaging experiments throughout this study were carried out at room temperature and mediator release assays at 37°C, the possibility was considered that synta 66 sensitivity is affected by temperature. Ca^{2+} imaging experiments like shown in figure 5.15 were repeated at 35°C, in the same donors (410 and 411). As shown in figure 5.20, synta 66 gave rise to partial inhibition of IgE-dependent Ca^{2+} entry in donors 410 and 411 at 35°C. There was no significant difference in $\Delta F_{340/380}$ corresponding to IgE-evoked Ca^{2+} entry in the presence or absence of synta 66 at the two different temperatures. Synta 66 therefore gave rise to partial inhibition of IgE-dependent Ca^{2+} entry in both donors tested. Although time and tissue availability did not permit more experiments, further investigations into the inhibition of IgE-induced Ca^{2+} entry by synta 66 using HLMCs from more donors would reveal whether similar donor-dependency exists in the contribution of TRPC channels to IgE-evoked Ca^{2+} entry as that observed in mediator release assays.

To summarise, donor variability exists in the sensitivity of IgE-evoked histamine and β-hexosaminidase to synta 66. These data indicate that Orai1 is the principal channel governing Ca^{2+} entry required for mediator release in HLMCs from some donors. In other donors however, the Gd^{3+} and SKF-96365 sensitivity of synta 66-insensitive mediator release suggests that TPRC channels, as well as Orai1 channels, may be important for degranulation in HLMCs.

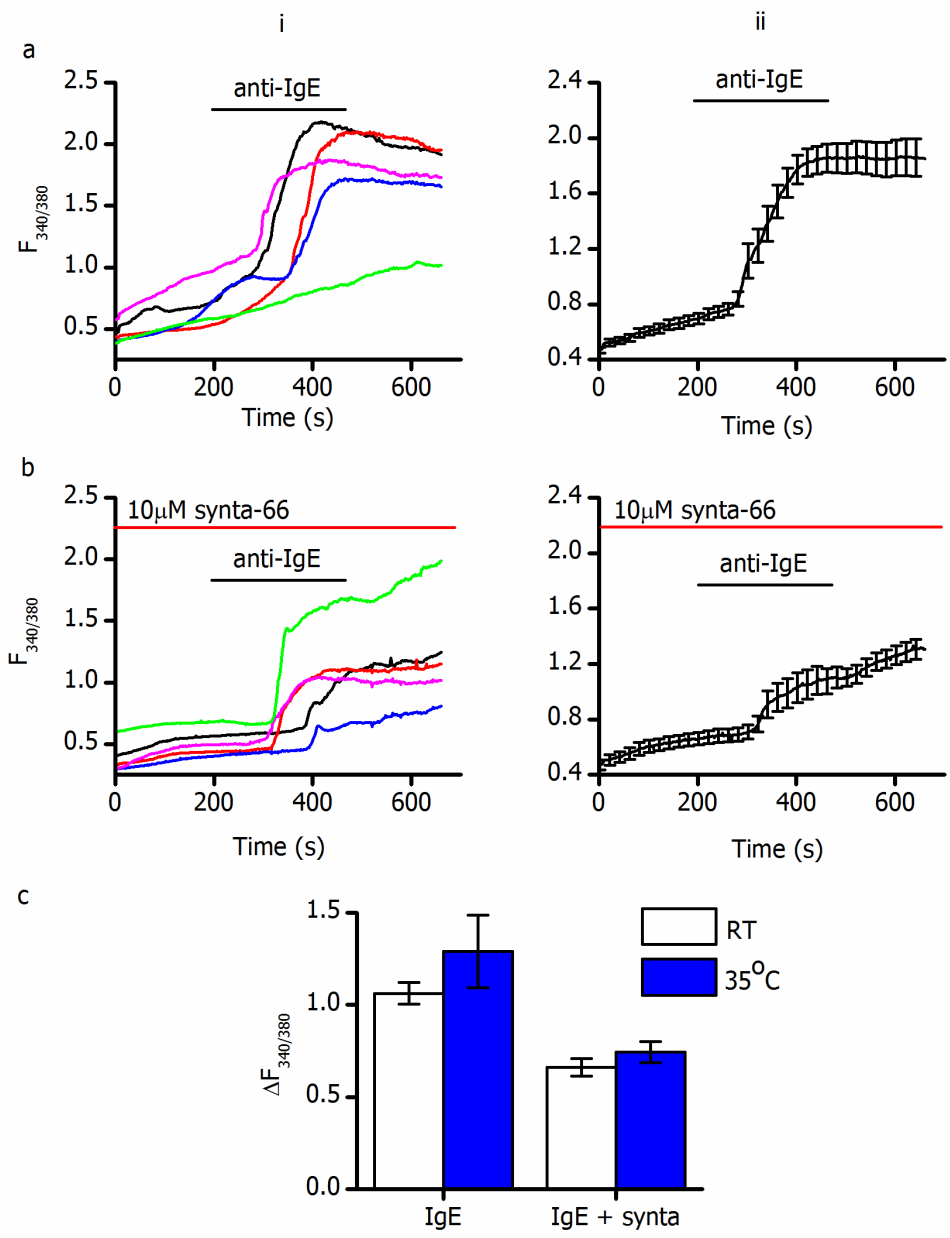

Figure 5.20. Synta-66 partially inhibits anti-IgE-induced calcium entry at 35°C

Fura 2-loaded HLMCs were perfused in standard external solution, which was heated to 35°C, and 1/300 anti-IgE was bath-applied where indicated by the horizontal bars. (a) shows anti-IgE-induced calcium entry, indicated by $F_{340/380}$, in control cells (no inhibitor); (i) shows traces from example cells and (ii) shows the mean ± SEM (n=14 cells, N=4 experiments, representative of 2 donors). (b): experiment as in (a), but 10μM synta-66 was present throughout the experiment. (ii) shows the mean response; n=17 cells, N=4 representative of 2 donors.

c: Bar chart comparing the size of IgE-induced calcium entry at room temperature ("RT", clear bars) and 35°C (blue bars) in the presence and absence of synta-66. There was no significant difference between room temperature and 35°C in control cells or in the presence of synta-66 (unpaired Student's T-test).

5.5 Assessment of TRPC5 channels' contribution to HLMC degranulation

As shown earlier in this chapter (figures 5.12 and 5.13), the TRPC5 activators S1P and 100μM Gd^{3+} gave rise to Ca^{2+} entry in HLMCs from 1/5 donors, indicating that these channels may be functionally expressed in some donors. To assess whether TRPC5 channel activation causes degranulation, histamine and β-hexosaminidase release in response to these agonists were assessed. Results are shown in figure 5.21; 100μM Gd^{3+} gave rise to histamine release of 3.43% ± 0.49 (N=6, 3 donors), and β-hexosaminidase release of 5.25% ± 4.75 (N=4, 2 donors). S1P induced histamine release of 0.33% ± 1.08 (n=4, 2 donors) and β-hexosaminidase release of 4.75% ± 2.07 (N=4, 2 donors). For comparison, anti-IgE application gave rise to histamine release of 38.13% ± 2.56 (N=8, 4 donors) and β-hexosaminidase release of 24.90% ± 4.54 (N=6, 3 donors). Both histamine and β-hexosaminidase release evoked by S1P were not significantly different from that induced by methanol (vehicle for S1P; unpaired Student's T-test). Therefore, application of agonists shown in this study to activate TRPC5 channels does not stimulate release of the granule-associated mediators histamine and β-hexosaminidase. Given that TRPC5 stimulation does not evoke degranulation in HLMCs, and Ca^{2+} entry in response to Gd^{3+} and S1P only occurred in 1/5 donors, it is unlikely that TRPC5 channels are responsible for the synta 66-insensitive FcεRI-evoked degranulation seen in figure 5.18. From the TRPC1/4/5 subgroup, TRPC1 is the most likely candidate to be involved in Ca^{2+} entry and degranulation downstream of FcεRI in HLMCs; as shown by RT-PCR, TRPC4 was not expressed in HLMCs from 3/3 donors tested. TRPC1 was present in all donors tested; synta 66-insensitive Ba^{2+} entry occurred following store depletion with thapsigargin, as well as receptor stimulation, in HLMCs, suggesting that this channel is activated by store depletion in these cells. Synta 66-insensitive Ca^{2+} entry was further reduced by 10μM Gd^{3+} and SKF-96365; further inhibition of degranulation was also seen in donors where synta 66 did not inhibit release by 100%. The I/V relationship of currents activated downstream of FcεRI cross-linking provides further evidence for the involvement of TRPC1 channels; TRPC1 currents are almost linear with a reversal potential close to 0mV (Rychkov & Barritt, 2007). Taken together with the likely involvement of TRPC1 in thapsigargin-evoked Ba^{2+} entry, these data suggest that TRPC1 could be involved in IgE-dependent degranulation. Further experiments employing selective molecular knock-down of TRPC1 channels would verify the involvement of these channels in FcεRI-dependent Ca^{2+} signalling and mediator release.

Of the DAG-activated TRPC3/6/7 subgroup, TRPC6 mRNA was expressed in HLMCs from 3/3 donors, TRPC7 in 1/3 donors and TRPC3 in 0/3 donors. As DAG is produced by PLCγ downstream of FcεRI cross-linking, it is possible that TRPC6 or perhaps TRPC7 channels could contribute to FcεRI-evoked Ca^{2+} signalling and mediator release. The functional expression of this subgroup of TRPC channels in HLMCs is characterised in chapter 6, and their contribution to FcεRI-dependent signalling is assessed.

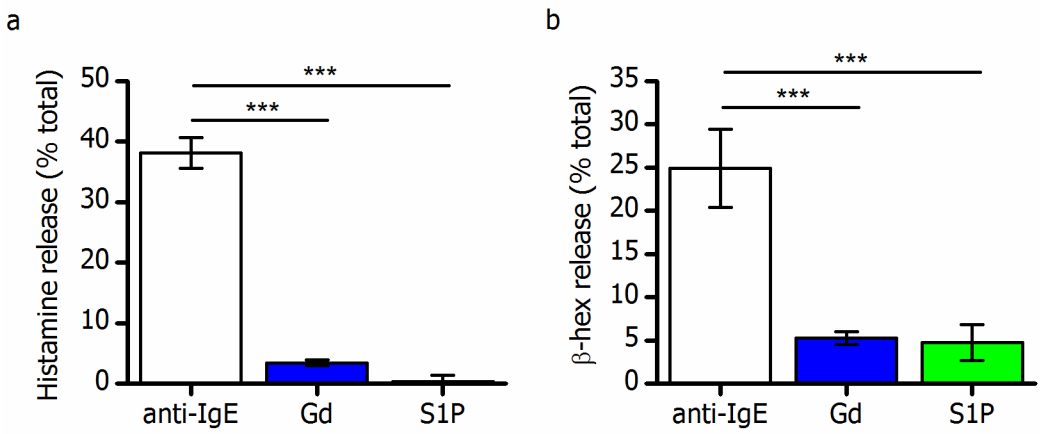

Figure 5.21. Activators of TRPC5 channels do not stimulate degranulation in HLMCs

a: Freshly isolated impure HLMCs were stimulated with the agonists shown and histamine release was measured as % total release, determined by lysis with 0.5% perchloric acid. Anti-IgE-induced histamine release in the donors tested for responsiveness to other agonists is shown for comparison. N=8, 4 donors for IgE (3µg/ml); N=6, 3 donors for Gd^{3+} (100µM); N=4, 2 donors for S1P (10µM). ***: release was significantly lower than that induced by anti-IgE, one-way ANOVA with Tukey post test. There was no significant difference between histamine release induced by DMSO and methanol (vehicles for OAG and S1P, respectively), and that induced by agonists. Histamine release experiments in 1 donor (N=2) were carried out by Jasmine Farrington.

b: Freshly isolated impure HLMCs were stimulated with the agonists shown and β-hexosaminidase release was measured as % total release, determined by lysis with 0.5% Triton X-100. Anti-IgE-induced β-hexosaminidase release in the donors tested for responsiveness to other agonists is shown for comparison. N=6, 4 donors for IgE (3µg/ml); N=4, 2 donors for Gd^{3+} (100µM); N=4, 2 donors for S1P (10µM). ***: release was significantly lower than that induced by anti-IgE, one-way ANOVA with Tukey post test.

5.6 Discussion

As detailed in chapter 1.3.2, Orai1 channels are not thought to be the sole mediators of SOCE in mast cells; divalent ions such as Ba^{2+}, Sr^{2+} and Mn^{2+} have been shown to support mast cell degranulation in the absence of Ca^{2+} (see chapter 3.3 and (Hide & Beaven, 1991; Ma *et al.*, 2008)). It has been proposed that TRPC channels, which lack the Ca^{2+} selectivity of I_{CRAC}, conducting other divalent ions including Ba^{2+} and Sr^{2+} (Ma *et al.*, 2008), form another type of SOCE channel, distinct from I_{CRAC} and sometimes referred to as I_{SOC} (Parekh & Putney, 2005; Cheng *et al.*, 2011). In the recently-proposed model for the role of TRPC channels in SOCE (depicted in figure 5.1 and based on studies in HSG cells), TRPC1 channels are present in recycling vesicles, and following store depletion they are retained at the plasma membrane by STIM1. TRPC1 and Orai1, whilst not forming the same channel, are maintained in discrete plasma membrane microdomains by cholesterol- and sphingomyelin- rich lipid raft regions (Brazer *et al.*, 2003; Lingwood & Simons, 2010; Calloway *et al.*, 2011). Ca^{2+} entry through Orai1 channels following store depletion is thought to enhance TRPC1 channel insertion in the plasma membrane and gating by STIM1, suggesting functional interactions of the three proteins.

As discussed in chapter 1.3.2, there is a lack of conclusive evidence implicating TRPC3, 6 and 7 channels in SOCE, whereas a number of studies suggest that TRPC1 channels, along with TRPC4 and TRPC5, are involved in SOCE. This discussion will therefore focus mainly on TRPC1 and TRPC5 channels, which were detected in both LAD 2 cells and HLMCs by RT-PCR.

The entry of Ba^{2+} ions in human mast cells following Ca^{2+} store depletion indicates that Orai1 channels are unlikely to be the sole mediators of SOCE, and suggests the involvement of TRPC channels, as discussed in chapter 3.5. The selective I_{CRAC} inhibitor, synta 66, was used in this chapter to further investigate the contribution of TRPC channels to SOCE. Synta 66 has been shown to inhibit I_{CRAC} currents in RBL cells with estimated IC_{50} values of 3μM (Ng *et al.*, 2008) and 1.4μM (Di Sabatino *et al.*, 2009), and in vascular SMCs with an estimated IC_{50} of 26nM (Li *et al.*, 2011). In our laboratory, synta 66 blocked I_{CRAC} currents in HEK-Orai/STIM cells with an IC_{50} of 70nM; of the published IC_{50} values for synta 66 inhibition of I_{CRAC}, this is closest to that reported in vascular SMCs (26nM). Li *et al.* (2011) suggest that the greater potency of synta 66 in SMCs could indicate a fundamental difference in the mechanisms of I_{CRAC} in vascular and immune cells, highlighting the importance of using an appropriate concentration of synta 66 to inhibit I_{CRAC} in a given cell type. In accordance with published results in both RBL cells (Ng *et al.*, 2008; Di Sabatino *et al.*, 2009) and vascular SMCs (Li *et al.*, 2011), 10μM synta 66 gave rise to complete inhibition of I_{CRAC} currents in HLMCs; this concentration was used for the remaining experiments in this chapter where synta 66 was used to inhibit Orai1 channels. In agreement with previous studies (detailed in chapter 1.3) showing that synta 66 is selective for I_{CRAC} inhibition (Di Sabatino *et al.*, 2009; Li *et al.*, 2011), 10μM synta 66 did not affect OAG-induced Ca^{2+} entry in HEK-TRPC6 cells, or S1P-induced Ca^{2+} entry in HEK-TRPC5 cells in this study,

confirming that it does not affect these channels. As both Orai1 and some TRPC channels can be activated by store depletion, synta 66 may be an important tool to study TRPC-mediated SOCE in isolation from Orai1 channel activity.

In LAD 2 cells, the presence of 10μM synta 66 caused significant reduction of Ca^{2+} entry following direct store depletion by thapsigargin, and via receptor-operated mechanisms, indicating the involvement of Orai1 channels in SOCE in these cells. Ba^{2+} entry was inhibited by 85% when thapsigargin was used to deplete Ca^{2+} stores, by 35% following FcεRI cross-linking, and by 41% when ADP was the stimulus. This result was unexpected, as Orai1 channels are not thought to permeate Ba^{2+} ions, and as discussed above, synta 66 is not expected to inhibit TRPC channels. As shown in figure 5.1, it is possible that Orai1 and TRPC1 are present in the same plasma membrane domains in LAD 2 cells, as previously demonstrated in HEK cells (Kim *et al.*, 2009b), platelets (Jardin *et al.*, 2008), HSG cells (Cheng *et al.*, 2011) and RBL cells (Ma & Beaven, 2011). If, as shown in figure 5.1, Orai1 enhances TRPC1 surface expression and gating by STIM1, inhibition of Orai1 by synta 66 could reduce TRPC1 activity due to the conformation coupling of the two channels, thus reducing Ba^{2+} entry through TRPC1. This hypothesis is depicted in figure 5.22. Orai1 inhibition would not be expected to completely inhibit TRPC1-mediated Ba^{2+} entry, as the surface expression of TRPC1 is not entirely dependent on Orai1. Cheng *et al.* (2011) showed that TRPC1 plasma membrane expression was reduced, but not prevented, by expression of the dominant negative Orai1 mutant E106Q, concluding that Orai1 increases the expression of TRPC1 at the membrane. It can therefore be hypothesised that when synta 66 is present, TRPC1-dependent divalent ion entry is reduced due to the inhibition of Orai1 channels. It is evident that the amplitude of synta 66-insensitive Ba^{2+} entry was smaller following store depletion with thapsigargin than downstream of P2Y receptor stimulation or FcεRI cross-linking. This could be because compartmentalised signalling occurs to a lesser degree when thapsigargin is the stimulus for store depletion, compared with receptor simulation. Whilst PLCβ and PLCγ are activated downstream of P2Y receptors and FcεRI, respectively, thapsigargin has been shown to cause minimal activation of PLC in RBL-2H3 cells (Cissel *et al.*, 1998). PtdIns(4,5)P_2, the target of PLC, is known to be maintained in discrete membrane lipid raft regions, giving rise to compartmentalised signalling and the activation of SOCE channels in discrete plasma membrane domains. It can be hypothesised that when TRPC1 and Orai1 channels are brought together in lipid rafts following PLC activation downstream of receptor stimulation, TRPC1 channels are more likely to be in the correct position for gating by STIM1. When thapsigargin is the stimulus, however, the channels are less likely to be brought together in specific membrane domains due to the lack of PLC involvement; when Orai1 is inhibited by synta 66, fewer TRPC1 channels could be in the correct location for gating by STIM1, giving rise to greater inhibition of Ba^{2+} entry.

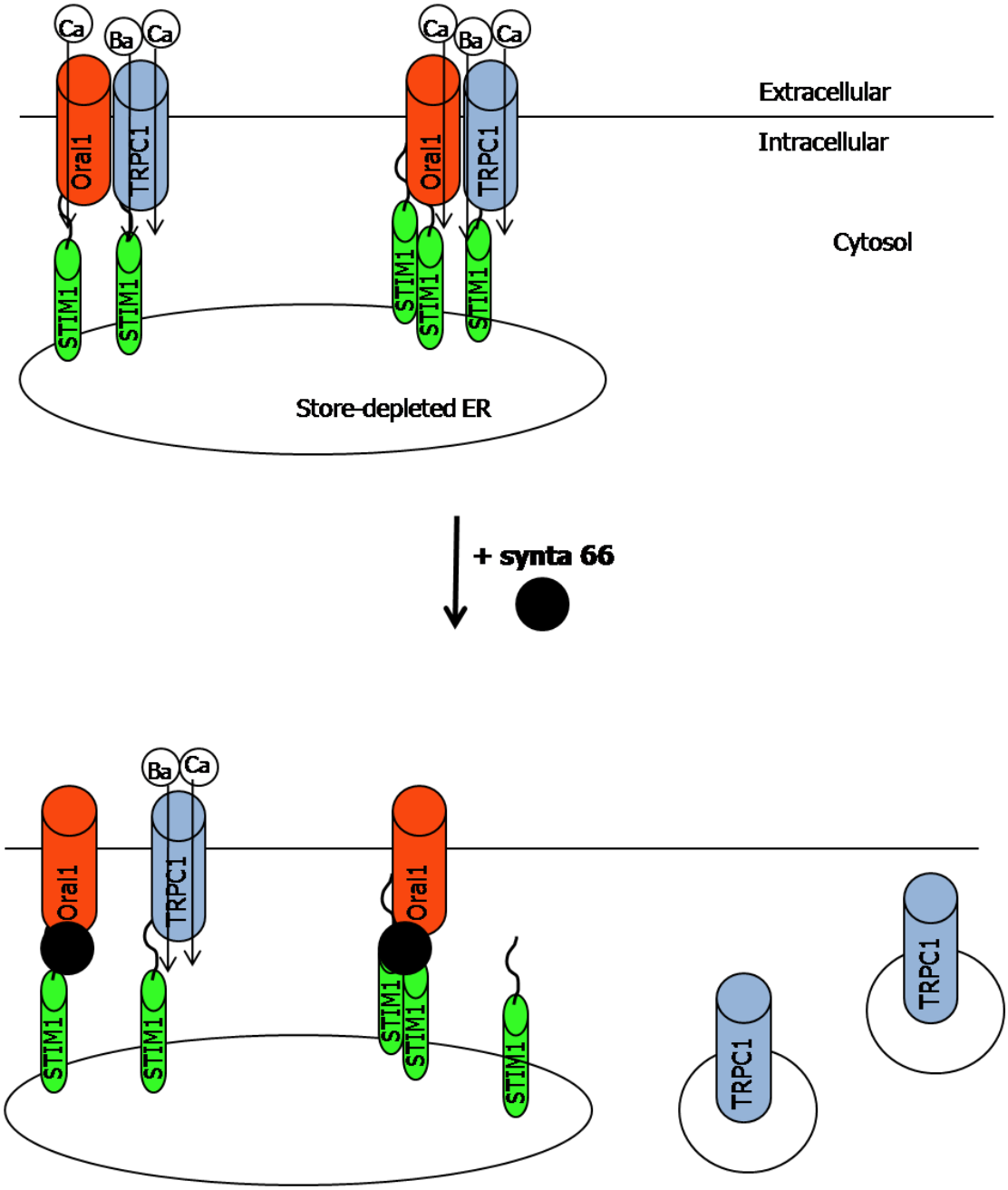

Figure 5.22. Model of Orai1 inhibition by synta 66 and the effects on TRPC1 channels. As shown in figure 6.1, Orai1 activation by STIM1 enhances TRPC1 expression at the plasma membrane and gating by STIM1. When both channels are active downstream of store depletion, Ca^{2+} ions enter the cell through Orai1 channels; Ba^{2+} and Ca^{2+} ions enter through TRPC1 channels (top). In the presence of synta 66 (black circle, bottom), Orai1 is inhibited, which could affect TRPC1 channel surface expression and gating by STIM1, thus reducing Ba^{2+} ion entry through TRPC1 channels.

Gd^{3+} sensitivity has been suggested as another means to isolate TRPC from I_{CRAC} channel activity; low (~1) μM concentrations of Gd^{3+} are thought to inhibit I_{CRAC} currents, whereas concentrations of 10μM and above inhibit TRPC1, 3, 6 and 7 channels (Broad *et al.*, 1999; DeHaven *et al.*, 2009). Ca^{2+} entry following thapsigargin-mediated store depletion was inhibited by Gd^{3+} in LAD 2 cells; the small but significant inhibition by 1μM Gd^{3+} is likely to represent reduction in I_{CRAC} only. This is confirmed by the lack of inhibition of Ba^{2+} entry by Gd^{3+} at this concentration. Concentrations of 10 and 30μM Gd^{3+} gave rise to much greater inhibition of Ba^{2+} and Ca^{2+} entry; this was expected, as TRPC and I_{CRAC} channels are both inhibited by Gd^{3+} at these concentrations. The partial inhibition of Ca^{2+} entry by 1μM Gd^{3+} is in accordance with partial inhibition by synta 66, as both antagonists inhibit Orai1 channels. However, 1μM Gd^{3+} did not inhibit Ba^{2+} entry, whereas synta 66 caused partial inhibition. This is likely to be due to the different mechanism of action of the two antagonists; Gd^{3+} blocks ion channels by pore occlusion, but the mechanism of action of synta 66 is unknown. As depicted above (figure 5.22), the presence of synta 66 could interfere with the functional interaction between TRPC1 and Orai1 in the membrane, reducing TRPC1 membrane expression and gating by STIM1. Gd^{3+}, however, may not have this effect due to its differential binding site, affecting Orai1 channels only at low concentrations, resulting in functional gating of TRPC1 channels by STIM1, and inhibiting both channel types at higher concentrations. Taken together, the presence of synta 66-insensitive and Gd^{3+} sensitive Ba^{2+} and Ca^{2+} entry in LAD 2 cells suggests that TRPC1 channels are involved in SOCE in these cell types. A contribution from TRPC5 channels, whose mRNA was expressed in LAD 2 cells, can be excluded as LAD 2 cells did not respond to the selective TRPC5 activators, S1P and 100μM Gd^{3+}.

In HLMCs, Ca^{2+} entry following store depletion with all methods was significantly inhibited by 10μM synta 66, indicating the involvement of Orai1 channels in SOCE in these cells. These data are in accordance with other results obtained in our laboratory, showing that currents with the expected biophysical properties of I_{CRAC} are activated in HLMCs following $InsP_3$- mediated store depletion (J. Farrington, unpublished data). Synta 66- insensitive Ba^{2+} and Ca^{2+} entry occurred in HLMCs following all methods of stimulation, indicating the involvement of TRPC channels in divalent ion entry. As with LAD 2 cells, the partial inhibition of Ba^{2+} entry following FcεRI cross-linking or P2Y receptor stimulation could be due to synta 66 interfering with the functional interaction of TRPC1 and Orai1 channels, giving rise to impaired gating of TRPC1 by STIM1, as illustrated in figure 5.22. However, unlike LAD 2 cells, Ba^{2+} entry was not inhibited by 10μM synta 66 following thapsigargin-mediated store depletion in HLMCs. This is indicative of the involvement of TRPC channels in Ba^{2+} entry, but was unexpected due to previous reports of interactions between TRPC1 and Orai1 (Ong *et al.*, 2007; Jardin *et al.*, 2008; Kim *et al.*, 2009b), and enhancement of TRPC1 cell surface expression by Orai1 (Cheng *et al.*, 2011). It is possible that the variation in synta 66-dependent inhibition of Ba^{2+} entry observed when different methods were used to deplete Ca^{2+} stores in HLMCs is due to differential spatial regulation of the TRPC channels. As discussed in detail in chapter 3.5, it is likely that PLCγ and PLCβ, which are

activated downstream of FcεRI and $P2Y_1$ receptors, respectively (Park *et al.*, 1991; Gilfillan & Tkaczyk, 2006), are targeted to distinct plasma membrane signalling microdomains. Differential expression of Orai1 in these signalling domains could lead to varied effects on TRPC1 channels when Orai1 is inhibited by synta 66. As discussed above, passive store depletion by thapsigargin is unlikely to give rise to spatial regulation of TRPC1 channels to the same degree as when ADP or anti-IgE were used as a stimulus. The lack of dependency of TRPC1 on Orai1 channels in this situation could account for the absence of inhibition of Ba^{2+} entry by synta 66 when thapsigargin was used to deplete stores.

Inhibition of thapsigargin-mediated Ba^{2+} entry by synta 66 could have occurred to a greater degree in LAD 2 cells than in HLMCs due to differential expression of TRPC1 channels in the two cell types. Maturation-dependent expression of proteins has previously been demonstrated in mast cells; terminally-differentiated skin mast cells were found to have higher levels of tryptase and chymase than less mature LAD 2 cells (Guhl *et al.*, 2010). Additionally, B cells have been reported to exhibit maturation stage-dependent differences in Ca^{2+} signalling (Benschop *et al.*, 2001). It is possible that TRPC1 channels are expressed at higher levels in HLMCs than in LAD 2 cells, and are thus present at high levels in the plasma membrane. As compartmentalised signalling is likely to occur to a lesser degree following thapsigargin stimulation than receptor stimulation, the requirement of Orai1 to enhance TRPC1 surface expression could be reduced as TRPC1 is already present at high levels in the plasma membrane at the correct location for gating by STIM1. In LAD 2 cells, however, lower expression levels of TRPC1 could mean that it is not expressed at the cell surface to the same degree as in HLMCs, and channels could be present in recycling vesicles, as suggested previously in HSG cells (Cheng *et al.*, 2011). As the channels are unlikely to be assembled in lipid rafts following thapsigargin-evoked store depletion to the same extent as following receptor stimulation, the lower expression levels could mean that fewer channels are correctly positioned for gating by STIM1 in LAD2 cells, giving rise to reduced Ba^{2+} entry through TRPC1 channels when Orai1 channels are inhibited by synta 66 and are thus unable to enhance the surface expression of TRPC1.

Whilst differences between the two cell types occur, which are likely to be accounted for by maturation-dependent variation, the existence of synta 66-senstitive and -insensitive Ba^{2+} and Ca^{2+} entry in LAD 2 cells and HLMCs provides evidence for the involvement of both Orai1 and TRPC channels in SOCE in both cell types. In HLMCs from the two donors (410 and 411) where synta 66-insensitive Ba^{2+} and Ca^{2+} entry was observed, 100μM Gd^{3+} and 10μM S1P did not give rise to Ca^{2+} influx, suggesting the lack of functional TRPC5 expression in these donors. These data were confirmed by RT-PCR (chapter 3.4) results, showing that mRNA transcripts for TRPC5 were not expressed in HLMCs from donors 410 and 411. TRPC1 mRNA was detected in all donors tested; it is therefore a likely candidate to mediate synta 66-insensitive SOCE in HLMCs. As depicted above (figure 5.22), interference with the functional interaction between Orai1 and

TRPC1 channels in discrete lipid raft microdomains could account for the partial reduction of Ba^{2+} entry following Ca^{2+} store release downstream of receptor activation.

The non-selective TRPC channel blocker SKF-96365 has been confirmed as an inhibitor of TRPC1 channels in mouse pulmonary artery smooth muscle cells. SOCE was abolished in these cells by a TRPC1 inhibitory antibody, an effect that was mimicked by SKF-96365 (Ng *et al.*, 2009). A similar study in bovine aortic endothelial cells showed that molecular knock-down of TRPC1 and SKF-96365 attenuated SOCE downstream of P2Y receptor activation to a similar degree (Bishara & Ding, 2010). In this study, SKF-96365 significantly inhibited Ba^{2+} and Ca^{2+} entry downstream of thapsigargin-mediated store depletion, providing further evidence for the contribution of TRPC1 channels to SOCE in HLMCs. As evidenced in figure 5.10, Ca^{2+} store release was potentiated in the presence of SKF-96365; this could be due to the off-target effects of SKF-96365. For example, Leung *et al*. (1996) showed that 30μM SKF-96365 promoted Ca^{2+} entry in HL-60 cells, and it was reported to stimulate phosphoinositide hydrolysis in human astrocytoma cells (Arias-Montano *et al.*, 1998). Such non-specific effects in HLMCs could lead to an increase in cytosolic Ca^{2+} and potentiation of Ca^{2+} store release. However, taken together with synta 66-insensitive Ba^{2+} and Ca^{2+} entry, the significant inhibition of divalent ion entry following thapsigargin stimulation by SKF-96365 provides further evidence for the involvement of TRPC1 channels in SOCE in HLMCs.
Further studies employing selective molecular knock-down techniques, although beyond the scope of this project, would confirm the activation of TRPC1 downstream of Ca^{2+} store release in HLMCs. Such studies would provide valuable information on the differential contribution of TRPC and Orai channels to SOCE downstream of different mechanisms of activation.

S1P was identified as an activator of TRPC5 in search for novel activators of the channel using tetracycline-inducible HEK-TRPC5 cells (the cell line used in this study). S1P was reported to give rise to Ca^{2+} entry in tetracycline-induced, but not non-induced, cells in a concentration-dependent manner. S1P was also shown to activate TRPC1-TRPC5 heteromeric assemblies expressed in HEK cells, but not TRPC1 channels alone (Xu *et al.*, 2006b). The authors described that S1P-evoked Ca^{2+} entry in human saphenous vein vascular SMCs has two phases, which are both sensitive to the inhibitory TRPC5 antibody T5E3. Treatment of HEK-TRPC5 cells with pertussis toxin or the PLC inhibitor U73122 inhibited S1P-evoked Ca^{2+} entry, indicating the respective involvement of Gi/o-coupled receptors and PLC in the activation of TRPC5 by S1P. A recent study suggested that group 6 phospholipase A2 (PLA2) enzymes, which release the fatty acids lysophosphatidylcholine (LPC) and arachidonic acid (AA) from glycerol, are involved in the activation of TRPC5 by extracellular S1P (Al-Shawaf *et al.*, 2011). An intracellular mechanism of action of S1P has also been suggested; it was reported to elicit single-channel events in inside-out patch clamp experiments of HEK-TRPC5 cells (Xu *et al.*, 2006b). As S1P can be transported across the membrane or accumulate intracellularly following activation of S1P receptors (Saba & Hla, 2004), it was concluded that TRPC5 can be activated by S1P by two different mechanisms; it

can act as an ionotropic receptor for intracellular S1P, or become activated downstream of PLC production following S1P receptor stimulation (Xu *et al.*, 2006b). Consistent with these reports, S1P gave rise to two phases of Ca^{2+} entry in HLMCs in this study. This is likely to be due to S1P acting in both an intracellular and extracellular manner to activate the channels. Unfortunately, technical difficulties prevented patch clamp experiments from being carried out on HLMCs from donor 387; future experiments investigating the I/V relationship of S1P-evoked currents in HLMCs will reveal whether homomeric TRPC5 channels are activated, or whether they form heteromeric assemblies with TRPC1. Inside-out patch clamp experiments, or whole-cell patch clamp experiments with S1P in the pipette solution would also reveal whether S1P acts intracellularly to activate TRPC5-containing channels in HLMCs.

The donor-dependent nature of TRPC5 expression in HLMCs could have important physiological consequences. Although relatively little is known about its biological roles, TRPC5 has been reported to mediate the Ca^{2+} entry in hippocampal neurones that hinders growth cone extension (Greka *et al.*, 2003). Ca^{2+} entry in arteriolar smooth muscle cells occurs through TRPC5 (Xu *et al.*, 2005b), and TRPC5-mediated Ca^{2+} entry has been implicated in vascular smooth muscle cell motility stimulated by S1P (Xu *et al.*, 2006b). Ca^{2+} permeability is thus central to all the known roles of TRPC5 channels in different systems. The possibility that Ca^{2+} entry through TRPC5 in HLMCs from 1/5 donors in this study could be important in the control of downstream mediators involved in lung disease was considered. From the medical records of HLMC donors, donor 387 (HLMCs expressing TRPC5) did not suffer from asthma, allergies or chronic obstructive pulmonary disease. Donors 410 and 411 (not expressing TRPC5) suffered from iodine allergies and COPD, respectively; TRPC5 expression does therefore not appear to correlate with lung disease incidence. Donor 387 smoked cigarettes until 3 months before the tissue was obtained; of the 4/5 donors not expressing TRPC5, 410 and 411 were non-smokers, and smoking data was not available for donors 360 and 370. Tobacco smoke is a complex mixture of over 4700 different chemicals including carbon oxides, esters, phenols, hydrocarbons and free radicals, which have multifaceted effects in the body (Borgerding & Klus, 2005). The expression of a number of genes is known to be up-regulated in response to cigarette smoke in rat pulmonary arteries (Wright *et al.*, 2002) and human airway epithelial cells (Beane *et al.*, 2007); this up-regulation can be transient, rapidly-reversible or irreversible (Beane *et al.*, 2007). It is possible that TRPC5 channels are expressed in donor 387 due to cigarette smoking. Interestingly, one study has suggested that TRPC6 channel expression is up-regulated in non-small cell lung cancer, which is most commonly caused by smoking (Zhang *et al.*, 2010a). Collecting more data on the functional expression of TRPC5 channels in HLMCs from smokers and non-smokers is necessary to draw reliable conclusions on whether chemicals in cigarette smoke up-regulate TRPC5 expression; data obtained in this study suggest that it is a possibility, and represents an interesting avenue for further investigation.

	Donor number				
	387	**360**	**370**	**410**	**411**
TRPC5 expression	Yes	No	No	No	No
Asthma	No			No	No
COPD	No			Yes	No
Allergies	No			No	Iodine
Smoking	Yes			Ex (40 years ago)	No
Medication	prodisimol atenolol	amlodipine perindopril simvastatin bendroflumeth azide	bendroflumeth azide felodipine quinapril ezetimibe lansoprazole cocodamol etodolac fluoxetine	ventolin seretide lansoprazole co-codamol quinine sulphate aspirin	atenalol aspirin oxytetracycline simastatin

Table 5.1. HLMC Donor information

Table summarising HLMC donor information and TRPC5 expression. Blank box=no data.

The possibility that the donors' drug history could affect TRPC5 expression was also considered. Known patient information is summarised in table 5.1; of interest is that whilst donor 387 was not taking aspirin or other oral anti-inflammatory medication, donors 410 and 411 were taking aspirin. Donor 370 was taking etodolac, another non-steroidal anti-inflammatory drug. These compounds work by inhibiting cyclo-oxygenase enzymes, which are responsible for the production of prostaglandins (Vane & Botting, 2003), second messengers that regulate inflammation. It is possible that the anti-inflammatory effects due to long-term use of aspirin and etodolac could include the down-regulation of ion channel expression in mast cells, which could account for the lack of TRPC5 expression in some donors. Donor 360 was taking amlodipine and donor 370 felodipine; these Ca^{2+} channel inhibitors block L-type voltage-gated Ca^{2+} channels, but could affect other channels. A study investigating the selectivity of amlodipine in *Xenopus* oocytes showed that it also significantly inhibits N-type Ca^{2+} channels (Furukawa *et al.*, 1999); complex cellular effects of this and other drugs could be responsible for the variation seen in TRPC5 expression between donors. Future analysis of TRPC5 activity in HLMCs from a greater pool of donors will provide insightful information on whether donors' drug history affects channel expression.

In conclusion, the data presented in the first part of this chapter suggest that TRPC1 and Orai1 channels are involved in SOCE in HLMCs, with a possible contribution from TRPC5 in some donors. The potential involvement of different channels in SOCE between donors could be important for mast cell functions in conditions such as asthma. Following Ca^{2+} influx, exocytic release of pre-formed pro-inflammatory mediators within secretory granules occurs as the mast

cell degranulates. Granule-associated mediators include biogenic amines such as histamine, which causes increased capillary permeability and bronchoconstriction (Lundequist & Pejler, 2011). Serotonin, which was previously thought to be restricted to rodent mast cells (Lundequist & Pejler, 2011), has recently been shown to be present in human peripheral blood-derived mast cells (Kushnir-Sukhov *et al.*, 2007), and gives rise to vasoconstriction and pain (Theoharides *et al.*, 2007). Lysosomal enzymes are also released in mast cell degranulation, including β-hexosaminidase, which is present in mast cells from all species and is thought to be involved in carbohydrate processing (Theoharides *et al.*, 2007; Lundequist & Pejler, 2011). Proteoglycans, proteases and pre-formed cytokines are also stored in mast cell granules and released upon degranulation (Lundequist & Pejler, 2011). Mast cells thus store an extensive array of pre-formed mediators in their cytoplasmic granules, which have a profound effect on surrounding tissues when released in response to mast cell activation.

Whilst TRPC channels have been reported to be involved in FcεRI-mediated Ca^{2+} entry and degranulation in RBL-2H3 cells (Ma *et al.*, 2008), the involvement of TRPC channels in human mast cell mediator release has not been investigated. In accordance with the results obtained by Ma *et al.* (2008), data obtained in this chapter suggest that both I_{CRAC} and TRPC channels are involved in Ca^{2+} entry downstream of FcεRI cross-linking in HLMCs; IgE-dependent Ca^{2+} entry was partially inhibited by synta 66, and synta 66-insensitive Ca^{2+} entry was further reduced by the non-selective TRPC channel inhibitors Gd^{3+} and SKF-96365. These data are in accordance with Ca^{2+} imaging data discussed above showing that TRPC1 channels are likely to be involved in Ba^{2+} and Ca^{2+} entry following FcεRI-dependent Ca^{2+} store depletion.

Electrophysiological experiments revealed TRPC-like currents activated downstream of FcεRI cross-linking in 3/7 cells, and I_{CRAC}-like currents in 1/7 cells. These data appear to contradict Ca^{2+} imaging data showing that IgE-dependent Ca^{2+} entry was partially inhibited by synta 66 in all cells. However, the electrophysiological recording conditions were not optimised to record I_{CRAC}-like currents. As Orai1 channels have very low conductance (Hogan *et al.*, 2010), they are very difficult to detect under standard recording conditions. Ca^{2+} ions are frequently replaced with Na^{+} ions when recording I_{CRAC} currents to increase the conductance and facilitate identification (Lepple-Wienhues & Cahalan, 1996; Mercer *et al.*, 2006; Prakriya *et al.*, 2006; Scrimgeour *et al.*, 2009). As the extracellular solution contained 2mM Ca^{2+} in this study and divalent ions were not replaced with Na^{+}, it is possible that I_{CRAC} currents were too small to detect in the presence of the larger non-selective TRPC currents. Electrophysiological data in this chapter therefore provide evidence for the activation of TRPC channels downstream of FcεRI cross-linking, but the contribution of I_{CRAC} cannot be ascertained under the experimental conditions used..

In accordance with the Ca^{2+} imaging data, synta 66 gave rise to partial inhibition of FcεRI-dependent histamine and β-hexosaminidase release in 50% of HLMCs. Synta 66-insensitive release was sensitive to the non-selective TRPC channel blockers Gd^{3+} and SKF-96365, providing

evidence for the involvement of both Orai1 and TRPC1 channels in HLMC degranulation. In the other 50% of donors, however, synta 66 completely inhibited histamine and β-hexosaminidase release. Repeating Ca^{2+} imaging experiments at 35°C showed that the temperature did not affect the sensitivity of FcεRI responses to synta 66. These data suggest that in some donors, I_{CRAC} alone is responsible for mediating the Ca^{2+} influx required for degranulation, whereas in other donors TRPC1 and I_{CRAC} channels are both involved. Two questions arise from these observations; why are two different Ca^{2+} channels involved in FcεRI-dependent Ca^{2+} entry and degranulation in HLMCs, and why does donor dependency exist?

To address the first question, it is possible that TRPC1 and Orai1 channels function together to bring about FcεRI-dependent Ca^{2+} entry, as discussed above and depicted in figure 5.1. It has been suggested, based on experiments in HSG cells, that TRPC1 and Orai1 channels have distinct downstream effects and are both required for HSG cell function. Orai1 mediated Ca^{2+} entry was reported to be sufficient for the activation of nuclear factor of activated T-cells (NFAT) transcription factor, but a higher concentration of intracellular Ca^{2+}, provided by TRPC1 activation, was shown to be required for the full activation of the transcription factor nuclear factor-κB (NFκB) and K_{Ca} channels (Cheng *et al.*, 2011). The existence of the two types of store-operated Ca^{2+} channel allows fine control of cellular functions regulated by store depletion. Both NFAT and NFκB are activated downstream of FcεRI cross-linking and regulate cytokine transcription in mast cells (Hutchinson & McCloskey, 1995; Marquardt & Walker, 2000). NFAT is important for the production of TNFα, a pro-inflammatory cytokine that activates the airway epithelium, antigen-presenting cells and macrophages in the asthmatic airway (Chung & Barnes, 1999). The production of IL-2 is also regulated by NFAT (Marquardt & Walker, 2000); this pro-inflammatory cytokine causes T cell differentiation and eosinophilia. NFκB enhances the transcription of many genes for proteins involved in inflammation including cytokines, adhesion molecules and growth factors (Marquardt & Walker, 2000). It has been shown in mouse mast cells that NFκB activated downstream of FcεRI is vital for the production of IL-6 (Marquardt & Walker, 2000), which acts as a growth factor for T and B cells in allergic inflammation (Chung & Barnes, 1999). Fine control of these transcription factors by differential Ca^{2+} entry through Orai1 and TRPC1 channels would allow the mast cell to tightly regulate downstream cytokine production, and thus activate different cells important in airway inflammation. Whilst the transcription of some cytokines is tightly controlled by Ca^{2+} and likely to be regulated by the different channels, it is possible that both TRPC1 and Orai1 channels contribute to the Ca^{2+} influx required for degranulation, which can be produced by Ca^{2+} ionophores in the absence of FcεRI cross-linking (Cochrane & Douglas, 1974). It can be speculated that the two channel types can bring about degranulation in HLMCs as a 'fail-safe' mechanism to ensure that mediator release still occurs when inactivating single nucleotide polymorphisms arise in the genes encoding one of the channels. Such a mechanism has been proposed to account for the evolution of complementary signalling cascades for mast cell activation (Gilfillan & Tkaczyk, 2006).

To address the second question of why donor dependency exists in the contribution of TRPC1 and Orai1 channels to HLMC degranulation, it is important to consider that compartmentalised signalling is likely to occur. As described previously, the plasma membrane localisation and association of ion channel subunits is tightly controlled by lipids, proteins and other signalling molecules; donor-dependent variations in these molecules could give rise to varied membrane expression of TRPC1 and Orai1 channels. For example, a higher level of ordered PtdIns(4,5)P_2 in some donors could give rise to a greater association of STIM1 and Orai1 (Calloway *et al.*, 2011) than in other donors, resulting in a greater contribution of I_{CRAC} to FcεRI-dependent Ca^{2+} entry and degranulation.

It is also possible that the expression of TRPC1 and Orai1 channels varies between donors, as discussed above for TRPC5. Unfortunately it was not possible to electrophysiologically investigate the contribution of the different ion channels in the same donors that were used for histamine and β-hexosaminidase secretion assays, as sufficient numbers of pure HLMCs were not able to be obtained in our laboratory to carry out functional assays. If TRPC1 and Orai1 were both expressed to a high level in one donor, they could both contribute to FcεRI-dependent Ca^{2+} signalling and degranulation as depicted in figure 5.1. If TRPC1 expression levels were low in another donor insufficient membrane trafficking could occur, and TRPC1 membrane expression may not be sufficient for gating by STIM1. Orai1 alone could mediate Ca^{2+} entry required for degranulation downstream of FcεRI cross-linking in these donors.

Differential contribution of Orai1 and TRPC1 to FcεRI-evoked Ca^{2+} entry between donors could have important functional consequences. Whilst degranulation occurred to a similar extent in all donors in this study regardless of the involvement of the different ion channels, it is likely that cytokine expression would be affected. As discussed above, the greater Ca^{2+} conductance effected by TRPC1 is required for the complete activation of NFκB (Cheng *et al.*, 2011). Cytokines play an integral role in asthmatic airway inflammation as they induce many of the characteristic symptoms of the disease including airway smooth muscle cell hyperplasia and the infiltration of other immune cells (Chung & Barnes, 1999). Donor-dependent TRPC1 and Orai1 channel contribution to Ca^{2+} entry could therefore have important consequences for the development of inflammation in the asthmatic airway. Although beyond the scope of this project, determining the cytokine expression profile of HLMCs from different donors in combination with molecular knock-down of TRPC1 and Orai1 would be an interesting avenue of investigation and would reveal whether TRPC1 and Orai1- mediated Ca^{2+} entry regulates the transcription of different cytokines.

To summarise the findings in this chapter, TRPC1 channels are likely to be involved in SOCE in human mast cells, possibly interacting functionally with Orai1. Results provide evidence for the involvement of TRPC channels in FcεRI-dependent Ca^{2+} signalling and mediator release in some donors.

Chapter 6: Diacylglycerol-sensitive TRPC3/6/7 channels in human mast cells

The results described in chapter 3 demonstrated that TRPC channels, which are expressed in both LAD 2 cells and HLMCs, may be involved in Ca^{2+} entry following receptor stimulation. Chapter 4 discussed the development of pharmacological methods to investigate second messenger-regulated TRPC3/6/7 channels using HEK-TRPC6 cells. Having established that LAD 2 cells express mRNA for all three TRPC channels in this subgroup, and HLMCs expressed TRPC6 in 3/3 donors and TRPC7 in 1/3 donors, these tools were then applied to study the functional expression and biophysical properties of TRPC3/6/7 channels in human mast cells.

6.1 OAG activation of TRPC3/6/7 channels in HLMCs

OAG was applied to fura-2-loaded HLMCs to test for functional expression of TRPC3/6/7 channels. As shown in figure 6.1, application of 100μM OAG to HLMCs in the presence of extracellular Ca^{2+} gave rise to Ca^{2+} entry in 97% of cells tested, where "responders" were classed as cells where the fluorescence increased by more than 10 standard deviations above the baseline fluorescence following OAG application. As similar results were obtained in four separate donors, figure 6.1a (ii) shows the mean response from all donors tested. OAG-induced Ca^{2+} entry was significantly reduced in the absence of extracellular Ca^{2+}; the change in fura-2 fluorescence ratio in response to OAG application was 0.68 ± 0.03 (n=95, N=7) in the presence of Ca^{2+}, compared with 0.05 ± 0.01 (n=7, N=3) in the absence of extracellular Ca^{2+}. DMSO at 1/1000 dilution (vehicle for OAG) did not result in Ca^{2+} entry when applied to cells.

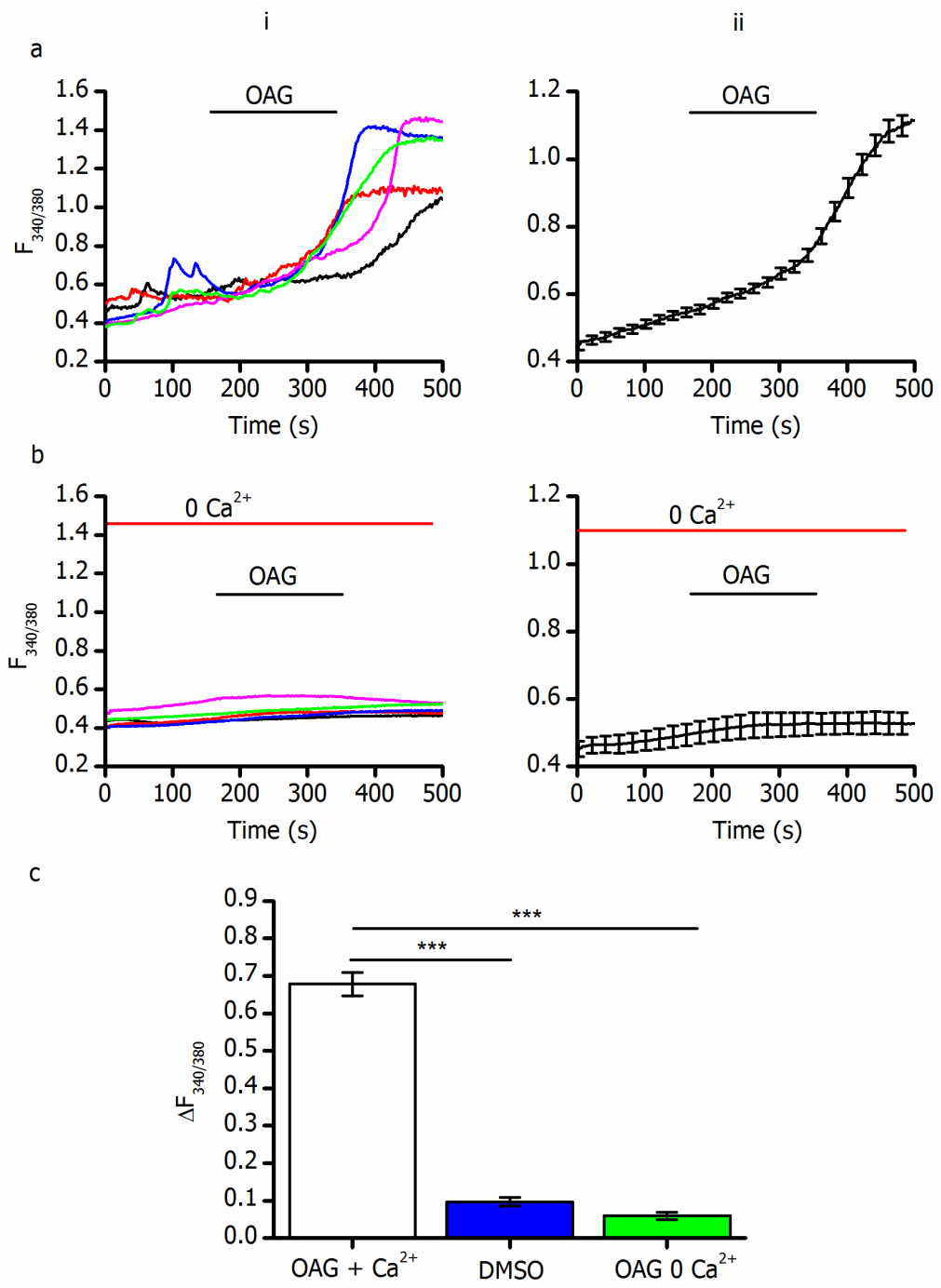

Figure 6.1. OAG-induced Ca^{2+} entry in HLMCs

Fura 2-loaded HLMCs were perfused in standard external solution, and OAG was bath-applied as indicated by the horizontal bars.

a: Ca^{2+} fluxes in HLMCs stimulated with OAG in the presence of extracellular Ca^{2+}. (i) shows individual example cells; (ii) shows the mean response (n=95 cells, N=7 experiments, representative of 4 donors). 97% of cells responded to OAG application.

b: Experiments as in (a), in the absence of extracellular Ca^{2+}; n=6, N=3, 1 donor.

c: Bar chart showing size of Ca^{2+} influx ($\Delta F_{340/380}$) in the presence (white) and absence (green) of extracellular Ca^{2+} and when applying 1/1000 DMSO (blue), the vehicle for OAG (n=48, N=4, representative of 2 donors). ***: means are significantly different, $p<0.0001$, one-way ANOVA with Tukey post-test.

The effect of the non-selective TRPC channel inhibitors Gd^{3+} and SKF-96365 on OAG-induced Ca^{2+} entry in HLMCs was then assessed. Gd^{3+} has previously been shown to block heterologously expressed TRPC3 and TRPC6 channels with IC_{50} values of 2.5μM and 2.3μM, respectively (Inoue *et al.*, 2001; Dietrich *et al.*, 2005b). SKF-96365 inhibits heterologously expressed TRPC6 channels with an IC_{50} of 4.2μM (Inoue *et al.*, 2001), and receptor-mediated Ca^{2+} entry in platelets with an IC_{50} of 8.5μM (Merritt *et al.*, 1990). Experiments like those shown in figure 6.1 were repeated in the presence of Gd^{3+} and SKF-96365; as shown in figure 6.2, both inhibitors caused concentration-dependent inhibition of OAG-induced Ca^{2+} entry in HLMCs. When analysing the single-cell traces shown in figure 6.2a, it is apparent that the both inhibitors caused a reduction in the amplitude of the Ca^{2+} signal in each cell; they did not cause fewer cells to respond. Figure 6.2c shows concentration-response curves for inhibition by Gd^{3+}; in donor A410 (5.2c (i)), the estimated IC_{50} for Gd^{3+} inhibition was 2.77μM, and complete inhibition was achieved by 10μM. Whilst the Gd^{3+} sensitivity varied between donors (estimated IC_{50} in donor 411= 18.4μM), the average estimated IC_{50} for N=2 donors (figure 6.2c (ii)) was 6.5μM. A sub-maximal concentration of 10μM Gd^{3+} was chosen for use in further experiments.

SKF-96365 also had concentration-dependent effects on OAG-induced Ca^{2+} entry; as shown in figure 6.2d (i), concentrations below 1μM appeared to potentiate Ca^{2+} entry. For example, $\Delta F_{340/380}$ was increased by 0.27 (from 0.68 to 0.95) in the presence of 0.001μM SKF-96365. Inhibition of OAG-induced Ca^{2+} entry occurred at concentrations greater than 1μM. Analysis of concentrations of 1μM SKF-96365 and above revealed an IC_{50} of 10.25μM, which is in range of previously reported values for the inhibition of heterologously expressed TRPC6 channels (Inoue *et al.*, 2001; Dietrich *et al.*, 2005b). Due to the potentiating effect of lower concentrations of SKF-956365, a "% inhibition" graph was not plotted as was done for Gd^{3+} inhibition. H_2O at 1/100 dilution (vehicle for maximal concentrations of Gd^{3+} and SKF-96365) did not have an effect on OAG-induced Ca^{2+} entry; see figure 6.2d (ii).

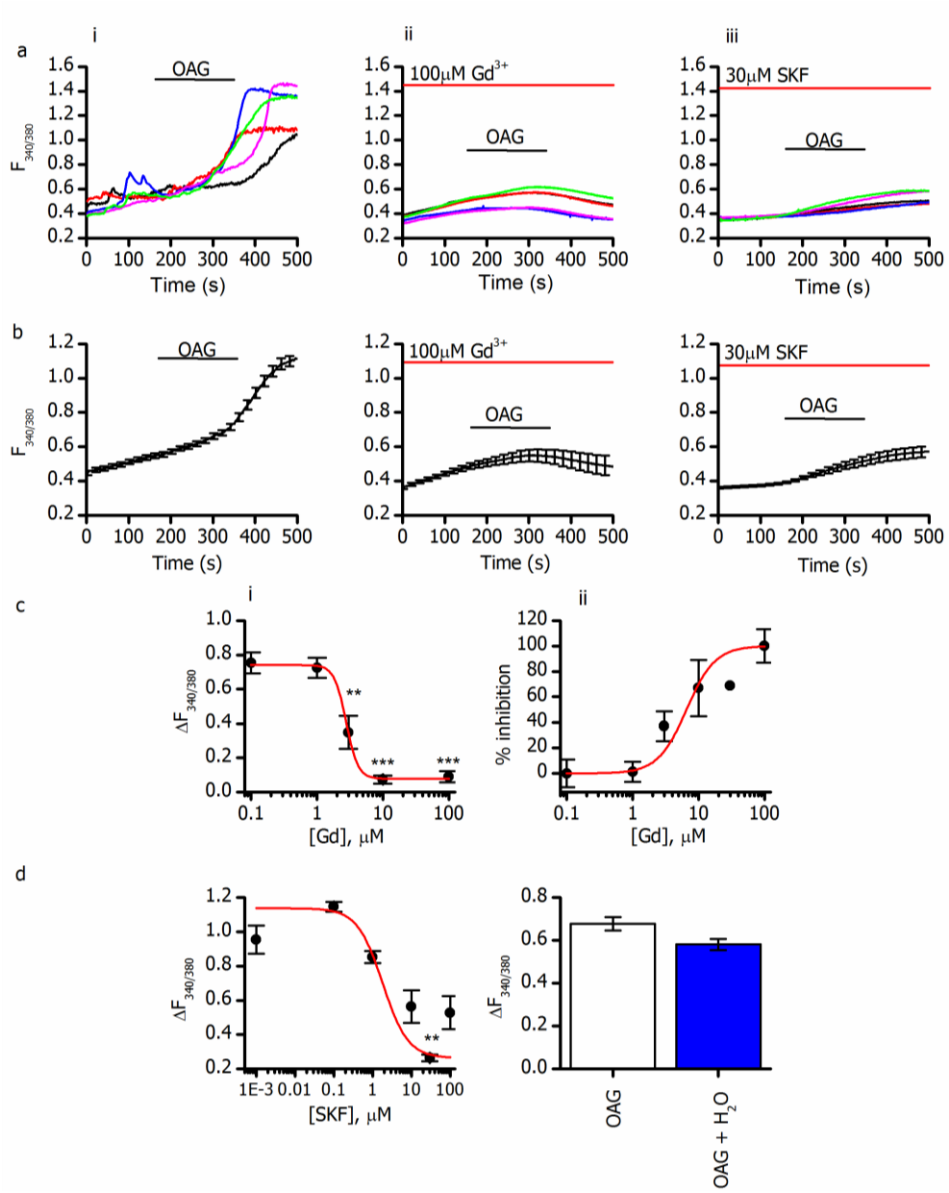

Figure 6.2. OAG-induced Ca^{2+} entry in HLMCs is inhibited by Gd^{3+} and SKF-96365.

a: Individual representative cell traces showing Ca^{2+} fluxes in HLMCs. (i) shows control responses to 100μM OAG; in (ii) and (iii) OAG was applied in the presence of 100μM Gd^{3+} and 30μM SKF-96365, respectively.

b: Mean traces ± SEM for experiments shown in (a); (i) shows control OAG response, (ii) shows OAG response in the presence of 100μM Gd^{3+} and (iii) shows OAG response in the presence of 30μM SKF-96365.

c (i): Concentration-response curve showing change in fluorescence ($\Delta F_{340/380}$) against Gd^{3+} concentration present in donor A410. IC_{50}=2.77μM. (ii) shows % inhibition of OAG-induced Ca^{2+} entry by different concentrations of Gd^{3+} compared to control data. Points show mean ± SEM for N=2 donors. IC_{50}=6.5μM. n numbers are as follows: Donor A410: 10 for 0.1μM, 8 for 1 μM, 10 for 3μM, 5 for 10μM, 8 for 100μM. Donor A411: 13 for 0.1μM, 9 for 1 μM, 7 for 3μM, 9 for 10μM, 7 for 30μM 3 for 100μM.

d (i): Concentration-response curve showing OAG-induced change in fluorescence against concentration of SKF-96365. n numbers are as follows: 7 for 0.001μM, 3 for 0.1μM, 7 for 1μM, 14 for 10μM, 8 for 30μM, 8 for 100μM. (ii) shows OAG-induced change in fluorescence in the presence and absence of 1/100 H_2O (vehicle for Gd^{3+} and SKF-96365 at minimal dilution); means were not significantly different (unpaired Student's T-test).

**: means were significantly different, p<0.01. ***: p<0.0001, one-way ANOVA with Tukey post-test.

N.B. Control OAG data is the same as that shown in figure 6.1.

Whole-cell patch clamp recordings were then carried out as detailed in chapter 2.6.9 in order to investigate the biophysical properties of OAG-induced currents in HLMCs. Cells were voltage-clamped at -60mV, and 1 second voltage ramps from -100mV to +100mV were applied. Results are shown in figure 6.3; focal application of OAG gave rise to an outwardly-rectifying current in 88% of cells. Currents had the expected biophysical properties of the DAG-activated TRPC channels, showing outward rectification and a reversal potential close to 0mV. In 37.5% of responding cells (3/8), the OAG-induced current was sustained; the mean inward current amplitude measured at -100mV was 11.1pA/pF±10.3, and the outward current measured at +100mV was 51.6pA/pF±41.5. 62.5% of responding cells (5/9) displayed a transient response; in these cells the mean inward current amplitude was 75.3pA/pF ± 36.35, and the mean outward current amplitude was 147.2pA/pF±52.34. For comparison, 50% of HEK-TRPC6 cells had a sustained response to OAG. Examples of cells showing sustained and transient responses are shown in figure 6.3a (i) and (ii), respectively. As with OAG-induced currents in HEK-TRPC6 cells, currents were classed as "sustained" when more than 50% of current remained at 2 minutes after the end of drug application. 2/3 cells displaying a sustained response to OAG application were from the same donor (370). The other cell displaying a sustained current was from donor 410; 2/3 cells from donor 410 had a transient current. Currents were transient in all cells tested from donor 360 (n=3). The kinetics of current onset were not found to be related to whether currents were transient or sustained; in cells with a transient OAG-induced current, the peak current occurred at 124.67 seconds ± 30.64 (n=5) after the beginning of OAG application. In cells displaying a sustained current, the peak occurred at 118.40 seconds ± 23.47 (n=3) after OAG application; there was no significant difference in the time taken for the current to peak between the cells displaying the two types of response (unpaired Student's T-test).

Example I/V relationships from time points 1–6 in figure 6.3a (i) and (ii) are shown in figure 6.3b (i) and (ii). In order to examine the relative size of the inward and outward currents in OAG-responding cells, a "rectification index" was calculated using the formula: rectification index = peak current at +100mV/ peak current at -100mV.

In the bar graph in figure 6.3b (iii), the rectification index in cells showing a sustained response to OAG is compared with that in cells showing a transient response. The rectification index was significantly higher in cells with a sustained response, showing that the current was more outwardly-rectifying in these cells. For comparison, in HEK-TRPC6 cells the rectification index of OAG-evoked currents was 6.86 ± 1.23 (n=4) for sustained currents and 4.78 ± 1.12 (n=4) for transient currents; these values were not significantly different.

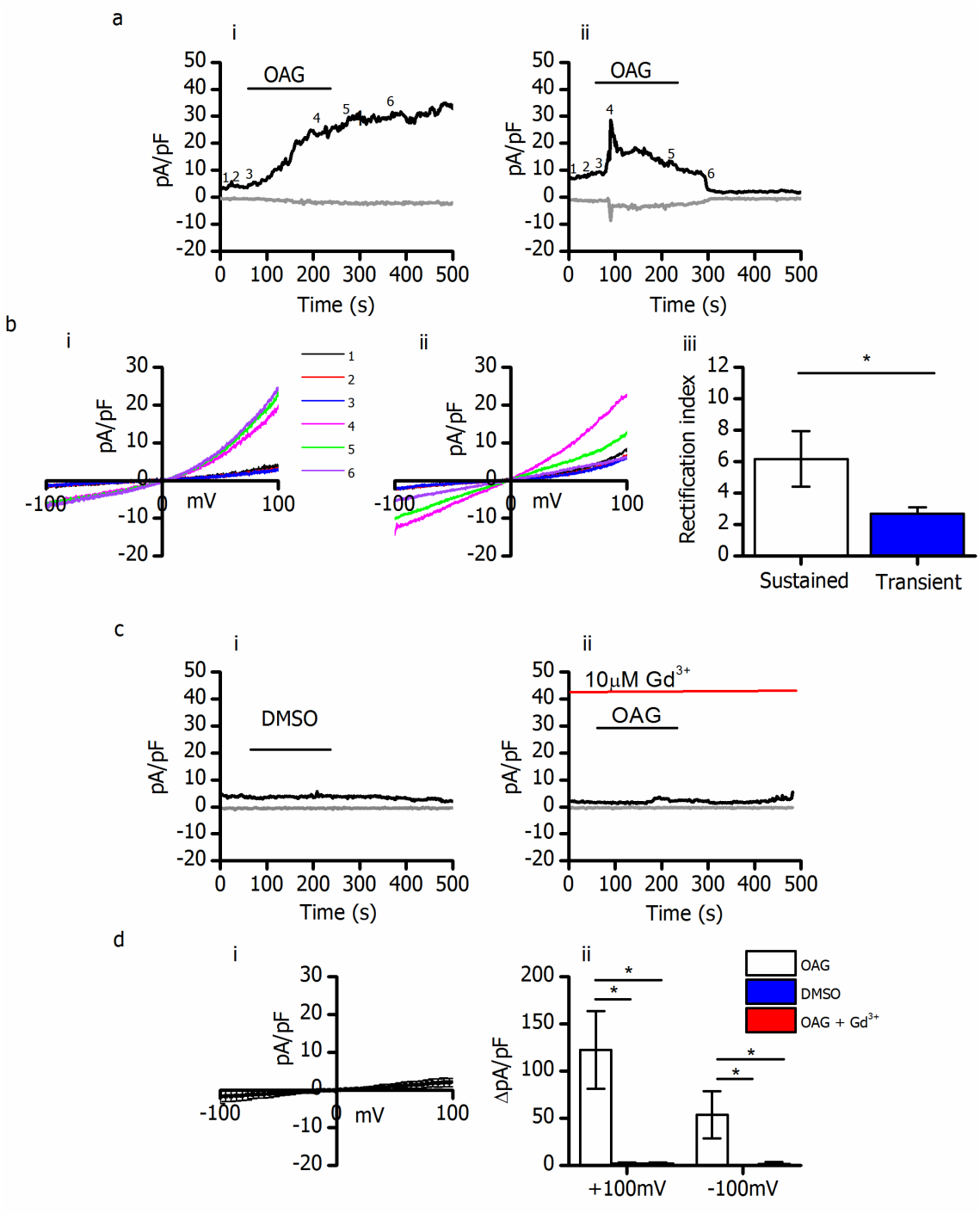
a
i
OAG
pA/pF
Time (s)
ii
OAG
pA/pF
Time (s)
b
i
pA/pF
mV
ii
pA/pF
mV
iii
Rectification index
Sustained
Transient
c
i
DMSO
pA/pF
Time (s)
ii
10μM Gd3+
OAG
pA/pF
Time (s)
d
i
pA/pF
mV
ii
ΔpA/pF
OAG
DMSO
OAG + Gd3+
+100mV
-100mV

Figure 6.3. OAG induces an outwardly-rectifying current in HLMCs that is sensitive to 10μM Gd^{3+}

a (i) and (ii): Current-time plots of whole-cell current induced by 100μM OAG in HLMCs.OAG was focally applied where indicated by the horizontal bars. Current was sampled at -100mV (grey trace) and +100mV (black trace). (i): example trace showing OAG-induced current that remained after washout, as observed in 25% of cells (3/9). (ii) shows example traces of a current that reached a peak in the presence of OAG, which then declined, as observed in 62.5% of cells (5/9). The remaining 12.5% of cells (1/9) did not respond to OAG application.

b (i): Current-voltage relationships taken from time points 1-6 in part a (i) from cell displaying a sustained current in response to OAG application. (ii): Current-voltage relationships taken from time points 1-6 in part a (ii) from cell showing a transient response. (iii): Bar chart comparing the rectification index (peak current at +100mV/peak current at -100mV) of OAG-induced current in cells displaying sustained versus transient responses. *: means are statistically significant, $p<0.05$, unpaired Student's T-test.

c (i): Current-time plot of whole-cell currents from an example cell when 1/1000 DMSO (vehicle for OAG) was focally applied. Similar results were obtained in 2 other cells. (ii): Current-time plot of OAG-induced current in the presence of 10μM Gd^{3+}, which was focally applied as indicated by red horizontal bar. Traces are shown for a single representative cell; similar currents were observed in 5 other cells.

d (i): Current-voltage relationship of OAG-induced current in the presence of 10μM Gd^{3+} showing mean current ±SEM; n=6 cells, N=2 donors. Currents had a mean reversal potential of -6.26mV ±1.84. (ii): Bar graph comparing size of currents induced by OAG (white), DMSO (blue) and OAG + Gd^{3+} (red). Current before agonist application was subtracted from the maximum current in the presence of agonist, to give "ΔpA/pF". *: Results are statistically significant, $p<0.05$, one-way ANOVA with Tukey post-test.

As shown in figure 6.3c, focal application of DMSO at 1/1000 dilution did not induced currents in HLMCs, and OAG-induced currents were significantly inhibited by 10μM Gd^{3+} (ΔpA/pF at +100mV = 122.5 ± 41.3 in the absence of Gd^{3+} and 2.2 ± 1.1 when Gd^{3+} was present. At -100mV ΔpA/pF = 53.0±24.8 in the absence of Gd^{3+} and 1.8 ± 1.7 in the presence of Gd^{3+}).

Experiments in HEK-TRPC6 cells (chapter 4.1) indicated that PKC may have a role in the negative regulation of TRPC6 channels as reported previously (Estacion *et al.*, 2004; Shi *et al.*, 2004; Bousquet *et al.*, 2010), giving rise to the transient currents seen in response to OAG application in some cells. To investigate whether such a mechanism regulates the kinetics of OAG-evoked currents in HLMCs, the effects of the selective PKC inhibitor, Ro-31-8425, were examined. Whole-cell patch clamp experiments like those shown in figure 6.3 were then repeated in the presence of 3μM Ro-31-8425. Unfortunately, due to experimental timings and the short-lived nature of HLMCs from some donors in culture, experiments in the presence of Ro-31-8425 were only able

to be carried out on one of the donors (410) shown in figure 6.3. Data obtained were culture-matched; control experiments using donor 410 were carried out on the same days as experiments in the presence of Ro-31-8425.

Data are shown in figure 6.4; the percentage of cells displaying a sustained current induced by OAG was increased from 33% (3/9) to 83% (5/6) when Ro-31-8425 was present. For comparison, the percentage of HEK-TRPC6 with a sustained current increased from 50% to 78% in the presence of Ro-31-8425. As shown in figure 6.4b (i), the peak current was reduced by 67pA/pF (from 128.4 to 60.93) at +100mV, and by 38.3pA/pF (from 55.0 to 16.7) at -100mV in the presence of Ro-31-8425. The peak currents were variable, indicated by the large error bars in figure 6.4b (i), and this reduction in peak current was not statistically significant. These data suggest that PKC is unlikely to have a role in determining the amplitude of the initial current evoked by OAG. The rectification index of the OAG-induced current was measured at 3.93 ± 0.31 (n=6) in the presence of Ro-31-8425, showing that the outward current amplitude was approximately 4 fold larger than the inward current. When comparing this value to the calculated rectification index values for currents obtained in the absence of Ro-31-8425 (6.17 ± 1.76 (n=3) and 2.69 ± 0.39 (n=5) for sustained and transient currents, respectively), it is apparent that it is more similar to that obtained for transient currents when Ro-31-8425 was not present. As few cells (3/9) displayed a sustained current in response to OAG application when Ro-31-8425 was absent, more n numbers would be required to draw conclusions about the direction of cation flow through TRPC3/6/7 channels under the different conditions from the rectification index values. Given the low availability of human lung tissue and limited time-frame in which HLMCs can be used for patch-clamp experiments, more n numbers were not able to be obtained in this study.

The percentage of the maximum current remaining at two minutes after the end of OAG application was significantly greater when Ro-31-8425 was present (figure 6.4b (ii)). The percentage of current remaining increased by 66.2% (from 36.8 to 103.0) at + 100mV, and by 54.3% (from 24.3 to 78.6) at -100mV. These data suggest that PKC does negatively regulate TRPC3/6/7 function in HLMCs following activation of the channels with OAG.

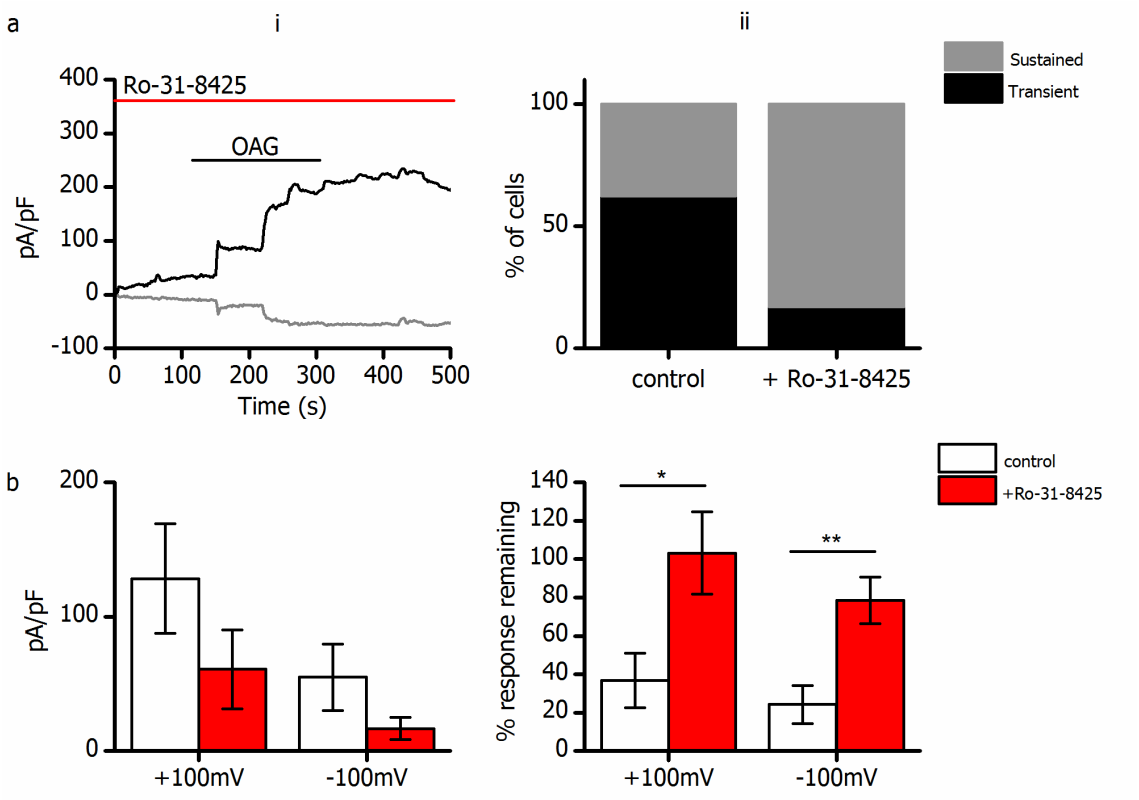

Figure 6.4. OAG-induced currents in HLMCs in the presence of Ro-31-8425.

Experiments like those described in figure 6.3 were repeated in the presence of 3μM Ro-31-8425. a (i): Diary plot of an example whole-cell recording; solutions containing drugs shown were focally applied as indicated by the horizontal bars. Grey trace shows current sampled at -100mV; black trace shows current at +100mV. (ii): Bar graph showing percentage of cells with a "sustained" or "transient" response in the presence vs absence of Ro-31-8425. A response was classed as "sustained" when more than 50% of current remained at 2 minutes after the end of drug application. In control cells, 33% (3/9) of cells had a sustained response; in the presence of Ro-31-8425, 83% of cells (5/6) had a sustained response.

b: (i) Comparison of peak current at +100mV and -100mV in the presence (red; 60.9pA/pF ±29.4 at +100mV, 16.7pA/pF ±8.2 at -100mV) and absence (white; 128.4pA/pF ±40.8 at +100mV, 55.0pA/pF ± 24.8 at -100mV) of Ro-31-8425. (ii): Current remaining at 2 minutes after drug application was calculated as a percentage of peak current in the presence of OAG. At +100mV, 36.8% ± 14.2 remained in the absence of Ro-31-8425; 103% ± 21.5 remained. At -100mV, 24.3% ± 10.0 remained in the absence of Ro-31-8425; 78.6% ± 12.1 remained. Means were significantly different; $p<0.05$ (*) or $p<0.01$ (**), unpaired Student's T-test of log-transformed data.

n numbers are as follows: n=6 cells, N=1 donor in the presence of Ro-31-8425, n=8 cells, N=3 donors in the absence of Ro-31-8425.

The results shown so far suggest that HLMCs express functional OAG-activated TRPC3/6/7 channels; it was then investigated whether LAD 2 cells are an appropriate model to study this subgroup of TRPC channels using fura-2 Ca^{2+} imaging and electrophysiology. As shown in figure 6.5a, very weak Ca^{2+} entry was observed in 25% (15/59) of cells tested, where "responding cells" were classed as those where the fluorescence in the presence of OAG rose by more than 10 standard deviations above the mean baseline fluorescence. The mean amplitude of OAG-induced Ca^{2+} entry in responding LAD 2 cells was 0.37 ± 0.09 (n=15, N=3); this was significantly lower than that observed in HLMCs (0.68 ± 0.03; n=95, N=7. $p<0.0001$, unpaired Student's T-test). Whole-cell patch clamp recordings revealed the activation of currents in response to focal application of OAG in 20% of LAD 2 cells (figure 6.5b); the currents were outwardly-rectifying with a reversal potential of -0.09 ± 0.09mV, typical properties of TRPC3/6/7 channel activity. The rectification index of OAG-induced currents in responding LAD 2 cells was calculated to be 4.4 ± 2.3 (n=3). OAG-induced currents were very small; the mean change in current in response to OAG application measured at +100mV in responding LAD 2 cells was 1.8pA/pF ± 0.4 (n=3), compared with 128.4pA/pF ± 40.8 (n=8) in HLMCs and 32.57pA/pF ± 8.00 (n=7) in HEK-TRPC6 cells. Taken together, these results suggest that LAD 2 cells are a poor model to study second messenger-regulated TRPC channel expression in human mast cells; the reasons for this will be discussed in section 6.5.

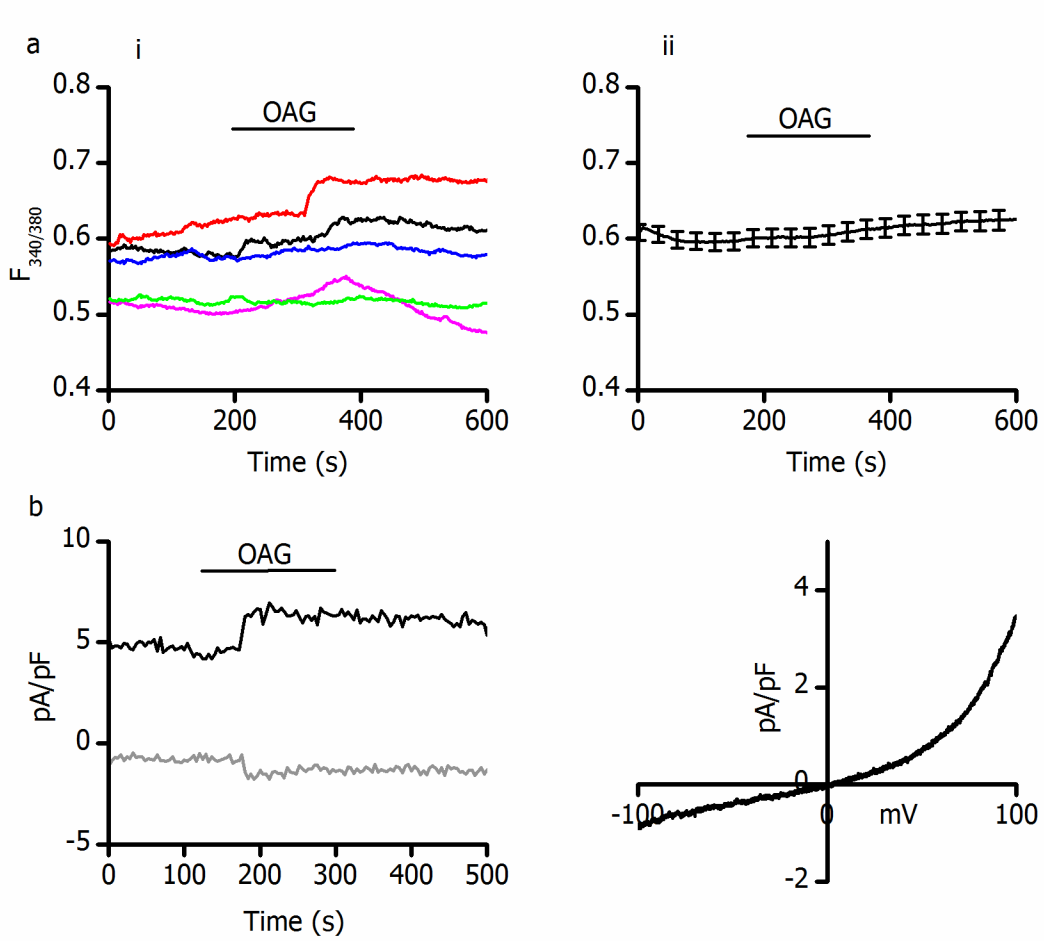

Figure 6.5. OAG-induced Ca^{2+} entry and currents in LAD 2 cells

a: Ca^{2+} fluxes in fura 2-loaded LAD 2 cells stimulated with100μM OAG as indicated by the horizontal bar. (i) shows Ca^{2+} fluxes, represented by fluorescence at 340/380nm, in individual responding and non-responding example cells. 25% of cells (15/59) responded to OAG application; "responders" were classified as cells where the fluorescence in the presence of OAG rose by more than 10 standard deviations above the mean baseline fluorescence. (ii): Mean ± SEM $F_{340/380}$ from n=59 cells, N=3 independent experiments.
b: whole-cell currents induced by 100μM OAG in LAD 2 cells, as observed in 20% (3/15) cells. (i): current-time plot of a representative responding cell. Cells were superfused with standard external solution and OAG was focally applied where indicated. Current was sampled at -100mV (grey trace) and +100mV (black trace). (ii) shows the current-voltage relationship of the OAG-induced current in a representative responding cell; similar I/V curves were obtained in the 2 other responding cells. Currents had a mean reversal potential of -0.09 ± 0.09mV (n=3).

6.2 Receptor activation of TRPC3/6/7 channels in HLMCs

The results obtained so far in this chapter show that OAG can activate Ca^{2+}-permeable channels in HLMCs with the expected biophysical and pharmacological properties of the TRPC3/6/7 channel subfamily. Receptor-mediated activation of the channels was then investigated, which is representative of the situation *in vivo*. DAG is produced downstream of PLCβ generation, which occurs following the stimulation of cell surface receptors, such as G protein-coupled $P2Y_1$ receptors (Gilfillan & Tkaczyk, 2006). ADP, an endogenous ligand for P2Y receptors, is found at sites of inflammation such as the asthmatic lung, and was shown in chapter 3 to stimulate Ca^{2+} influx in HLMCs. It may therefore represent an important mechanism for inflammatory activation of HLMCs; studies in this chapter aimed to elucidate whether channels from the TRPC3/6/7 subfamily are activated downstream of P2Y receptor activation by ADP.

It was firstly investigated which P2Y receptor subtype was being switched on by ADP in HLMCs; whilst $P2Y_1$, $P2Y_{12}$ and $P2Y_{13}$ are all activated by ADP (Bulanova & Bulfone-Paus, 2010), only $P2Y_1$ mRNA has been detected in HLMCs (Schulman *et al.*, 1999). N^6-methyl-2'-deoxyadenosine-3',5'-bisphosphate (MRS2179) is a potent and selective $P2Y_1$ receptor antagonist (Camaioni *et al.*, 1998; Kaiser & Buxton, 2002); the IC_{50} for $P2Y_1$ receptor inhibition in turkey erythrocytes is 0.3μM, and maximal inhibition achieved with 10μM (Camaioni *et al.*, 1998). ADP-induced Ca^{2+} entry was assessed in the presence of 10μM MRS2179 in order to investigate the involvement of $P2Y_1$ receptors in ADP-induced Ca^{2+} entry in HLMCs. As shown in figure 6.6b, ADP-induced Ca^{2+} entry was significantly reduced in the presence of MRS2179; $\Delta F_{340/380}$ was reduced by 0.18 (from 0.26 to 0.08). As similar results were obtained in two separate donors, the mean trace in figure 6.6b (ii) is representative of data from both donors. This sensitivity to MRS2179 is indicative of Gq-coupled $P2Y_1$ receptor involvement, as 10-100μM MRS2179 has previously been shown to have no effect on the other P2Y receptor subtypes (von Kugelgen, 2006).

To assess the contribution of the TRPC3/6/7 subfamily of channels to ADP-induced, $P2Y_1$-mediated Ca^{2+} entry in HLMCs, Ca^{2+} entry was assessed in the presence of 10μM Gd^{3+} (figure 6.6c) and 10μM SKF-96365 (figure 6.6d). Both antagonists significantly reduced ADP-induced Ca^{2+} entry; $\Delta F_{340/380}$ was reduced by 0.19 (from 0.26 to 0.07) in the presence of 10μM Gd^{3+}, and to by 0.19 (from 0.26 to 0.07) in the presence of 10μM SKF-96365. The change in fluorescence elicited by ADP in the presence of all three antagonists is summarised in figure 6.7.

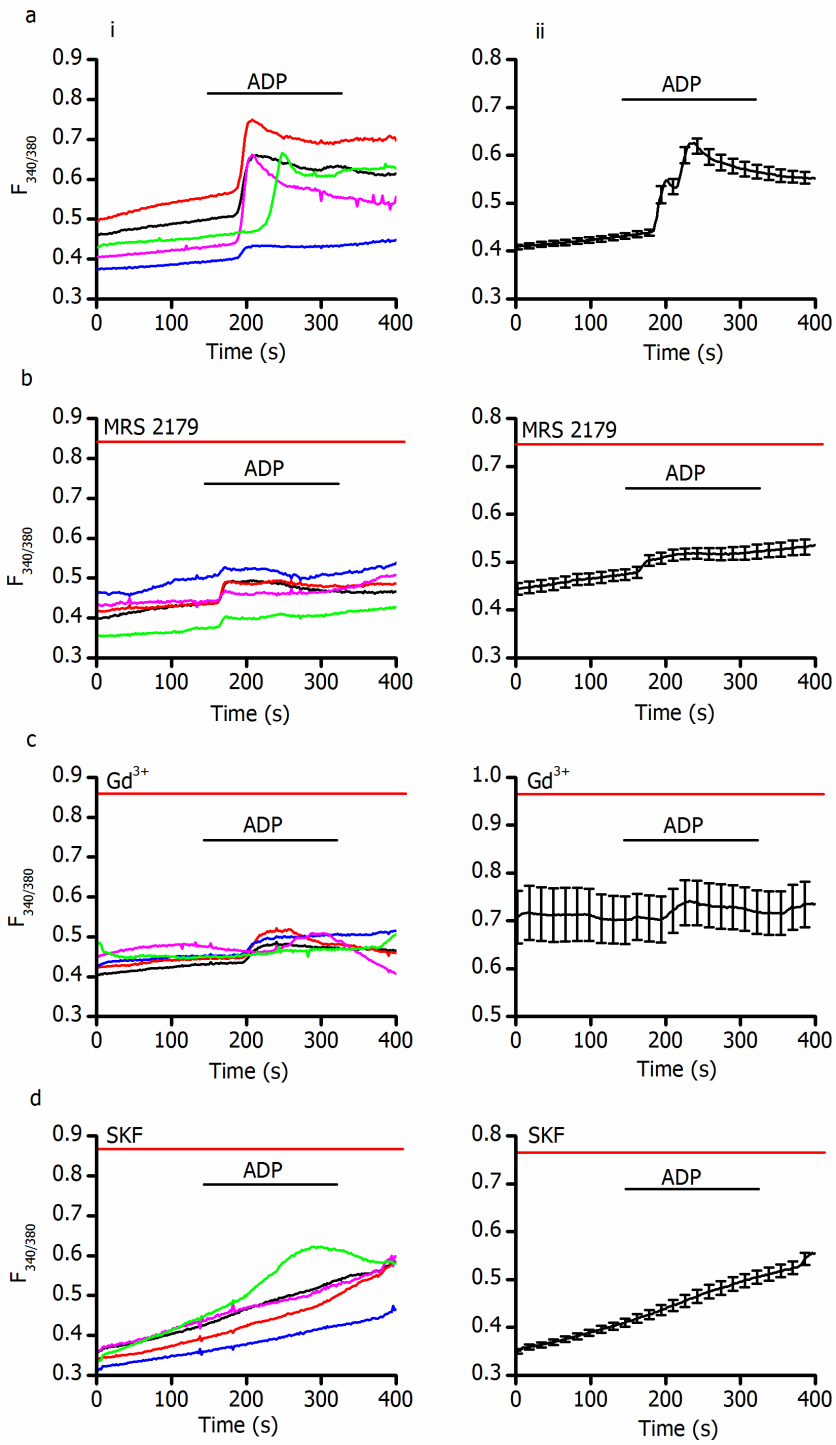

Figure 6.6. ADP-induced Ca^{2+} entry is sensitive to MRS 2179, Gd^{3+} and SKF-96365.

Fura 2-loaded HLMCs were perfused in standard external solution and 100μM ADP was bath-applied where indicated by the horizontal bars. (a) shows Ca^{2+} entry, indicated by $F_{340/380}$, in control cells (no inhibitor); in all sections (i) shows traces from example cells and (ii) shows the mean ± SEM. (a) (ii): n=53 cells, N=8 experiments, representative of 4 donors. (b): experiment as in (a), but 10μM MRS 2179 was present throughout the experiment; n=30, N=4, 2 donors. In (c) 10μM Gd^{3+} was present throughout the experiment (n=26, N=3, 2 donors) and in (d) 10μM SKF-96365 was present (n=25, N=3, 1 donor).

N.B. Control data is the same as that shown in figure 3.3.

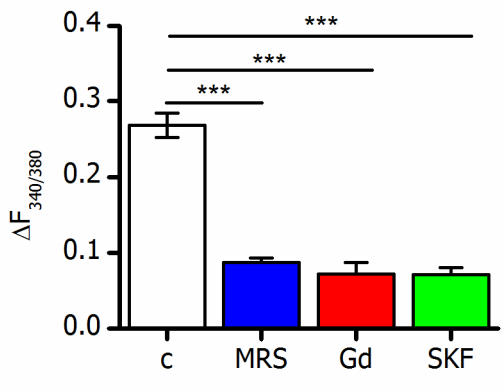

Figure 6.7. Inhibition of ADP-induced Ca^{2+} entry by MRS 2179, Gd^{3+} and SKF-96365.

Bar graph comparing the size of ADP-induced Ca^{2+} entry ($\Delta F_{340/380}$) in control experiments ("c", white) and in the presence of 10μM MRS2179 (blue), 10μM Gd^{3+} and 10μM SKF-96365. ***: means were significantly different compared to control, $p<0.0001$, one-way ANOVA with Tukey post-test.

As shown above, MRS2179 and the TRPC channel inhibitors Gd^{3+} and SKF-96365 significantly inhibited ADP-induced Ca^{2+} entry in HLMCs, suggesting the involvement of $P2Y_1$ receptors and TRPC channels, respectively. Whole-cell patch clamp recordings were then carried out to investigate the biophysical properties of ADP-induced currents and to further evaluate the contribution of the DAG-activated TRPC channels. As shown in figure 6.8a, focal application of 100μM ADP to HLMCs gave rise to outwardly-rectifying currents in 100% of cells tested; 78% of cells (7/9) exhibited a sustained current, and 22% of cells (2/9) displayed a transient current. One cell from each donor tested displayed a transient current in response to ADP. The amplitude of the ADP-induced current was 51.21pA/pF ± 36.0 (n=9, N=2 donors) at +100mV and 10.5pA/pF ± 7.9 (n=9, N=2) at -100mV. The I/V relationship of the ADP-induced current (figure 6.8a (iii)) was similar to that induced by OAG in HLMCs (figure 6.3a (iii)), showing inward and outward current with outward rectification, and a reversal potential of -4.38mV± 2.0 (n=9, N=2). The rectification index of ADP-induced currents in HLMCs was calculated at 4.83 ± 1.61 (n=9, N=2). As with OAG-induced currents, the presence of 10μM Gd^{3+} throughout the experiment inhibited the activation of currents by ADP (figure 6.8b); current amplitudes at +100mV were reduced by 49.53pA/pF (from 51.21 to 1.68), and those at -100mV were reduced by 9.52pA/pF (from 10.50 to 0.98). This inhibition did not reach statistical significance due to the large variation in peak current when 10μM Gd^{3+} was not present.

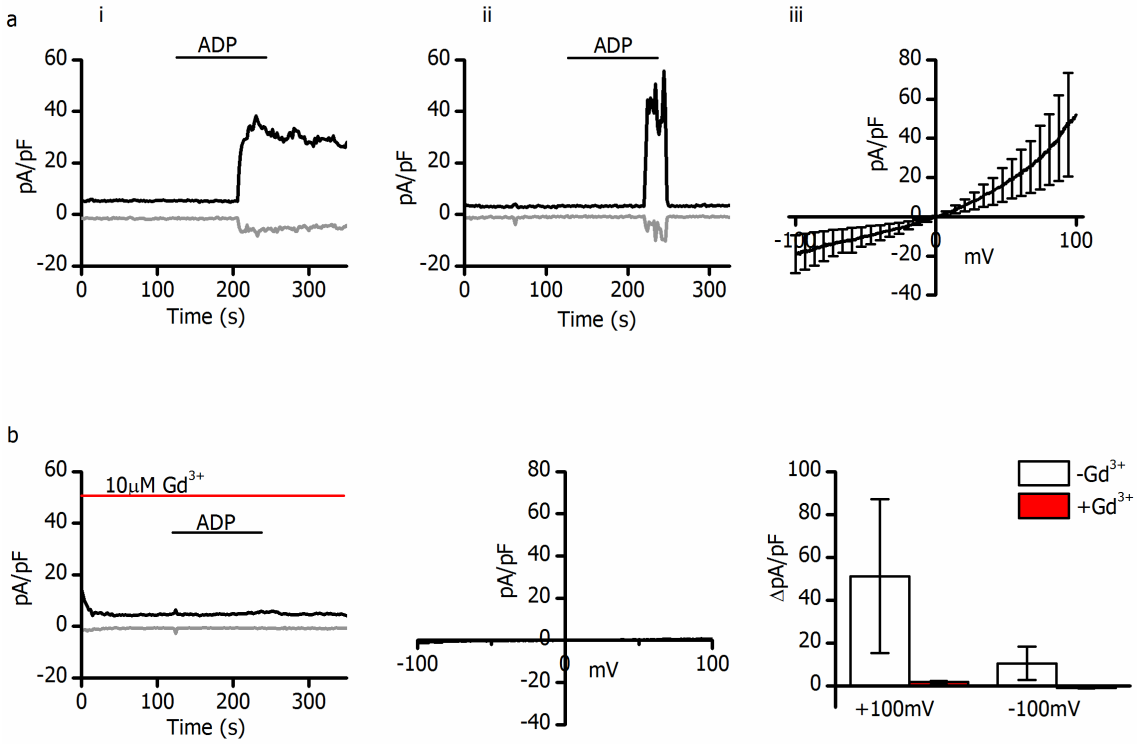

Figure 6.8. ADP induces an outwardly-rectifying current in HLMCs that is sensitive to 10μM Gd^{3+}

a: Whole-cell current induced by 100μM ADP in HLMCs. (i) and (ii): Cells were superfused with standard external solution; ADP was focally applied where indicated by the horizontal bars. (i): example traces showing ADP-induced current at -100mV (grey) and +100mV (black) that remained after washout, as observed in 62.5% of cells (5/8). (ii) shows an example of a transient current activated by ADP, as seen in 37.5% of cells (3/8). The current-voltage relationship of the ADP-induced current is shown in (iii); mean ± SEM, n=8 cells, representative of 2 donors. The mean reversal potential of the ADP-induced current was -4.38mV± 2.

b (i): ADP was focally applied in the presence of 10μM Gd^{3+} as indicated by the horizontal bars. Current at +100mV is shown in black; -100mV is in grey. Traces are for an example cell; similar currents were observed in 5 other cells. (ii): I/V relationship in the presence of 100μM ADP and 10μM Gd^{3+}; current reversed at -5.75mV ± 2.23 (n=6 cells, representative of 2 donors). (iii): Bar graph comparing ADP-induced current at +100mV and -100mV in the presence and absence of 10μM Gd^{3+}. Current before drug application was subtracted from the maximum current in the presence of ADP, to give "Δ pA/pF". White bars indicate ADP-induced current in the absence of Gd^{3+}; red bars show current in the presence of Gd^{3+}.

	HEK-TRPC6 OAG (n=8)	**HLMC OAG** (n=9)	**LAD 2 OAG** (n=15)	**HEK-TRPC6 ADP** (n=5)	**HLMC ADP** (n=9)
% cells responding	100	88	20	100	100
Peak current +100mV (pA/pF)	89.03 ± 28.61	122.52 ± 41.28	1.8 ± 0.4	105.48 ± 45.10	51.21 ± 36.0
Peak current -100mV (pA/pF)	18.73 ± 5.37	53.78 ± 24.84	1.03 ± 0.66	24.75 ± 12.68	10.49 ± 7.86
Rectification index	5.81 ± 0.89	3.99 ± 0.89	4.4 ± 2.3	4.39 ± 1.28	4.38 ± 2.0
% cells with sustained current	50	33	13	60	78
Reversal potential (mV)	0.06 ± 0.31	-5.31 ± 2.59	-0.09 ± 0.09	1.44 ± 0.38	4.83 ± 1.61

Table 6.1. Summary of OAG- and ADP-induced currents in HEK-TRPC6 cells, LAD 2 cells and HLMCs.

In conclusion, ADP activates Ca^{2+}-permeable channels in HLMCs via $P2Y_1$ receptor stimulation that are sensitive to the TRPC channel blockers Gd^{3+} and SKF-96365. ADP-induced currents in HLMCs have the expected biophysical properties of TRPC channels, displaying outward rectification, a reversal potential close to 0mV and sensitivity to 10μM Gd^{3+}. Table 6.1 summarises the properties of OAG- and ADP-evoked currents in HEK-TRPC6 cells, LAD 2 cells and HLMCs. As shown, ADP-induced currents in HLMCs have similar properties to those activated by OAG and to ADP-evoked currents in HEK-TRPC6 cells, indicating that the same channels could be involved.

6.3 Flufenamic acid-induced activation of human mast cells

Flufenamic acid (FFA) is a nonselective cation channel blocker (Popp *et al.*, 1993), but it has been shown to potentiate mouse TRPC6 channel activity at 100-500μM in HEK-TRPC6 cells (Inoue *et al.*, 2001), A7r5 smooth muscle cells (Jung *et al.*, 2002), primary megakaryocytes (Carter *et al.*, 2006) and cortical neurons (Tu *et al.*, 2009b), whilst inhibiting the other TRPC channels (Inoue *et al.*, 2001). It has recently been shown in human podocytes that 200μM FFA stimulates 2-APB and SKF-96365- sensitive Ca^{2+} entry, which is abolished by dominant negative TRPC6 expression; the authors concluded that FFA is a tool to selectively activate TRPC6 channels and study them in native cells (Foster *et al.*, 2009). FFA activation of LAD 2 cells and HLMCs was therefore investigated in this study.

As shown in figure 6.9a, FFA application gave rise to concentration-dependent Ca^{2+} entry in LAD 2 cells, with an estimated EC_{50} of 99.5μM. Whole-cell patch clamp recordings showed that focal application of 100μM FFA to voltage-clamped LAD 2 cells switched on an outwardly-rectifying current in 100% of cells tested (figure 6.9c), with a mean reversal potential of 0.25mV±0.09 (n=6). The mean FFA-induced current amplitude was 17.46pA/pF ± 4.71 (n=6) at +100mV and 9.35pA/pF ± 1.60 (n=6) at -100mV. The rectification index of the FFA-induced current was measured at 1.79 ± 0.21 (n=6). Ethanol at a 1/666.7 dilution (vehicle for FFA at the minimal dilution) did not give rise to Ca^{2+} entry or currents in LAD 2 cells; see figure 6.9 parts b (iii) and c (ii). Whilst these data are in agreement with results obtained previously (Carter *et al.*, 2006; Foster *et al.*, 2009; Tu *et al.*, 2009b) and suggest the activation of TRPC6 channels, 100μM FFA also elicited a large increase in cytosolic Ca^{2+} in 100% of cells tested when the experiment was carried out in the absence of extracellular Ca^{2+} (figure 6.9b). The change in fura-2 fluorescence evoked by 100μM FFA was measured at 0.17 ± 0.01 (n=47, N=3) in the presence of extracellular Ca^{2+}, and 0.27 ± 0.02 (n=41, N=3) in the absence of extracellular Ca^{2+}; this is illustrated in figure 6.9b (iii). This Ca^{2+} influx elicited by FFA in the absence of extracellular Ca^{2+} suggests that FFA causes Ca^{2+} release from intracellular stores, and contests the theory that it is a selective activator of TRPC6; this will be discussed in section 6.5.

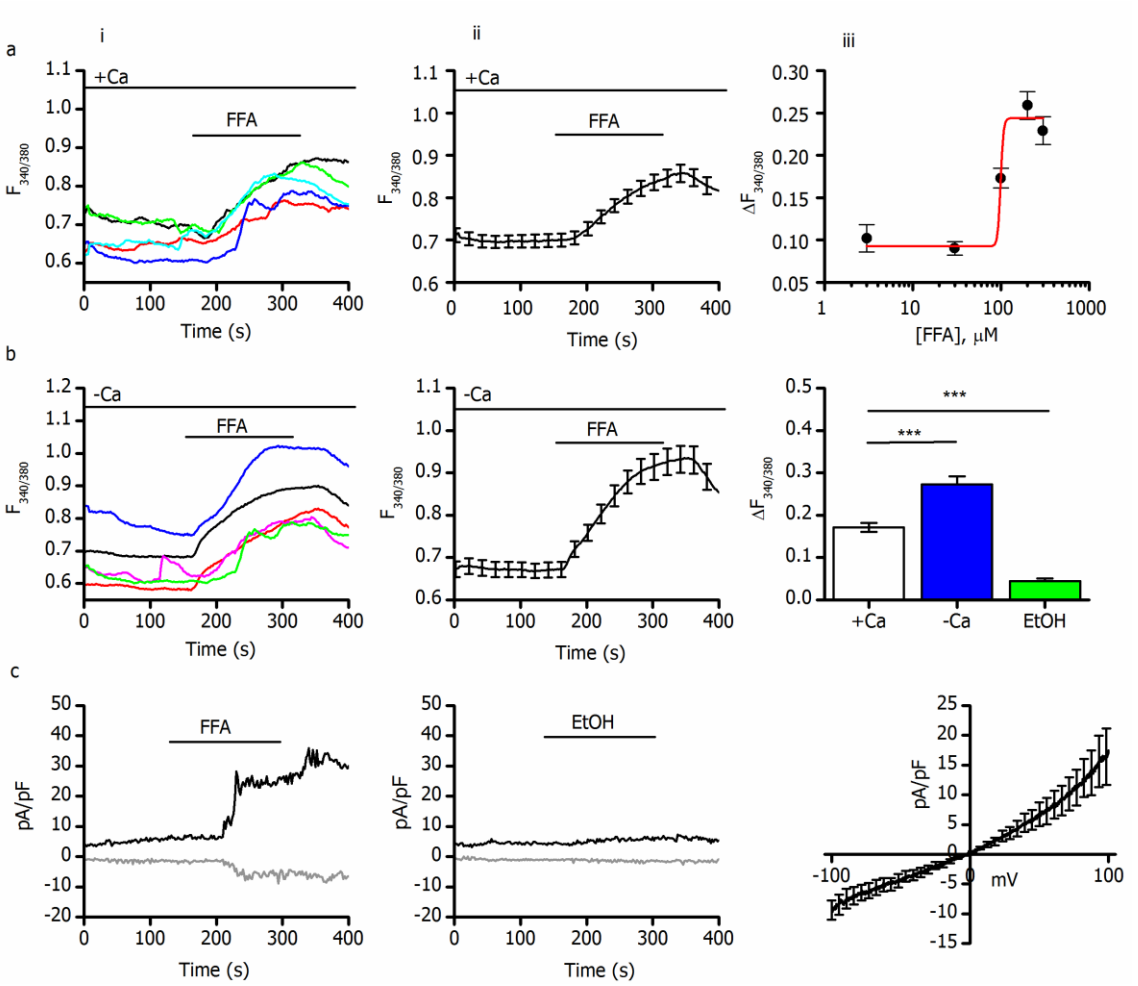

Figure 6.9. Flufenamic acid-induced Ca^{2+} entry and currents in LAD 2 cells

a: Fura 2-loaded LAD 2 cells were perfused in standard Ca^{2+}-containing extracellular solution and 100μM flufenamic acid (FFA) was bath-applied as indicated by the horizontal bar. (i) shows individual representative cells; (ii) shows mean ± SEM (n=47 cells, N=3 experiments). (iii): Concentration-response curve showing size of FFA-induced Ca^{2+} entry ($\Delta F_{340/380}$) at different concentrations. n numbers are as follows: 29 for 3μM, 62 for 30μM, 47 for 100μM, 31 for 200μM, 30 for 300μM. N≥2 experiments for each concentration.

b (i) and (ii): 100μM FFA was applied to cells in the absence of extracellular Ca^{2+} (n=41, N=3). (iii): Bar graph comparing Ca^{2+} entry induced by 100μM FFA in the presence and absence of extracellular Ca^{2+}, and that induced by ethanol at 1/666.7 dilution (solvent control for maximum concentration of FFA; n=26, N=2). ***: means are significantly different, p<0.0001, one-way ANOVA.

c: FFA-induced currents in LAD 2 cells. (i): Diary plot from an example cell showing whole-cell currents measured at +100mV (black trace) and -100mV (grey trace); FFA was focally applied as indicated by the horizontal bar. Similar results were obtained in 5 other cells. (ii): Example traces where ethanol at 1/666.7 dilution was focally applied as indicated. Similar results were obtained in 2 other cells. (iii): Current-voltage relationship of FFA-induced currents, calculated by subtracting current before FFA application from peak current in the presence of FFA. Trace shows mean ± SEM, n=6 cells. Currents had a mean reversal potential of 0.25mV±0.09.

FFA-induced activation of HLMCs was then assessed; as shown in figure 6.10, 100μM FFA gave rise to Ca^{2+} entry in the presence and absence of extracellular Ca^{2+} in 100% of cells tested. When comparing the Ca^{2+} traces in LAD 2 cells in the presence and absence of extracellular Ca^{2+} (figure 6.9a and b), the time-course is very similar. In HLMCs, however, the time-course was altered when extracellular Ca^{2+} was removed. Figure 6.10c compares the peak change in fluorescence in HLMCs induced by FFA in the presence (0.26 ± 0.03; n=20, N=3, 1 donor) and absence (0.21 ± 0.01; n=13, N=3, 1 donor) of extracellular Ca^{2+}; there was no significant difference. When the change in fluorescence 4 minutes after FFA application was compared, however, it was significantly greater in the presence of extracellular Ca^{2+} (0.15 ± 0.03; n=20, N=3) than when Ca^{2+} was not present (0.05 ± 0.01; n=13, N=3). Therefore, FFA-induced Ca^{2+} was more sustained in the HLMCs when extracellular Ca^{2+} was present, suggesting that a more transient Ca^{2+} release seen in the absence of extracellular Ca^{2+} could be mediated by release from stores, with Ca^{2+} entry from outside the cell following. This difference was not seen in LAD 2 cells, implying that similar Ca^{2+} entry from outside the cell does not occur in LAD 2 cells.

To summarise, whilst FFA is reported to be a selective activator of TRPC6 and has been shown in this study to activate currents with the expected biophysical properties of TRPC6 channels, Ca^{2+} imaging data show that FFA stimulates cytosolic Ca^{2+} rises in the absence of extracellular Ca^{2+}. Therefore FFA has other effects on human mast cells in addition to TRPC6 activation, so cannot be considered a selective activator.

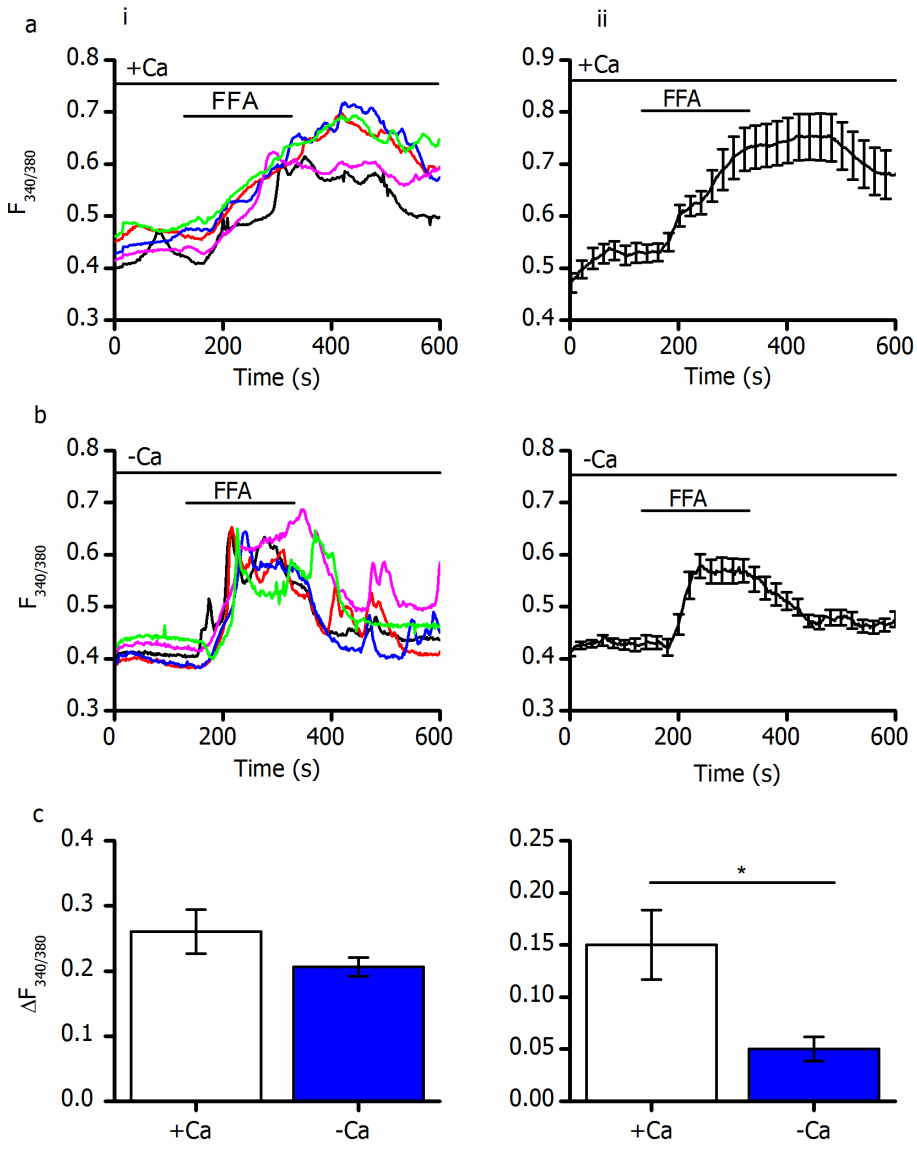

Figure 6.10. Flufenamic acid-induced Ca^{2+} entry and currents in HLMCs

a: Fura 2-loaded HLMCs were perfused in standard Ca^{2+}-containing extracellular solution and 100μM flufenamic acid (FFA) was bath-applied as indicated by the horizontal bar. (i) shows individual representative cells; (ii) shows mean ± SEM (n=20 cells, N=3 experiments, representative of 1 donor).

b (i) and (ii): Experiments as in (a), but in the absence of extracellular Ca^{2+} (n=13, N=3, 1 donor).

c (i): Bar graph comparing peak change in fluorescence ($\Delta F_{340/380}$) induced by 100μM FFA in the presence (white) and absence (blue) of extracellular Ca^{2+}. Means were not significantly different. (ii) compares the change in fluorescence at 4 minutes after FFA application in the presence and absence of extracellular Ca^{2+}; means were significantly different, $p<0.05$, unpaired Student's T-test.

6.4 Functional roles of the DAG-sensitive TRPC channels and involvement in the IgE response

As discussed in chapter 5.6, it is likely that store-operated TRPC1 channels are involved in FcεRI-dependent Ca^{2+} signalling and degranulation in HLMCs. As DAG is produced by PLCγ downstream of FcεRI cross-linking, it is possible that TRPC6 or perhaps TRPC7 channels could also contribute to FcεRI-evoked Ca^{2+} signalling and mediator release. Synta 66-insensitive Ca^{2+} entry induced by anti-IgE was further inhibited by 10μM Gd^{3+} and SKF-96365 (figure 5.15), and currents activated by anti-IgE (figure 5.14) had similar properties to OAG-activated currents in HLMCs (figure 6.3). Both currents had a similar rectification index, measured at 4.46 ± 0.08 (n=3) for IgE-induced currents and 3.99 ± 0.89 (n=9) for OAG-activated currents. The mean reversal potential of TRPC-like currents activated by anti-IgE (0.58 ± 0.16, n=3) was not significantly different (unpaired Student's T-test) to that for OAG-induced currents (0.75 ± 0.74, n=9). These similar properties suggest that the same channel (i.e. TRPC6) could be activated by FcεRI cross-linking and OAG. To address this possibility, Ca^{2+} imaging experiments were carried out to assess whether applying OAG to cells following FcεRI cross-linking stimulated further Ca^{2+} entry. If TRPC6 was already activated, OAG should not have caused further rises in Ca^{2+}. Data are shown in figure 6.11.

As shown in figure 6.11a, no further increases in $F_{340/380}$ occurred when OAG was applied to cells already stimulated with anti-IgE; this suggests that TRPC6 channels are activated downstream of FcεRI cross-linking so could not be switched on by subsequent application of OAG. However, when the experiment was repeated in the presence of 3μM Ro-31-8425 to inhibit PKC, OAG caused further increases in $F_{340/380}$ in 67% of cells (8/12). The amplitude of OAG-activated Ca^{2+} entry in responding cells following FcεRI cross-linking in the presence of Ro-31-8425 was not significantly different to that in the absence of FcεRI cross-linking (unpaired Student's T-test). These data suggest that TRPC6 channels are not activated by FcεRI cross-linking, but that PKC activation by DAG produced downstream of FcεRI prevented the activation of TRPC6 channels by OAG. It is therefore likely that TRPC6 channels are not the main contributors to the TRPC-like currents seen in response to FcεRI cross-linking.

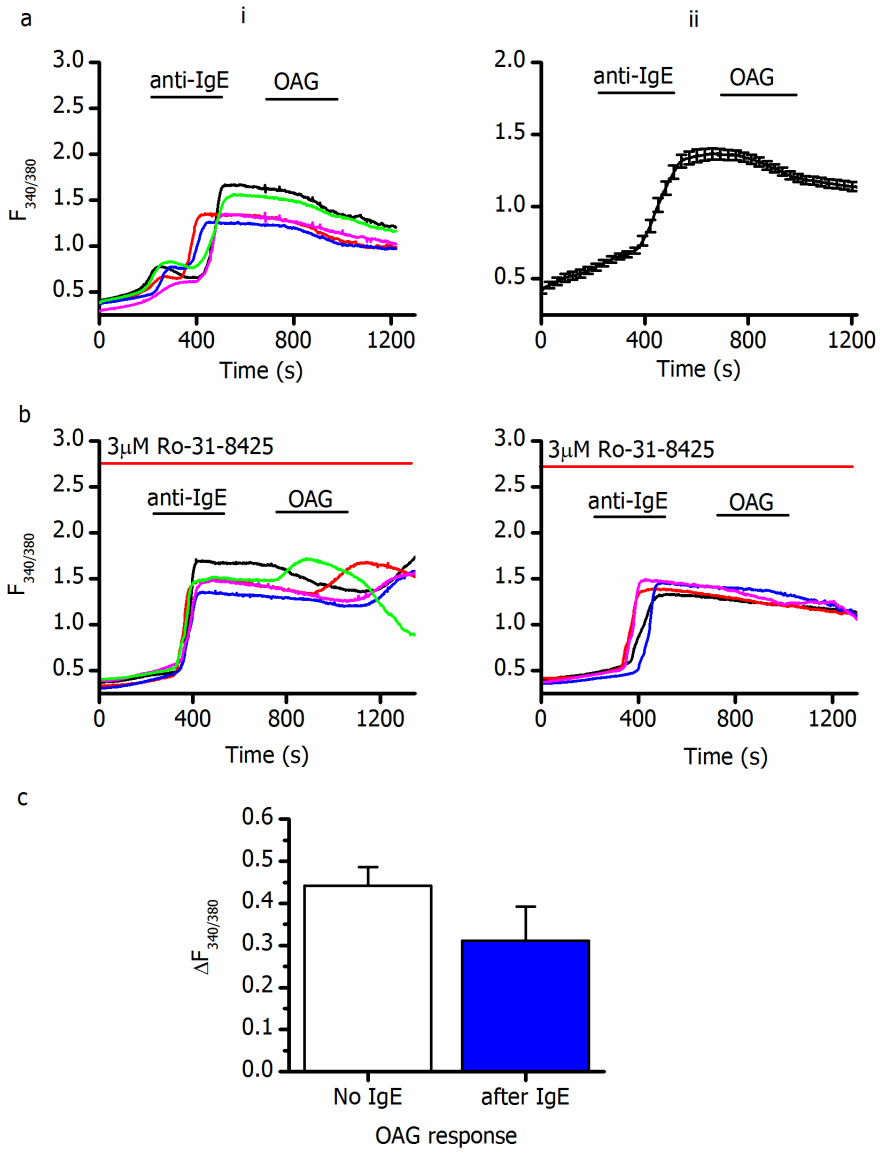

Figure 6.11. OAG responses in HLMCs following IgE receptor crosslinking.

HLMCs were perfused in standard external solution and agonists were applied as indicated by the horizontal bars.

a: 100μM OAG was applied following anti-IgE stimulation of cells; no further calcium entry occurred when OAG was applied to cells. Part (i) shows individual representative cell traces; part (ii) shows mean ± SEM (n=29 cells, N=4, representative of 2 donors).

b: 100μM OAG was applied following anti-IgE stimulation in the presence of the 3μM Ro-31-8425. In 67% of cells (8/12), OAG caused a further calcium rise when applied after IgE receptor stimulation. Individual representative cells where this occurred are shown in part (i). In 33% of cells (4/12), OAG stimulation did not lead to further calcium entry in the presence of Ro-31-8425; representative cell traces are shown in part (ii).

c: Bar graph comparing size of OAG response in responding cells following anti-IgE stimulation in the presence of Ro-31-8425 ("after IgE", blue, n=8) with a time-matched control where OAG was applied in the presence of DMSO (vehicle for Ro-31-8425, n=7) and without pre-application of anti-IgE ("no IgE", white). There was no significant difference in $\Delta F_{340/380}$ in response to OAG between control cells and those that had previously been stimulated with anti-IgE.

It was then investigated whether the activation of TRPC6-containing channels using OAG and ADP stimulates histamine and β-hexosaminidase release in impure suspensions of HLMCs. Results are shown in figure 6.12; 100μM OAG and 100μM ADP did not induce histamine release, giving rise to 0.03% ± 0.52 (N=8, 4 donors) and 0.12% ± 0.82 (N=8, 4 donors) release, respectively. For comparison, anti-IgE application gave rise to 38.13% ± 2.56 (N=8, 4 donors) histamine release; this was significantly higher than that induced by the TRPC6 channel agonists. Similar results were obtained for β-hexosaminidase release; OAG application gave rise to 2.44% ± 1.91 (N=6, 3 donors) release and ADP -1.73% ± 0.89 (N=6, 3 donors), compared with 24.90% ± 4.54 (N=6, 3 donors) release induced by anti-IgE. Therefore, application of agonists shown in this chapter to activate TRPC6-like channels does not stimulate release of the granule-associated mediators histamine and β-hexosaminidase. It is possible that DAG-regulated TRPC6 channels have other important functional roles in HLMCs, such as the regulation of cytokine transcription or prostaglandin and leukotriene release. Although beyond the scope of this study, a thorough assessment of the role of TRPC channels in these processes is required to determine their function in HLMCs.

In addition to mediator and cytokine release, the migration of mast cells is also an important determinant of the asthmatic phenotype. The micro-localisation of mast cells in airway smooth muscle bundles contributes to the symptoms of asthma; it has been shown that smooth muscle-derived chemokines stimulate HLMC migration and accumulation with airway smooth muscle cells through CXCR3 activation (Brightling *et al.*, 2005). Transforming growth factor-β (TGF-β) isoforms have also been shown to mediate migration of HMC-1 and human cord blood-derived mast cells. The ion channels activated downstream of chemokine receptors involved in mast cell migration, however, have not been investigated. It has been shown in neutrophils that TRPC6 channels are required for migration stimulated by OAG or macrophage inflammatory protein-2 (MIP-2) (Damann *et al.*, 2009); TRPC channels have also been suggested to have a role in monocyte migration induced by lysophosphatidylcholine (LPC). Pilot experiments were carried out in LAD 2 cells to assess whether DAG-activated TRPC channels are involved in mast cell motility; very little effect was observed, and investigations were not taken further as sufficient numbers of HLMCs were not available.

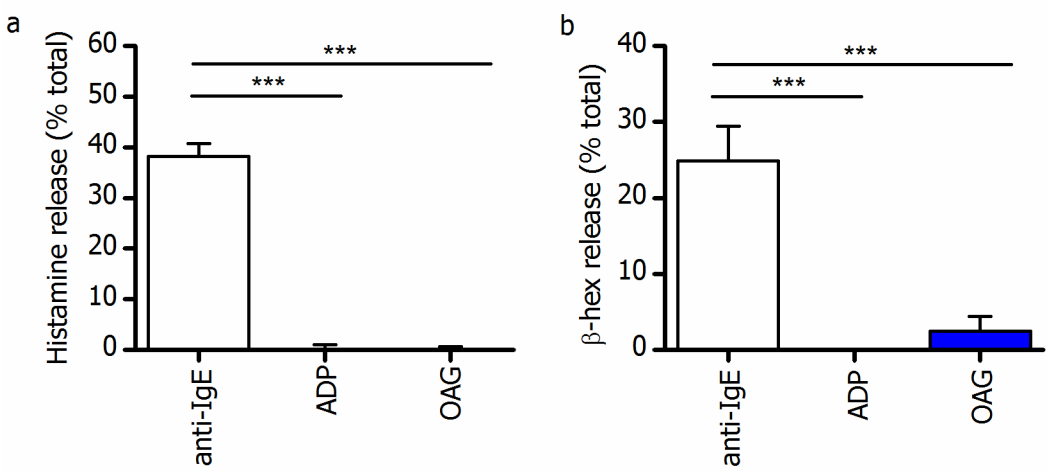

Figure 6.12. Activators of TRPC3/6/7 channels do not stimulate degranulation in HLMCs

a: Freshly isolated impure HLMCs were stimulated with the agonists shown and histamine release was measured as % total release, determined by lysis with 0.5% perchloric acid. Anti-IgE-induced histamine release in the donors tested for responsiveness to other agonists is shown for comparison. N=8, 4 donors for IgE (3µg/ml); N=8, 4 donors for OAG (100µM) and ADP (100µM). Histamine release experiments in 1 donor (N=2) were carried out by Jasmine Farrington.

b: Freshly isolated impure HLMCs were stimulated with the agonists shown and β-hexosaminidase release was measured as % total release, determined by lysis with 0.5% Triton X-100. Anti-IgE-induced β-hexosaminidase release in the donors tested for responsiveness to other agonists is shown for comparison. N=6, 4 donors for IgE (3µg/ml); N=6, 3 donors for OAG (100µM) and ADP (100µM). ***: release was significantly lower than that induced by anti-IgE, one-way ANOVA with Tukey post test.

6.5 Discussion

6.5.1 OAG activation of TRPC3/6/7 channels

TRPC3/6/7 channels are activated directly by DAG in a PKC-independent, store depletion-independent manner (Hofmann *et al.*, 1999). OAG, the membrane-permeable DAG analogue, is used extensively to study TRPC channels from this subfamily in heterologous expression systems (Venkatachalam *et al.*, 2003; Estacion *et al.*, 2004; Shi *et al.*, 2004; Estacion *et al.*, 2006) and in native cells (El Boustany *et al.*, 2008; Guilbert *et al.*, 2008; Tu *et al.*, 2009b). In this study, OAG stimulated Ca^{2+} entry in 97% of HLMCs tested (figure 6.1a), suggesting that functional TRPC3/6/7 channels could be present. RT-PCR (chapter 3.4) was carried out on two of the four donors exhibiting Ca^{2+} entry in response to OAG; TRPC6 was present in both donors, TRPC7 in one donor, and TRPC3 was not found to be present in HLMCs in this study. RT-PCR in one further donor not tested for OAG responsiveness was found to express mRNA for TRPC6 only from this subgroup. It is therefore likely that TRPC6 could mediate the Ca^{2+} entry shown in figure 6.1a, with a possible contribution from TRPC7 in one donor. Although the contribution of TRPC3 cannot be definitively excluded because mRNA expression was not assessed in all donors, transcripts were not detected in 3/3 donors tested, and have not been detected in previous studies (Bradding *et al.*, 2003). TRPC3 is predominantly expressed in the brain and embryonic tissues (Eder *et al.*, 2007), and TRPC3-deficient mice exhibit defects in walking behaviour, indicating a key role of the channel in motor co-ordination (Hartmann *et al.*, 2008). These mice have not been reported to show any immune phenotypes. Based on these roles of TRPC3 and lack of expression in HLMCs from 2/3 donors, it is unlikely to be required for HLMC function. The remainder of this discussion will therefore focus mainly on TRPC6 channels.

The results obtained in figure 6.1 are in accordance with those obtained in HEK-TRPC6 cells in this study (chapter 4.1) and previous reports showing that OAG stimulates Ca^{2+} influx in TRPC6-expressing cells (Boulay *et al.*, 1997; Hofmann *et al.*, 1999). A study by Venkatachalam *et al.* (2003) showed that OAG inhibits channels from the TRPC1/4/5 subgroup via the activation of PKC, in contrast to the direct stimulatory action on channels from the TRPC3/6/7 subgroup, which is known to be PKC- independent (Hofmann *et al.*, 1999; Inoue *et al.*, 2001; Venkatachalam *et al.*, 2003; Estacion *et al.*, 2004). The observed OAG-induced Ca^{2+} entry in HLMCs therefore suggests the direct activation of TRPC3/6/7 channels, without contribution from the TRPC1/4/5 subfamily. The lack of Ca^{2+} entry in the absence of extracellular Ca^{2+} (figure 6.1b) indicates that an increase in fura-2 fluorescence did not occur as a result of Ca^{2+} release from internal stores, but from the outside of the cell as expected.

Whilst studies such as that by Boulay *et al.* (1997) illustrate that OAG stimulation is associated with an increase in cytosolic Ca^{2+}, it has been reported that increasing extracellular Ca^{2+} concentration in Na^{+}-containing solutions during patch clamp recordings of TRPC6 and TRPC7 channels causes a reduction in channel activity (Inoue *et al.*, 2001; Shi *et al.*, 2004), suggesting

that Ca^{2+} blocks TRPC6 and TRPC7 channels. Estacion *et al.* (2006) showed, using simultaneous recordings of current and fura-2 fluorescence in HEK-TRPC6 cells, that at a membrane potential of 0mV, the Ca^{2+} conductance of TRPC6 channels is low relevant to Na^{+}; very little OAG-induced Ca^{2+} entry was observed. At a holding potential of -50mV, however, Ca^{2+} permeability was increased and OAG was shown to increase intracellular Ca^{2+} to 100nM. The authors propose that the Ca^{2+} permeability of TRPC6 is dependent upon the holding potential of the cell; in cells with a less negative membrane potential, TRPC6 channel activation primarily causes Na^{+} influx and depolarisation, which attenuates Ca^{2+} entry. In cells with a negative membrane potential, however, the depolarising effect of Na^{+} influx through TRPC6 is reduced, thus enhancing the driving force for Ca^{2+} entry (Estacion *et al.*, 2006).

When comparing OAG-induced Ca^{2+} entry in HLMCs (figure 6.1) and HEK-TRPC6 cells (figure 4.1), it is apparent that the time-course differs between the two cell types. Ca^{2+} entry in HLMCs was more sustained, whereas fura-2 fluorescence peaked and returned to baseline in the presence of OAG in HEK-TRPC6 cells. This could be due to differential ion channel expression in the two cell types affecting the membrane potential following OAG-mediated stimulation. HEK-293 cells express a number of voltage-activated ion channels (Varghese *et al.*, 2006); it is possible that initial Ca^{2+} and Na^{+} influx in HEK-TRPC6 cells caused depolarisation, thus inhibiting Ca^{2+} entry and causing a drop in fura-2 fluorescence. Another possibility is that PKC-mediated regulation occurs to a different degree in the two cell types. As discussed in chapter 4, a number of studies have demonstrated that PKC, which is activated by OAG (Bell *et al.*, 1986), negatively regulates TRPC6 channels. Results obtained in HEK-TRPC6 cells (figure 4.4) and HLMCs (figure 6.4) in this study also suggest that PKC negatively regulates TRPC6 channels; different levels of PKC in the two cell types may result in channel deactivation to a greater degree in HEK-TRPC6 cells, giving rise to the more transient Ca^{2+} response. Patch clamp data in this study suggests that PKC-mediated inactivation of TRPC6 channels occurs to a similar degree in the two cell types, but dialysis of PKC in the whole-cell configuration could have resulted in apparently similar regulation when the enzyme was in fact present at higher levels in HEK-TRPC6 cells.

As discussed in chapter 1.3.2, lanthanides can be used as diagnostic tools for the involvement of TRPC3/6/7 channels in Ca^{2+} signalling. Gd^{3+} inhibited OAG-induced Ca^{2+} entry with an average estimated IC_{50} of 6.5μM (N=2 donors). This is in the range of the estimated IC_{50} value obtained for the inhibition of heterologously expressed TRPC6 channels, 2.3μM (Inoue *et al.*, 2001). This was donor-dependent; in donor 410 the estimated IC_{50} was 2.77μM, with complete inhibition occurring at 10μM. In donor 411, however, Gd^{3+} inhibited OAG-induced Ca^{2+} entry with an estimated IC_{50} of 18.4μM. This could be due to donor-dependent expression of the DAG-activated TRPC channels; donor 410 expressed mRNA for TRPC6 and TRPC7, whereas donor 411 expressed TRPC6 mRNA only. Differential assembly of the TRPC channel pore into homomeric or heteromeric channels depending on their expression in different donors could result in distinct sensitivity to blockade. If the inhibition of TRPC channels by Gd^{3+} is mediated from the cytosolic

side of the membrane in HLMCs, as has been described for the regulation of TRPC3 in CHO cells (Halaszovich *et al.*, 2000)), donor-dependent variability in the rate at which intracellular and extracellular Gd^{3+} concentrations reach equilibrium could account for the differences seen in the inhibition of OAG-induced Ca^{2+} entry. Cell membranes were previously thought to be impermeable for lanthanides (Evans *et al.*, 1990), but it has been shown using fluorescent imaging techniques that lanthanides enter red blood cells (Cheng *et al.*, 1999) and ventricular cells (Peeters *et al.*, 1989), as well as CHO cells (Halaszovich *et al.*, 2000). Quicker uptake or slower extrusion of Gd^{3+} ions in HLMCs from donor 410 could therefore be responsible for the lower IC_{50} value observed for Gd^{3+} inhibition of OAG-induced Ca^{2+} entry. As only two donors were able to be tested in this study, significant conclusions about the donor-dependency of Gd^{3+} inhibition of TRPC3/6/7 channels cannot be drawn; investigating this in HLMCs from a larger pool of donors could reveal donor-dependent differences, and represents an interesting avenue of investigation for future projects.

The non-selective cation channel blocker SKF-96365 has also been used extensively to characterise TRPC channels (Eder *et al.*, 2007), inhibiting mTRPC6 channels expressed in HEK cells with an IC_{50} of 4.2μM, and receptor- activated TRPC6 currents in rabbit portal vein smooth muscle with an IC_{50} of 5.1μM (Inoue *et al.*, 2001). More recently, 10μM SKF-96365 has been reported to abolish OAG-induced TRPC6 currents in human epithelial breast cancer cells (Guilbert *et al.*, 2008). In this study, SKF-96365 inhibited OAG-induced Ca^{2+} entry in a concentration-dependent manner at concentrations greater than 1μM, but potentiation of OAG-induced Ca^{2+} entry occurred at concentrations less than 1μM. This potentiation is likely to be due to the non-specific effects of SKF-96365 that have been reported in some systems. As well as inhibiting TRPC channels, 10μM SKF-96365 has been shown to inhibit the voltage-gated Ca^{2+} channels Ca_v1, Ca_v2 and Ca_v3 expressed in HEK-293 cells (Singh *et al.*, 2010). In human leukaemic HL-60 cells, SKF-96365 has been reported to have dual effects, causing partial inhibition of Ca^{2+} entry at 1-3μM, but promoting Ca^{2+} entry at 30-100μM (Leung *et al.*, 1996). This SKF-96365- induced Ca^{2+} entry was not observed in human astrocytoma cells (Arias-Montano *et al.*, 1998), but it was reported to stimulate phosphoinositide hydrolysis in these cells. It has been suggested that SKF-96365 inhibits intracellular Ca^{2+} store refilling (Leung *et al.*, 1996; Arias-Montano *et al.*, 1998), which could lead to Ca^{2+} re-entry in some cells. The non-specific effects of SKF-96365 at concentrations less than 1μM have not been investigated, but it is evident from previous reports that the compound has other cellular effects in addition to the inhibition of TRPC channels. It is possible that in this study, SKF-96365 inhibited the re-uptake of Ca^{2+} into intracellular stores, as has been demonstrated in human astrocytoma cells (Arias-Montano *et al.*, 1998). This could have caused passive store depletion and the concomitant activation of store-operated Ca^{2+} channels such as Orai1 channels (Feske *et al.*, 2006; Prakriya *et al.*, 2006; Vig *et al.*, 2006b), and possibly store-operated TRPC channels (Ong et al., 2007; Liao et al., 2008; Ma et al., 2008). SKF-96365 has been reported to inhibit I_{CRAC} currents, which have since been shown to be mediated by Orai1 channels, with an IC_{50} of 4μM in rat peritoneal mast cell (Franzius *et al.*, 1994). TRPC1,

which is expressed in HLMCs from all donors in this study and has been suggested to be activated by store depletion (Zagranichnaya *et al.*, 2005; Ong *et al.*, 2007; Yuan *et al.*, 2007; Cheng *et al.*, 2011), can be inhibited by 10μM SKF-96365 (Zagranichnaya *et al.*, 2005). Therefore, at concentrations greater than 1μM, SKF-96365 would be expected to inhibit channels activated by passive store depletion, as well as OAG-activated TRPC3/6/7 channels. This would result in a reduced overall Ca^{2+} signal, as seen with concentrations of SKF-96365 above 1μM. At lower concentrations of SKF-96365, however, inhibition of TRPC3/6/7 channels does not occur, and store-operated Ca^{2+} channels would not be inhibited. If passive store depletion by inhibition of re-uptake into intracellular stores occurs at 0.001-1μM SKF-96365, store-operated Ca^{2+} channels could be activated, but SKF-96365 at these concentrations would not cause inhibition of these channels. This, along with the activation of TRPC6/7 channels by OAG that are not inhibited by 0.001-1μM SKF-96365, could lead to an overall increase in cytosolic Ca^{2+} and apparent potentiation of OAG-induced Ca^{2+} entry.

When a concentration-response curve was fitted using concentrations of 1μM and above only, the estimated IC_{50} for the inhibition of OAG-induced Ca^{2+} entry by SKF-96365 was 10.25μM; this value is close to that obtained by Inoue *et al.* (2001) for the inhibition of TRPC6 channels in rabbit portal vein smooth muscle cells (5.1μM). It is evident from previous studies showing that SKF-96365 has off-target effects that caution must be applied when using SKF-96365 as the sole pharmacological agent to identify the contribution of TRPC channels to Ca^{2+} entry. However, taken together with the RT-PCR data and the concentration-dependent inhibition by Gd^{3+}, the reduction of OAG-induced Ca^{2+} entry by SKF-96365 with an IC_{50} of 10.25μM suggests that TRPC6 channels, with a possible contribution from TRPC7, are activated by OAG and mediate Ca^{2+} entry in HLMCs.

The biophysical properties of OAG-induced currents in HLMCs were then investigated using whole-cell patch clamp electrophysiology. Data in this study and published data have shown that OAG activation of TRPC6 channels in HEK-293 cells gives rise to outwardly-rectifying currents with a reversal potential close to 0mV (Inoue *et al.*, 2001; Estacion *et al.*, 2004; Shi *et al.*, 2004; Estacion *et al.*, 2006). These properties have been used to identify native TRPC6 currents in rabbit portal vein smooth muscle cells (Inoue *et al.*, 2001), mouse cortical neurons (Tu *et al.*, 2009b) and mouse megakaryocytes (Carter *et al.*, 2006). In accordance with previous reports, data obtained in this study show that OAG activates outwardly-rectifying currents in HLMCs with a reversal potential of -5.31mV ± 2.59 (n=8). As observed with HEK-TRPC6 in chapter 4, some cells (55%) showed a transient response to OAG and others (33%) exhibited a sustained response. The rectification index (peak current at +100mV/ peak current at -100mV) was significantly higher in cells with a sustained response compared to those with a transient response, indicating that the current was more outwardly-rectifying in cells with a sustained response. This could be due to the negative regulation of TRPC6 channels by Ca^{2+}; as described in chapter 1.3.2, both intracellular and extracellular Ca^{2+} can cause channel deactivation (Shi *et*

al., 2004). A more inwardly-rectifying current is likely to have a greater inward Ca^{2+} current, which could give rise to Ca^{2+}-dependent deactivation and a more transient current. The patch clamp solutions and protocols in this study were not designed to assess the presence of other ion channels, but differences in expression of other ion channels between donors could give rise to variations in rectification. The mean inward current measured at -100mV at the start of experiments was 14.9pA ± 3.22 (n=8); the mean outward current measured at +100mV was 77.14pA ± 19.95 (n=8), indicating that channels could be active. A detailed characterisation of the ion channels expressed in HLMCs would be a valuable avenue of investigation in future studies. Current-clamp experiments in HLMCs following OAG stimulation would reveal changes in the membrane potential and provide insightful information on the driving force for cation entry when the membrane potential is not clamped.

It is also possible that the composition of the OAG-activated TRPC channels varied in different HLMCs, giving rise to responses with different kinetics and rectification. The kinetics of the response showed some donor-dependency; 2/3 cells displaying a sustained response were from the same donor (370), and all cells tested from donor 360 had a transient response (n=3). 2/3 cells from donor 410 had a transient current. Unfortunately, due to the time taken to optimise RNA extraction from small cell numbers, RT-PCR was only carried out on one of the donors used to study OAG-induced currents in HLMCs (donor 410, which expressed TRPC6 and TRPC7); differential expression of TRPC6 and TRPC7 channels could give rise to different channel assemblies with different pore properties. The contribution of TRPC3 in the donors where RT-PCR was not carried out cannot be excluded, although this channel was not present in 3/3 donors where RT-PCR was carried out, and has not been detected in HLMCs in previous studies (Bradding *et al.*, 2003).

The time taken for the OAG-induced current to reach a peak was variable in this study. Estacion *et al*. (2004) reported that currents activated by OAG in HEK-hTRPC6 cells were slow to activate; the authors suggest that this could reflect a time-dependent insertion of TRPC6 channels into the membrane. Cayouette *et al.* (2004) showed that OAG stimulates the externalisation of mTRPC6 channels via an exocytic mechanism prior to Ca^{2+} entry. TRPC6 channels are thought to be located in vesicles, which fuse with the plasma membrane upon cell stimulation, increasing the level of TRPC6 channels at the plasma membrane (Cayouette *et al.*, 2004). It is possible that the variation in the time taken to reach a peak current in this study was due to the availability of vesicles close to the plasma membrane; in some cells TRPC6 channels may have already been present in the membrane, giving rise to a current with a quicker rate of onset.

In accordance with the Ca^{2+} imaging data obtained in this study (figure 6.2), and previous reports showing that Gd^{3+} inhibits TRPC3/6/7 channels (Zhu *et al.*, 1998; Broad *et al.*, 1999; Halaszovich *et al.*, 2000; Inoue *et al.*, 2001; Jung *et al.*, 2002), the presence of 10μM Gd^{3+} inhibited the activation of OAG-induced currents in this study. This sensitivity of OAG-induced

currents in HLMCs to Gd^{3+}, along with the currents having the expected biophysical properties of TRPC3/6/7, Ca^{2+} permeability and sensitivity to SKF-96365, provides strong evidence for the functional expression of DAG-activated TRPC channels in HLMCs. Taken together with the RT-PCR data (chapter 3.4), these data suggest that TRPC6 channels mediate OAG-induced currents in HLMCs. Further studies employing specific molecular knockdown of TRPC6, along with TRPC3 and TRPC7, are necessary to confirm the results obtained using Gd^{3+} and SKF-96365, and to verify which DAG-activated TRPC channel(s) is/are responsible for mediating OAG-induced currents in HLMCs. siRNA or dominant negative pore mutants could be used for selective channel knock-down. Dominant negative TRPC6 has successfully been used in human microvascular endothelial cells using an adenoviral delivery method to show that TRPC6 is involved in receptor-evoked Ca^{2+} entry, proliferation and migration in these cells (Hamdollah Zadeh *et al.*, 2008). As RT-PCR data revealed donor-dependent expression of TRPC7 channels, assessing the relative contribution of this channel and that of TRPC6 to OAG-induced Ca^{2+} entry in different donors would be an interesting avenue of investigation.

The role of PKC in the negative regulation of TRPC3/6/7 channels was discussed extensively in chapter 4.3 so will not be described in detail here. Briefly, previous studies have shown that PKC is involved in the negative regulation of hTRPC6 expressed in HEK-293 cells (Estacion *et al.*, 2004), and hTRPC3 expressed in the DT40 chicken B-cell line (Venkatachalam *et al.*, 2003). The results obtained in HLMCs are in accordance with published observations (figure 6.4); the presence of the PKC inhibitor Ro-31-8425 did not have a significant effect on the current amplitude, but did increase the number of cells displaying a sustained current in response to OAG application from 33% (3/9) to 83% (5/6), and the percentage of the peak current remaining at 2 minutes after OAG application was significantly increased in the presence of Ro-31-8425. These data suggest that PKC does have a role in the inactivation of TRPC6 channels, in agreement with the results obtained in HEK-TRPC6 cells in this study, and with previous published work.

PKC levels may vary between recordings as discussed in chapter 4.3.1, as a result of dialysis into the patch pipette in the whole-cell recording configuration or cell cycle-dependent variation. It was previously thought that terminally differentiated mast cells did not proliferate, and that their increased numbers at tissue sites such as the asthmatic lung were due to the diversion of a larger proportion of haematopoietic progenitor cells into a mast cell fate, or increased survival of mast cells (Kambe *et al.*, 2001). However, it has since been shown that primary human skin mast cells (Kambe *et al.*, 2001) and HLMCs (Duffy *et al.*, 2003; Cruse *et al.*, 2006) do proliferate; HLMC numbers were reported to increase by 5 fold over 4 weeks when cultured in the presence of SCF, IL-6 and IL-10 (Duffy *et al.*, 2003), meaning their doubling time is approximately 1.6 weeks. HEK-293 cells have a doubling time of approximately 22 hours (Hopper-Borge *et al.*, 2004), therefore the cell cycle in HEK-293 cells would be expected to progress a great deal more quickly than that in HLMCs. This difference in the two cell types could account for the greater

variation in the percentage of OAG-induced current remaining at 2 minutes after OAG application seen in HEK cells (51.72 ± 26.11, n=7) compared with HLMCs (36.8 ± 14.2, n=8) when Ro-31-8425 was not present.

Whilst PKC is likely to have a role in TRPC6 regulation in HLMCs, 17% of cells still had a transient current when PKC was inhibited. It is therefore likely that other mechanisms also contribute to the inactivation of the channels. As discussed in chapter 4.3, dialysis of OAG or other important signalling molecules into the patch pipette could account for the deactivation of TRPC6 channels. Interacting molecules such as the $InsP_3$ receptor and PtdIns(4,5)P_2 have been suggested to be important for TRPC6-mediated cation entry; TRPC6 and the $InsP_3$ receptor have been shown to interact (Boulay *et al.*, 1999; Cayouette *et al.*, 2004), although the functional significance is not yet known as TRPC6 channels are believed to be activated independently of store depletion (Dietrich & Gudermann, 2007). PtdIns(4,5)P_2 binding has also been proposed to be important for the regulation of TRPC6; OAG and receptor stimulation have been shown to synergistically activate hTRPC6 (Estacion *et al.*, 2004), and the authors suggest that PtdIns(4,5)P_2 hydrolysis *per se* could be an important event in channel activation. A number of other ion channels including TRPV1 (Chuang *et al.*, 2001) and TRPM7 (Runnels *et al.*, 2002) are thought to be regulated by PtdIns(4,5)P_2. It is known that membrane PtdIns(4,5)P_2 levels gradually deplete in the absence of PLC hydrolysis; lipid kinases including phosphatidyl inositol 4 kinases (PI4K) are required in the presence of ATP to resynthesise PtdIns(4,5)P_2. It has been shown in HEK-293 cells that inhibition of PI4K leads to rundown of PtdIns(4,5)P_2 levels (Suh & Hille, 2002). The dialysis of important molecules such as PI4K and ATP in the whole-cell recording configuration used in this study could have a role in the depletion of PtdIns(4,5)P_2 levels in the membrane and the deactivation of TRPC6 channels. OAG-induced Ca^{2+} entry measured in intact HLMCs did not decline in the presence of OAG (see figure 6.1), suggesting that dialysis of signalling molecules may be a key factor in the inactivation of TRPC6 channels seen in whole-cell patch clamp recordings.

As described in chapter 4.3, it is also known that TRPC6 and TRPC7 channels undergo complex regulation by Ca^{2+} from both sides of the membrane, dependently and independently of calmodulin (Shi *et al.*, 2004). Cell-dependent differences in the levels of molecules involved in Ca^{2+}- dependent channel regulation, perhaps due to differing degrees of dialysis in the whole-cell recording configuration, could also contribute to the inactivation of OAG-induced currents in HLMCs. Experiments carried out in the presence of different concentrations of intracellular and extracellular Ca^{2+}, and in the presence of a calmodulin antagonist such as calmidazolum (Shi *et al.*, 2004), would reveal whether Ca^{2+} regulation contributes to the inactivation of OAG-mediated currents. Recording OAG-induced currents in HLMCs using the perforated patch clamp technique would reveal whether the dialysis of PKC, OAG or other signalling molecules contributes to the deactivation of the channels.

To summarise, whilst a number of different factors may be responsible for the kinetics of the response, the TRPC3/6/7 channel activator OAG gave rise to Gd^{3+}-sensitive, outwardly-rectifying currents in HLMCs with a reversal potential close to 0mV; these properties are typical of TRPC3/6/7 channels. Taken together with the Ca^{2+} imaging results showing that OAG mediates Gd^{3+}- and SKF-96365- sensitive Ca^{2+} entry in HLMCs, and PCR data showing that TRPC6 mRNA present in 3/3 donors tested and TRPC7 mRNA in 1/3 donors, results suggest that functional TRPC6 channels are expressed in HLMCs.

LAD 2 cells were the only human mast cell line reported to degranulate in response to FcεRI cross-linking (Kirshenbaum *et al.*, 2003) at the time this work was done, and have previously been shown in our laboratory to be a good model to ion channels in human mast cells (Wykes *et al.*, 2007; Wareham *et al.*, 2009). Therefore, LAD 2 cells represented a potentially good model to study the functional expression of DAG-activated TRPC3/6/7 channels in human mast cells. mRNA transcripts for all channels from this subgroup were present, but Ca^{2+} entry only occurred in 25% of LAD 2 cells in response to OAG application, compared with 97% of HLMCs. Similarly, 20% of LAD 2 cells exhibited outwardly-rectifying currents following OAG stimulation, compared with 89% of HLMCs; LAD 2 cells are therefore a poor model to study second messenger-regulated TRPC channels in human mast cells. Maturation stage-dependent expression of proteins has previously been reported in mast cells; terminally differentiated skin mast cells were found to contain higher levels of tryptase and chymase than the less mature LAD 2 cells (Guhl *et al.*, 2010). It has also been reported that B cells exhibit maturation stage-dependent expression of signalling molecules activated downstream of B cell antigen receptor, including PLCγ, B cell linker protein and Bruton's tyrosine kinase (Benschop *et al.*, 2001). It is therefore possible that the DAG-activated TRPC channels, the mRNA for which is expressed in LAD 2 cells, are not expressed at the protein level in immature LAD 2 cells. Immature mast cell progenitors migrate to tissues such as the lung, where they terminally differentiate under the influence of the tissue environment (Kitamura, 1989). It is possible that the DAG-activated TRPC channels are not fully expressed in human mast cells until terminal differentiation has occurred, which would give rise to only a small percentage of LAD 2 cells responding to OAG. TRPC6 channels are known be present at the plasma membrane at rest in HEK-293 cells, and the number of channels at the membrane increases upon activation by OAG or GPCRs (Cayouette *et al.*, 2004); it is also possible that TRPC6 protein is present in LAD 2 cells but it is ineffectively trafficked to the membrane. Unsuccessful attempts were made to characterise the surface expression of TRPC6 channels in LAD 2 cells with flow cytometry and immunocytochemistry using a rabbit anti-hTRPC6 antibody, which was a gift from a collaborator, Thierry Capiod. This antibody has previously been used to detect TRPC6 surface expression in human hepatoma cell lines by immunocytochemistry (El Boustany *et al.*, 2008). . Whilst 99% of cells were found to be positive for c-kit expression, demonstrated with flow cytometry using a PE-tagged anti-c-kit antibody, all cells appeared negative for TRPC6 expression. Similar results were obtained with immunocytochemistry. When the antibody was tested in HEK-TRPC6 cells it also failed to reveal

TRPC6 expression, suggesting that the antibody was unsuitable for this kind of experiment. Analysis of surface expression with a more suitable antibody would reveal whether TRPC6 protein is expressed at the surface; Western Blotting could also be used to determine whether the protein is produced in LAD 2 cells.

6.5.2 Receptor activation of TRPC3/6/7 channels in HLMCs

As discussed in chapter 1.3.2, stimulation of PLC-linked receptors represents a physiological mode of activation for TRPC6 channels. As shown in chapter 3.2 and in accordance with previous studies showing that $P2Y_1$ is expressed in HLMCs and causes mediator release (Saito *et al.*, 1991; Schulman *et al.*, 1999), application of ADP to HLMCs stimulates Ca^{2+} entry. It is known that $P2Y_1$, $P2Y_{12}$ and $P2Y_{13}$ receptors are all ADP-sensitive; whilst $P2Y_1$ couples to Gq proteins and PLCβ, $P2Y_{12}$ and $P2Y_{13}$ are coupled to Gi proteins (Communi *et al.*, 2001; Nicholas, 2001), causing downstream inhibition of cyclic adenosine monophosphate (cAMP) production. ADP-induced Ca^{2+} entry in the presence of the selective $P2Y_1$ antagonist, MRS2179 (Camaioni *et al.*, 1998; Kaiser & Buxton, 2002), was significantly inhibited in this study (see figures 6.6 and 6.7), showing that Ca^{2+} entry occurs downstream of Gq-coupled $P2Y_1$ receptors in HLMCs stimulated with ADP. The possibility that TRPC3/6/7 channels are activated downstream of $P2Y_1$ receptors in HLMCs was therefore considered. As previously discussed, Gd^{3+} is a commonly-used inhibitor of TRPC channels (Zhu *et al.*, 1998; Broad *et al.*, 1999; Halaszovich *et al.*, 2000; Inoue *et al.*, 2001; Jung *et al.*, 2002), and inhibited OAG-induced Ca^{2+} entry in this study with an estimated IC_{50} of 6.5μM. SKF-96365 has also been used extensively for the characterisation of TRPC channels in various systems (Merritt *et al.*, 1990; Halaszovich *et al.*, 2000; Inoue *et al.*, 2001; Eder *et al.*, 2007; Guilbert *et al.*, 2008; Finney-Hayward *et al.*, 2010), and caused concentration-dependent inhibition of OAG-induced Ca^{2+} entry in HLMCs in this study. 10μM Gd^{3+} or SKF-96365 caused significant inhibition of ADP-induced Ca^{2+} entry in HLMCs (see figures 5.6 and 5.7), suggesting that TRPC channels are involved in mediating Ca^{2+} entry downstream of $P2Y_1$ receptor activation in HLMCs. This is the first demonstration of a $P2Y_1$-mediated TRPC current in HLMCs, indicating that TRPC-mediated Ca^{2+} entry occurring downstream of P2Y receptor activation in HLMCs could be important in HLMC activation.

It is evident that the amplitude of the OAG-induced Ca^{2+} signal in HLMCs is much larger than that occurring in response to ADP. The same four donors were used for experiments using both agonists, so this difference is not donor-dependent. It is likely to be due to the different mechanisms of action of the two agonists. Evidence from platelets suggests that $PLC\beta_2$ is the predominant isoform activated downstream of $P2Y_1$ receptors (Kahner *et al.*, 2006); platelets from $PLC\beta_2/\beta_3$ knockout mice have defects in Ca^{2+} mobilisation and secretion in response to $P2Y_1$ stimulation (Lian *et al.*, 2005). Impaired $InsP_3$ production and Ca^{2+} signalling have been reported in platelets from patients with reduced $PLC\beta_2$ expression (Mao *et al.*, 2002), again demonstrating that $PLC\beta_2$ is a key effector molecule involved in $P2Y_1$ receptor signalling. $PLC\beta_2$ catalyses the

production of $InsP_3$ and DAG at the membrane from $PtdIns(4,5)P_2$; $InsP_3$ triggers Ca^{2+} release from intracellular stores, and DAG is thought to activate PKCδ (Kahner *et al.*, 2006), as well as TRPC3/6/7 channels (Hofmann *et al.*, 1999). The complex signalling cascade activated downstream of $P2Y_1$ receptors is therefore likely to have multiple effects on the cell, in addition to the activation of TRPC channels. Ca^{2+} release from stores and the activation of store-operated Ca^{2+} channels such as Orai1, and possibly TRPC channels including TRPC1, occurs following $InsP_3$ production. An increase in intracellular Ca^{2+} has been shown to cause inactivation of TRPC6 and 7 channels, which is associated with decreased single channel conductance. The activation of Ca^{2+} store depletion by $P2Y_1$-mediated stimulation, but not by OAG, could therefore down-regulate DAG-activated TRPC channels switched on downstream of $P2Y_1$.

It is also possible that TRPC6 channels are activated to a greater extent when directly stimulated with OAG, in comparison with activation downstream of the $P2Y_1$-mediated signalling cascade. Estacion *et al.* (2004), as well as data shown in chapter 4.1 in this study, showed that 100μM OAG caused maximal activation of TRPC6 channels; increasing the concentration to 300μM did not stimulate further channel activity. It is possible that whilst OAG activated TRPC6 channels maximally in this study, DAG activated downstream of $P2Y_1$ was not present at a sufficient concentration to maximally activate the channel. As a large number of signalling molecules are involved in the production of DAG downstream of $P2Y_1$ receptor stimulation, one of them could be a limiting factor in channel activation. As discussed in chapter 3, phosphoinositides such as $PtdIns(4,5)P_2$ are maintained in distinct membrane compartments (Mao & Yin, 2007), giving rise to specific microdomains of Ca^{2+} signalling at regions where ion channels are located. TRPC channels, Orai1 channels and voltage-gated Ca^{2+} channels have been shown to localise in distinct plasma membrane regions (Brazer *et al.*, 2003; Pani & Singh, 2009). Activation of Ca^{2+} entry downstream of $P2Y_1$ receptor stimulation would therefore be expected to occur only at membrane regions where $PtdIns(4,5)P_2$ and Ca^{2+} channels are clustered together. Unlike DAG, OAG is membrane-permeable and was applied directly to cells, so the activation of TRPC3/6/7 channels would not be expected to occur only at distinct regions where other signalling molecules are present. This could result in a much larger, non-physiological, Ca^{2+} signal in cells stimulated with OAG compared to those stimulated with ADP.

Although the amplitude of the Ca^{2+} signals was different following OAG and ADP stimulation of HLMCs, the sensitivity to Gd^{3+} was very similar. These observations suggest that, although the two stimuli may have activated the channels to a different extent, it is likely that the TRPC6 (and possibly TRPC7) channels activated by OAG were also activated downstream of $P2Y_1$ receptor stimulation.

The currents induced by OAG and $P2Y_1$ receptor stimulation were similar, as shown in table 6.1. The current properties are also similar to those in the study by Carter *et al.* (2006) showing that ADP stimulates outwardly-rectifying currents mediated by TRPC6 in mouse megakaryocytes. The

reversal potential for ADP-induced currents in HLMCs was measured at 4.38mV ± 2.00 (n=9, N=2 donors), and that for ADP-induced TRPC6 currents in mouse megakaryocytes was around 0mV (Carter *et al.*, 2006). Receptor operated TRPC6 currents measured in HEK cells in this study had a reversal potential of 1.44mV ± 0.38 (n=5), and those in previous studies have a reversal potential of around 0mV (Hofmann *et al.*, 1999; Estacion *et al.*, 2004; Shi *et al.*, 2004; Estacion *et al.*, 2006). When examining the example current-voltage relationship for ADP-induced currents in mouse megakaryocytes, the outward current appears to be approximately 4 fold larger than the inward current (Carter *et al.*, 2006), which would give rise to a rectification index of around 4, suggesting that similar channels are activated in both systems. The rectification of ADP-induced currents measured in HLMCs in this study also appears similar to that of receptor-operated TRPC6 channels expressed in HEK cells; carbachol-induced currents recorded in HEK-TRPC6 cells by Shi *et al*. (2004) appear to have an outward current that is around 3 fold larger than the inward current. ADP-induced currents in HEK-TRPC6 cells in this study (chapter 4.1) had a rectification index of 4.39 ± 1.28 (n=5); OAG-induced currents in HLMCs had a mean rectification index of 3.99 ± 0.89 (n=8, N=3 donors). The similar rectification properties of ADP-induced currents to those induced by OAG in HLMCs, and receptor-operated TRPC6 channels in heterologous expression systems, suggest that TRPC6-like channels are activated downstream of $P2Y_1$ receptor stimulation by ADP in HLMCs. The sensitivity of ADP-induced currents to 10μM Gd^{3+} also provides evidence for the activation of TRPC channels downstream of $P2Y_1$ receptor activation. The exact mechanism for receptor- mediated activation of TRPC6 channels remains elusive; whilst Hofmann *et al.* (1999) showed that DAG directly activates the channels, Estacion *et al*. (2004) reported that TRPC6-mediated currents in the presence of carbachol plus OAG were larger than the sum of the currents induced by either agent alone. The authors concluded that DAG production alone may not cause complete activation of TRPC6, and it may act synergistically with other events downstream of receptor stimulation to maximally activate TRPC6 (Estacion *et al.*, 2004). It is known that PLC is necessary for receptor activation of TRPC6 channels, because pre-incubation with the PLC inhibitor U73122 inhibited histamine-induced Mn^{2+} influx in CHO cells expressing hTRPC6 (Hofmann *et al.*, 1999). Estacion *et al*. (2004) suggested that PtdIns(4,5)P_2 hydrolysis *per se* may have a role in receptor-mediated TRPC6 channel activation in synergy with DAG. To verify the involvement of DAG in the activation of TRPC6-like currents activated downstream of $P2Y_1$ receptor activation, experiments could be carried out in the presence of DAG kinase, which breaks down DAG; a reduction in the current would indicate that DAG is required for channel activation. Co-immunoprecipitation studies using antibodies to TRPC6 and other signalling proteins could be used to reveal whether other second messengers activated downstream of $P2Y_1$ receptor stimulation, such as PtdIns(4,5)P_2, are associated with TRPC6 following ADP stimulation.

Given that $InsP_3$ is produced downstream of $P2Y_1$ stimulation (Kahner *et al.*, 2006), and $InsP_3$-mediated store release is sensed by STIM1, which has been shown to translocate to distinct puncta in the plasma membrane (Stathopulos *et al.*, 2006) and activate I_{CRAC} currents mediated

by Orai1 in mast cells (Feske *et al.*, 2006; Prakriya *et al.*, 2006; Vig *et al.*, 2006b), it might be expected that I_{CRAC} activation downstream of $P2Y_1$ receptor stimulation could occur. . I_{CRAC}-like currents (properties described in chapter 1.3.1) were not observed following ADP stimulation of HLMCs; as conditions in this study were not optimised to measure I_{CRAC} activation, it is possible that the current was active following $P2Y_1$ stimulation but was not visible in the recording conditions used. Stimulating cells with ADP in recording conditions designed to detect I_{CRAC} currents, such as the application of divalent-free solution during recordings, would reveal whether such currents are activated. Another possibility is that I_{CRAC} currents are not activated downstream of $P2Y_1$ receptor activation; distinct pools of $PtsIns(4,5)P_2$ in the membrane may interact with different isoforms of PLC, targeting them to different regions. It has been suggested that Orai1 and TRPC channels are localised in distinct membrane regions; experiments using MβCD, which sequesters cholesterol, have shown that TRPC3 channel function is suppressed by cholesterol sequestration, whereas Orai1 function is unaffected (DeHaven *et al.*, 2009). The authors concluded that the two types of channels exist in distinct plasma domains; it is possible in this study that following $P2Y_1$ activation by ADP, PLCβ is targeted to distinct plasma membrane regions containing discrete pools of $PtdIns(4,5)P_2$ to activate TRPC channels but not Orai1 channels. Distinct receptor signalling pathways, such as FcεRI-mediated signalling, may result in the recruitment of PLCγ to regions of the plasma membrane containing Orai1 and the activation of I_{CRAC}. This hypothesis is in accordance with results in chapter 3.3 showing that IgE and ADP activate Ca^{2+} store release and entry with different amplitudes, which can be explained by PLCβ and PLCγ activating different ion channels depending on their spatial orientation in the membrane. Therefore, it is possible that I_{CRAC} currents were not observed following $P2Y_1$ receptor stimulation in this study because the two ion channel types (TRPC and Orai1) are subject to tight spatial regulation and differentially activated depending on the stimulus and concomitant signalling cascade.

Attempts were made to verify the involvement of TRPC6 in OAG- and ADP- activated currents using FFA. As discussed in chapter 1.3.2, FFA has been used as a diagnostic tool for TRPC6 channel activation in a number of studies, as it activates TRPC6 whilst suppressing other TRPC channels. In this study, application of FFA to LAD 2 cells and HLMCs gave rise to Ca^{2+} entry and currents with the typical biophysical properties of TRPC6 channels. However, a number of observations challenge the view that FFA is a selective activator of TRPC6. Firstly, FFA application gave rise to Ca^{2+} entry in 100% of LAD 2 cells tested; as shown in figure 6.5, Ca^{2+} entry following OAG application only occurred in 25% of LAD 2 cells. As discussed above, it is likely that LAD 2 cells are not an appropriate model to study TRPC6 channels in human mast cells because they are not fully differentiated. Secondly, a large increase in cytosolic Ca^{2+} occurred when FFA was applied to LAD 2 cells in the absence of extracellular Ca^{2+}, showing that Ca^{2+} was being released from inside the cell not entering across the plasma membrane. A similar observation was made by Tu *et al.* (2009a), who reported that FFA caused a rise in cytosolic calcium in cultured cortical neurons even in cells kept in calcium-free extracellular solution or

when intracellular stores were depleted with thapsigargin. The FFA-induced calcium rise was shown to be strongly diminished by bongkrekic acid, which is a ligand of the mitochondrial ADP/ATP carrier, and the authors suggested that FFA exerts its effects on plasma membrane channels by affecting the mitochondria (Tu *et al.*, 2009a). Mitochondria exert complex effects on calcium signalling in the cell, therefore interfering with their function could have many downstream effects.

To summarise, data in this chapter shows that OAG stimulates Gd^{3+} and SKF-96365- sensitive Ca^{2+} entry in HLMCs; OAG-evoked currents have the expected biophysical properties of TRPC3/6/7 channels. Taken together with the RT-PCR data shown in figure 3.9, these data suggest that TRPC6 channels, possibly along with TRPC7, are functionally expressed in HLMCs. ADP stimulation of $P2Y_1$ receptors in HLMCs activates Gd^{3+} and SKF-96365- sensitive Ca^{2+} entry and currents with similar properties to those activated by OAG, suggesting that TRPC6 channels may be switched on downstream of $P2Y_1$ receptor activation in HLMCs. This is the first demonstration of TRPC6-like current activation in HLMCs.

6.5.3 Functional roles of DAG-activated TRPC channels

The lack of histamine and β-hexosaminidase release in response to OAG suggests that TRPC3/6/7 channels are not required for HLMC degranulation. This observation is in accordance with Ca^{2+} imaging results showing that OAG stimulates Ca^{2+}influx following FcεRI cross-linking, suggesting that TRPC3/6/7 channels are not required for FcεRI-dependent Ca^{2+} entry. ADP has previously been shown to stimulate histamine release in mouse BMMCs (Saito *et al.*, 1991) and RBL-2H3 cells (Gao *et al.*, 2010), but HLMCs did not release histamine and β-hexosaminidase in response to ADP in this study. It is known that species-dependent differences exist between human and rodent mast cells (Bischoff, 2007); this discrepancy highlights the need to use primary human mast cells to study their activation mechanisms.

The observation that HLMCs degranulate in response to FcεRI cross-linking but not $P2Y_1$ receptor stimulation supports the theory that PLCγ and PLCβ are subject to spatial regulation in the cell and differentially couple to downstream signalling molecules. As discussed in chapter 1.3, signalling molecules and ion channels are brought together in lipid raft complexes in the plasma membrane (Lingwood & Simons, 2010; Calloway *et al.*, 2011); the coupling of PLCγ and PLCβ to different signalling molecules and ion channels would give rise to differential downstream effects. It is known that the secretion of granule-associated mediators in mast cells is controlled by SNARE proteins. Specific SNARE proteins on intracellular vesicles (v-SNAREs) bind to their cognate SNAREs on the target plasma membrane (t-SNAREs) to mediate fusion and the release of granule contents (Puri & Roche, 2008). It has recently been shown that mast cells possess distinct subsets of mediators contained in different secretory granules, and different SNARE isoforms are required for their release. VAMP-8, for example, mediates the secretion of serotonin but not histamine from mouse mast cells (Puri & Roche, 2008). It is possible that PLCγ- and

PLCβ-dependent signalling cascades couple to differential SNARE proteins to effect the secretion of distinct mediators. The study by Puri & Roche (2008) highlights that the release of histamine and β-hexosaminidase may not accurately reflect the behaviour of all granule-associated mediators in HLMCs; it is possible that other mediators such as proteoglycans, proteases or pre-formed cytokines stored in distinct granules are released downstream of PLCβ signalling. Further studies investigating the release of other granule-associated mediators are required to elucidate whether $P2Y_1$ receptor stimulation is involved in HLMC degranulation.

In addition to the plethora of granule-associated mediators released by the mast cell, newly-synthesised mediators are produced upon mast cell activation. It is known that mast cells are capable of differential mediator release without degranulation as they are involved in the pathogenesis of inflammatory diseases without causing anaphylactic shock (Theoharides *et al.*, 2007). Eicosanoids including prostaglandin D_2 and leukotriene C_4 are released by the mast cell and contribute to inflammation, and the transcription of a range of cytokines occurs following Ca^{2+} entry (Gilfillan & Tkaczyk, 2006). As degranulation is a rapid process taking place over minutes, whereas transcriptional regulation of cytokine production occurs over hours, a more sustained Ca^{2+} signal is required for *de novo* synthesis of mediators (Gilfillan & Tkaczyk, 2006). As discussed in the previous chapter, it is likely that store-operated TRPC1 channels, along with Orai1 channels, are activated downstream of FcεRI cross-linking. It is possible that $P2Y_1$ receptor activation and PLCβ are coupled to TRPC6 channels in HLMCs whereas FcεRI and PLCγ are coupled to TRPC1. Whilst TRPC6-mediated Ca^{2+} entry may not be coupled to the release of granule-associated mediators, it could provide a more sustained Ca^{2+} signal required for cytokine transcription. A comprehensive investigation of HLMC mediator release following ADP stimulation in future studies would reveal whether signalling downstream of $P2Y_1$ receptors contributes to allergic inflammation in the asthmatic airway.

To summarise, data in this chapter show for the first time that TRPC6-like channels are functionally expressed in HLMCs, and they can be activated directly by OAG, or via ADP stimulation of $P2Y_1$ receptors. These channels were not found to have a role in HLMC degranulation or motility, but it is possible that Ca^{2+} entry through TRPC6 channels has another role, such as the *de novo* synthesis of cytokines, which could be important in the development of asthma.

Chapter 7: Discussion and future directions

7.1 Discussion

This study demonstrated for the first time that TRPC channels are functionally expressed in human lung mast cells. Of the DAG-sensitive TRPC family, it is likely that TRPC6 is present in HLMCs; TRPC6-like currents were activated by the DAG analogue OAG and downstream of $P2Y_1$ receptor activation by ADP. TRPC6 channel activation by these methods was not found to stimulate release of the granule-associated mediators histamine and β-hexosaminidase, suggesting that the channels are unlikely to have a role in HLMC degranulation. As further Ca^{2+} rises could be stimulated by OAG following FcεRI cross-linking, it is unlikely that TRPC6 channels contribute to IgE-dependent mast cell activation.

As discussed in chapter 1.2, the IgE-dependent pathway is not the only important mechanism of mast cell activation; they express receptors for many other physiological ligands, which may induce degranulation, promote survival, growth or chemotaxis of mast cells, prime cells for activation by FcεRI cross-linking, or provide co-stimulatory signals (Gilfillan & Tkaczyk, 2006). Nucleotides such as ATP and ADP are thought to be among the first released and most abundant molecules released from cells in response to tissue injury, infection and hypoxia (Feng *et al.*, 2004; Bulanova & Bulfone-Paus, 2010). The sources of extracellular nucleotides are summarised in figure 7.1. The demonstration in this study that ADP can activate TRPC6-like currents downstream of $P2Y_1$ receptor activation indicates that TRPC6-mediated Ca^{2+} entry could be an important mechanism of HLMC activation in the inflammatory response. Whilst β-hexosaminidase and histamine release are not likely to be dependent on Ca^{2+} entry through TRPC6 channels, a rise in cytosolic Ca^{2+} is also essential for the *de novo* synthesis and release of other pro-inflammatory mediators, including prostaglandins, leukotrienes and cytokines (Chung *et al.*, 1986; Metcalfe *et al.*, 1997; Theoharides *et al.*, 2007). TRPC6-dependent Ca^{2+} entry could be coupled to eicosanoid or cytokine production in HLMCs, thus coupling nucleotide release in inflammation to HLMC activation. It has recently been shown in T cells that the product of *ORMDL3*, a genetic risk factor for asthma (Moffatt *et al.*, 2007), inhibits the SERCA pump (Cantero-Recasens *et al.*, 2010). This gives rise to reduced Ca^{2+} concentration in the ER, which triggers the unfolded-protein response (UPR), increasing the expression of genes involved in the onset of inflammation (Cantero-Recasens *et al.*, 2010). A genome-wide association study found that genetic variants in the IL-6 receptor (IL-6R) gene were associated with atopic asthma, and it has been suggested that tocilizumab, an IL-6R antagonist approved to treat rheumatoid arthritis, could also be used in the treatment of asthma (Ferreira *et al.*, 2011). These studies indicate that genetic dysregulation of cytokine signalling in immune cells is important in the development of asthma (Ferreira *et al.*, 2011); elucidating the role of TRPC channels in mast cell cytokine production may unveil new therapeutic targets for aberrant cytokine signalling.

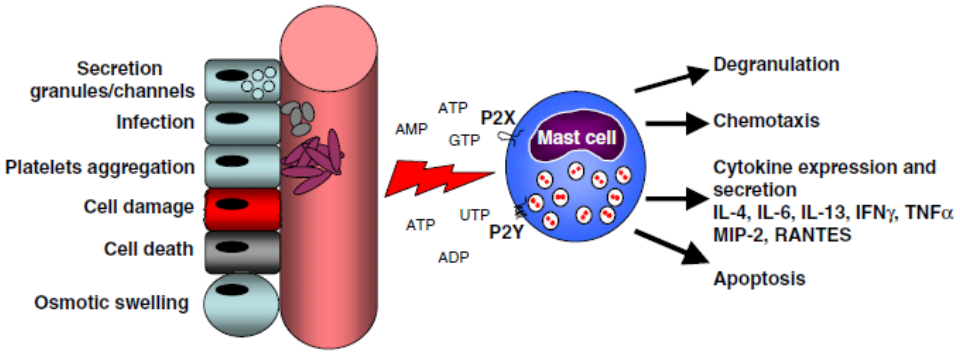

Figure 7.1. Sources of extracellular nucleotides and mast cell responses
Reproduced with permission from (Bulanova & Bulfone-Paus, 2010)

The migration of mast cells is also an important determinant of the asthmatic phenotype; their micro-localisation in airway smooth muscle bundles contributes to the symptoms of asthma, and they migrate to these sites through CXCR3 activation (Brightling *et al.*, 2005). It has been shown in neutrophils that TRPC6 channels are required for migration stimulated by OAG or macrophage inflammatory protein-2 (MIP-2) (Damann *et al.*, 2009); TRPC channels have also been suggested to have a role in monocyte migration induced by lysophosphatidylcholine (LPC) (Schilling & Eder, 2009). The ion channels involved in HLMC migration have not been investigated; given the importance of TRPC6 channels for neutrophil migration, it can be hypothesised that they have a similar importance in HLMCs. The involvement of TRPC channels in HLMC migration was unable to be assessed in this study due to insufficient cell availability, but would represent an interesting avenue for future investigation.

This study is the first known demonstration of a TRPC-like current in response to $P2Y_1$ receptor activation in HLMCs; the existence of this current indicates that TRPC channels could be important in regulating mast cell activation in the inflammatory response, suggesting that they could be involved in the development of allergic asthma. Nucleotides are known to have important effects on other cells involved in the asthmatic phenotype, giving rise to neutrophil and eosinophil chemotaxis (Myrtek & Idzko, 2007), along with the release of the pro-inflammatory cytokines IL-1β and TNF-α from macrophages (Ferrari *et al.*, 1997; Myrtek & Idzko, 2007). Given the importance of P2 receptor-mediated activation in these other cell types, it is reasonable to hypothesise that $P2Y_1$ receptors, which are sensitive to both ADP and ATP, are important for mast cell activation.

Elevated concentrations of ATP (Idzko *et al.*, 2007) and its breakdown product adenosine (Driver *et al.*, 1993) have been detected in BALF from patients with asthma compared with non-asthmatics, highlighting the importance of purinergic signalling in the development of asthma. The demonstration that TRPC-like currents are activated downstream of $P2Y_1$ receptor activation provides a mechanism by which $P2Y_1$ stimulation leads to elevated Ca^{2+} entry and mast cell

activation, and highlights TRPC channels in HLMCs as potential therapeutic targets for asthma. Selective molecular knock-down of TRPC6 channels in HLMCs is required in future studies to verify their activation downstream of $P2Y_1$ receptors. This could be carried out using a dominant negative TRPC6 pore mutant; this approach has successfully been used to inhibit TRPC6 channels in human microvascular endothelial cells and human podocytes (Hamdollah Zadeh *et al.*, 2008; Foster *et al.*, 2009). As techniques to transfect human mast cells are currently being optimised in our laboratory, it should be possible to use dominant negative mutants to verify the contribution of TRPC6 channels to Ca^{2+} entry downstream of $P2Y_1$ receptor activation in the near future. Molecular knock-down studies used in combination with mediator release screens could be used to reveal whether TRPC6 channels activated following $P2Y_1$ receptor stimulation are important for the synthesis and release of eicosanoids and cytokines that could contribute to the asthmatic phenotype.

It has previously been shown that ATP can enhance IgE-dependent histamine release in HLMCs (Schulman *et al.*, 1999). This enhancement was unaffected by a P2X purinoceptor antagonist, pyridoxalphosphate-6-azophenyl-2',4'-disulphonic acid (PPADS) , suggesting a P2Y-dependent mechanism (Schulman *et al.*, 1999). It is therefore possible that $P2Y_1$ receptor activation by ADP in HLMCs could have a role in modifying FcεRI-dependent mediator release. Ca^{2+} entry through TRPC channels downstream of PLCβ-dependent DAG generation could provide a co-stimulatory signal for IgE-dependent mediator release, or the phosphorylation of key adaptor molecules following Gq protein stimulation could enhance FcεRI signalling. This hypothesis could be tested in future studies by comparing mediator release and Ca^{2+} entry in HLMCs stimulated with anti-IgE alone, or anti-IgE together with ADP. If TRPC channels activated downstream of $P2Y_1$ receptors provide a co-stimulatory signal for FcεRI-dependent mediator release, they could be a potential therapeutic target for the attenuation of the allergic response.

Whilst HLMCs are most well-known for their involvement in allergic asthma, making them an attractive therapeutic target in allergic individuals, it must also be considered that mast cells have an important role in protective immunity. As described in chapter 1.1.4, studies in mice have shown that mast cell-derived mediators are important for the recruitment of other inflammatory cells to sites of infection, and that mast cells are essential for survival in bacterial infections (Echtenacher *et al.*, 1996; Malaviya *et al.*, 1996; Metz & Maurer, 2007). They are thought to have a role in both innate and acquired immunity. Nucleotides including ATP and ADP are considered "danger signals" in the immune system; their role is to alert the body to potential danger and activate the immune response to destroy invading pathogens (Di Virgilio, 2005). $P2Y_1$ receptor activation and subsequent Ca^{2+} entry by TRPC channels could thus have a protective role in the lung; mediators released by HLMCs in response to invading pathogens could activate other components of the immune system to efficiently destroy the pathogen. As asthmatic patients have increased numbers of mast cells in the lung (Broide *et al.*, 1991; Brightling *et al.*, 2002; Bradding *et al.*, 2006), it is possible that TRPC channels activated downstream of $P2Y_1$

receptors could contribute to mast cells' protective role in non-asthmatics, but play a role in the development of the asthmatic phenotype in hypersensitive individuals. Comparison of TRPC channel expression between asthmatic and non-asthmatic individuals would reveal whether the channels are likely to have an immunoprotective role or whether they specifically contribute to mast cell activation in hypersensitive individuals. mRNA expression could be compared by quantitative PCR and protein expression by flow cytometry or immunohistochemistry. HLMC ADP responsiveness and the comparison of mediator release between asthmatic and non-asthmatic individuals would also reveal whether TRPC channels activated downstream of $P2Y_1$ receptors are important in the allergic response, protective immunity, or both. The demonstration that DAG-activated TRPC channels are likely to cause Ca^{2+} entry in HLMCs following $P2Y_1$ receptor activation is a significant development in the field of mast cell biology, and will lead to further investigations like those discussed above to elucidate their role in mast cell function.

This study also revealed for the first time that TRPC1 channels are expressed in HLMCs, and that they are likely to be involved in SOCE. As described in chapter 1.3, SOCE is an important mechanism for Ca^{2+} entry in mast cells; following allergic activation via FcεRI cross-linking, PLCγ generates $InsP_3$ from $PtdIns(4,5)P_2$, which causes Ca^{2+} release from stores in the ER and subsequent activation of SOC channels in the plasma membrane (Gilfillan & Tkaczyk, 2006). The resulting Ca^{2+} influx is essential for mast cell degranulation, as well as cytokine transcription and eicosanoid production (Cochrane & Douglas, 1974; Gilfillan & Tkaczyk, 2006; Melicoff *et al.*, 2009). The demonstration that TRPC1 channels are likely to be involved in SOCE in human mast cells adds to a growing body of evidence, described in chapter 1.3.2, that these channels are important components of SOCE in a number of different cell types (Liu *et al.*, 2007; Yuan *et al.*, 2007; Liao *et al.*, 2008; Ma *et al.*, 2008; Ng *et al.*, 2009; Zhang *et al.*, 2010a; Cheng *et al.*, 2011; Hong *et al.*, 2011). Results indicate that both non-selective TRPC1 and highly Ca^{2+}-selective Orai1 channels are likely to be involved in SOCE in human mast cells; as described in chapter 1.3.2, it is likely that the channels function together to bring about FcεRI-dependent Ca^{2+} entry, but give rise to distinct downstream effects. In HSG cells, Orai1 mediated Ca^{2+} entry activates the transcription factor NFAT, but a higher concentration of intracellular Ca^{2+} provided by TRPC1 activation is required for the full activation of NFκB (Cheng *et al.*, 2011). In mast cells, NFAT is required for TNFα and IL-2 production; TNFα is a pro-inflammatory cytokine that is centrally involved in asthma, activating the airway epithelium, antigen-presenting cells and macrophages in the airway (Chung & Barnes, 1999). The transcription factor NFκB enhances the transcription of genes for cytokines, adhesion molecules and growth factors (Marquardt & Walker, 2000). Fine control of these transcription factors by differential Ca^{2+} entry through Orai1 and TRPC1 channels could allow the mast cell to tightly regulate downstream cytokine production, and thus activate different cells important in airway inflammation. Given the importance of the cytokines produced following NFAT and NFκB activation in mast cells, it can be hypothesised that if a similar dependence on TRPC1- and Orai1- mediated Ca^{2+} entry exists in HLMCs as that for described for

HSG cells, both channels would be important in the pathophysiology of asthma. These channels could thus be important therapeutic targets for future asthma treatments.

Also shown for the first time in this study is that TRPC1 channels, along with Orai1 channels, are likely to be involved in FcεRI-dependent Ca^{2+} entry and degranulation. As a number of mast cell mediators are released upon degranulation that contribute to asthmatic airway inflammation, these findings are of significance for the development of future mast cell-stabilising drugs. Inhibition of the essential Ca^{2+} influx required for degranulation following FcεRI cross-linking would inhibit the release of mediators such as histamine, chymase and tryptase, all of which contribute to airway inflammation (Metcalfe *et al.*, 1997). The clinical potential of inhibiting the IgE-dependent pathway of mast cell activation has recently been demonstrated by the success of the humanised monoclonal antibody omalizumab in clinical trials. This antibody treatment works by binding to circulating IgE, thus preventing it from binding to FcεRI (Thomson *et al.*, 2011). It has been shown to improve symptoms in patients with allergic asthma and reduce airway inflammation (Walker *et al.*, 2006; Rodrigo *et al.*, 2011), highlighting the importance of this pathway in mast cells as a therapeutic target. Whilst the safety and efficacy of omalizumab is generally good, preliminary data has indicated a possible increase in cardiovascular problems (Thomson *et al.*, 2011). As existing drugs for asthma lack potency or are ineffective in some patients (Church & Hiroi, 1987; Giannini *et al.*, 1996; Rodrigo *et al.*, 2011), there is a need for the development of new therapies. This study identifies TRPC1 channels as a target for new asthma therapies; inhibiting TRPC1- mediated Ca^{2+} influx in HLMCs could attenuate the release of mediators and consequently reduce asthmatic airway inflammation.

7.2 Future directions

This study reveals TRPC1 as a potentially important therapeutic target for HLMC stabilisation to improve the symptoms of asthma; as mast cells are involved in the pathophysiology of many other allergic diseases including allergic rhinitis, coeliac disease, inflammatory bowel disease and rheumatoid arthritis (Sellge & Bischoff, 2006; Nigrovic & Lee, 2007; Owen, 2007; Beaven, 2009), TRPC1 channels may also contribute to mast cell activation in these diseases. Analysis of mRNA expression in mast cells from different sites including the human intestine, skin and synovial fluid in the joints would indicate whether TRPC channels are likely to have a role in the activation of mast cells from different sites. Results from an oligonucleotide probe array screen to identify ion channel genes in mast cells indicate that TRPC1 mRNA is present in human skin mast cells (Bradding *et al.*, 2003), suggesting that the channel may also have an important role in Ca^{2+} entry in mast cells from other sources. As mast cells display heterogeneity between species and between sites within the same organism (Bischoff, 2007), it is important to study primary human mast cells from the site of interest where possible to gain insight into their mechanisms of activation.

The functional expression of TRPC5 was found to be highly variable between donors; investigation of its expression in a larger pool of donors is necessary to elucidate whether environmental factors such as cigarette smoking or medication affect the expression of this channel. Quantitative PCR could be used to compare mRNA levels between donors; comparisons between asthmatic and non-asthmatic patients could show whether the channel has a role in the development of asthma.

An interesting avenue for future investigation for TRPC channels from both subfamilies would be assessing their role in the secretion of different mediators. This study addressed the secretion of the granule-associated mediators β-hexosaminidase and histamine; further investigation is required to elucidate whether TRPC channels have a role in FcεRI- and $P2Y_1$- evoked release of other mediators. Again the specific role of TRPC1 and TRPC6 in regulating the functions of primary human mast cells will require gene knockdown studies (siRNA) and targeted loss of function studies by expression of dominant-negative pore mutants. As FcεRI is coupled to PLCγ and $P2Y_1$ to PLCβ (Gilfillan & Tkaczyk, 2006), it is likely that the two signalling pathways are coupled to different ion channels in distinct membrane lipid raft domains (Lingwood & Simons, 2010). PLCβ-coupled Ca^{2+} entry could thus give rise to differential mediator secretion compared with PLCγ-coupled Ca^{2+} entry. It has been shown in mouse BMMCs that different SNARE proteins regulate the exocytosis of distinct mediators; serotonin secretion was inhibited, but histamine secretion was unaffected, in BMMCs from mice lacking the SNARE protein vesicle-associated membrane protein 8 (VAMP-8) (Puri & Roche, 2008). Analysis of the mediators secreted downstream of the different PLC isoforms would reveal whether similar differential mediator release occurs in human mast cells. siRNA could be used to inhibit the different isoforms of PLC, as has been described for PLCβ in rat fibroblasts (Kelley *et al.*, 2006), in order to determine their involvement in mediator release.

Results in this study indicate that TRPC1 and Orai1 may functionally interact to mediate SOCE in HLMCs. To confirm this conclusion, which is based on data using the selective pharmacological Orai1 inhibitor synta 66, specific molecular knock-down of Orai1 channels could be used to assess the effect on TRPC1 current. Combined patch clamp and Ca^{2+} imaging experiments could be used to compare store-activated TRPC1 currents in the presence and absence of Orai1 inhibition. Such experiments would verify the functional dependence of the channels, and would provide insight into whether pharmacological inhibition of one or both channels would be beneficial for the modulation of mast cell secretion. The I_{CRAC} inhibitor synta 66 has been shown to inhibit Orai1 channels with potency and selectivity (Ng *et al.*, 2008; Di Sabatino *et al.*, 2009; Li *et al.*, 2011), thus has the potential to be developed into a mast cell-modulating drug. If TRPC1 channel activation is indeed modulated by Orai1 channel inhibition, agents targeting Orai1 such as synta 66 could sufficiently reduce the activity of both channels to attenuate mast cell mediator secretion.

Although more donors were assayed for IgE-dependent mediator release than Ca^{2+} entry in this study, donor variability in the contribution of TRPC channels was apparent in mediator release assays but Ca^{2+} imaging experiments revealed a contribution from TRPC channels in 100% of donors tested. Whilst mediator release assays were carried out on freshly isolated HLMCs, cultured HLMCs were used for Ca^{2+} imaging experiments. It would be interesting to assess whether culture conditions affect the surface expression of TRPC channels; it is known that the mast cell microenvironment determines its phenotype (Metcalfe *et al.*, 1997; Metz & Maurer, 2007), and it is possible that TRPC channel expression is up-regulated in cultured HLMCs compared with freshly isolated cells. mRNA expression could be compared in freshly isolated cells and in those kept in culture using quantitative PCR, and flow cytometry using anti-TRPC antibodies could be employed to quantify the surface expression.

In order to determine the *in vivo* role of TRPC channels in mast cells, knockout mouse models could be used. Such models have been extremely useful in determining some *in vivo* functions of TRPC channels. For example, TRPC1-deficient mice were used to show that TRPC1 channels are essential for salivary gland function and SOCE in salivary gland cells (Liu *et al.*, 2007). Knockout mice are available for all TRPC channels, with the exception of TRPC7 (Wu *et al.*, 2010). Such models could be used to assess the localisation of mast cells to identify whether TRPC channels have an important role in microlocalisation in the lung, for example. Mast cells from different sites in the knockout mouse could be compared with those in wild-type mice to assess effects on Ca^{2+} signalling and mediator release. TRPC-deficient mouse models could would also be useful to assess whether the absence of a particular TRPC channel has adverse effects on the whole organism; this would provide valuable information on whether pharmacologically inhibiting TRPC channels as a target for asthma therapy would have systemic effects. Whilst experiments using mouse mast cells have disadvantages due to the species-dependent differences that occur (Bischoff, 2007), meaning that all results would need to be verified in human mast cells, experiments using knockout mice would be extremely valuable to assess the *in vivo* roles of TRPC channels in mast cells.

In summary, there are many avenues of work that can be pursued following the results of this study. It has shown for the first time that TRPC channels are functionally expressed in human lung mast cells, and are likely to represent an important route for Ca^{2+} entry. These channels are thus an exciting potential therapeutic target for the modulation of allergic diseases such as asthma.

Bibliography

Abbracchio MP & Burnstock G. (1994). Purinoceptors: are there families of P2X and P2Y purinoceptors? *Pharmacol Ther* **64,** 445-475.

Abrink M, Grujic M & Pejler G. (2004). Serglycin is essential for maturation of mast cell secretory granule. *J Biol Chem* **279,** 40897-40905.

Al-Shawaf E, Tumova S, Naylor J, Majeed Y, Li J & Beech DJ. (2011). GVI phospholipase A2 role in the stimulatory effect of sphingosine-1-phosphate on TRPC5 cationic channels. *Cell Calcium*.

Alicia S, Angelica Z, Carlos S, Alfonso S & Vaca L. (2008). STIM1 converts TRPC1 from a receptor-operated to a store-operated channel: moving TRPC1 in and out of lipid rafts. *Cell Calcium* **44,** 479-491.

Ammit AJ, Hastie AT, Edsall LC, Hoffman RK, Amrani Y, Krymskaya VP, Kane SA, Peters SP, Penn RB, Spiegel S & Panettieri RA, Jr. (2001). Sphingosine 1-phosphate modulates human airway smooth muscle cell functions that promote inflammation and airway remodeling in asthma. *Faseb J* **15,** 1212-1214.

Arias-Montano JA, Gibson WJ & Young JM. (1998). SK&F 96365 (1-[beta-[3-(4-methoxyphenyl)propoxy]-4-methoxyphenylethyl]-1H- imidazole hydrochloride) stimulates phosphoinositide hydrolysis in human U373 MG astrocytoma cells. *Biochem Pharmacol* **56,** 1023-1027.

Arinobu Y, Iwasaki H, Gurish MF, Mizuno S, Shigematsu H, Ozawa H, Tenen DG, Austen KF & Akashi K. (2005). Developmental checkpoints of the basophil/mast cell lineages in adult murine hematopoiesis. *Proc Natl Acad Sci U S A* **102,** 18105-18110.

Baba Y, Nishida K, Fujii Y, Hirano T, Hikida M & Kurosaki T. (2008). Essential function for the calcium sensor STIM1 in mast cell activation and anaphylactic responses. *Nat Immunol* **9,** 81-88.

Bansal G, DiVietro JA, Kuehn HS, Rao S, Nocka KH, Gilfillan AM & Druey KM. (2008). RGS13 controls g protein-coupled receptor-evoked responses of human mast cells. *J Immunol* **181,** 7882-7890.

Barbara G, Stanghellini V, De Giorgio R & Corinaldesi R. (2006). Functional gastrointestinal disorders and mast cells: implications for therapy. *Neurogastroenterol Motil* **18,** 6-17.

Barsumian EL, Isersky C, Petrino MG & Siraganian RP. (1981). IgE-induced histamine release from rat basophilic leukemia cell lines: isolation of releasing and nonreleasing clones. *Eur J Immunol* **11,** 317-323.

Beane J, Sebastiani P, Liu G, Brody JS, Lenburg ME & Spira A. (2007). Reversible and permanent effects of tobacco smoke exposure on airway epithelial gene expression. *Genome Biol* **8,** R201.

Beaven MA. (2009). Our perception of the mast cell from Paul Ehrlich to now. *Eur J Immunol* **39,** 11-25.

Beech DJ. (2007). Canonical transient receptor potential 5. *Handb Exp Pharmacol***,** 109-123.

Bell RM, Hannun YA & Loomis CR. (1986). Mechanism of regulation of protein kinase C by lipid second messengers. *Symp Fundam Cancer Res* **39,** 145-156.

Benschop RJ, Brandl E, Chan AC & Cambier JC. (2001). Unique signaling properties of B cell antigen receptor in mature and immature B cells: implications for tolerance and activation. *J Immunol* **167,** 4172-4179.

Berry MA, Hargadon B, Shelley M, Parker D, Shaw DE, Green RH, Bradding P, Brightling CE, Wardlaw AJ & Pavord ID. (2006). Evidence of a role of tumor necrosis factor alpha in refractory asthma. *N Engl J Med* **354,** 697-708.

Birnbaumer L. (2009). The TRPC class of ion channels: a critical review of their roles in slow, sustained increases in intracellular Ca($^{2+}$) concentrations. *Annu Rev Pharmacol Toxicol* **49,** 395-426.

Bischoff SC. (2007). Role of mast cells in allergic and non-allergic immune responses: comparison of human and murine data. *Nat Rev Immunol* **7,** 93-104.

Bischoff SC, Sellge G, Schwengberg S, Lorentz A & Manns MP. (1999). Stem cell factor-dependent survival, proliferation and enhanced releasability of purified mature mast cells isolated from human intestinal tissue. *Int Arch Allergy Immunol* **118,** 104-107.

Bishara NB & Ding H. (2010). Glucose enhances expression of TRPC1 and calcium entry in endothelial cells. *Am J Physiol Heart Circ Physiol* **298,** H171-178.

Borgerding M & Klus H. (2005). Analysis of complex mixtures--cigarette smoke. *Exp Toxicol Pathol* **57 Suppl 1,** 43-73.

Boulay G, Brown DM, Qin N, Jiang M, Dietrich A, Zhu MX, Chen Z, Birnbaumer M, Mikoshiba K & Birnbaumer L. (1999). Modulation of Ca($^{2+}$) entry by polypeptides of the inositol 1,4, 5-trisphosphate receptor (IP3R) that bind transient receptor potential (TRP): evidence for roles of TRP and IP3R in store depletion-activated Ca($^{2+}$) entry. *Proc Natl Acad Sci U S A* **96,** 14955-14960.

Boulay G, Zhu X, Peyton M, Jiang M, Hurst R, Stefani E & Birnbaumer L. (1997). Cloning and expression of a novel mammalian homolog of Drosophila transient receptor potential (Trp) involved in calcium entry secondary to activation of receptors coupled by the Gq class of G protein. *The Journal of biological chemistry* **272,** 29672-29680.

Bousquet SM, Monet M & Boulay G. (2010). Protein kinase C-dependent phosphorylation of transient receptor potential canonical 6 (TRPC6) on serine 448 causes channel inhibition. *J Biol Chem* **285,** 40534-40543.

Bradding P, Feather IH, Howarth PH, Mueller R, Roberts JA, Britten K, Bews JP, Hunt TC, Okayama Y, Heusser CH & et al. (1992). Interleukin 4 is localized to and released by human mast cells. *J Exp Med* **176,** 1381-1386.

Bradding P, Okayama Y, Kambe N & Saito H. (2003). Ion channel gene expression in human lung, skin, and cord blood-derived mast cells. *J Leukoc Biol* **73,** 614-620.

Bradding P, Walls AF & Holgate ST. (2006). The role of the mast cell in the pathophysiology of asthma. *J Allergy Clin Immunol* **117,** 1277-1284.

Brazer SC, Singh BB, Liu X, Swaim W & Ambudkar IS. (2003). Caveolin-1 contributes to assembly of store-operated Ca^{2+} influx channels by regulating plasma membrane localization of TRPC1. *J Biol Chem* **278,** 27208-27215.

Brightling CE, Ammit AJ, Kaur D, Black JL, Wardlaw AJ, Hughes JM & Bradding P. (2005). The CXCL10/CXCR3 axis mediates human lung mast cell migration to asthmatic airway smooth muscle. *Am J Respir Crit Care Med* **171,** 1103-1108.

Brightling CE, Bradding P, Symon FA, Holgate ST, Wardlaw AJ & Pavord ID. (2002). Mast-cell infiltration of airway smooth muscle in asthma. *N Engl J Med* **346,** 1699-1705.

Broad LM, Cannon TR & Taylor CW. (1999). A non-capacitative pathway activated by arachidonic acid is the major Ca^{2+} entry mechanism in rat A7r5 smooth muscle cells stimulated with low concentrations of vasopressin. *J Physiol* **517 (Pt 1),** 121-134.

Broide DH, Gleich GJ, Cuomo AJ, Coburn DA, Federman EC, Schwartz LB & Wasserman SI. (1991). Evidence of ongoing mast cell and eosinophil degranulation in symptomatic asthma airway. *J Allergy Clin Immunol* **88,** 637-648.

Bulanova E & Bulfone-Paus S. (2010). P2 receptor-mediated signaling in mast cell biology. *Purinergic Signal* **6,** 3-17.

Burd PR, Rogers HW, Gordon JR, Martin CA, Jayaraman S, Wilson SD, Dvorak AM, Galli SJ & Dorf ME. (1989). Interleukin 3-dependent and -independent mast cells stimulated with IgE and antigen express multiple cytokines. *J Exp Med* **170,** 245-257.

Butterfield JH, Weiler D, Dewald G & Gleich GJ. (1988). Establishment of an immature mast cell line from a patient with mast cell leukemia. *Leuk Res* **12,** 345-355.

Calloway N, Owens T, Corwith K, Rodgers W, Holowka D & Baird B. (2011). Stimulated association of STIM1 and Orai1 is regulated by the balance of PtdIns(4,5)P2 between distinct membrane pools. *J Cell Sci* **124,** 2602-2610.

Camaioni E, Boyer JL, Mohanram A, Harden TK & Jacobson KA. (1998). Deoxyadenosine bisphosphate derivatives as potent antagonists at P2Y1 receptors. *J Med Chem* **41,** 183-190.

Cantero-Recasens G, Fandos C, Rubio-Moscardo F, Valverde MA & Vicente R. (2010). The asthma-associated ORMDL3 gene product regulates endoplasmic reticulum-mediated calcium signaling and cellular stress. *Human molecular genetics* **19,** 111-121.

Carter RN, Tolhurst G, Walmsley G, Vizuete-Forster M, Miller N & Mahaut-Smith MP. (2006). Molecular and electrophysiological characterization of transient receptor potential ion channels in the primary murine megakaryocyte. *J Physiol* **576,** 151-162.

Cass R, Riley JF, West GB, Head KW & Stroud SW. (1954). Heparin and histamine in mast-cell tumours from dogs. *Nature* **174,** 318-319.

Caterina MJ, Schumacher MA, Tominaga M, Rosen TA, Levine JD & Julius D. (1997). The capsaicin receptor: a heat-activated ion channel in the pain pathway. *Nature* **389,** 816-824.

Cavalie A. (2007). Ionic channels formed by TRPC4. *Handb Exp Pharmacol***,** 93-108.

Cayouette S, Lussier MP, Mathieu EL, Bousquet SM & Boulay G. (2004). Exocytotic insertion of TRPC6 channel into the plasma membrane upon Gq protein-coupled receptor activation. *J Biol Chem* **279,** 7241-7246.

Chang WC, Di Capite J, Nelson C & Parekh AB. (2007). All-or-none activation of CRAC channels by agonist elicits graded responses in populations of mast cells. *J Immunol* **179,** 5255-5263.

Chen CC, Grimbaldeston MA, Tsai M, Weissman IL & Galli SJ. (2005). Identification of mast cell progenitors in adult mice. *Proc Natl Acad Sci U S A* **102,** 11408-11413.

Cheng KT, Liu X, Ong HL & Ambudkar IS. (2008). Functional requirement for Orai1 in store-operated TRPC1-STIM1 channels. *J Biol Chem* **283,** 12935-12940.

Cheng KT, Liu X, Ong HL, Swaim W & Ambudkar IS. (2011). Local Ca(2)+ entry via Orai1 regulates plasma membrane recruitment of TRPC1 and controls cytosolic Ca(2)+ signals required for specific cell functions. *PLoS Biol* **9,** e1001025.

Cheng Y, Huo Q, Lu J, Li R & Wang K. (1999). The transport kinetics of lanthanide species in a single erythrocyte probed by confocal laser scanning microscopy. *J Biol Inorg Chem* **4,** 447-456.

Chuang HH, Prescott ED, Kong H, Shields S, Jordt SE, Basbaum AI, Chao MV & Julius D. (2001). Bradykinin and nerve growth factor release the capsaicin receptor from PtdIns(4,5)P2-mediated inhibition. *Nature* **411,** 957-962.

Chung KF & Barnes PJ. (1999). Cytokines in asthma. *Thorax* **54,** 825-857.

Chung SW, Wong PM, Shen-Ong G, Ruscetti S, Ishizaka T & Eaves CJ. (1986). Production of granulocyte-macrophage colony-stimulating factor by Abelson virus-induced tumorigenic mast cell lines. *Blood* **68,** 1074-1081.

Church MK & Hiroi J. (1987). Inhibition of IgE-dependent histamine release from human dispersed lung mast cells by anti-allergic drugs and salbutamol. *Br J Pharmacol* **90,** 421-429.

Cissel DS, Fraundorfer PF & Beaven MA. (1998). Thapsigargin-induced secretion is dependent on activation of a cholera toxin-sensitive and phosphatidylinositol-3-kinase-regulated phospholipase D in a mast cell line. *J Pharmacol Exp Ther* **285,** 110-118.

Clapham DE, Runnels LW & Strubing C. (2001). The TRP ion channel family. *Nat Rev Neurosci* **2,** 387-396.

Cochrane DE & Douglas WW. (1974). Calcium-induced extrusion of secretory granules (exocytosis) in mast cells exposed to 48-80 or the ionophores A-23187 and X-537A. *Proc Natl Acad Sci U S A* **71,** 408-412.

Colton CK & Zhu MX. (2007). 2-Aminoethoxydiphenyl borate as a common activator of TRPV1, TRPV2, and TRPV3 channels. *Handb Exp Pharmacol***,** 173-187.

Communi D, Gonzalez NS, Detheux M, Brezillon S, Lannoy V, Parmentier M & Boeynaems JM. (2001). Identification of a novel human ADP receptor coupled to G(i). *J Biol Chem* **276,** 41479-41485.

Communi D, Janssens R, Suarez-Huerta N, Robaye B & Boeynaems JM. (2000). Advances in signalling by extracellular nucleotides. the role and transduction mechanisms of P2Y receptors. *Cell Signal* **12,** 351-360.

Corteling RL, Li S, Giddings J, Westwick J, Poll C & Hall IP. (2004). Expression of transient receptor potential C6 and related transient receptor potential family members in human airway smooth muscle and lung tissue. *Am J Respir Cell Mol Biol* **30,** 145-154.

Cruse G, Duffy SM, Brightling CE & Bradding P. (2006). Functional KCa3.1 K+ channels are required for human lung mast cell migration. *Thorax* **61,** 880-885.

Cruse G, Kaur D, Yang W, Duffy SM, Brightling CE & Bradding P. (2005). Activation of human lung mast cells by monomeric immunoglobulin E. *Eur Respir J* **25,** 858-863.

Damann N, Owsianik G, Li S, Poll C & Nilius B. (2009). The calcium-conducting ion channel transient receptor potential canonical 6 is involved in macrophage inflammatory protein-2-induced migration of mouse neutrophils. *Acta Physiol (Oxf)* **195,** 3-11.

Dare E, Kifor O, Brown EM & Weber G. (1998). Characterization of the phosphatidylinositol-specific phospholipase C isozymes present in the bovine parathyroid and in human

kidney HEK-293 cells stably transfected with the human parathyroid Ca^{2+}-sensing receptor. *J Mol Endocrinol* **21,** 7-17.

DeHaven WI, Jones BF, Petranka JG, Smyth JT, Tomita T, Bird GS & Putney JW, Jr. (2009). TRPC channels function independently of STIM1 and Orai1. *J Physiol* **587,** 2275-2298.

DeHaven WI, Smyth JT, Boyles RR & Putney JW, Jr. (2007). Calcium inhibition and calcium potentiation of Orai1, Orai2, and Orai3 calcium release-activated calcium channels. *J Biol Chem* **282,** 17548-17556.

Di Sabatino A, Rovedatti L, Kaur R, Spencer JP, Brown JT, Morisset VD, Biancheri P, Leakey NA, Wilde JI, Scott L, Corazza GR, Lee K, Sengupta N, Knowles CH, Gunthorpe MJ, McLean PG, MacDonald TT & Kruidenier L. (2009). Targeting gut T cell Ca^{2+} release-activated Ca^{2+} channels inhibits T cell cytokine production and T-box transcription factor T-bet in inflammatory bowel disease. *J Immunol* **183,** 3454-3462.

Di Virgilio F. (2005). Purinergic mechanism in the immune system: A signal of danger for dendritic cells. *Purinergic Signal* **1,** 205-209.

Dietrich A & Gudermann T. (2007). Trpc6. *Handb Exp Pharmacol***,** 125-141.

Dietrich A, Kalwa H, Rost BR & Gudermann T. (2005a). The diacylgylcerol-sensitive TRPC3/6/7 subfamily of cation channels: functional characterization and physiological relevance. *Pflugers Arch* **451,** 72-80.

Dietrich A, Kalwa H, Storch U, Mederos y Schnitzler M, Salanova B, Pinkenburg O, Dubrovska G, Essin K, Gollasch M, Birnbaumer L & Gudermann T. (2007). Pressure-induced and store-operated cation influx in vascular smooth muscle cells is independent of TRPC1. *Pflugers Arch* **455,** 465-477.

Dietrich A, Mederos y Schnitzler M, Emmel J, Kalwa H, Hofmann T & Gudermann T. (2003). N-linked protein glycosylation is a major determinant for basal TRPC3 and TRPC6 channel activity. *J Biol Chem* **278,** 47842-47852.

Dietrich A, Mederos y Schnitzler M, Kalwa H, Storch U & Gudermann T. (2005b). Functional characterization and physiological relevance of the TRPC3/6/7 subfamily of cation channels. *Naunyn Schmiedebergs Arch Pharmacol* **371,** 257-265.

Dietrich A, Mederos YSM, Gollasch M, Gross V, Storch U, Dubrovska G, Obst M, Yildirim E, Salanova B, Kalwa H, Essin K, Pinkenburg O, Luft FC, Gudermann T & Birnbaumer L. (2005c). Increased vascular smooth muscle contractility in TRPC6-/- mice. *Mol Cell Biol* **25,** 6980-6989.

Dohke Y, Oh YS, Ambudkar IS & Turner RJ. (2004). Biogenesis and topology of the transient receptor potential Ca^{2+} channel TRPC1. *J Biol Chem* **279,** 12242-12248.

Drazen JM & Austen KF. (1987). Leukotrienes and airway responses. *Am Rev Respir Dis* **136,** 985-998.

Driver AG, Kukoly CA, Ali S & Mustafa SJ. (1993). Adenosine in bronchoalveolar lavage fluid in asthma. *Am Rev Respir Dis* **148,** 91-97.

Dubyak GR & el-Moatassim C. (1993). Signal transduction via P2-purinergic receptors for extracellular ATP and other nucleotides. *Am J Physiol* **265,** C577-606.

Duffy SM, Lawley WJ, Kaur D, Yang W & Bradding P. (2003). Inhibition of human mast cell proliferation and survival by tamoxifen in association with ion channel modulation. *J Allergy Clin Immunol* **112,** 965-972.

Duncan LM, Deeds J, Hunter J, Shao J, Holmgren LM, Woolf EA, Tepper RI & Shyjan AW. (1998). Down-regulation of the novel gene melastatin correlates with potential for melanoma metastasis. *Cancer Res* **58,** 1515-1520.

Dvorak AM. (1989). Human mast cells. *Adv Anat Embryol Cell Biol* **114,** 1-107.

Eccleston E, Leonard BJ, Lowe JS & Welford HJ. (1973). Basophilic leukaemia in the albino rat and a demonstration of the basopoietin. *Nat New Biol* **244,** 73-76.

Echtenacher B, Mannel DN & Hultner L. (1996). Critical protective role of mast cells in a model of acute septic peritonitis. *Nature* **381,** 75-77.

Eder P, Poteser M & Groschner K. (2007). TRPC3: a multifunctional, pore-forming signalling molecule. *Handb Exp Pharmacol***,** 77-92.

Eder P, Poteser M, Romanin C & Groschner K. (2005). Na(+) entry and modulation of Na(+)/Ca($^{2+}$) exchange as a key mechanism of TRPC signaling. *Pflugers Arch* **451,** 99-104.

Eisfeld J & Luckhoff A. (2007). Trpm2. *Handb Exp Pharmacol***,** 237-252.

El Boustany C, Bidaux G, Enfissi A, Delcourt P, Prevarskaya N & Capiod T. (2008). Capacitative calcium entry and transient receptor potential canonical 6 expression control human hepatoma cell proliferation. *Hepatology* **47,** 2068-2077.

Erdei A, Andreev S & Pecht I. (1995). Complement peptide C3a inhibits IgE-mediated triggering of rat mucosal mast cells. *Int Immunol* **7,** 1433-1439.

Estacion M, Li S, Sinkins WG, Gosling M, Bahra P, Poll C, Westwick J & Schilling WP. (2004). Activation of human TRPC6 channels by receptor stimulation. *J Biol Chem* **279,** 22047-22056.

Estacion M, Sinkins WG, Jones SW, Applegate MA & Schilling WP. (2006). Human TRPC6 expressed in HEK 293 cells forms non-selective cation channels with limited Ca^{2+} permeability. *J Physiol* **572,** 359-377.

Evans RJ, Lewis C, Buell G, Valera S, North RA & Surprenant A. (1995). Pharmacological characterization of heterologously expressed ATP-gated cation channels (P2x purinoceptors). *Mol Pharmacol* **48,** 178-183.

Falkenburger BH, Jensen JB, Dickson EJ, Suh BC & Hille B. (2010). Phosphoinositides: lipid regulators of membrane proteins. *J Physiol* **588,** 3179-3185.

Feng C, Mery AG, Beller EM, Favot C & Boyce JA. (2004). Adenine nucleotides inhibit cytokine generation by human mast cells through a Gs-coupled receptor. *J Immunol* **173,** 7539-7547.

Fenwick EM, Marty A & Neher E. (1982). A patch-clamp study of bovine chromaffin cells and of their sensitivity to acetylcholine. *J Physiol* **331,** 577-597.

Fernihough J, Gentry C, Bevan S & Winter J. (2005). Regulation of calcitonin gene-related peptide and TRPV1 in a rat model of osteoarthritis. *Neurosci Lett* **388,** 75-80.

Ferrari D, Chiozzi P, Falzoni S, Dal Susino M, Melchiorri L, Baricordi OR & Di Virgilio F. (1997). Extracellular ATP triggers IL-1 beta release by activating the purinergic P2Z receptor of human macrophages. *J Immunol* **159,** 1451-1458.

Ferreira MA, Matheson MC, Duffy DL, Marks GB, Hui J, Le Souef P, Danoy P, Baltic S, Nyholt DR, Jenkins M, Hayden C, Willemsen G, Ang W, Kuokkanen M, Beilby J, Cheah F, de Geus EJ, Ramasamy A, Vedantam S, Salomaa V, Madden PA, Heath AC, Hopper JL, Visscher PM,

Musk B, Leeder SR, Jarvelin MR, Pennell C, Boomsma DI, Hirschhorn JN, Walters H, Martin NG, James A, Jones G, Abramson MJ, Robertson CF, Dharmage SC, Brown MA, Montgomery GW & Thompson PJ. (2011). Identification of IL6R and chromosome 11q13.5 as risk loci for asthma. *Lancet* **378,** 1006-1014.

Feske S, Gwack Y, Prakriya M, Srikanth S, Puppel SH, Tanasa B, Hogan PG, Lewis RS, Daly M & Rao A. (2006). A mutation in Orai1 causes immune deficiency by abrogating CRAC channel function. *Nature* **441,** 179-185.

Field KA, Holowka D & Baird B. (1999). Structural aspects of the association of FcepsilonRI with detergent-resistant membranes. *J Biol Chem* **274,** 1753-1758.

Finney-Hayward TK, Popa MO, Bahra P, Li S, Poll CT, Gosling M, Nicholson AG, Russell RE, Kon OM, Jarai G, Westwick J, Barnes PJ & Donnelly LE. (2010). Expression of transient receptor potential c6 channels in human lung macrophages. *Am J Respir Cell Mol Biol* **43,** 296-304.

Flockerzi V. (2007). An introduction on TRP channels. *Handb Exp Pharmacol***,** 1-19.

Foreman JC & Mongar JL. (1972). The role of the alkaline earth ions in anaphylactic histamine secretion. *J Physiol* **224,** 753-769.

Forsythe P & Ennis M. (1999). Adenosine, mast cells and asthma. *Inflamm Res* **48,** 301-307.

Foster RR, Zadeh MA, Welsh GI, Satchell SC, Ye Y, Mathieson PW, Bates DO & Saleem MA. (2009). Flufenamic acid is a tool for investigating TRPC6-mediated calcium signalling in human conditionally immortalised podocytes and HEK-293 cells. *Cell Calcium* **45,** 384-390.

Franzius D, Hoth M & Penner R. (1994). Non-specific effects of calcium entry antagonists in mast cells. *Pflugers Arch* **428,** 433-438.

Freichel M, Suh SH, Pfeifer A, Schweig U, Trost C, Weissgerber P, Biel M, Philipp S, Freise D, Droogmans G, Hofmann F, Flockerzi V & Nilius B. (2001). Lack of an endothelial store-operated Ca^{2+} current impairs agonist-dependent vasorelaxation in TRP4-/- mice. *Nat Cell Biol* **3,** 121-127.

Furuichi K, Rivera J & Isersky C. (1985). The receptor for immunoglobulin E on rat basophilic leukemia cells: effect of ligand binding on receptor expression. *Proc Natl Acad Sci U S A* **82,** 1522-1525.

Furukawa T, Yamakawa T, Midera T, Sagawa T, Mori Y & Nukada T. (1999). Selectivities of dihydropyridine derivatives in blocking $Ca(^{2+})$ channel subtypes expressed in Xenopus oocytes. *J Pharmacol Exp Ther* **291,** 464-473.

Galli SJ, Nakae S & Tsai M. (2005). Mast cells in the development of adaptive immune responses. *Nat Immunol* **6,** 135-142.

Galli SJ, Tsai M & Wershil BK. (1993). The c-kit receptor, stem cell factor, and mast cells. What each is teaching us about the others. *Am J Pathol* **142,** 965-974.

Gao ZG, Ding Y & Jacobson KA. (2010). P2Y(13) receptor is responsible for ADP-mediated degranulation in RBL-2H3 rat mast cells. *Pharmacol Res* **62,** 500-505.

Garcia-Anoveros J & Nagata K. (2007). Trpa1. *Handb Exp Pharmacol***,** 347-362.

Giannini D, Carletti A, Dente FL, Bacci E, Di Franco A, Vagaggini B & Paggiaro PL. (1996). Tolerance to the protective effect of salmeterol on allergen challenge. *Chest* **110,** 1452-1457.

Gilfillan AM & Tkaczyk C. (2006). Integrated signalling pathways for mast-cell activation. *Nat Rev Immunol* **6,** 218-230.

Gilfillan AM, Wiggan GA & Welton AF. (1990). Pertussis toxin pretreatment reveals differential effects of adenosine analogs on IgE-dependent histamine and peptidoleukotriene release from RBL-2H3 cells. *Biochim Biophys Acta* **1052,** 467-474.

Gimborn K, Lessmann E, Kuppig S, Krystal G & Huber M. (2005). SHIP down-regulates FcepsilonR1-induced degranulation at supraoptimal IgE or antigen levels. *J Immunol* **174,** 507-516.

Gordon JR & Galli SJ. (1990). Mast cells as a source of both preformed and immunologically inducible TNF-alpha/cachectin. *Nature* **346,** 274-276.

Greka A, Navarro B, Oancea E, Duggan A & Clapham DE. (2003). TRPC5 is a regulator of hippocampal neurite length and growth cone morphology. *Nat Neurosci* **6,** 837-845.

Grimbaldeston MA, Chen CC, Piliponsky AM, Tsai M, Tam SY & Galli SJ. (2005). Mast cell-deficient W-sash c-kit mutant Kit W-sh/W-sh mice as a model for investigating mast cell biology in vivo. *Am J Pathol* **167,** 835-848.

Grimm C, Kraft R, Sauerbruch S, Schultz G & Harteneck C. (2003). Molecular and functional characterization of the melastatin-related cation channel TRPM3. *J Biol Chem* **278,** 21493-21501.

Grimm C, Kraft R, Schultz G & Harteneck C. (2005). Activation of the melastatin-related cation channel TRPM3 by D-erythro-sphingosine [corrected]. *Mol Pharmacol* **67,** 798-805.

Gross SA, Guzman GA, Wissenbach U, Philipp SE, Zhu MX, Bruns D & Cavalie A. (2009). TRPC5 is a Ca^{2+}-activated channel functionally coupled to Ca^{2+}-selective ion channels. *J Biol Chem* **284,** 34423-34432.

Guhl S, Babina M, Neou A, Zuberbier T & Artuc M. (2010). Mast cell lines HMC-1 and LAD2 in comparison with mature human skin mast cells--drastically reduced levels of tryptase and chymase in mast cell lines. *Exp Dermatol* **19,** 845-847.

Guilbert A, Dhennin-Duthille I, Hiani YE, Haren N, Khorsi H, Sevestre H, Ahidouch A & Ouadid-Ahidouch H. (2008). Expression of TRPC6 channels in human epithelial breast cancer cells. *BMC Cancer* **8,** 125.

Gurish MF, Tao H, Abonia JP, Arya A, Friend DS, Parker CM & Austen KF. (2001). Intestinal mast cell progenitors require CD49dbeta7 (alpha4beta7 integrin) for tissue-specific homing. *J Exp Med* **194,** 1243-1252.

Halaszovich CR, Zitt C, Jungling E & Luckhoff A. (2000). Inhibition of TRP3 channels by lanthanides. Block from the cytosolic side of the plasma membrane. *J Biol Chem* **275,** 37423-37428.

Hamdollah Zadeh MA, Glass CA, Magnussen A, Hancox JC & Bates DO. (2008). VEGF-mediated elevated intracellular calcium and angiogenesis in human microvascular endothelial cells in vitro are inhibited by dominant negative TRPC6. *Microcirculation* **15,** 605-614.

Hamill OP, Marty A, Neher E, Sakmann B & Sigworth FJ. (1981). Improved patch-clamp techniques for high-resolution current recording from cells and cell-free membrane patches. *Pflugers Arch* **391,** 85-100.

Hardie RC & Minke B. (1992). The trp gene is essential for a light-activated Ca^{2+} channel in Drosophila photoreceptors. *Neuron* **8,** 643-651.

Hartmann J, Dragicevic E, Adelsberger H, Henning HA, Sumser M, Abramowitz J, Blum R, Dietrich A, Freichel M, Flockerzi V, Birnbaumer L & Konnerth A. (2008). TRPC3 channels are required for synaptic transmission and motor coordination. *Neuron* **59,** 392-398.

Hartmann K, Henz BM, Kruger-Krasagakes S, Kohl J, Burger R, Guhl S, Haase I, Lippert U & Zuberbier T. (1997). C3a and C5a stimulate chemotaxis of human mast cells. *Blood* **89,** 2863-2870.

Havard S, Scola AM, Kay LJ, Ishmael SS, MacGlashan DW, Jr. & Peachell PT. (2011). Characterization of syk expression in human lung mast cells: relationship with function. *Clin Exp Allergy* **41,** 378-388.

Henz BM, Maurer M, Lippert U, Worm M & Babina M. (2001). Mast cells as initiators of immunity and host defense. *Exp Dermatol* **10,** 1-10.

Hide M & Beaven MA. (1991). Calcium influx in a rat mast cell (RBL-2H3) line. Use of multivalent metal ions to define its characteristics and role in exocytosis. *J Biol Chem* **266,** 15221-15229.

Hisatsune C, Kuroda Y, Nakamura K, Inoue T, Nakamura T, Michikawa T, Mizutani A & Mikoshiba K. (2004). Regulation of TRPC6 channel activity by tyrosine phosphorylation. *J Biol Chem* **279,** 18887-18894.

Hodgkin AL, Huxley AF & Katz B. (1952). Measurement of current-voltage relations in the membrane of the giant axon of Loligo. *J Physiol* **116,** 424-448.

Hofmann T, Obukhov AG, Schaefer M, Harteneck C, Gudermann T & Schultz G. (1999). Direct activation of human TRPC6 and TRPC3 channels by diacylglycerol. *Nature* **397,** 259-263.

Hofmann T, Schaefer M, Schultz G & Gudermann T. (2002). Subunit composition of mammalian transient receptor potential channels in living cells. *Proc Natl Acad Sci U S A* **99,** 7461-7466.

Hogan PG, Lewis RS & Rao A. (2010). Molecular basis of calcium signaling in lymphocytes: STIM and ORAI. *Annu Rev Immunol* **28,** 491-533.

Hong JH, Li Q, Kim MS, Shin DM, Feske S, Birnbaumer L, Cheng KT, Ambudkar IS & Muallem S. (2011). Polarized but differential localization and recruitment of STIM1, Orai1 and TRPC channels in secretory cells. *Traffic* **12,** 232-245.

Hopper-Borge E, Chen ZS, Shchaveleva I, Belinsky MG & Kruh GD. (2004). Analysis of the drug resistance profile of multidrug resistance protein 7 (ABCC10): resistance to docetaxel. *Cancer Res* **64,** 4927-4930.

Hoth M. (1995). Calcium and barium permeation through calcium release-activated calcium (CRAC) channels. *Pflugers Arch* **430,** 315-322.

Hoth M & Penner R. (1992). Depletion of intracellular calcium stores activates a calcium current in mast cells. *Nature* **355,** 353-356.

Hoth M & Penner R. (1993). Calcium release-activated calcium current in rat mast cells. *J Physiol* **465,** 359-386.

Howarth PH, Babu KS, Arshad HS, Lau L, Buckley M, McConnell W, Beckett P, Al Ali M, Chauhan A, Wilson SJ, Reynolds A, Davies DE & Holgate ST. (2005). Tumour necrosis factor (TNFalpha) as a novel therapeutic target in symptomatic corticosteroid dependent asthma. *Thorax* **60,** 1012-1018.

Huang GN, Zeng W, Kim JY, Yuan JP, Han L, Muallem S & Worley PF. (2006). STIM1 carboxyl-terminus activates native SOC, I(crac) and TRPC1 channels. *Nat Cell Biol* **8,** 1003-1010.

Huber M, Helgason CD, Damen JE, Liu L, Humphries RK & Krystal G. (1998). The src homology 2-containing inositol phosphatase (SHIP) is the gatekeeper of mast cell degranulation. *Proc Natl Acad Sci U S A* **95,** 11330-11335.

Hughes PJ, Holgate ST & Church MK. (1984). Adenosine inhibits and potentiates IgE-dependent histamine release from human lung mast cells by an A2-purinoceptor mediated mechanism. *Biochem Pharmacol* **33,** 3847-3852.

Hundley TR, Gilfillan AM, Tkaczyk C, Andrade MV, Metcalfe DD & Beaven MA. (2004). Kit and FcepsilonRI mediate unique and convergent signals for release of inflammatory mediators from human mast cells. *Blood* **104,** 2410-2417.

Hutchinson LE & McCloskey MA. (1995). Fc epsilon RI-mediated induction of nuclear factor of activated T-cells. *J Biol Chem* **270,** 16333-16338.

Idzko M, Hammad H, van Nimwegen M, Kool M, Willart MA, Muskens F, Hoogsteden HC, Luttmann W, Ferrari D, Di Virgilio F, Virchow JC, Jr. & Lambrecht BN. (2007). Extracellular ATP triggers and maintains asthmatic airway inflammation by activating dendritic cells. *Nat Med* **13,** 913-919.

Inoue R, Okada T, Onoue H, Hara Y, Shimizu S, Naitoh S, Ito Y & Mori Y. (2001). The transient receptor potential protein homologue TRP6 is the essential component of vascular alpha(1)-adrenoceptor-activated Ca($^{2+}$)-permeable cation channel. *Circ Res* **88,** 325-332.

Irani AA, Schechter NM, Craig SS, DeBlois G & Schwartz LB. (1986). Two types of human mast cells that have distinct neutral protease compositions. *Proc Natl Acad Sci U S A* **83,** 4464-4468.

Irani AM, Bradford TR, Kepley CL, Schechter NM & Schwartz LB. (1989). Detection of MCT and MCTC types of human mast cells by immunohistochemistry using new monoclonal anti-tryptase and anti-chymase antibodies. *J Histochem Cytochem* **37,** 1509-1515.

Ishizaka K & Ishizaka T. (1967). Identification of gamma-E-antibodies as a carrier of reaginic activity. *J Immunol* **99,** 1187-1198.

Iwata Y, Katanosaka Y, Arai Y, Komamura K, Miyatake K & Shigekawa M. (2003). A novel mechanism of myocyte degeneration involving the Ca^{2+}-permeable growth factor-regulated channel. *J Cell Biol* **161,** 957-967.

Jaffar ZH & Pearce FL. (1990). Histamine secretion from mast cells stimulated with ATP. *Agents Actions* **30,** 64-66.

Jardin I, Lopez JJ, Salido GM & Rosado JA. (2008). Orai1 mediates the interaction between STIM1 and hTRPC1 and regulates the mode of activation of hTRPC1-forming Ca^{2+} channels. *J Biol Chem* **283,** 25296-25304.

Jolly PS, Bektas M, Olivera A, Gonzalez-Espinosa C, Proia RL, Rivera J, Milstien S & Spiegel S. (2004). Transactivation of sphingosine-1-phosphate receptors by FcepsilonRI triggering is required for normal mast cell degranulation and chemotaxis. *J Exp Med* **199,** 959-970.

Jung S, Muhle A, Schaefer M, Strotmann R, Schultz G & Plant TD. (2003). Lanthanides potentiate TRPC5 currents by an action at extracellular sites close to the pore mouth. *J Biol Chem* **278,** 3562-3571.

Jung S, Strotmann R, Schultz G & Plant TD. (2002). TRPC6 is a candidate channel involved in receptor-stimulated cation currents in A7r5 smooth muscle cells. *Am J Physiol Cell Physiol* **282,** C347-359.

Kahner BN, Shankar H, Murugappan S, Prasad GL & Kunapuli SP. (2006). Nucleotide receptor signaling in platelets. *J Thromb Haemost* **4,** 2317-2326.

Kaiser RA & Buxton IL. (2002). Nucleotide-mediated relaxation in guinea-pig aorta: selective inhibition by MRS2179. *Br J Pharmacol* **135,** 537-545.

Kambe N, Kambe M, Kochan JP & Schwartz LB. (2001). Human skin-derived mast cells can proliferate while retaining their characteristic functional and protease phenotypes. *Blood* **97,** 2045-2052.

Kanki H, Kinoshita M, Akaike A, Satoh M, Mori Y & Kaneko S. (2001). Activation of inositol 1,4,5-trisphosphate receptor is essential for the opening of mouse TRP5 channels. *Mol Pharmacol* **60,** 989-998.

Kelley GG, Kaproth-Joslin KA, Reks SE, Smrcka AV & Wojcikiewicz RJ. (2006). G-protein-coupled receptor agonists activate endogenous phospholipase Cepsilon and phospholipase Cbeta3 in a temporally distinct manner. *J Biol Chem* **281,** 2639-2648.

Kim EY, Alvarez-Baron CP & Dryer SE. (2009a). Canonical transient receptor potential channel (TRPC)3 and TRPC6 associate with large-conductance Ca^{2+}-activated K+ (BKCa) channels: role in BKCa trafficking to the surface of cultured podocytes. *Mol Pharmacol* **75,** 466-477.

Kim MS, Zeng W, Yuan JP, Shin DM, Worley PF & Muallem S. (2009b). Native Store-operated Ca^{2+} Influx Requires the Channel Function of Orai1 and TRPC1. *J Biol Chem* **284,** 9733-9741.

Kinet JP. (1999). The high-affinity IgE receptor (Fc epsilon RI): from physiology to pathology. *Annu Rev Immunol* **17,** 931-972.

Kirshenbaum AS, Akin C, Wu Y, Rottem M, Goff JP, Beaven MA, Rao VK & Metcalfe DD. (2003). Characterization of novel stem cell factor responsive human mast cell lines LAD 1 and 2 established from a patient with mast cell sarcoma/leukemia; activation following aggregation of FcepsilonRI or FcgammaRI. *Leuk Res* **27,** 677-682.

Kirshenbaum AS, Goff JP, Semere T, Foster B, Scott LM & Metcalfe DD. (1999). Demonstration that human mast cells arise from a progenitor cell population that is CD34(+), c-kit(+), and expresses aminopeptidase N (CD13). *Blood* **94,** 2333-2342.

Kitamura Y. (1989). Heterogeneity of mast cells and phenotypic change between subpopulations. *Annu Rev Immunol* **7,** 59-76.

Kitamura Y, Go S & Hatanaka K. (1978). Decrease of mast cells in W/Wv mice and their increase by bone marrow transplantation. *Blood* **52,** 447-452.

Koarai A, Ichinose M, Ishigaki-Suzuki S, Yamagata S, Sugiura H, Sakurai E, Makabe-Kobayashi Y, Kuramasu A, Watanabe T, Shirato K, Hattori T & Ohtsu H. (2003). Disruption of L-histidine decarboxylase reduces airway eosinophilia but not hyperresponsiveness. *Am J Respir Crit Care Med* **167,** 758-763.

Kuehn HS & Gilfillan AM. (2007). G protein-coupled receptors and the modification of FcepsilonRI-mediated mast cell activation. *Immunol Lett* **113,** 59-69.

Kushnir-Sukhov NM, Brown JM, Wu Y, Kirshenbaum A & Metcalfe DD. (2007). Human mast cells are capable of serotonin synthesis and release. *J Allergy Clin Immunol* **119,** 498-499.

Laidlaw TM, Steinke JW, Tinana AM, Feng C, Xing W, Lam BK, Paruchuri S, Boyce JA & Borish L. (2011). Characterization of a novel human mast cell line that responds to stem cell factor and expresses functional FcepsilonRI. *J Allergy Clin Immunol* **127,** 815-822 e811-815.

Landsteiner K & Simms S. (1923). Production of Heterogenetic Antibodies with Mixtures of the Binding Part of the Antigen and Protein. *J Exp Med* **38,** 127-138.

Lee KP, Yuan JP, Hong JH, So I, Worley PF & Muallem S. (2010). An endoplasmic reticulum/plasma membrane junction: STIM1/Orai1/TRPCs. *FEBS Lett* **584,** 2022-2027.

Lee N, Chen J, Sun L, Wu S, Gray KR, Rich A, Huang M, Lin JH, Feder JN, Janovitz EB, Levesque PC & Blanar MA. (2003a). Expression and characterization of human transient receptor potential melastatin 3 (hTRPM3). *J Biol Chem* **278,** 20890-20897.

Lee RJ & Oliver JM. (1995). Roles for Ca^{2+} stores release and two Ca^{2+} influx pathways in the Fc epsilon R1-activated Ca^{2+} responses of RBL-2H3 mast cells. *Mol Biol Cell* **6,** 825-839.

Lee YM, Kim BJ, Kim HJ, Yang DK, Zhu MH, Lee KP, So I & Kim KW. (2003b). TRPC5 as a candidate for the nonselective cation channel activated by muscarinic stimulation in murine stomach. *Am J Physiol Gastrointest Liver Physiol* **284,** G604-616.

Lepple-Wienhues A & Cahalan MD. (1996). Conductance and permeation of monovalent cations through depletion-activated Ca^{2+} channels (ICRAC) in Jurkat T cells. *Biophys J* **71,** 787-794.

Leung YM, Kwan CY & Loh TT. (1996). Dual effects of SK&F 96365 in human leukemic HL-60 cells. Inhibition of calcium entry and activation of a novel cation influx pathway. *Biochem Pharmacol* **51,** 605-612.

Li J, McKeown L, Ojelabi O, Stacey M, Foster R, O'Regan D, Porter KE & Beech DJ. (2011). Nanomolar potency and selectivity of a CRAC channel blocker against store-operated $Ca(^{2+})$ -entry and migration of vascular smooth muscle cells. *Br J Pharmacol*.

Li J, Sukumar P, Milligan CJ, Kumar B, Ma ZY, Munsch CM, Jiang LH, Porter KE & Beech DJ. (2008). Interactions, functions, and independence of plasma membrane STIM1 and TRPC1 in vascular smooth muscle cells. *Circ Res* **103,** e97-104.

Li S, Gosling M & Poll C. (2005). Determining the functional role of TRPC channels in primary cells. *Pflugers Arch* **451,** 43-52.

Lian L, Wang Y, Draznin J, Eslin D, Bennett JS, Poncz M, Wu D & Abrams CS. (2005). The relative role of PLCbeta and PI3Kgamma in platelet activation. *Blood* **106,** 110-117.

Liao Y, Erxleben C, Abramowitz J, Flockerzi V, Zhu MX, Armstrong DL & Birnbaumer L. (2008). Functional interactions among Orai1, TRPCs, and STIM1 suggest a STIM-regulated heteromeric Orai/TRPC model for SOCE/Icrac channels. *Proc Natl Acad Sci U S A* **105,** 2895-2900.

Liao Y, Plummer NW, George MD, Abramowitz J, Zhu MX & Birnbaumer L. (2009). A role for Orai in TRPC-mediated Ca^{2+} entry suggests that a TRPC:Orai complex may mediate store and receptor operated Ca^{2+} entry. *Proc Natl Acad Sci U S A* **106,** 3202-3206.

Lievremont JP, Bird GS & Putney JW, Jr. (2005). Mechanism of inhibition of TRPC cation channels by 2-aminoethoxydiphenylborane. *Mol Pharmacol* **68,** 758-762.

Liman ER. (2007). TRPM5 and taste transduction. *Handb Exp Pharmacol***,** 287-298.

Lingwood D & Simons K. (2010). Lipid rafts as a membrane-organizing principle. *Science* **327,** 46-50.

Liou J, Kim ML, Heo WD, Jones JT, Myers JW, Ferrell JE, Jr. & Meyer T. (2005). STIM is a Ca^{2+} sensor essential for Ca^{2+}-store-depletion-triggered Ca^{2+} influx. *Curr Biol* **15,** 1235-1241.

Lis A, Peinelt C, Beck A, Parvez S, Monteilh-Zoller M, Fleig A & Penner R. (2007). CRACM1, CRACM2, and CRACM3 are store-operated Ca^{2+} channels with distinct functional properties. *Curr Biol* **17,** 794-800.

Liu X, Bandyopadhyay BC, Singh BB, Groschner K & Ambudkar IS. (2005). Molecular analysis of a store-operated and 2-acetyl-sn-glycerol-sensitive non-selective cation channel. Heteromeric assembly of TRPC1-TRPC3. *J Biol Chem* **280,** 21600-21606.

Liu X, Cheng KT, Bandyopadhyay BC, Pani B, Dietrich A, Paria BC, Swaim WD, Beech D, Yildrim E, Singh BB, Birnbaumer L & Ambudkar IS. (2007). Attenuation of store-operated Ca^{2+} current impairs salivary gland fluid secretion in TRPC1(-/-) mice. *Proc Natl Acad Sci U S A* **104,** 17542-17547.

Liu X, Singh BB & Ambudkar IS. (2003). TRPC1 is required for functional store-operated Ca^{2+} channels. Role of acidic amino acid residues in the S5-S6 region. *J Biol Chem* **278,** 11337-11343.

Lockwich T, Singh BB, Liu X & Ambudkar IS. (2001). Stabilization of cortical actin induces internalization of transient receptor potential 3 (Trp3)-associated caveolar Ca^{2+} signaling complex and loss of Ca^{2+} influx without disruption of Trp3-inositol trisphosphate receptor association. *J Biol Chem* **276,** 42401-42408.

Lundequist A & Pejler G. (2011). Biological implications of preformed mast cell mediators. *Cell Mol Life Sci* **68,** 965-975.

Lytton J, Westlin M & Hanley MR. (1991). Thapsigargin inhibits the sarcoplasmic or endoplasmic reticulum Ca-ATPase family of calcium pumps. *J Biol Chem* **266,** 17067-17071.

Ma HT & Beaven MA. (2011). Regulators of $Ca(^{2+})$ signaling in mast cells: potential targets for treatment of mast cell-related diseases? *Adv Exp Med Biol* **716,** 62-90.

Ma HT, Peng Z, Hiragun T, Iwaki S, Gilfillan AM & Beaven MA. (2008). Canonical transient receptor potential 5 channel in conjunction with Orai1 and STIM1 allows Sr^{2+} entry, optimal influx of Ca^{2+}, and degranulation in a rat mast cell line. *J Immunol* **180,** 2233-2239.

Mahaut-Smith MP, Ennion SJ, Rolf MG & Evans RJ. (2000). ADP is not an agonist at P2X(1) receptors: evidence for separate receptors stimulated by ATP and ADP on human platelets. *Br J Pharmacol* **131,** 108-114.

Malaviya R, Twesten NJ, Ross EA, Abraham SN & Pfeifer JD. (1996). Mast cells process bacterial Ags through a phagocytic route for class I MHC presentation to T cells. *J Immunol* **156,** 1490-1496.

Mao GF, Vaidyula VR, Kunapuli SP & Rao AK. (2002). Lineage-specific defect in gene expression in human platelet phospholipase C-beta2 deficiency. *Blood* **99,** 905-911.

Mao YS & Yin HL. (2007). Regulation of the actin cytoskeleton by phosphatidylinositol 4-phosphate 5 kinases. *Pflugers Arch* **455,** 5-18.

Maroto R, Raso A, Wood TG, Kurosky A, Martinac B & Hamill OP. (2005). TRPC1 forms the stretch-activated cation channel in vertebrate cells. *Nat Cell Biol* **7,** 179-185.

Marquardt DL & Walker LL. (2000). Dependence of mast cell IgE-mediated cytokine production on nuclear factor-kappaB activity. *J Allergy Clin Immunol* **105,** 500-505.

Mazurek N, Regazzi R, Borner C, Wyss R, Conscience JF, Erne P, Eppenberger U & Fabbro D. (1987). Altered protein kinase C in a mast cell variant defective in exocytosis. *Proc Natl Acad Sci U S A* **84,** 1277-1281.

McDermott JR, Bartram RE, Knight PA, Miller HR, Garrod DR & Grencis RK. (2003). Mast cells disrupt epithelial barrier function during enteric nematode infection. *Proc Natl Acad Sci U S A* **100,** 7761-7766.

McKay RR, Szymeczek-Seay CL, Lievremont JP, Bird GS, Zitt C, Jungling E, Luckhoff A & Putney JW, Jr. (2000). Cloning and expression of the human transient receptor potential 4 (TRP4) gene: localization and functional expression of human TRP4 and TRP3. *Biochem J* **351 Pt 3,** 735-746.

McLachlan JB, Hart JP, Pizzo SV, Shelburne CP, Staats HF, Gunn MD & Abraham SN. (2003). Mast cell-derived tumor necrosis factor induces hypertrophy of draining lymph nodes during infection. *Nat Immunol* **4,** 1199-1205.

Melicoff E, Sansores-Garcia L, Gomez A, Moreira DC, Datta P, Thakur P, Petrova Y, Siddiqi T, Murthy JN, Dickey BF, Heidelberger R & Adachi R. (2009). Synaptotagmin-2 controls regulated exocytosis but not other secretory responses of mast cells. *J Biol Chem* **284,** 19445-19451.

Mensenkamp AR, Hoenderop JG & Bindels RJ. (2007). TRPV5, the gateway to Ca^{2+} homeostasis. *Handb Exp Pharmacol***,** 207-220.

Mercer JC, Dehaven WI, Smyth JT, Wedel B, Boyles RR, Bird GS & Putney JW, Jr. (2006). Large store-operated calcium selective currents due to co-expression of Orai1 or Orai2 with the intracellular calcium sensor, Stim1. *J Biol Chem* **281,** 24979-24990.

Merritt JE, Armstrong WP, Benham CD, Hallam TJ, Jacob R, Jaxa-Chamiec A, Leigh BK, McCarthy SA, Moores KE & Rink TJ. (1990). SK&F 96365, a novel inhibitor of receptor-mediated calcium entry. *Biochem J* **271,** 515-522.

Merritt JE, Sullivan JA, Tse J, Wilkinson S & Nixon JS. (1997). Different sensitivities of neutrophil responses to a selective protein kinase C inhibitor Ro 31-8425; redundancy in signal transduction. *Cell Signal* **9,** 53-57.

Mery L, Strauss B, Dufour JF, Krause KH & Hoth M. (2002). The PDZ-interacting domain of TRPC4 controls its localization and surface expression in HEK-293 cells. *J Cell Sci* **115,** 3497-3508.

Metcalfe DD, Baram D & Mekori YA. (1997). Mast cells. *Physiol Rev* **77,** 1033-1079.

Metcalfe DD, Lewis RA, Silbert JE, Rosenberg RD, Wasserman SI & Austen KF. (1979). Isolation and characterization of heparin from human lung. *J Clin Invest* **64,** 1537-1543.

Metz M & Maurer M. (2007). Mast cells--key effector cells in immune responses. *Trends Immunol* **28,** 234-241.

Meyer zu Heringdorf D, Lass H, Kuchar I, Lipinski M, Alemany R, Rumenapp U & Jakobs KH. (2001). Stimulation of intracellular sphingosine-1-phosphate production by G-protein-coupled sphingosine-1-phosphate receptors. *Eur J Pharmacol* **414,** 145-154.

Moffatt MF, Kabesch M, Liang L, Dixon AL, Strachan D, Heath S, Depner M, von Berg A, Bufe A, Rietschel E, Heinzmann A, Simma B, Frischer T, Willis-Owen SA, Wong KC, Illig T, Vogelberg C, Weiland SK, von Mutius E, Abecasis GR, Farrall M, Gut IG, Lathrop GM & Cookson WO. (2007). Genetic variants regulating ORMDL3 expression contribute to the risk of childhood asthma. *Nature* **448,** 470-473.

Moller A, Lippert U, Lessmann D, Kolde G, Hamann K, Welker P, Schadendorf D, Rosenbach T, Luger T & Czarnetzki BM. (1993). Human mast cells produce IL-8. *J Immunol* **151,** 3261-3266.

Montell C, Jones K, Hafen E & Rubin G. (1985). Rescue of the Drosophila phototransduction mutation trp by germline transformation. *Science* **230,** 1040-1043.

Mori Y, Wakamori M, Miyakawa T, Hermosura M, Hara Y, Nishida M, Hirose K, Mizushima A, Kurosaki M, Mori E, Gotoh K, Okada T, Fleig A, Penner R, Iino M & Kurosaki T. (2002). Transient receptor potential 1 regulates capacitative Ca($^{2+}$) entry and Ca($^{2+}$) release from endoplasmic reticulum in B lymphocytes. *J Exp Med* **195,** 673-681.

Munsch T, Freichel M, Flockerzi V & Pape HC. (2003). Contribution of transient receptor potential channels to the control of GABA release from dendrites. *Proc Natl Acad Sci U S A* **100,** 16065-16070.

Musio S, Gallo B, Scabeni S, Lapilla M, Poliani PL, Matarese G, Ohtsu H, Galli SJ, Mantegazza R, Steinman L & Pedotti R. (2006). A key regulatory role for histamine in experimental autoimmune encephalomyelitis: disease exacerbation in histidine decarboxylase-deficient mice. *J Immunol* **176,** 17-26.

Myrtek D & Idzko M. (2007). Chemotactic activity of extracellular nucleotideson human immune cells. *Purinergic Signal* **3,** 5-11.

Nakayama H, Wilkin BJ, Bodi I & Molkentin JD. (2006). Calcineurin-dependent cardiomyopathy is activated by TRPC in the adult mouse heart. *Faseb J* **20,** 1660-1670.

Neher E & Sakmann B. (1976). Single-channel currents recorded from membrane of denervated frog muscle fibres. *Nature* **260,** 799-802.

Ng LC, McCormack MD, Airey JA, Singer CA, Keller PS, Shen XM & Hume JR. (2009). TRPC1 and STIM1 mediate capacitative Ca^{2+} entry in mouse pulmonary arterial smooth muscle cells. *J Physiol* **587,** 2429-2442.

Ng SW, di Capite J, Singaravelu K & Parekh AB. (2008). Sustained activation of the tyrosine kinase Syk by antigen in mast cells requires local Ca^{2+} influx through Ca^{2+} release-activated Ca^{2+} channels. *J Biol Chem* **283,** 31348-31355.

Nicholas RA. (2001). Identification of the P2Y(12) receptor: a novel member of the P2Y family of receptors activated by extracellular nucleotides. *Mol Pharmacol* **60,** 416-420.

Nigrovic PA & Lee DM. (2007). Synovial mast cells: role in acute and chronic arthritis. *Immunol Rev* **217,** 19-37.

Nilius B, Owsianik G, Voets T & Peters JA. (2007). Transient receptor potential cation channels in disease. *Physiol Rev* **87,** 165-217.

Nilsson G, Blom T, Kusche-Gullberg M, Kjellen L, Butterfield JH, Sundstrom C, Nilsson K & Hellman L. (1994). Phenotypic characterization of the human mast-cell line HMC-1. *Scand J Immunol* **39,** 489-498.

North RA & Surprenant A. (2000). Pharmacology of cloned P2X receptors. *Annu Rev Pharmacol Toxicol* **40,** 563-580.

Numaga T, Wakamori M & Mori Y. (2007). Trpc7. *Handb Exp Pharmacol***,** 143-151.

Oberwinkler J & Phillipp SE. (2007). Trpm3. *Handb Exp Pharmacol***,** 253-267.

Obukhov AG & Nowycky MC. (2002). TRPC4 can be activated by G-protein-coupled receptors and provides sufficient Ca($^{2+}$) to trigger exocytosis in neuroendocrine cells. *J Biol Chem* **277,** 16172-16178.

Oda M, Sato-Nakamura N & Azuma T. (2004). Molecular characterization of monovalent and multivalent hapten-protein conjugates for analysis of the antigen--antibody interaction. *Anal Biochem* **333,** 365-371.

Oda M, Uchiyama S, Noda M, Nishi Y, Koga M, Mayanagi K, Robinson CV, Fukui K, Kobayashi Y, Morikawa K & Azuma T. (2009). Effects of antibody affinity and antigen valence on molecular forms of immune complexes. *Mol Immunol* **47,** 357-364.

Ohkawara Y, Yamauchi K, Tanno Y, Tamura G, Ohtani H, Nagura H, Ohkuda K & Takishima T. (1992). Human lung mast cells and pulmonary macrophages produce tumor necrosis factor-alpha in sensitized lung tissue after IgE receptor triggering. *Am J Respir Cell Mol Biol* **7,** 385-392.

Ohya Y, Kitamura K & Kuriyama H. (1988). Regulation of calcium current by intracellular calcium in smooth muscle cells of rabbit portal vein. *Circ Res* **62,** 375-383.

Okada T, Inoue R, Yamazaki K, Maeda A, Kurosaki T, Yamakuni T, Tanaka I, Shimizu S, Ikenaka K, Imoto K & Mori Y. (1999). Molecular and functional characterization of a novel mouse transient receptor potential protein homologue TRP7. Ca($^{2+}$)-permeable cation channel that is constitutively activated and enhanced by stimulation of G protein-coupled receptor. *J Biol Chem* **274,** 27359-27370.

Okada T, Shimizu S, Wakamori M, Maeda A, Kurosaki T, Takada N, Imoto K & Mori Y. (1998). Molecular cloning and functional characterization of a novel receptor-activated TRP Ca^{2+} channel from mouse brain. *J Biol Chem* **273,** 10279-10287.

Okayama Y, Hunt TC, Kassel O, Ashman LK & Church MK. (1994). Assessment of the anti-c-kit monoclonal antibody YB5.B8 in affinity magnetic enrichment of human lung mast cells. *J Immunol Methods* **169,** 153-161.

Olivera A, Mizugishi K, Tikhonova A, Ciaccia L, Odom S, Proia RL & Rivera J. (2007). The sphingosine kinase-sphingosine-1-phosphate axis is a determinant of mast cell function and anaphylaxis. *Immunity* **26,** 287-297.

Olivera A & Rivera J. (2005). Sphingolipids and the balancing of immune cell function: lessons from the mast cell. *J Immunol* **174,** 1153-1158.

Ong HL, Cheng KT, Liu X, Bandyopadhyay BC, Paria BC, Soboloff J, Pani B, Gwack Y, Srikanth S, Singh BB, Gill DL & Ambudkar IS. (2007). Dynamic assembly of TRPC1-STIM1-Orai1 ternary complex is involved in store-operated calcium influx. Evidence for similarities in store-operated and calcium release-activated calcium channel components. *J Biol Chem* **282,** 9105-9116.

Ortega E, Schweitzer-Stenner R & Pecht I. (1988). Possible orientational constraints determine secretory signals induced by aggregation of IgE receptors on mast cells. *Embo J* **7,** 4101-4109.

Osipchuk Y & Cahalan M. (1992). Cell-to-cell spread of calcium signals mediated by ATP receptors in mast cells. *Nature* **359,** 241-244.

Owen CE. (2007). Immunoglobulin E: role in asthma and allergic disease: lessons from the clinic. *Pharmacol Ther* **113,** 121-133.

Ozawa K, Szallasi Z, Kazanietz MG, Blumberg PM, Mischak H, Mushinski JF & Beaven MA. (1993). Ca($^{2+}$)-dependent and Ca($^{2+}$)-independent isozymes of protein kinase C mediate exocytosis in antigen-stimulated rat basophilic RBL-2H3 cells. Reconstitution of secretory responses with Ca^{2+} and purified isozymes in washed permeabilized cells. *J Biol Chem* **268,** 1749-1756.

Pani B, Ong HL, Liu X, Rauser K, Ambudkar IS & Singh BB. (2008). Lipid rafts determine clustering of STIM1 in endoplasmic reticulum-plasma membrane junctions and regulation of store-operated Ca^{2+} entry (SOCE). *J Biol Chem* **283,** 17333-17340.

Pani B & Singh BB. (2009). Lipid rafts/caveolae as microdomains of calcium signaling. *Cell Calcium* **45,** 625-633.

Paolini R, Jouvin MH & Kinet JP. (1991). Phosphorylation and dephosphorylation of the high-affinity receptor for immunoglobulin E immediately after receptor engagement and disengagement. *Nature* **353,** 855-858.

Paredes RM, Etzler JC, Watts LT, Zheng W & Lechleiter JD. (2008). Chemical calcium indicators. *Methods* **46,** 143-151.

Parekh AB & Putney JW, Jr. (2005). Store-operated calcium channels. *Physiol Rev* **85,** 757-810.

Park DJ, Min HK & Rhee SG. (1991). IgE-induced tyrosine phosphorylation of phospholipase C-gamma 1 in rat basophilic leukemia cells. *J Biol Chem* **266,** 24237-24240.

Parravicini V, Gadina M, Kovarova M, Odom S, Gonzalez-Espinosa C, Furumoto Y, Saitoh S, Samelson LE, O'Shea JJ & Rivera J. (2002). Fyn kinase initiates complementary signals required for IgE-dependent mast cell degranulation. *Nat Immunol* **3,** 741-748.

Peeters GA, Kohmoto O & Barry WH. (1989). Detection of La^{3+} influx in ventricular cells by indo-1 fluorescence. *Am J Physiol* **256,** C351-357.

Peinelt C, Vig M, Koomoa DL, Beck A, Nadler MJ, Koblan-Huberson M, Lis A, Fleig A, Penner R & Kinet JP. (2006). Amplification of CRAC current by STIM1 and CRACM1 (Orai1). *Nat Cell Biol* **8,** 771-773.

Penner R & Fleig A. (2007). The Mg^{2+} and $Mg(^{2+})$-nucleotide-regulated channel-kinase TRPM7. *Handb Exp Pharmacol***,** 313-328.

Philipp S, Cavalie A, Freichel M, Wissenbach U, Zimmer S, Trost C, Marquart A, Murakami M & Flockerzi V. (1996). A mammalian capacitative calcium entry channel homologous to Drosophila TRP and TRPL. *Embo J* **15,** 6166-6171.

Philipp S, Strauss B, Hirnet D, Wissenbach U, Mery L, Flockerzi V & Hoth M. (2003). TRPC3 mediates T-cell receptor-dependent calcium entry in human T-lymphocytes. *J Biol Chem* **278,** 26629-26638.

Pingle SC, Matta JA & Ahern GP. (2007). Capsaicin receptor: TRPV1 a promiscuous TRP channel. *Handb Exp Pharmacol***,** 155-171.

Plant TD & Schaefer M. (2003). TRPC4 and TRPC5: receptor-operated Ca^{2+}-permeable nonselective cation channels. *Cell Calcium* **33,** 441-450.

Plant TD & Strotmann R. (2007). Trpv4. *Handb Exp Pharmacol***,** 189-205.

Popp R, Englert HC, Lang HJ & Gogelein H. (1993). Inhibitors of nonselective cation channels in cells of the blood-brain barrier. *Exs* **66,** 213-218.

Prakriya M, Feske S, Gwack Y, Srikanth S, Rao A & Hogan PG. (2006). Orai1 is an essential pore subunit of the CRAC channel. *Nature* **443,** 230-233.

Prakriya M & Lewis RS. (2001). Potentiation and inhibition of $Ca(^{2+})$ release-activated $Ca(^{2+})$ channels by 2-aminoethyldiphenyl borate (2-APB) occurs independently of IP(3) receptors. *J Physiol* **536,** 3-19.

Prouvost-Danon A, Wyczolkowska J, Binaghi R & Abadie A. (1975). Mouse and rat IgE Cross-sensitization of mast cells and antigenic relationships. *Immunology* **29,** 151-162.

Puri N & Roche PA. (2008). Mast cells possess distinct secretory granule subsets whose exocytosis is regulated by different SNARE isoforms. *Proc Natl Acad Sci U S A* **105,** 2580-2585.

Putney JW, Jr. (1986). A model for receptor-regulated calcium entry. *Cell Calcium* **7,** 1-12.

Rae J, Cooper K, Gates P & Watsky M. (1991). Low access resistance perforated patch recordings using amphotericin B. *J Neurosci Methods* **37,** 15-26.

Ramkumar V, Stiles GL, Beaven MA & Ali H. (1993). The A3 adenosine receptor is the unique adenosine receptor which facilitates release of allergic mediators in mast cells. *J Biol Chem* **268,** 16887-16890.

Rao GK & Kaminski NE. (2006). Induction of intracellular calcium elevation by Delta9-tetrahydrocannabinol in T cells involves TRPC1 channels. *J Leukoc Biol* **79,** 202-213.

Reiser J, Polu KR, Moller CC, Kenlan P, Altintas MM, Wei C, Faul C, Herbert S, Villegas I, Avila-Casado C, McGee M, Sugimoto H, Brown D, Kalluri R, Mundel P, Smith PL, Clapham DE & Pollak MR. (2005). TRPC6 is a glomerular slit diaphragm-associated channel required for normal renal function. *Nat Genet* **37,** 739-744.

Rhee JS, Ebihara S & Akaike N. (1994). Gramicidin perforated patch-clamp technique reveals glycine-gated outward chloride current in dissociated nucleus solitarii neurons of the rat. *J Neurophysiol* **72,** 1103-1108.

Riccio A, Li Y, Moon J, Kim KS, Smith KS, Rudolph U, Gapon S, Yao GL, Tsvetkov E, Rodig SJ, Van't Veer A, Meloni EG, Carlezon WA, Jr., Bolshakov VY & Clapham DE. (2009). Essential role for TRPC5 in amygdala function and fear-related behavior. *Cell* **137,** 761-772.

Riccio A, Mattei C, Kelsell RE, Medhurst AD, Calver AR, Randall AD, Davis JB, Benham CD & Pangalos MN. (2002). Cloning and functional expression of human short TRP7, a candidate protein for store-operated Ca^{2+} influx. *J Biol Chem* **277,** 12302-12309.

Riley JF. (1953). The effects of histamine-liberators on the mast cells of the rat. *J Pathol Bacteriol* **65,** 471-479.

Riley JF & West GB. (1952). Histamine in tissue mast cells. *J Physiol* **117,** 72P-73P.

Rodrigo GJ, Neffen H & Castro-Rodriguez JA. (2011). Efficacy and safety of subcutaneous omalizumab vs placebo as add-on therapy to corticosteroids for children and adults with asthma: a systematic review. *Chest* **139,** 28-35.

Roedding AS, Li PP & Warsh JJ. (2006). Characterization of the transient receptor potential channels mediating lysophosphatidic acid-stimulated calcium mobilization in B lymphoblasts. *Life Sci* **80,** 89-97.

Roos J, DiGregorio PJ, Yeromin AV, Ohlsen K, Lioudyno M, Zhang S, Safrina O, Kozak JA, Wagner SL, Cahalan MD, Velicelebi G & Stauderman KA. (2005). STIM1, an essential and conserved component of store-operated Ca^{2+} channel function. *J Cell Biol* **169,** 435-445.

Rosado JA, Brownlow SL & Sage SO. (2002). Endogenously expressed Trp1 is involved in store-mediated Ca^{2+} entry by conformational coupling in human platelets. *J Biol Chem* **277,** 42157-42163.

Runnels LW, Yue L & Clapham DE. (2002). The TRPM7 channel is inactivated by PIP(2) hydrolysis. *Nat Cell Biol* **4,** 329-336.

Rychkov G & Barritt GJ. (2007). TRPC1 Ca($^{2+}$)-permeable channels in animal cells. *Handb Exp Pharmacol***,** 23-52.

Saba JD & Hla T. (2004). Point-counterpoint of sphingosine 1-phosphate metabolism. *Circ Res* **94,** 724-734.

Saito H, Ebisawa M, Reason DC, Ohno K, Kurihara K, Sakaguchi N, Ohgimi A, Saito E, Akasawa A, Akimoto K & et al. (1991). Extracellular ATP stimulates interleukin-dependent cultured mast cells and eosinophils through calcium mobilization. *Int Arch Allergy Appl Immunol* **94,** 68-70.

Sakura H & Ashcroft FM. (1997). Identification of four trp1 gene variants murine pancreatic beta-cells. *Diabetologia* **40,** 528-532.

Salido GM, Sage SO & Rosado JA. (2009). TRPC channels and store-operated Ca($^{2+}$) entry. *Biochim Biophys Acta* **1793,** 223-230.

Sanchez-Miranda E, Ibarra-Sanchez A & Gonzalez-Espinosa C. (2010). Fyn kinase controls FcepsilonRI receptor-operated calcium entry necessary for full degranulation in mast cells. *Biochem Biophys Res Commun* **391,** 1714-1720.

Sanmugalingam D, Wardlaw AJ & Bradding P. (2000). Adhesion of human lung mast cells to bronchial epithelium: evidence for a novel carbohydrate-mediated mechanism. *J Leukoc Biol* **68,** 38-46.

Sato E, Suzuki T, Hoshi N, Sugino T & Hasegawa H. (2008). Sodium azide induces necrotic cell death in rat squamous cell carcinoma SCC131. *Med Mol Morphol* **41,** 211-220.

Schaefer M, Plant TD, Obukhov AG, Hofmann T, Gudermann T & Schultz G. (2000). Receptor-mediated regulation of the nonselective cation channels TRPC4 and TRPC5. *J Biol Chem* **275,** 17517-17526.

Schilling T & Eder C. (2009). Non-selective cation channel activity is required for lysophosphatidylcholine-induced monocyte migration. *J Cell Physiol* **221,** 325-334.

Schilling WP, Rajan L & Strobl-Jager E. (1989). Characterization of the bradykinin-stimulated calcium influx pathway of cultured vascular endothelial cells. Saturability, selectivity, and kinetics. *J Biol Chem* **264,** 12838-12848.

Schulman ES, Glaum MC, Post T, Wang Y, Raible DG, Mohanty J, Butterfield JH & Pelleg A. (1999). ATP modulates anti-IgE-induced release of histamine from human lung mast cells. *Am J Respir Cell Mol Biol* **20,** 530-537.

Schwartz LB, Austen KF & Wasserman SI. (1979). Immunologic release of beta-hexosaminidase and beta-glucuronidase from purified rat serosal mast cells. *J Immunol* **123,** 1445-1450.

Schwartz LB, Irani AM, Roller K, Castells MC & Schechter NM. (1987). Quantitation of histamine, tryptase, and chymase in dispersed human T and TC mast cells. *J Immunol* **138,** 2611-2615.

Scrimgeour N, Litjens T, Ma L, Barritt GJ & Rychkov GY. (2009). Properties of Orai1 mediated store-operated current depend on the expression levels of STIM1 and Orai1 proteins. *J Physiol* **587,** 2903-2918.

Segal DM, Taurog JD & Metzger H. (1977). Dimeric immunoglobulin E serves as a unit signal for mast cell degranulation. *Proc Natl Acad Sci U S A* **74,** 2993-2997.

Sellge G & Bischoff SC. (2006). Isolation, culture, and characterization of intestinal mast cells. *Methods Mol Biol* **315,** 123-138.

Shi J, Mori E, Mori Y, Mori M, Li J, Ito Y & Inoue R. (2004). Multiple regulation by calcium of murine homologues of transient receptor potential proteins TRPC6 and TRPC7 expressed in HEK-293 cells. *J Physiol* **561,** 415-432.

Shim JY, Kim BS, Cho SH, Min KU & Hong SJ. (2003). Allergen-specific conventional immunotherapy decreases immunoglobulin E-mediated basophil histamine releasability. *Clin Exp Allergy* **33,** 52-57.

Singh A, Hildebrand ME, Garcia E & Snutch TP. (2010). The transient receptor potential channel antagonist SKF96365 is a potent blocker of low-voltage-activated T-type calcium channels. *Br J Pharmacol* **160,** 1464-1475.

Singh BB, Liu X, Tang J, Zhu MX & Ambudkar IS. (2002). Calmodulin regulates Ca($^{2+}$)-dependent feedback inhibition of store-operated Ca($^{2+}$) influx by interaction with a site in the C terminus of TrpC1. *Mol Cell* **9,** 739-750.

Sinkins WG, Estacion M & Schilling WP. (1998). Functional expression of TrpC1: a human homologue of the Drosophila Trp channel. *Biochem J* **331 (Pt 1),** 331-339.

Siraganian RP. (1974). An automated continuous-flow system for the extraction and fluorometric analysis of histamine. *Anal Biochem* **57,** 383-394.

Siraganian RP, Kulczycki A, Jr., Mendoza G & Metzger H. (1975). Ionophore A-23187 induced histamine release from rat mast cells and rat basophil leukemia (RBL-1) cells. *J Immunol* **115,** 1599-1602.

Sossey-Alaoui K, Lyon JA, Jones L, Abidi FE, Hartung AJ, Hane B, Schwartz CE, Stevenson RE & Srivastava AK. (1999). Molecular cloning and characterization of TRPC5 (HTRP5), the human homologue of a mouse brain receptor-activated capacitative Ca^{2+} entry channel. *Genomics* **60,** 330-340.

Stathopulos PB, Li GY, Plevin MJ, Ames JB & Ikura M. (2006). Stored Ca^{2+} depletion-induced oligomerization of stromal interaction molecule 1 (STIM1) via the EF-SAM region: An initiation mechanism for capacitive Ca^{2+} entry. *J Biol Chem* **281,** 35855-35862.

Strub GM, Maceyka M, Hait NC, Milstien S & Spiegel S. (2010). Extracellular and intracellular actions of sphingosine-1-phosphate. *Adv Exp Med Biol* **688,** 141-155.

Strubing C, Krapivinsky G, Krapivinsky L & Clapham DE. (2003). Formation of novel TRPC channels by complex subunit interactions in embryonic brain. *J Biol Chem* **278,** 39014-39019.

Suh BC & Hille B. (2002). Recovery from muscarinic modulation of M current channels requires phosphatidylinositol 4,5-bisphosphate synthesis. *Neuron* **35,** 507-520.

Suzuki R, Liu X, Olivera A, Aguiniga L, Yamashita Y, Blank U, Ambudkar I & Rivera J. (2010). Loss of TRPC1-mediated Ca^{2+} influx contributes to impaired degranulation in Fyn-deficient mouse bone marrow-derived mast cells. *J Leukoc Biol* **88,** 863-875.

Sweeney ZK, Minatti A, Button DC & Patrick S. (2009). Small-molecule inhibitors of store-operated calcium entry. *ChemMedChem* **4,** 706-718.

Swystun VA, Gordon JR, Davis EB, Zhang X & Cockcroft DW. (2000). Mast cell tryptase release and asthmatic responses to allergen increase with regular use of salbutamol. *J Allergy Clin Immunol* **106,** 57-64.

Tabata H, Tanaka S, Sugimoto Y, Kanki H, Kaneko S & Ichikawa A. (2002). Possible coupling of prostaglandin E receptor EP(1) to TRP5 expressed in Xenopus laevis oocytes. *Biochem Biophys Res Commun* **298,** 398-402.

Tadesse MG & Ibrahim JG. (2004). A bayesian hierarchical model for the analysis of Affymetrix arrays. *Ann N Y Acad Sci* **1020,** 41-48.

Tang J, Lin Y, Zhang Z, Tikunova S, Birnbaumer L & Zhu MX. (2001). Identification of common binding sites for calmodulin and inositol 1,4,5-trisphosphate receptors on the carboxyl termini of trp channels. *J Biol Chem* **276,** 21303-21310.

Tani D, Monteilh-Zoller MK, Fleig A & Penner R. (2007). Cell cycle-dependent regulation of store-operated I(CRAC) and Mg^{2+}-nucleotide-regulated MagNuM (TRPM7) currents. *Cell Calcium* **41,** 249-260.

Theoharides TC, Kempuraj D, Tagen M, Conti P & Kalogeromitros D. (2007). Differential release of mast cell mediators and the pathogenesis of inflammation. *Immunol Rev* **217,** 65-78.

Thienemann F, Henz BM & Babina M. (2004). Regulation of mast cell characteristics by cytokines: divergent effects of interleukin-4 on immature mast cell lines versus mature human skin mast cells. *Arch Dermatol Res* **296,** 134-138.

Thomson NC, Chaudhuri R & Spears M. (2011). Emerging therapies for severe asthma. *BMC Med* **9,** 102.

Tkaczyk C, Beaven MA, Brachman SM, Metcalfe DD & Gilfillan AM. (2003). The phospholipase C gamma 1-dependent pathway of Fc epsilon RI-mediated mast cell activation is regulated independently of phosphatidylinositol 3-kinase. *J Biol Chem* **278,** 48474-48484.

Tkaczyk C, Horejsi V, Iwaki S, Draber P, Samelson LE, Satterthwaite AB, Nahm DH, Metcalfe DD & Gilfillan AM. (2004). NTAL phosphorylation is a pivotal link between the signaling cascades leading to human mast cell degranulation following Kit activation and Fc epsilon RI aggregation. *Blood* **104,** 207-214.

Trebak M, Bird GS, McKay RR & Putney JW, Jr. (2002). Comparison of human TRPC3 channels in receptor-activated and store-operated modes. Differential sensitivity to channel blockers suggests fundamental differences in channel composition. *J Biol Chem* **277,** 21617-21623.

Trebak M, Vazquez G, Bird GS & Putney JW, Jr. (2003). The TRPC3/6/7 subfamily of cation channels. *Cell Calcium* **33,** 451-461.

Tsien RY. (1980). New calcium indicators and buffers with high selectivity against magnesium and protons: design, synthesis, and properties of prototype structures. *Biochemistry* **19,** 2396-2404.

Tsujimura T, Furitsu T, Morimoto M, Kanayama Y, Nomura S, Matsuzawa Y, Kitamura Y & Kanakura Y. (1995). Substitution of an aspartic acid results in constitutive activation of c-kit receptor tyrosine kinase in a rat tumor mast cell line RBL-2H3. *Int Arch Allergy Immunol* **106,** 377-385.

Tu P, Brandolin G & Bouron A. (2009a). The anti-inflammatory agent flufenamic acid depresses store-operated channels by altering mitochondrial calcium homeostasis. *Neuropharmacology* **56,** 1010-1016.

Tu P, Kunert-Keil C, Lucke S, Brinkmeier H & Bouron A. (2009b). Diacylglycerol analogues activate second messenger-operated calcium channels exhibiting TRPC-like properties in cortical neurons. *J Neurochem* **108,** 126-138.

Turner H, del Carmen KA & Stokes A. (2007). Link between TRPV channels and mast cell function. *Handb Exp Pharmacol***,** 457-471.

Uehara K. (2005). Localization of TRPC1 channel in the sinus endothelial cells of rat spleen. *Histochem Cell Biol* **123,** 347-356.

Uvelius B, Sigurdsson SB & Johansson B. (1974). Strontium and barium as Substitutes for calcium on electrical and mechanical activity in rat portal vein. *Blood Vessels* **11,** 245-259.

van Abel M, Hoenderop JG & Bindels RJ. (2005). The epithelial calcium channels TRPV5 and TRPV6: regulation and implications for disease. *Naunyn Schmiedebergs Arch Pharmacol* **371,** 295-306.

Vane JR & Botting RM. (2003). The mechanism of action of aspirin. *Thromb Res* **110,** 255-258.

Vanhaesebroeck B, Leevers SJ, Ahmadi K, Timms J, Katso R, Driscoll PC, Woscholski R, Parker PJ & Waterfield MD. (2001). Synthesis and function of 3-phosphorylated inositol lipids. *Annu Rev Biochem* **70,** 535-602.

Varga-Szabo D, Authi KS, Braun A, Bender M, Ambily A, Hassock SR, Gudermann T, Dietrich A & Nieswandt B. (2008). Store-operated Ca($^{2+}$) entry in platelets occurs independently of transient receptor potential (TRP) C1. *Pflugers Arch* **457,** 377-387.

Varghese A, Tenbroek EM, Coles J, Jr. & Sigg DC. (2006). Endogenous channels in HEK cells and potential roles in HCN ionic current measurements. *Prog Biophys Mol Biol* **90,** 26-37.

Vasudevan L, Jeromin A, Volpicelli-Daley L, De Camilli P, Holowka D & Baird B. (2009). The beta- and gamma-isoforms of type I PIP5K regulate distinct stages of Ca^{2+} signaling in mast cells. *J Cell Sci* **122,** 2567-2574.

Vazquez G, Wedel BJ, Trebak M, St John Bird G & Putney JW, Jr. (2003). Expression level of the canonical transient receptor potential 3 (TRPC3) channel determines its mechanism of activation. *J Biol Chem* **278,** 21649-21654.

Venkatachalam K, Zheng F & Gill DL. (2003). Regulation of canonical transient receptor potential (TRPC) channel function by diacylglycerol and protein kinase C. *J Biol Chem* **278,** 29031-29040.

Venkatesha RT, Berla Thangam E, Zaidi AK & Ali H. (2005). Distinct regulation of C3a-induced MCP-1/CCL2 and RANTES/CCL5 production in human mast cells by extracellular signal regulated kinase and PI3 kinase. *Mol Immunol* **42,** 581-587.

Vennekens R & Nilius B. (2007). Insights into TRPM4 function, regulation and physiological role. *Handb Exp Pharmacol***,** 269-285.

Vig M, Beck A, Billingsley JM, Lis A, Parvez S, Peinelt C, Koomoa DL, Soboloff J, Gill DL, Fleig A, Kinet JP & Penner R. (2006a). CRACM1 multimers form the ion-selective pore of the CRAC channel. *Curr Biol* **16,** 2073-2079.

Vig M, DeHaven WI, Bird GS, Billingsley JM, Wang H, Rao PE, Hutchings AB, Jouvin MH, Putney JW & Kinet JP. (2008). Defective mast cell effector functions in mice lacking the CRACM1 pore subunit of store-operated calcium release-activated calcium channels. *Nat Immunol* **9,** 89-96.

Vig M & Kinet JP. (2009). Calcium signaling in immune cells. *Nat Immunol* **10,** 21-27.

Vig M, Peinelt C, Beck A, Koomoa DL, Rabah D, Koblan-Huberson M, Kraft S, Turner H, Fleig A, Penner R & Kinet JP. (2006b). CRACM1 is a plasma membrane protein essential for store-operated Ca^{2+} entry. *Science* **312,** 1220-1223.

Voets T, Owsianik G & Nilius B. (2007). Trpm8. *Handb Exp Pharmacol***,** 329-344.

von Kugelgen I. (2006). Pharmacological profiles of cloned mammalian P2Y-receptor subtypes. *Pharmacol Ther* **110,** 415-432.

Vonakis BM, Gibbons S, Jr., Sora R, Langdon JM & MacDonald SM. (2001). Src homology 2 domain-containing inositol 5' phosphatase is negatively associated with histamine release to human recombinant histamine-releasing factor in human basophils. *J Allergy Clin Immunol* **108,** 822-831.

Walker S, Monteil M, Phelan K, Lasserson TJ & Walters EH. (2006). Anti-IgE for chronic asthma in adults and children. *Cochrane Database Syst Rev*, CD003559.

Wang GX & Poo MM. (2005). Requirement of TRPC channels in netrin-1-induced chemotropic turning of nerve growth cones. *Nature* **434,** 898-904.

Wang J, Laurier LG, Sims SM & Preiksaitis HG. (2003). Enhanced capacitative calcium entry and TRPC channel gene expression in human LES smooth muscle. *Am J Physiol Gastrointest Liver Physiol* **284,** G1074-1083.

Wang W, O'Connell B, Dykeman R, Sakai T, Delporte C, Swaim W, Zhu X, Birnbaumer L & Ambudkar IS. (1999). Cloning of Trp1beta isoform from rat brain: immunodetection and localization of the endogenous Trp1 protein. *Am J Physiol* **276,** C969-979.

Wang Y, Chen X, Lian L, Tang T, Stalker TJ, Sasaki T, Kanaho Y, Brass LF, Choi JK, Hartwig JH & Abrams CS. (2008). Loss of PIP5KIbeta demonstrates that PIP5KI isoform-specific PIP2 synthesis is required for IP3 formation. *Proc Natl Acad Sci U S A* **105,** 14064-14069.

Wareham K, Vial C, Wykes RC, Bradding P & Seward EP. (2009). Functional evidence for the expression of P2X1, P2X4 and P2X7 receptors in human lung mast cells. *Br J Pharmacol* **157,** 1215-1224.

Warnat J, Philipp S, Zimmer S, Flockerzi V & Cavalie A. (1999). Phenotype of a recombinant store-operated channel: highly selective permeation of Ca^{2+}. *J Physiol* **518 (Pt 3),** 631-638.

Wilde JI & Watson SP. (2001). Regulation of phospholipase C gamma isoforms in haematopoietic cells: why one, not the other? *Cell Signal* **13,** 691-701.

Wilkinson SE, Parker PJ & Nixon JS. (1993). Isoenzyme specificity of bisindolylmaleimides, selective inhibitors of protein kinase C. *Biochem J* **294 (Pt 2),** 335-337.

Winn MP, Daskalakis N, Spurney RF & Middleton JP. (2006). Unexpected role of TRPC6 channel in familial nephrotic syndrome: does it have clinical implications? *J Am Soc Nephrol* **17,** 378-387.

Wissenbach U & Niemeyer BA. (2007). Trpv6. *Handb Exp Pharmacol*, 221-234.

Witzgall R. (2007). TRPP2 channel regulation. *Handb Exp Pharmacol*, 363-375.

Woolhiser MR, Okayama Y, Gilfillan AM & Metcalfe DD. (2001). IgG-dependent activation of human mast cells following up-regulation of FcgammaRI by IFN-gamma. *Eur J Immunol* **31,** 3298-3307.

Wright JL, Tai H, Dai J & Churg A. (2002). Cigarette smoke induces rapid changes in gene expression in pulmonary arteries. *Lab Invest* **82,** 1391-1398.

Wu LJ, Sweet TB & Clapham DE. (2010). International Union of Basic and Clinical Pharmacology. LXXVI. Current progress in the mammalian TRP ion channel family. *Pharmacol Rev* **62,** 381-404.

Wu X, Babnigg G & Villereal ML. (2000). Functional significance of human trp1 and trp3 in store-operated Ca($^{2+}$) entry in HEK-293 cells. *Am J Physiol Cell Physiol* **278,** C526-536.

Wykes RC, Lee M, Duffy SM, Yang W, Seward EP & Bradding P. (2007). Functional transient receptor potential melastatin 7 channels are critical for human mast cell survival. *J Immunol* **179,** 4045-4052.

Xu SZ & Beech DJ. (2001). TrpC1 is a membrane-spanning subunit of store-operated Ca($^{2+}$) channels in native vascular smooth muscle cells. *Circ Res* **88,** 84-87.

Xu SZ, Boulay G, Flemming R & Beech DJ. (2006a). E3-targeted anti-TRPC5 antibody inhibits store-operated calcium entry in freshly isolated pial arterioles. *Am J Physiol Heart Circ Physiol* **291,** H2653-2659.

Xu SZ, Muraki K, Zeng F, Li J, Sukumar P, Shah S, Dedman AM, Flemming PK, McHugh D, Naylor J, Cheong A, Bateson AN, Munsch CM, Porter KE & Beech DJ. (2006b). A sphingosine-1-phosphate-activated calcium channel controlling vascular smooth muscle cell motility. *Circ Res* **98,** 1381-1389.

Xu SZ, Sukumar P, Zeng F, Li J, Jairaman A, English A, Naylor J, Ciurtin C, Majeed Y, Milligan CJ, Bahnasi YM, Al-Shawaf E, Porter KE, Jiang LH, Emery P, Sivaprasadarao A & Beech DJ. (2008). TRPC channel activation by extracellular thioredoxin. *Nature* **451,** 69-72.

Xu SZ, Zeng F, Boulay G, Grimm C, Harteneck C & Beech DJ. (2005a). Block of TRPC5 channels by 2-aminoethoxydiphenyl borate: a differential, extracellular and voltage-dependent effect. *Br J Pharmacol* **145,** 405-414.

Xu SZ, Zeng F, Lei M, Li J, Gao B, Xiong C, Sivaprasadarao A & Beech DJ. (2005b). Generation of functional ion-channel tools by E3 targeting. *Nat Biotechnol* **23,** 1289-1293.

Yamada H, Wakamori M, Hara Y, Takahashi Y, Konishi K, Imoto K & Mori Y. (2000). Spontaneous single-channel activity of neuronal TRP5 channel recombinantly expressed in HEK-293 cells. *Neurosci Lett* **285,** 111-114.

Yiangou Y, Facer P, Dyer NH, Chan CL, Knowles C, Williams NS & Anand P. (2001). Vanilloid receptor 1 immunoreactivity in inflamed human bowel. *Lancet* **357,** 1338-1339.

Yildirim E & Birnbaumer L. (2007). TRPC2: molecular biology and functional importance. *Handb Exp Pharmacol***,** 53-75.

Yildirim E, Kawasaki BT & Birnbaumer L. (2005). Molecular cloning of TRPC3a, an N-terminally extended, store-operated variant of the human C3 transient receptor potential channel. *Proc Natl Acad Sci U S A* **102,** 3307-3311.

Yuan JP, Zeng W, Dorwart MR, Choi YJ, Worley PF & Muallem S. (2009). SOAR and the polybasic STIM1 domains gate and regulate Orai channels. *Nat Cell Biol* **11,** 337-343.

Yuan JP, Zeng W, Huang GN, Worley PF & Muallem S. (2007). STIM1 heteromultimerizes TRPC channels to determine their function as store-operated channels. *Nat Cell Biol* **9,** 636-645.

Zagranichnaya TK, Wu X & Villereal ML. (2005). Endogenous TRPC1, TRPC3, and TRPC7 proteins combine to form native store-operated channels in HEK-293 cells. *J Biol Chem* **280,** 29559-29569.

Zeng F, Xu SZ, Jackson PK, McHugh D, Kumar B, Fountain SJ & Beech DJ. (2004). Human TRPC5 channel activated by a multiplicity of signals in a single cell. *J Physiol* **559,** 739-750.

Zeng W, Yuan JP, Kim MS, Choi YJ, Huang GN, Worley PF & Muallem S. (2008). STIM1 gates TRPC channels, but not Orai1, by electrostatic interaction. *Mol Cell* **32,** 439-448.

Zhang Q, He J, Lu W, Yin W, Yang H, Xu X & Wang D. (2010a). [Expression of transient receptor potential canonical channel proteins in human non-small cell lung cancer]. *Zhongguo Fei Ai Za Zhi* **13,** 612-616.

Zhang W, Trible RP, Zhu M, Liu SK, McGlade CJ & Samelson LE. (2000). Association of Grb2, Gads, and phospholipase C-gamma 1 with phosphorylated LAT tyrosine residues. Effect of LAT tyrosine mutations on T cell angigen receptor-mediated signaling. *J Biol Chem* **275,** 23355-23361.

Zhang ZY, Pan LJ & Zhang ZM. (2010b). Functional interactions among STIM1, Orai1 and TRPC1 on the activation of SOCs in HL-7702 cells. *Amino Acids* **39,** 195-204.

Zhu M, Liu Y, Koonpaew S, Granillo O & Zhang W. (2004). Positive and negative regulation of FcepsilonRI-mediated signaling by the adaptor protein LAB/NTAL. *J Exp Med* **200,** 991-1000.

Zhu X, Chu PB, Peyton M & Birnbaumer L. (1995). Molecular cloning of a widely expressed human homologue for the Drosophila trp gene. *FEBS Lett* **373,** 193-198.

Zhu X, Jiang M & Birnbaumer L. (1998). Receptor-activated Ca^{2+} influx via human Trp3 stably expressed in human embryonic kidney (HEK)293 cells. Evidence for a non-capacitative Ca^{2+} entry. *J Biol Chem* **273,** 133-142.

Zhu X, Jiang M, Peyton M, Boulay G, Hurst R, Stefani E & Birnbaumer L. (1996). trp, a novel mammalian gene family essential for agonist-activated capacitative Ca^{2+} entry. *Cell* **85,** 661-671.

Zhuang L, Peng JB, Tou L, Takanaga H, Adam RM, Hediger MA & Freeman MR. (2002). Calcium-selective ion channel, CaT1, is apically localized in gastrointestinal tract epithelia and is aberrantly expressed in human malignancies. *Lab Invest* **82,** 1755-1764.

Zitt C, Zobel A, Obukhov AG, Harteneck C, Kalkbrenner F, Luckhoff A & Schultz G. (1996). Cloning and functional expression of a human Ca^{2+}-permeable cation channel activated by calcium store depletion. *Neuron* **16,** 1189-1196.

Zweifach A & Lewis RS. (1995). Rapid inactivation of depletion-activated calcium current (ICRAC) due to local calcium feedback. *J Gen Physiol* **105,** 209-226.